

NASA Contractor Report 4714

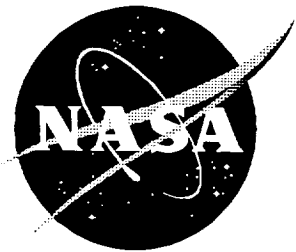
Aircraft Emissions Deposited in the Stratosphere and Within the Arctic Polar Vortex

Steven L. Baughcum

Contract NAS1-19360
Prepared for Langley Research Center

April 1996





NASA Contractor Report 4714

Aircraft Emissions Deposited in the Stratosphere and Within the Arctic Polar Vortex

*Steven L. Baughcum
Boeing Commercial Airplane Group • Seattle Washington*

National Aeronautics and Space Administration
Langley Research Center • Hampton, Virginia 23681-0001

Prepared for Langley Research Center
under Contract NAS1-19360

April 1996

Printed copies available from the following:

NASA Center for AeroSpace Information
800 Elkridge Landing Road
Linthicum Heights, MD 21090-2934
(301) 621-0390

National Technical Information Service (NTIS)
5285 Port Royal Road
Springfield, VA 22161-2171
(703) 487-4650

Executive Summary

This report describes analyses of aircraft emission inventories to evaluate the amount of emissions that might be deposited within the Arctic polar vortex due to a fleet of Mach 2.4 HSCTs. It also describes preliminary calculations to evaluate the amount of emissions occurring in the lower stratosphere due to subsonic aircraft. This work was performed under the NASA High Speed Research Systems Studies (HSRSS) contract NAS1-19360, Task Assignment 36.

The analysis shows that approximately 1-3% of the global emissions from a fleet of 500 Mach 2.4 HSCTs would occur directly in the Arctic polar vortex, based on analyses of the meteorological data for the winters of 1979 to 1994. Considering the data for 1979-1994, only a few HSCT flights would be expected to occur within the vortex for most days of each winter. For a few days each winter, however, the vortex extends south into the North Atlantic. On those days, as much as 10-20% of HSCT cruise emissions could be deposited within the vortex.

Assuming the emissions are well mixed within the vortex, the water vapor in the vortex would be expected to increase by 1.9-4.1% and NO_y by 1.2-2.6% due to emissions deposited directly within the vortex by a fleet of 500 Mach 2.4 HSCTs with EI(NO_x)=5 combustors. If EI(NO_x)=15 combustors were used, the NO_y perturbation would be 3.6-7.8%.

For a fleet of 1000 HSCTs, the effect is approximately 2-3 times larger than for a fleet of 500 HSCTs. It is not just a factor of two because the geographical distribution changes as the fleet size expands due to increases in market penetration and the number of city-pairs served.

These calculations have provided an estimate of total mass deposition of water vapor and NO_y directly into the vortex. They indicate that, on average, the direct emissions will be far less than the amount emitted by the global fleet and otherwise transported into the vortex. Previous estimates due to steady state fleet emissions have been approximately 10-20% increase in water vapor and 50-100% increase in NO_y in the lower stratosphere.

It is important to point out that these calculations do not consider the total perturbations to water vapor and NO_y which would occur within the polar vortex due to a fleet of HSCTs but only consider direct injection within the vortex to help in the evaluation of processes due to localized perturbations. Emissions would occur globally over the entire year and be transported into high latitudes before and during the time that the vortex forms. These emissions will be well mixed prior to the formation of the vortex and may lead to perturbations of the PSC formation probability. The effects of these perturbations must be treated separately by chemical transport models.

These calculations do not consider the effect of local increases in water vapor, NO_y, or sulfate aerosols in the vicinity of HSCT flights. Localized microphysical processes such as aerosol or ice particle growth (e.g., contrail formation) in the plume were not addressed by this study and must be considered separately from this analysis. As noted above, for each winter, episodes occur in which the vortex penetrates into the North Atlantic where a significant fraction of the HSCT flights are projected to occur. Microphysical processes may be more important during those brief events.

As localized effects are taken into account using microphysical models, the results presented here should provide an upper limit of the mass deposition within the vortex. With that information, it may be possible to scale the results of microphysical models to evaluate their impact on chemical perturbations within the vortex.

The preliminary analysis of the amount of subsonic emissions deposited within the stratosphere based on one month (May 1990) of aircraft emissions data shows that approximately 17% of the global fuel burned by the subsonic fleet may occur in the stratosphere. Averaged globally, approximately 16% of the fuel burned occurs within 1 kilometer of the tropopause and 29% occurs within 2 kilometers of the tropopause. The results for NO_x emissions are similar.

Both air traffic and tropopause heights are seasonally dependent. Higher tourist traffic in the summer months results in higher emission levels. The tropopause, a function of vertical temperature gradient, is also located at higher altitudes in the summer season in the northern hemisphere. Since both air traffic and tropopause heights are seasonally dependent, a more detailed analysis is required to provide a reliable answer to the question of how much water vapor and NO_x is emitted to the stratosphere from the subsonic fleet. Such an analysis is now being conducted using the tropopause height data described here and monthly aircraft emission inventories that have recently been developed. The results of that study will be reported in a future report.

Table of Contents

Section	Title	Page
Executive Summary		iii
Table of Contents		v
List of Figures		vi
List of Tables		viii
Glossary		ix
1. Introduction		1
2. Direct Deposition of HSCT Emissions with the Arctic polar vortex		5
2.1 HSCT Emission Distribution		5
2.2 Potential Vorticity Data		7
2.3 Deposition Analysis		11
2.4 Discussion		19
2.5 Conclusions		21
3. Emissions Deposited Directly in the Stratosphere		23
3.1 Tropopause Data		23
3.2 Analysis of Emissions above the Tropopause		34
3.3 Conclusions		45
4. References		46
Appendix A	Arctic Polar Vortex, Winter of 1992-93	A-1
Appendix B	Plots of Emissions within the Polar Vortex for the winters of 1979-94	B-1
Appendix C	Tables of Results for the Polar Vortex Calculations	C-1

List of Figures

Figure No.	Title	Page
Figure 2-1	NO _x emissions for a fleet of 500 Mach 2.4 HSCTs on the universal airline network as a function of altitude and latitude and as a function of latitude and longitude.	6
Figure 2-2	Plot of the relative potential vorticity as a function of latitude and longitude for January 13, 1993 and January 30, 1993.	10
Figure 2-3	HSCT fuel use within the polar vortex for the meteorology of 1992-3 for a fleet of 500 HSCTs on the universal airline network, using the conservative analysis.	13
Figure 2-4	HSCT fuel use within the polar vortex for the meteorology of 1992-3 for a fleet of 500 HSCTs on the universal airline network, using the liberal analysis.	14
Figure 2-5	Fuel use within the Arctic polar vortex for the winters 1979-94 for a fleet of 500 Mach 2.4 HSCTs on the universal airline network.	16
Figure 2-6	Fuel use within the Arctic polar vortex for the winters 1979-94 for a fleet of 500 Mach 2.4 HSCTs on the 1993 AESA Assessment network.	17
Figure 2-7	Fuel use within the Arctic polar vortex for the winters 1979-94 for a fleet of 1000 Mach 2.4 HSCTs on the universal airline network.	18
Figure 3-1	Tropopause heights in kilometers for January 1, 1990 and July 1, 1990.	24
Figure 3-2	Tropopause heights in kilometers for January and July monthly averages for 1990.	25
Figure 3-3	Comparison of the zonal mean tropopause heights for January and July averaged over the time period of 1983 to 1993.	27
Figure 3-4	Monthly average tropopause heights in kilometers for 1990.	28
Figure 3-5	Monthly average tropopause heights in kilometers for the time period 1983-93.	31

List of Figures (cont)

Figure No.	Title	Page
Figure 3-6	NO _x emissions for all 1990 aircraft traffic as a function of altitude and latitude and as a function of latitude and longitude.	35
Figure 3-7	Fraction of emissions (fuel burned, NO _x , CO, and hydrocarbons) deposited in the stratosphere globally from scheduled air traffic in 1990, based on air traffic data for May 1990, using tropopause heights for 1990.	36
Figure 3-8	Fraction of emissions (fuel burned, NO _x , CO, and hydrocarbons) deposited in the stratosphere globally from scheduled air traffic in 1990, based on air traffic data for May 1990, using daily tropopause heights for 1989.	39
Figure 3-9	Fraction of emissions (fuel burned, NO _x , CO, and hydrocarbons) deposited in the stratosphere globally from scheduled air traffic in 1990, based on air traffic data for May 1990, using daily tropopause heights for 1991.	40
Figure 3-10	Fraction of emissions (fuel burned, NO _x , CO, and hydrocarbons) deposited in the stratosphere globally from all air traffic in 1990, based on air traffic data for May 1990 and using daily tropopause heights for 1990.	41
Figure 3-11	Fraction of emissions (fuel burned, NO _x , CO, and hydrocarbons) deposited in the stratosphere in the North Atlantic from scheduled air traffic in 1990, based on air traffic data for May 1990 and daily tropopause heights for 1990.	42
Figure 3-12	Sensitivity of amount of fuel use in the stratosphere globally to the aircraft flight altitudes for scheduled air traffic in 1990 using May 1990 as representative.	43
Figure 3-13	Fraction of emissions (fuel burned, NO _x , CO, and hydrocarbons) deposited in the stratosphere globally from a fleet of 500 Mach 2.4 HSCTs for tropopause heights for 1990.	44

List of Tables

Table No.	Title	Page
Table 2-1	Potential temperatures for US Standard Atmosphere conditions	7
Table 2-2	Summary of data available for the vortex analysis	9
Table 2-3	Recommended emission indices in units of grams of emissions/kilogram fuel burned for the year 2015	12
Table 2-4	Average daily fuel use within the Arctic vortex for the winters of 1979-94	15
Table 2-5	Calculated direct mass deposition of water vapor and NO _y by HSCTs (EI(NO _x)=5) flying within the polar vortex averaged over the winters between 1979 and 1994	20
Table 2-6	Calculated local perturbations of water vapor and NO _y by HSCTs (EI(NO _x)=5) flying within the polar vortex averaged over the winters between 1979 and 1994	20

GLOSSARY

AEAP	Atmospheric Effects of Aviation Project
AESA	Atmospheric Effects of Stratospheric Aircraft
APU	Auxiliary power unit
ASM	Available seat mile (the number of seats an airline provides times the number of miles they are flown)
ATC	Air traffic control
ATM	Available ton-miles (the number of tons capable of being carried times the number of miles flown)
BCAG	Boeing Commercial Airplane Group
BMAP	Boeing Mission Analysis Process
CAC	Climate Prediction Center
CAEP	ICAO Committee on Aviation Environmental Protection
CIAP	Climatic Impact Assessment Program (US Dept. of Transportation program in the early 1970s)
CIONO ₂	Chlorine nitrate
CO	Carbon Monoxide
CO ₂	Carbon Dioxide
EI(CO)	Emission Index (grams CO/kg fuel burn)
EI(HC)	Emission Index [grams hydrocarbon (as CH ₄)/kg fuel burn]
EI(NO _x)	Emission Index (grams NO _x (as NO ₂)/kg fuel burn)
Epv	Ertel's potential vorticity
ESAD	Equivalent Still Air Distance
FAA	Federal Aviation Administration
GAEC	Global Atmospheric Emissions Code
GCD	Great circle distance
GDAS	Global Data Acquisition System
GE	General Electric
GSFC	Goddard Space Flight Center (NASA)
gm	gram
HC	Unburned hydrocarbon
H ₂ O	Water
HSCT	High Speed Civil Transport
HSRP	High Speed Research Program (NASA)
ICAO	International Civil Aviation Organization
IDL	Interactive Data Language (Research Systems, Inc.)
ISA	International standard atmosphere
kg	kilogram
km	kilometer
lb	pound
Load Factor	Percentage of an airplane's seat capacity occupied by passengers on a given flight
LTO cycle	Landing takeoff cycle
M	Mach number
MDC	McDonnell Douglas Corporation
MTOW	Maximum takeoff weight
NASA	National Aeronautics and Space Administration

GLOSSARY (cont)

NCEP	National Center for Environmental Prediction (formerly NMC)
NMC	National Meteorological Center (now NCEP)
nmi	Nautical mile
NOx	Oxides of nitrogen (NO + NO ₂) in units of gram equivalent NO ₂
NOy	Reactive odd nitrogen (NO + NO ₂ + NO ₃ + HNO ₃ + 2 x N ₂ O ₅ + HNO ₄ + HONO + ClONO ₂ + BrONO ₂)
OAG	Official Airline Guide
OEW	Operating Empty Weight
P&W	Pratt & Whitney
PAX	passengers
ppb	parts per billion
ppbv	parts per billion by volume
ppm	parts per million
ppmv	parts per million by volume
PSC	Polar Stratospheric Cloud
PV	Potential Vorticity
RAM	Revenue air mile
RPM	Revenue passenger miles (the number of paying passengers times the number of miles they fly)
RTM	Revenue ton-miles (number of tons carried times the number of miles flown)
SO ₂	Sulfur dioxide
TBE	Turbine bypass engine
TOGW	Takeoff gross weight
ton	2000 pounds
US	United States
WMO	World Meteorological Organization
2D	Two dimensional (latitude x altitude)
3D	Three dimensional

1. Introduction

The NASA Atmospheric Effects of Aviation Project (AEAP) is investigating the effects of aircraft emissions on the atmosphere. This includes evaluating the impact of a projected high speed civil transport (HSCT) fleet on the stratosphere and the effects of subsonic aircraft emissions on the stratosphere and troposphere.

To support these analyses, 3-dimensional (1° latitude $\times 1^{\circ}$ longitude $\times 1$ km altitude) inventories of fuel burned and emissions (NOx, CO, and HC) have been developed for May 1990 and for projected fleets of HSCTs and subsonic aircraft in the year 2015. [Baughcum, et. al., 1994; Wuebbles, et. al., 1993; Baughcum and Henderson, 1995]. Additional emission inventories for scheduled air traffic for each month of 1992 [Baughcum, et. al., 1996a] and for selected months of 1976 and 1984 have also recently been developed [Baughcum, et. al., 1996b]. Similar studies for charter, military, and non-OAG scheduled air traffic in the former Soviet Union have been completed for 1992 [Metwally, 1995] and are underway for 1976 and 1984 [M. Metwally, private communication].

In this report, we examine two issues that relate to how the geographical location of the aircraft routes and flight altitudes might affect the calculated perturbations:

- How much water vapor and NOx would be emitted directly into the Arctic polar vortex from projected fleets of HSCTs and how would this change the ambient concentrations of water and NOy?
- What fraction of the subsonic emissions calculated for 1990 were emitted in the lower stratosphere and how sensitive is this answer to the flight altitudes used in the calculations of the emission inventories?

The chemistry and dispersion of aircraft emissions will depend on where they occur (altitude and geographical location) and the meteorological conditions. Most of the modeling studies have focused on the use of zonally averaged 2-dimensional chemical transport models to evaluate the effects of fleets of HSCTs. [Albritton, et. al., 1993; Stolarski, et. al., 1995] But three-dimensional effects will be important for understanding both the dynamics and chemistry of the perturbations.

The dynamics of the polar vortex has been reviewed by Schoeberl and Hartmann (1991) and discussed in detail by Schoeberl and co-workers (1992). The vortex forms in the late fall as the polar regions fall into darkness. Radiative cooling then quickly lowers the temperature in the high-latitude stratosphere to temperatures much lower than those at mid-latitudes. As a consequence, a latitudinal pressure gradient develops between the pole and mid-latitudes. Combined with the Earth's rotation, this produces a circumpolar belt of westerly winds referred to as the polar vortex. The vortex breaks up in late winter/early

spring as the polar stratosphere is exposed to sunlight, resulting in solar heating and temperature increases. The vortex is much larger and more persistent in the Antarctic than in the Arctic. Much colder temperatures are observed in the Antarctic polar vortex than in the Arctic.

Sharp gradients in tracer concentrations are observed between air within the vortex and outside of it. This is an indicator of the ability of the polar vortex to inhibit mixing [Schoeberl and Hartmann, 1991].

Chemical reactions are sensitive to temperature and pressure. Under extremely cold conditions, such as within the Arctic or Antarctic polar vortex, polar stratospheric clouds (PSCs) can form and chemical reactions will occur on ice surfaces. Reactions on PSCs have been shown to be particularly important for the activation of chlorine species during polar winter via the heterogeneous conversion of ClONO₂ [see WMO (1995) and references cited therein].

Emissions of water vapor and NOx from an HSCT fleet could perturb the chemistry in the polar vortex by two mechanisms:

- 1.) Transport of emissions occurring globally over the entire year into high latitudes before and during the time that the vortex forms. These emissions will be well mixed prior to the formation of the vortex and could lead to changes in PSC formation probability [Peter, et. al., 1991]. These perturbations must be treated by chemical transport models.
- 2.) Direct injection by flights in the late fall, winter, and early spring which occur within the vortex. These perturbations will primarily be localized and must be treated by considering the microphysics of the plume and plume dispersion.

The work presented here will focus on estimating the mass deposition of emissions which would contribute to the second mechanism.

Since the polar vortex is a relatively confined air mass, direct injection of water vapor and NOx from HSCTs might lead to local production of PSCs which might in turn affect the stratospheric chemistry. In addition, under these cold conditions, water emissions from HSCTs may lead to the formation of persistent ice contrails. Additional chemical processes could occur on these ice particles.

The polar vortex is not symmetric as a function of longitude and shows much lower temperatures than would be calculated for a zonal average (averaged over longitude) which would include regions outside the vortex. Although many of the zonally averaged 2-dimensional (altitude and latitude) models currently being used in the HSCT assessment include some parameterization of PSC chemistry, they generally do not include the vortex isolation. To characterize the perturbations due to ice particles and PSC in the wake of an HSCT would require a microphysical model of ice particle formation and chemistry.

No HSCT flights are expected over the Antarctic where the polar vortex is long-lived and relatively stable during austral winter. Although most HSCT flights are predicted to occur at northern mid-latitudes, a few HSCT flights are expected to occur in the high northern latitudes where the less-stable, shorter-lived Arctic polar vortex occurs. [see Schoeberl, et. al., 1992 and WMO, 1995 for in-depth discussions of the polar vortex]

In this report, potential vorticity data for the time period 1978-94 is used to estimate the amount of HSCT emissions that would be deposited directly within the Arctic vortex. The potential vorticity data was obtained from Dr. Paul Newman (NASA Goddard Space Flight Center) and was derived using an objective criteria developed by Nash, Newman, Rosenfield, and Schoeberl (1996). The total mass loading for each winter over that time period has been calculated and then compared to the ambient water vapor and NO_y concentrations expected to be present. This provides a first-order estimate of how the NO_y and water mass loading in the polar vortex would be altered by flights occurring directly within the vortex.

This analysis only considers direct injection into the vortex during the winter. In addition, water vapor and NO_y concentrations would be perturbed by emissions deposited throughout the year in other regions and transported to the polar regions. Those processes are treated in global 2-D and 3-D models and are beyond the scope of this analysis. If microphysical processes occurring in the plume of the HSCT were found to be important in evaluating the HSCT ozone impact, this estimate of the amount of direct injection of water vapor and NO_y should be useful in scaling the plume calculation on one aircraft to the effects due to a fleet of HSCTs.

Emissions deposited in the stratosphere will stay in the atmosphere longer than if injected in the troposphere. One issue that has been raised is whether aircraft emissions by the current subsonic fleet provide a significant source of NO_x and water vapor to the stratosphere. To evaluate this, we have used tropopause height data* for the time period 1983-93 and combined that with aircraft emission inventories calculated for May 1990 for both scheduled aircraft and for all aircraft emissions combined (scheduled passenger and cargo jets, scheduled turboprops, military, charter, and non-scheduled flights within the former Soviet Union and China). From these calculations, the total mass loading of water vapor and NO_x into the stratosphere has been calculated. The fraction of aircraft emissions occurring in the stratosphere has also been calculated.

For these preliminary analyses, May 1990 data has been used to represent the annual average. Subsequent studies of the seasonal variability of aircraft emissions have shown that this was a good assumption [Baughcum,

* Obtained from the National Centers for Environmental Prediction (NCEP) Climate Analysis Center (CAD) (formerly the National Meteorological Center (NMC)) via Dr. Paul Newman at NASA Goddard Space Flight Center.

et. al., 1996a]. Emission inventories have recently been calculated to take into account the monthly variation of scheduled air traffic [Baughcum, et.al., 1996a]. That analysis showed a strong seasonal dependence in emissions from air traffic, particularly in some regions. Aircraft emissions are highest during the summer, which is when the tropopause is highest. During winter when the tropopause is lower, the volume of air traffic is also lower. Since both the tropopause heights and aircraft emissions show seasonal cycles, the results presented here should be considered a preliminary analysis. Work is currently underway to do a more complete analysis using the seasonal aircraft emission inventories.

The work described in this report was conducted under NASA Langley Contract NAS1-19360, Task 36. The NASA Langley Task Manager was Donald L. Maiden.

Within the Boeing HSCT engineering group, overall program management was provided by John D. Vachal and John H. Gerstle for most of the research activities. The principal investigator of the task was Steven L. Baughcum. Peter S. Hertel did part of the computer programming.

The author gratefully acknowledges the help of Paul Newman (NASA Goddard Space Flight Center), Eric Nielsen (Applied Research Corporation at NASA Goddard Space Flight Center), and Karen Sage (NASA Langley Research Center). Datafiles of rescaled potential vorticity on the National Meteorological Center (NMC) grid were provided by Paul Newman. NMC tropopause height data was provided by Paul Newman and Eric Nielsen. They also provided routines written in IDL (Interactive Data Language, Research Systems, Inc.) which were used in the initial tropopause analyses and later modified. Karen Sage helped solve several problems in the code used to display the tropopause data.

The author is grateful to Paul Newman, Don Maiden, and Debra Maggiora for reviewing the draft of this report.

2. Direct Deposition of HSCT Emissions within the Arctic Polar Vortex

The primary objective of this work was to evaluate the amount of water vapor and NO_x emitted directly into the Arctic polar vortex from projected fleets of Mach 2.4 HSCTs. An estimate was made of how this would change the concentrations of water vapor and NO_y compared to ambient conditions.

Three-dimensional inventories of emissions from projected HSCT fleets have been calculated previously. [Baughcum, *et. al.*, 1994; Baughcum and Henderson, 1995] Although the majority of flights are projected to occur at mid-latitudes, some flights are projected at high northern latitudes. Also, episodes occur in which the Arctic polar vortex extends into the North Atlantic or over Europe.

In the study described below, the amount of emissions which would occur within the polar vortex were calculated using polar vortex data derived from National Meteorological Center (NMC)* wind and temperature data. The approach was to calculate the amount of emissions for each day of available data using both conservative and liberal definitions of the vortex.

2.1 HSCT Emission Distribution

The HSCT emission inventories have been described extensively [Baughcum, *et. al.*, 1994; Baughcum and Henderson, 1995]. For the analyses presented here, both the newer emission inventories corresponding to fleets of 500 and 1000 Mach 2.4 HSCTs on the universal airline network and the revised emission inventory of 500 HSCTs on the 1993 AESA assessment network [Baughcum and Henderson, 1995] were used.

The geographical distribution of a fleet of 500 Mach 2.4 HSCTs on the universal airline network is shown in Figure 2-1. Many of the routes are between North America and Europe and North America and the Far East. Supersonic aircraft produce sonic booms which are generally unacceptable to people on the ground. Because of these sonic booms, it is anticipated that the HSCT would only be allowed to fly supersonically over water. Flights over the pole are relatively few in number due to the long range required for such flights and the restrictions on overland flight.

* The National Meteorological Center is now called the National Center for Environmental Prediction (NCEP).

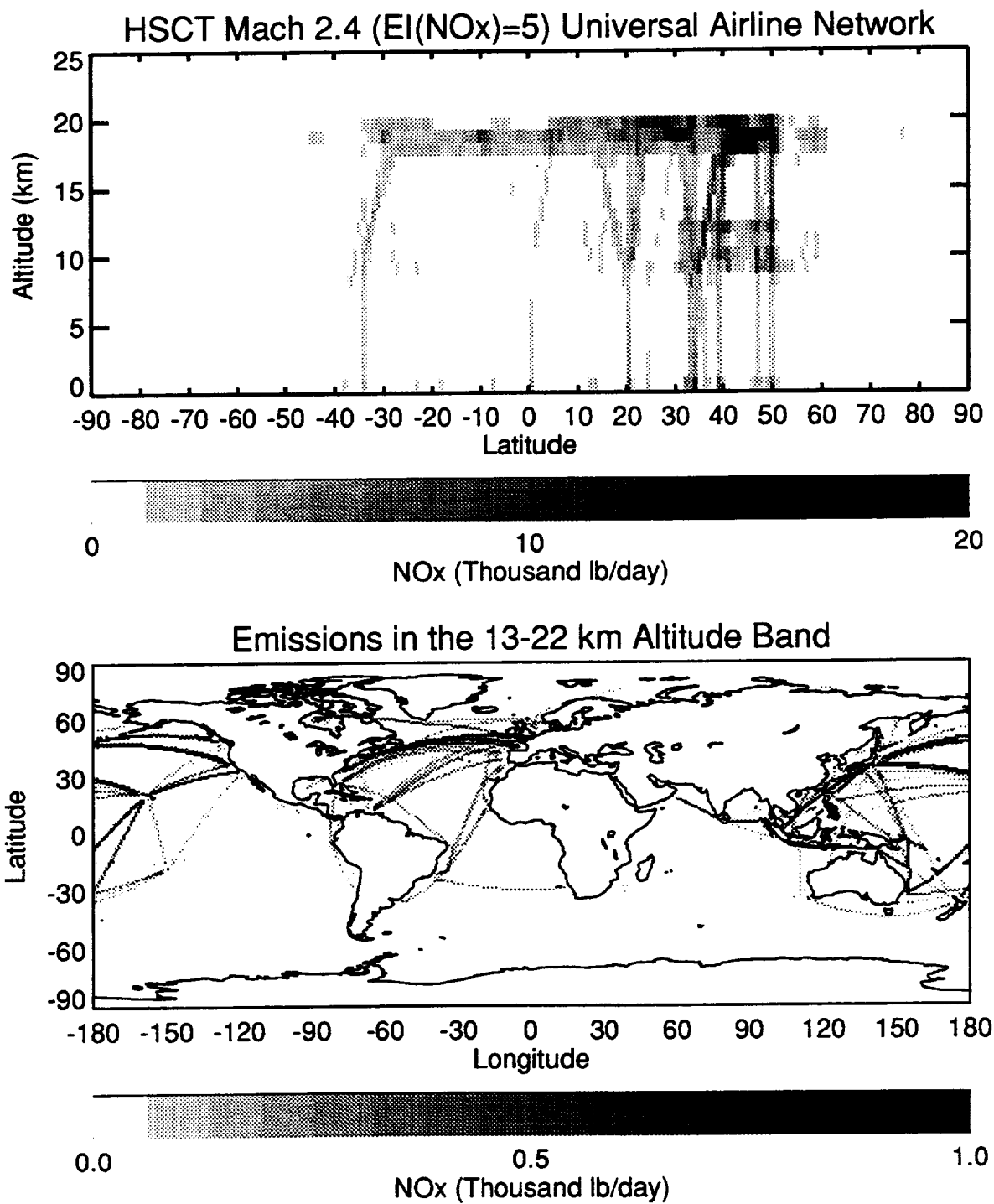


Figure 2-1. NOx emissions for a fleet of 500 Mach 2.4 HSCTs on the Universal Airline Network, as a function of altitude and latitude (summed over longitude, top panel) and as a function of latitude and longitude (summed over the 13-22 km altitude band, bottom panel). (Values greater than maximum are plotted as black.)

The global fuel burned calculated for a fleet of 500 active Mach 2.4 HSCTs on the universal airline network was 8.21×10^{10} kg/year, with 66% of this occurring above 17 kilometers altitude [Baughcum and Henderson, 1995]. A fleet of 1000 HSCTs was calculated to use 1.57×10^{11} kg/year, with 63% above 17 km altitude.

The supersonic cruise altitudes for the Mach 2.4 fleet are between 18 and 21 kilometers. For a US Standard Atmosphere, the corresponding potential temperatures (isentropes) are given in Table 2-1.

Table 2-1. Potential temperatures for US Standard Atmosphere conditions.

Altitude (km)	Pressure (mb)	Potential Temperature (K)
18	75.7	453
19	64.7	474
20	55.3	496
21	47.3	519

2.2 Potential Vorticity Data

Data files of rescaled potential vorticity (PV) were obtained from Dr. Paul Newman at the NASA Goddard Space Flight Center (GSFC). The data covered the winters of 1978 to 1994 and corresponded to PV on the 500 K potential temperature surface. This potential temperature corresponds reasonably well with the supersonic cruise altitudes of a Mach 2.4 HSCT. (see Table 2-1) The rescaled PV data were provided on the NMC grid (2° latitude $\times 5^{\circ}$ longitude).

The calculation of the potential vorticity data and the derivation of the vortex edge at GSFC are described in detail by Nash and co-workers (1996). A brief summary is provided below.

The NMC* analyses consist of geopotential heights and temperatures, with winds derived at GSFC via a balanced wind approximation. Tropospheric heights and temperatures (1000-100 mb) are produced from the NMC Global Data Acquisition System (GDAS), while stratospheric heights and temperatures (70 - 0.4 mb) are produced by the NMC Climate Analysis Center (CAC). The GDAS data are extensively described in Trenberth and Olson [1988], while the NMC CAC data are described in Newman et al. [1989, 1993]. The data have been documented in a number of climatologies [Wu et al., 1987; Randel, 1987; and Nagatani et al., 1988]. The CAC system generates heights and temperatures for 70 hPa to 10 hPa in the Northern Hemisphere, and is a successive correction method [Cressman, 1959; Finger et al., 1965]. The

* The National Meteorological Center is now called the National Center for Environmental Prediction (NCEP).

analysis for levels above 10 hPa and the Southern Hemisphere stratosphere (70 to 0.4 hPa) uses a similar successive corrections method [Yanai, 1964], but the successive scans are around the data rather than the gridpoints. The net result is a map that essentially uses the same analysis system for the whole stratosphere. The first guess for all maps is the previous day's map. Satellite data are then injected into the analysis for the current map. NMC data quality is generally quite good in the lower stratosphere [Gelman et al., 1986; Nagatani et al., 1988; Nagatani et al., 1990; Trenberth and Olson, 1988].

From the geopotential heights, balanced winds and vorticity are calculated on the 65 x 65 grid [Randel, 1987; Newman et al., 1988]. This 'balanced wind' is iteratively derived via a vorticity advection balance. The vorticity of the field is a byproduct of the 'balanced wind' calculation. The temperature, winds, and rescaled vorticity were then interpolated to a 5 degree longitude by 2 degree latitude grid. This method produced more realistic polar winds and vorticity fields than if the heights were first interpolated to the latitude-longitude grid. Potential vorticity is derived via the product of the absolute vorticity and the pressure derivative of the potential temperature. The potential vorticity values are then interpolated in potential temperatures to the appropriate isentropic level.

Plotting Ertel's potential vorticity (Epv) against equivalent latitude results in a distribution that has an 'S' shape in the vortex region. The method for determining the vortex edge is based on this shape. The vortex edge is defined to be the location of the highest Epv gradient between latitudes 45°N and 87°N. The upper latitude was chosen to prevent the edge effect of an increasing derivative at the pole point. The boundary is further defined to be the region which lies between the local maximum convex and concave curvature in the Epv curve that surrounds the vortex edge. The two additional edge values define liberal and conservative vortex edge estimates. The liberal vortex estimate provides a large vortex estimate, while the conservative vortex value is a relatively smaller vortex. These boundaries are considered to be limits for the location of the vortex edge. Kinematic studies of parcel behavior indicate that these boundaries represent excellent estimates of the air confined to the vortex.

The vortex files provided for the analysis described here are scaled to reflect these edge values. The Epv values are calculated by subtracting off the liberal vortex edge estimate, and then scaling those Epv values with the conservative minus liberal value.

$$Q_s = (Q - Q_{\text{liberal edge}})/(Q_{\text{conservative edge}} - Q_{\text{liberal edge}})$$

Hence, values of the rescaled potential vorticity (Q_s) less than zero are outside the vortex, while values greater than 1 are inside. Intermediate values are in the vortex edge region.

Data files of Q_s and the vortex edge were calculated by Paul Newman using the method of Nash, Newman, Rosenthal, and Schoeberl (1996) and were provided by him to Boeing for this analysis. Q_s will be referred to in this

section as rescaled potential vorticity. Data were available for the 1978-94 time period.

Figure 2-2 shows the rescaled potential vorticity as a function of latitude and longitude for two days. The top two plots show January 13, 1993 when the polar vortex extended into the North Atlantic. On this day, much of the HSCT supersonic cruise from Europe to North America would have been within the polar vortex. A more normal occurrence is shown in the bottom two figures a few days later, January 30, 1993. On this day, most of the HSCT traffic would have been outside of the vortex. The zero contour line on the plots corresponds to the liberal definition of the vortex edge, while the contour line plotted on the right corresponds to the vortex edge as defined by Nash and co-workers (1996).

Appendix A shows plots of Q_s and the vortex edge for each day of available data for the winter of 1992-93. That winter was chosen as representative of a typical winter [P. Newman, private communication]. A summary of data that was available for this analysis is given in Table 2-2.

Table 2-2. Summary of data available for the vortex analysis.

Winter	First Day of Available Vortex data	Last Day of Available Vortex Data	# of Days of Data Available
1978-79	1-Dec-78	28-Feb-79	68
1979-80	1-Dec-79	29-Feb-80	66
1980-81	1-Dec-80	28-Feb-81	67
1981-82	1-Dec-81	28-Feb-82	58
1982-83	1-Dec-82	16-Feb-83	65
1983-84	4-Dec-83	29-Feb-84	66
1984-85	1-Dec-84	25-Feb-85	62
1985-86	2-Dec-85	27-Feb-86	53
1986-87	4-Dec-86	28-Feb-87	71
1987-88	2-Dec-87	29-Feb-88	65
1988-89	1-Dec-88	25-Feb-89	58
1989-90	1-Dec-89	28-Feb-90	69
1990-91	1-Dec-90	28-Feb-91	72
1991-92	1-Dec-91	29-Feb-92	70
1992-93	1-Dec-92	28-Feb-93	69
1993-94	1-Dec-93	28-Feb-94	73

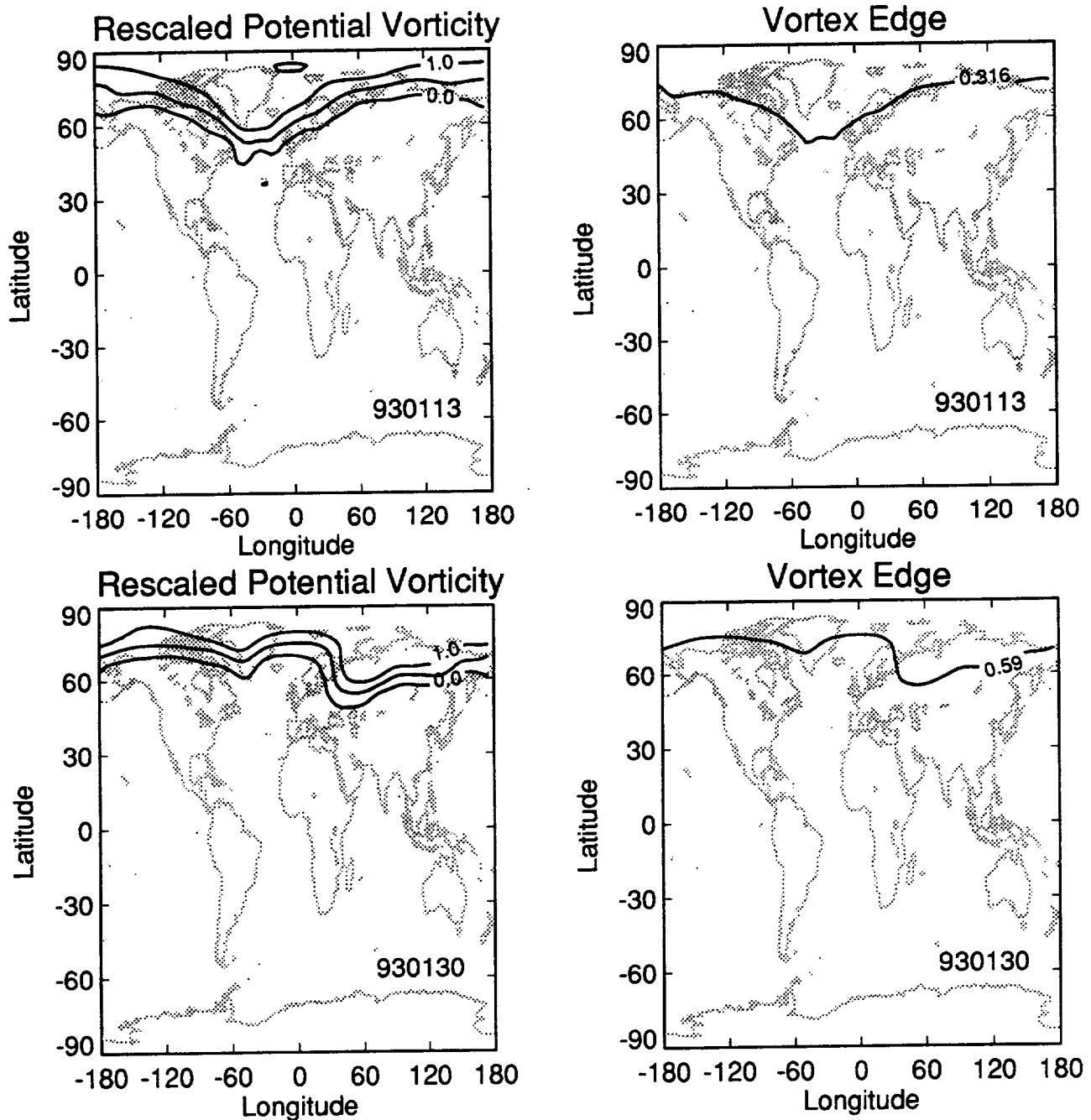


Figure 2-2. Plot of the rescaled potential vorticity as a function of latitude and longitude. The top two panels show the results for January 13, 1993 and the bottom two for January 30, 1993. The figures on the left show the rescaled potential vorticity with zero corresponding to a liberal definition of the vortex edge. The plots on the right correspond to the vortex edge as defined by Nash and co-workers (1996).

2.3 Deposition Analysis

To calculate the overlap of the emissions with the polar vortex, the emission inventories were first interpolated onto the NMC 2° latitude $\times 5^{\circ}$ longitude grid. The HSCT emissions over the altitude range 17-22 kilometers were summed for each latitude \times longitude cell. This altitude band includes all the supersonic cruise emissions and corresponds roughly to the 500 K isentropic surface used for the PV calculations (see Table 2-1). Since part of the cruise emissions would occur at potential temperatures < 500 K, the calculations presented below should provide an upper limit to the amount of emissions directly deposited with the vortex. As a reference, for a fleet of 500 Mach 2.4 HSCTs on the universal airline network, approximately 66% of the global fuel burn occurs at altitudes above 17 kilometers.

The rescaled potential vorticity files consisted of Q_s on a 2° latitude $\times 5^{\circ}$ longitude grid for each day of available data. Each data file also contained a value for Q_s corresponding to the vortex edge [$Q(\text{edge})$] as defined by Nash and co-workers (1996). Calculations of the amount of emissions deposited within the vortex were done using two cases:

Conservative Analysis:

For each latitude \times longitude cell in which $Q_s \geq Q(\text{edge})$, the emissions above 17 km were counted as within the vortex

Liberal Analysis:

For each cell in which Q_s was greater than zero, the emissions above 17 km were counted as within the vortex using the liberal definition of the vortex.

Analyses were done using three Mach 2.4 HSCT emission scenarios. These were for fleets of 500 HSCTs on the universal airline network, 1000 HSCTs on the universal airline network, and 500 HSCTs on the network used for the 1993 AESA assessment. Runs used the meteorological data available for the time period, 1978-94, to estimate how the results might vary from year.

The results discussed below will be presented in terms of fuel burned within the vortex. Since all of the HSCT emissions within the vortex are expected to occur during supersonic cruise, the other emissions can be calculated from the fuel use by applying the emission indices shown in Table 2-3.

Table 2-3. Recommended emission indices in units of grams of emission/kilogram fuel burned for the year 2015.

Emission	Emission Index
NOx (as NO ₂)	5.0
Carbon Monoxide (CO)	2.9
Hydrocarbons	0.3
Carbon Dioxide (CO ₂)	3155
Water (H ₂ O)	1237
Sulfur oxides (as SO ₂)	0.4

The amount of fuel burned in the Arctic polar vortex by the 500 HSCT fleet on the universal network fleet are shown for the meteorology of the winter of 1992-93 in Figures 2-3 and 2-4. The top panel of Figure 2-3 shows the amount of fuel burned per day within the vortex using the conservative analysis described above. The solid line corresponds to the mean value of the fuel burned within the vortex and the dashed line to the mean plus one standard deviation. The results show that for most days of that winter HSCT flights would have been outside of the vortex. Episodes occurred in mid-January in which the vortex edge moved south into the North Atlantic. During that episode, a significant fraction of the HSCT emissions would be within the vortex. The bottom panel of the figure shows the fraction of the global fuel burn above 17 kilometers altitude which occurred within the vortex. Averaged over each day of available data, 0.9% of the supersonic cruise fuel use would have been within the vortex during that winter.

Similar results using the liberal analysis described earlier are shown in Figure 2-4. Using the liberal definition of the vortex, 2.6% of the supersonic cruise fuel use would have been within the vortex. Similar plots for each winter of the 1979-94 time period are provided in Appendix B for both the conservative and liberal analyses. The calculations in Appendix B use a fleet of 500 Mach 2.4 HSCTs on the universal airline network. Similar results were obtained with the other two networks and will be summarized below. Tables summarizing the results are included as Appendix C.

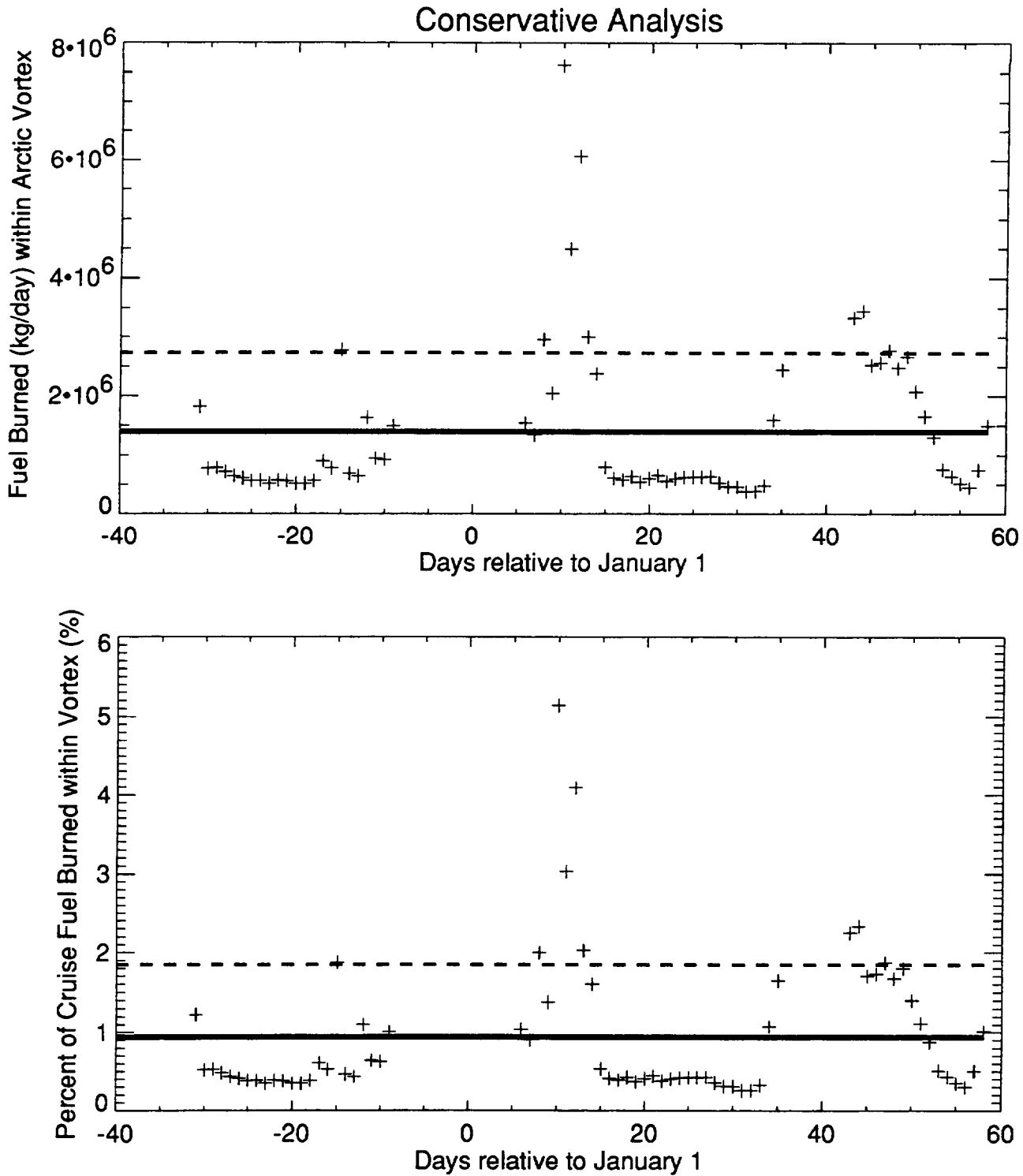


Figure 2-3. HSCT fuel use within the polar vortex (top panel) for the meteorology of 1992-3, for a fleet of 500 Mach 2.4 HSCTs on the universal airline network using the conservative analysis. The percent of global stratospheric cruise fuel use occurring within the vortex is shown in the bottom panel. The mean value (solid line) and mean + 1 standard deviation (dashed line) are shown.

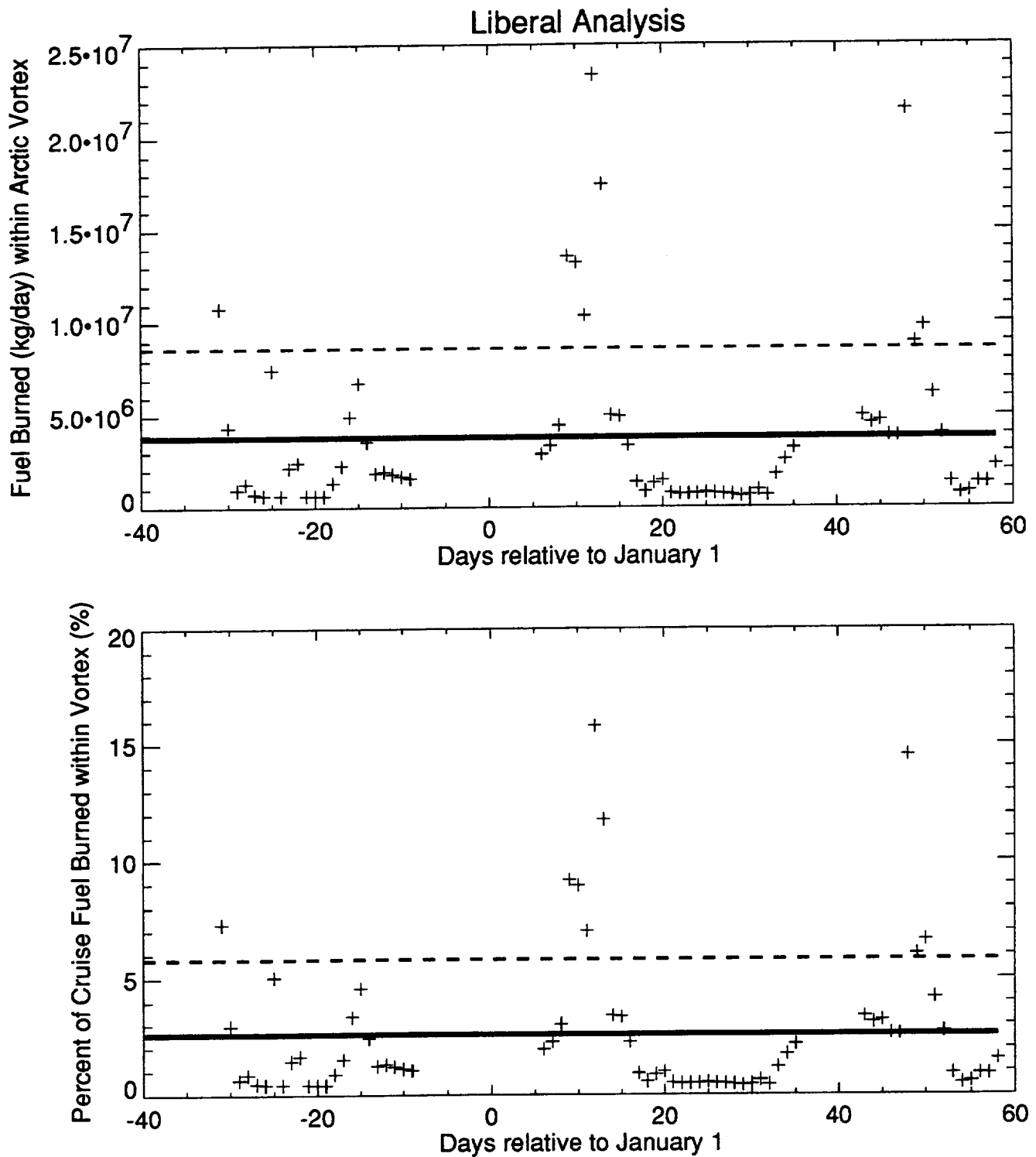


Figure 2-4. HSCT fuel use within the polar vortex (top panel) for the meteorology of 1992-3, for a fleet of 500 Mach 2.4 HSCTs on the universal airline network using the liberal analysis. The percent of global stratospheric cruise fuel use occurring within the vortex is shown in the bottom panel. The mean value (solid line) and mean + 1 standard deviation (dashed line) are shown.

Figure 2-5 shows the average daily deposition for each year beginning with the winter of 1979 (December 1978–February 1979) for the 500 aircraft fleet on the universal airline network. For each winter of data, the mean and standard deviation were calculated using the available rescaled potential vorticity data. The error bars plotted for each winter of data correspond to the standard deviation from that analysis. For this emission scenario, 1.1% of the daily cruise emissions would occur within the vortex using the conservative analysis for the deposition, while the liberal analysis would predict 2.5 % of the daily cruise emissions would be within the vortex.

To test the sensitivity to the details of the HSCT network, similar analyses are shown in Figure 2-6 for the 500 aircraft fleet used in the 1993 HSCT assessment. For this scenario, the conservative analysis would predict 1.8 % of the daily cruise emissions would be in the vortex, while the liberal analysis predicts 3.2 %.

To evaluate how the result might differ for a larger HSCT fleet, the 1000 HSCT emission inventory was evaluated and the results shown in Figure 2-7. The total amount of fuel burned in the vortex increases with increasing fleet size. Some geographical changes occur in the distribution as the fleet size grows because market penetration between some city-pairs increases and the number of city-pairs served increases [Baughcum and Henderson, 1995]. This has relatively little impact, however, on the fraction of the emissions that would be deposited in the vortex, yielding 1.8% of the daily cruise emissions for the conservative definition and 3.2% for the liberal definition.

The results are summarized in Table 2-4.

Table 2-4. Average daily fuel use within the Arctic vortex for the winters of 1979-94.

Scenario	Conservative Analysis		Liberal Analysis	
	Mean Daily Fuel (million kg/day)	Mean Fraction	Mean Daily Fuel (million kg/day)	Mean Fraction
Universal HSCT network (500 HSCTs)	1.7	1.1%	3.7	2.5%
Universal HSCT network (1000 HSCTs)	4.8	1.8%	8.6	3.2%
1993 AESA assessment network	2.6	1.8%	4.5	3.2%

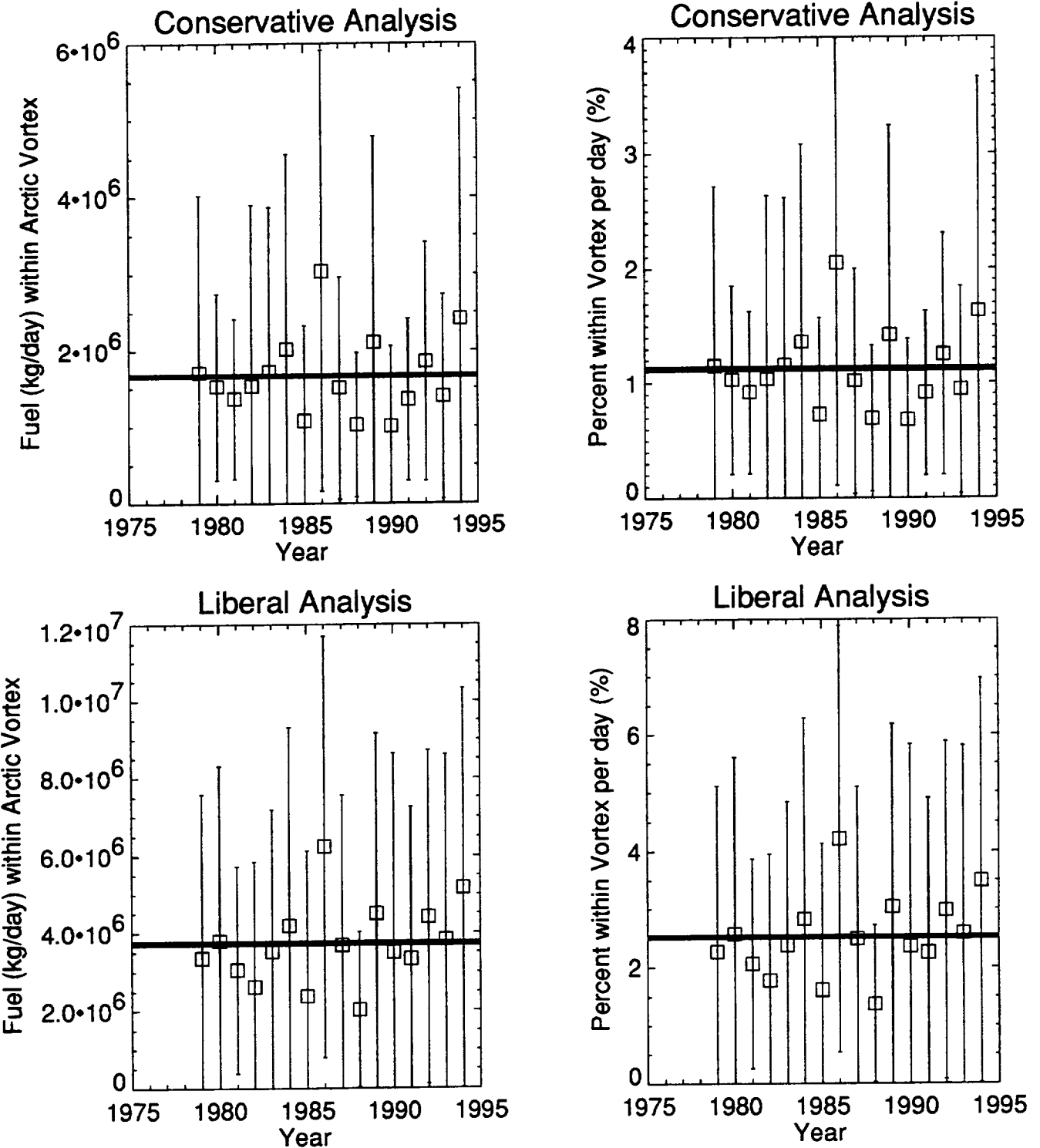


Figure 2-5. Fuel use within the Arctic polar vortex for the winters 1979-94 for a fleet of 500 Mach 2.4 HSCTs on the universal airline network. The top panels show the result for the conservative analysis and the bottom panels show the results for the liberal analysis. The solid horizontal lines are the average over the 1979 to 1994 time period.

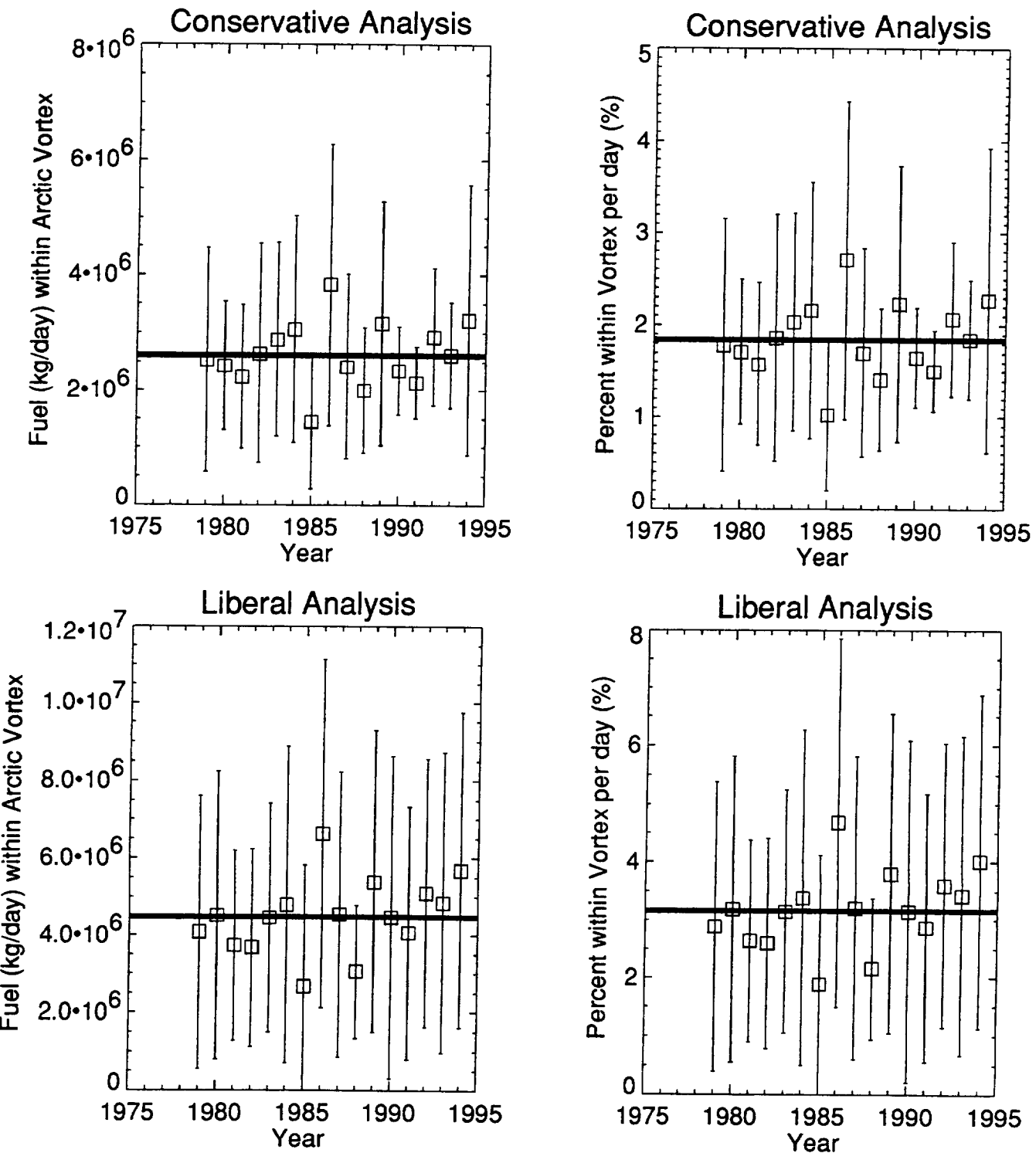


Figure 2-6. Fuel use within the Arctic polar vortex for the winters 1979-94 for a fleet of 500 Mach 2.4 HSCTs on the 1993 AESA Assessment network. The top panels show the result for the conservative analysis and the bottom panels show the results for the liberal analysis. The solid horizontal lines are the average over the 1979 to 1994 time period.

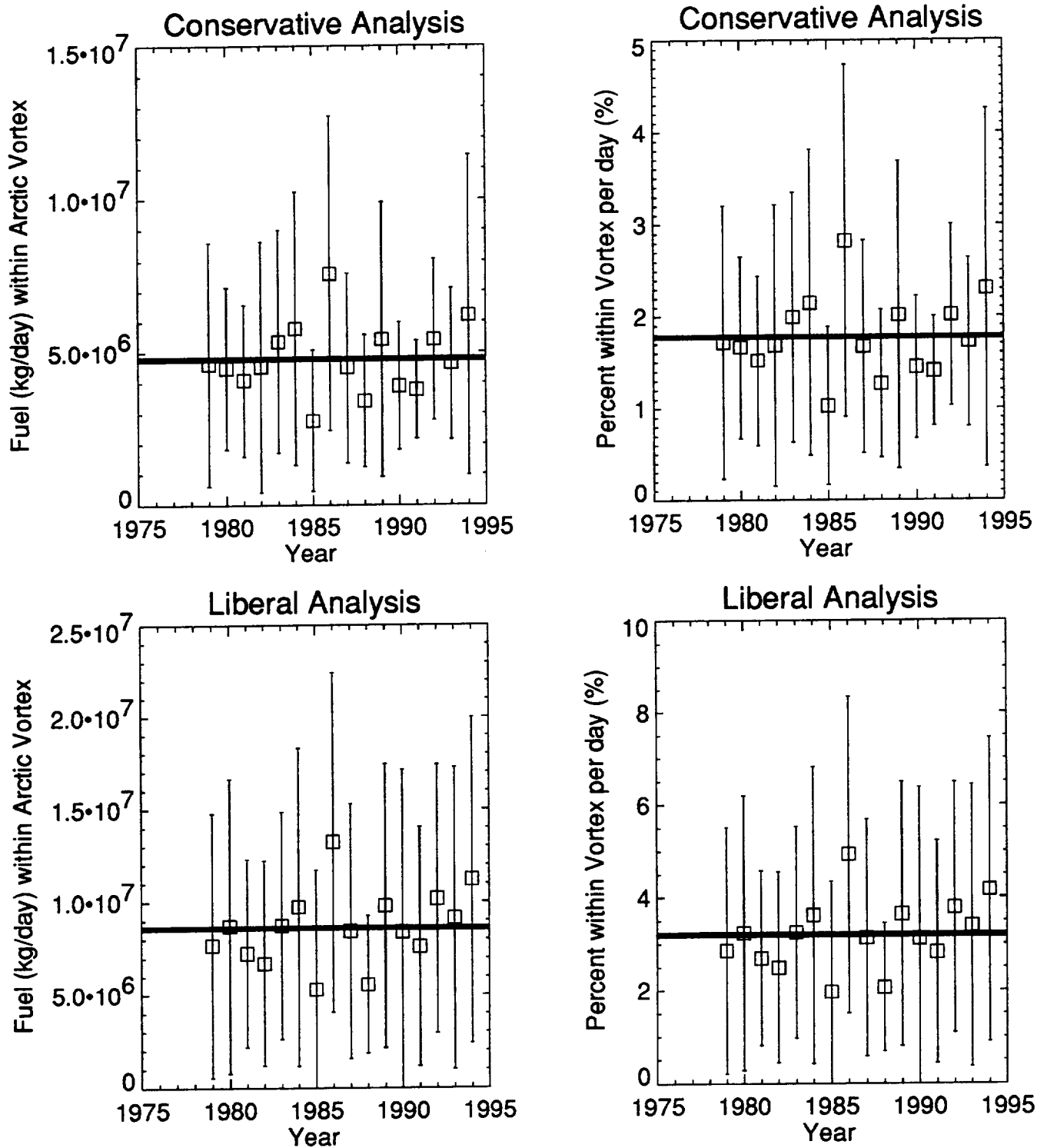


Figure 2-7. Fuel use within the Arctic polar vortex for the winters 1979-94 for a fleet of 1000 Mach 2.4 HSCTs on the universal airline network. The top panels show the result for the conservative analysis and the bottom panels show the results for the liberal analysis. The solid horizontal lines are the average over the 1979 to 1994 time period.

2.4 Discussion

The results show that for the time period of 1979-94 approximately 1-3% of the cruise emissions from a Mach 2.4 HSCT fleet would be deposited directly into the polar vortex. In the worse case considered (winter of 1985-86), approximately 2.8- 4.9 % of the cruise emissions would be within the vortex depending on which definition of the vortex edge was chosen. (see Appendices B and C)

To evaluate the perturbations of water vapor and NO_y in the vortex from the HSCT fleet, we assume background water vapor and NO_y concentrations of 4 ppmv [Kelly, et. al., 1990] and 10 ppbv [Kawa, et. al., 1990], respectively, based on measurements from the AASE campaign at these flight altitudes.

The Arctic vortex for the winter of 1992-1993 occurs at an average equivalent latitude of about 65°N [Nash, et. al., 1996] which corresponds to about 9% of the area of the Northern Hemisphere. This corresponds to a vortex area of $2.3 \times 10^{13} \text{ m}^2$.

The vortex data which was provided covered the time periods from December to February of each year. The Arctic vortex typically spins up in mid-November and breaks up in late-March to early April. For the winter of 1992-1993, Nash and co-workers calculated that the lower stratospheric vortex formed on 10 November 1992 and broke down on 20 April 1993 [Nash, et. al., 1996]. To estimate the total mass deposition from a fleet of HSCTs during the winter, 135 days was used as the average duration of the vortex.

Using the results from Table 2-4 for the daily fuel use within the vortex and the average duration of the vortex, the total emissions deposited within the vortex for an average winter were calculated. These results are summarized in Table 2-5 for an EI(NO_x)=5 combustor.

Assuming that the emissions were uniformly mixed over a 3 kilometer altitude band within the vortex and the average area of the vortex, the changes in water vapor and NO_y concentrations were calculated. The results are summarized in Table 2-6. The results shown assume an EI(NO_x) of 5. If EI(NO_x)=15 were used, the NO_y perturbation would be three times larger. The calculation does not consider local contrail formation, ice particle formation, or sedimentation of any particles.

The results shown in Table 2-6 indicate that the perturbation increases with fleet size as would be expected. The results are smaller than the water vapor and NO_y concentration changes expected due to the dispersion of the global fleet emissions. Previous estimates due to steady state fleet emissions have been approximately 10-20% increase in water vapor and 50-100% increase in NO_y in the lower stratosphere [Stolarski, et. al., 1995 and references cited therein].

Table 2-5. Calculated direct mass deposition of water vapor and NOy by HSCTs ($EI(NOx)=5$) flying within the polar vortex averaged over the winters between 1979 and 1994. The calculations do not account for additional emissions which were deposited throughout the year and transported into polar regions.

	Universal Network (500 HSCTs) (kilograms)	Universal Network (1000 HSCTs) (kilograms)	1993 AESA assessment network (500 HSCTs) (kilograms)
Conservative Analysis			
H ₂ O	2.8×10^8	8.0×10^8	4.3×10^8
NOy	1.2×10^6	3.2×10^6	1.8×10^6
Liberal Analysis			
H ₂ O	6.2×10^8	14.4×10^8	7.5×10^8
NOy	2.5×10^6	5.8×10^6	3.0×10^6

Table 2-6. Calculated local perturbations to water vapor and NOy by HSCTs ($EI(NOx)=5$) flying within the polar vortex averaged over the winters between 1979 and 1994. The calculations do not account for additional emissions which were deposited throughout the year and transported into polar regions.

	Universal Network (500 HSCTs)	Universal Network (1000 HSCTs)	1993 AESA assessment network (500 HSCTs)
Conservative Analysis			
H ₂ O Perturbation	1.9%	5.3%	2.9%
NOy Perturbation	1.2%	3.3%	1.8%
Liberal Analysis			
H ₂ O Perturbation	4.1%	9.4%	4.9%
NOy Perturbation	2.6%	6.0%	3.1%

2.5 Conclusions

The analysis shows that approximately 1-3% of the global emissions from a fleet of Mach 2.4 HSCTs would occur directly in the Arctic polar vortex, based on analyses of rescaled potential vorticity data for the winters of 1979 to 1994. Considering the data for 1979-1994, only a few HSCT flights would be expected to occur within the vortex for most days of each winter. For a few days each winter, the vortex extends south into the North Atlantic. On those days, as much as 10-20% of HSCT cruise emissions could be deposited within the vortex.

Assuming the emissions are well mixed within the vortex, the water vapor would be expected to increase by 1.9-4.1% and NO_y by 1.2-2.6% by flights within the vortex by a fleet of 500 Mach 2.4 HSCTs with EI(NO_x)=5 combustors. If EI(NO_x)=15 combustors were used, the NO_y perturbation would be 3.6-7.8%. For a fleet of 1000 HSCTs, the effect is approximately a factor of 2-3 times larger than for a fleet of 500 HSCTs. It is not just a factor of two because some changes occur in the geographical distribution as the fleet size increases because market penetration between some city-pairs increases and the number of city-pairs served increases [Baughcum and Henderson, 1995].

These calculations have provided an estimate of total mass deposition of water vapor and NO_y directly into the vortex. They indicate that, on average, the direct emissions will be far less than the amount emitted by the global fleet and otherwise transported into the vortex. Previous estimates due to steady state fleet emissions have been approximately 10-20% increase in water vapor and 50-100% increase in NO_y in the lower stratosphere [Stolarski, et. al., 1995 and references cited therein].

It is important to point out that these calculations do not consider the total perturbations to water vapor and NO_y which would occur within the polar vortex due to a fleet of HSCTs but only consider direct injection within the vortex to help in the evaluation of processes due to localized perturbations. Emissions would occur globally over the entire year and be transported into high latitudes before and during the time that the vortex forms. These emissions will be well mixed prior to the formation of the vortex and may lead to perturbations of the PSC formation probability [Peter, et. al., 1991]. The effects of these perturbations must be treated separately by chemical transport models.

These calculations do not consider the effect of local increases in water vapor, NO_y, or sulfate aerosols in the vicinity of HSCT flights. Localized microphysical processes such as aerosol or ice particle growth (e.g., contrail formation) in the plume could occur, were not addressed by this study, and must be considered separately from this analysis. As noted above, for each winter, episodes occur in which the vortex penetrates into the North Atlantic where a significant fraction of the HSCT flights are projected to occur. Microphysical processes may be more important during those brief events.

As localized effects are taken into account using microphysical models, the results presented in Table 2-5 should provide an upper limit of the mass deposition within the vortex. With that information, it may be possible to scale the results of microphysical models to evaluate their impact on chemical perturbations within the vortex.

3. Emissions Deposited Directly in the Stratosphere

The tropopause is the boundary between the troposphere and the stratosphere. The tropopause height varies with both season and geographical location. Within the troposphere, vertical mixing is relatively fast, while in the stratosphere it is much slower. Commercial aircraft fly at altitudes which are comparable to the height of the tropopause. Since the lifetime and chemistry of aircraft emissions into the stratosphere may be quite different from those injected into the troposphere, this analysis attempts to quantify the amount of emissions from aircraft deposited directly into the stratosphere.

3.1 Tropopause Data

There are both dynamical and thermal definitions of the tropopause. The data used in this analysis were standard National Meteorological Center (NMC)* tropopause height files and were obtained from NMC via Paul Newman and Eric Nielsen of the NASA Goddard Space Flight Center (GSFC). The tropopause heights were derived by NMC using the WMO thermal definition. The tropopause is defined as the lowest level above 500 mb in which the lapse rate decreases to 2° C/kilometer or less and that the average lapse rate from this level to any level within the next higher 2 km does not exceed 2° C/km. The tropopause heights (in mb) were provided on the standard NMC grid which is 2° latitude x 5° longitude.

Tropopause heights vary with season and geographical location. Day to day variations occur due to synoptic scale processes. This is illustrated in Figure 3-1 which shows the tropopause heights for January 1, 1990 and July 1, 1990. The structure in the contour plots is due to synoptic scale events.

Figure 3-2 shows the monthly average tropopause heights for January and July 1990. For these figures, much of the synoptic scale events have been averaged out and it is easier to see the seasonal differences. In the Northern Hemisphere, the tropopause is lower during the winter than during the summer. For example, compare the tropopause heights in January over the United States with those of July.

* The National Meteorological Center is now called the National Center for Environmental Prediction (NCEP) Climate Analysis Center (CAC).

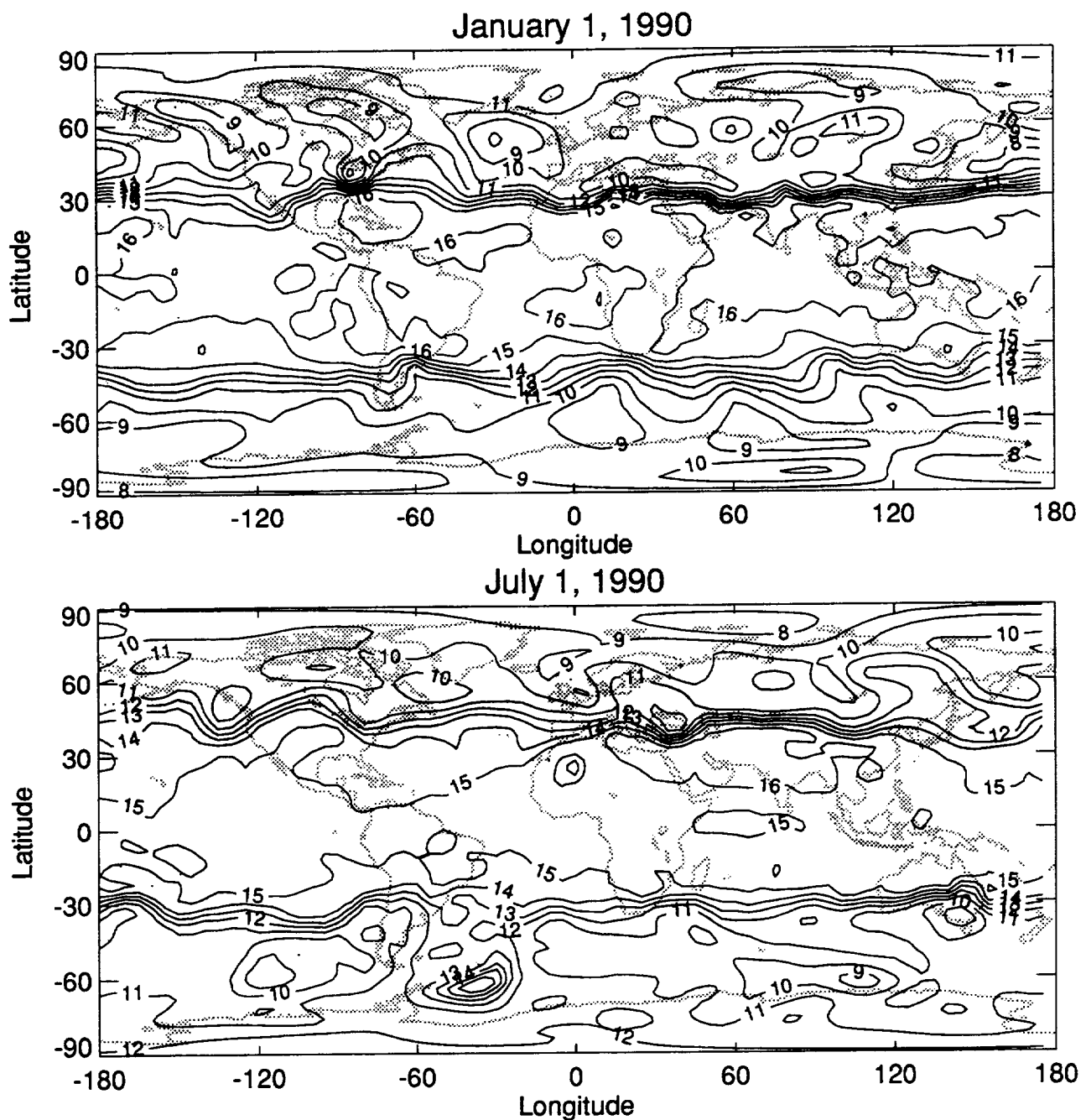


Figure 3-1. Tropopause heights in kilometers for January 1, 1990 (top panel) and July 1, 1990 (bottom panel).

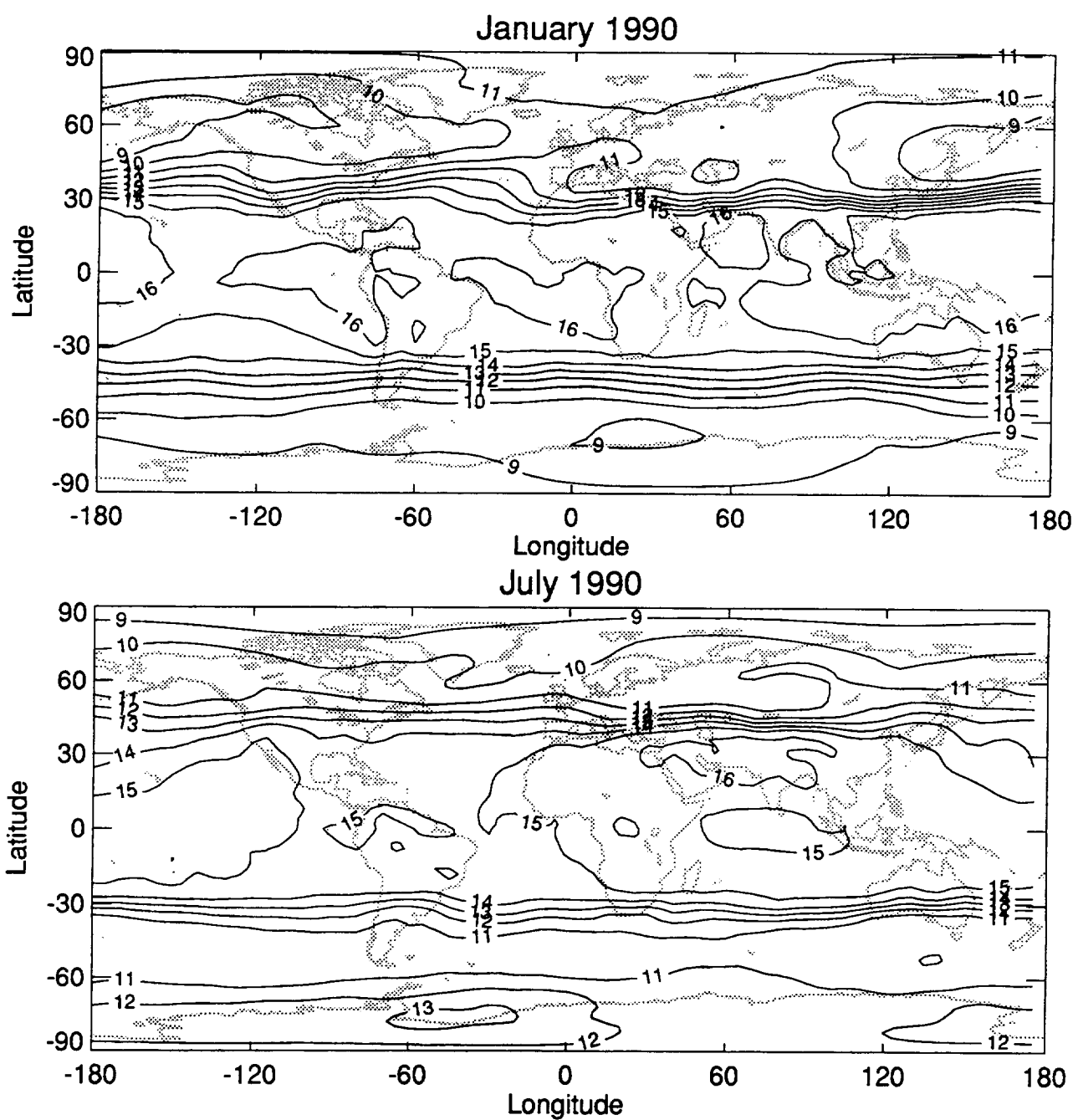


Figure 3-2. Tropopause heights in kilometers for January (top panel) and July (bottom panel) monthly averages for 1990.

The seasonal variation in tropopause is seen by comparing the zonal averaged (averaged over longitude) tropopause heights for summer and winter. Figure 3-3 shows the zonal mean tropopause heights as a function of latitude averaged over the 1983 to 1993 time period.** The tropopause height in the 30°N-50°N latitude band (where much of the commercial air traffic flies) is much lower in January than in July. Commercial aircraft cruise at altitudes between 9 and 13 kilometers and thus, we expect to see that the amount of emissions deposited above the tropopause will be seasonally dependent.

Figure 3-4 shows the monthly average tropopause heights for each month of 1990 to show how they vary through one year of data. Figure 3-5 shows the monthly average tropopause heights averaged over the years 1983-93.

** Because we are using the WMO definition of the tropopause and the lapse rate in the winter at high latitudes is small, the tropopause heights in the high-latitude winter are overestimated. This discrepancy is seen most clearly in the Antarctic but does not matter for this analysis because no commercial air traffic flies there. During polar winter, emissions deposited in the lower stratosphere would be expected to be transported downward because of the net descent of the air masses in that region. Since 99% of fuel burned by commercial air traffic occurs south of 70°N, we do not expect that the definition of the tropopause during polar winter to be critical to this analysis.

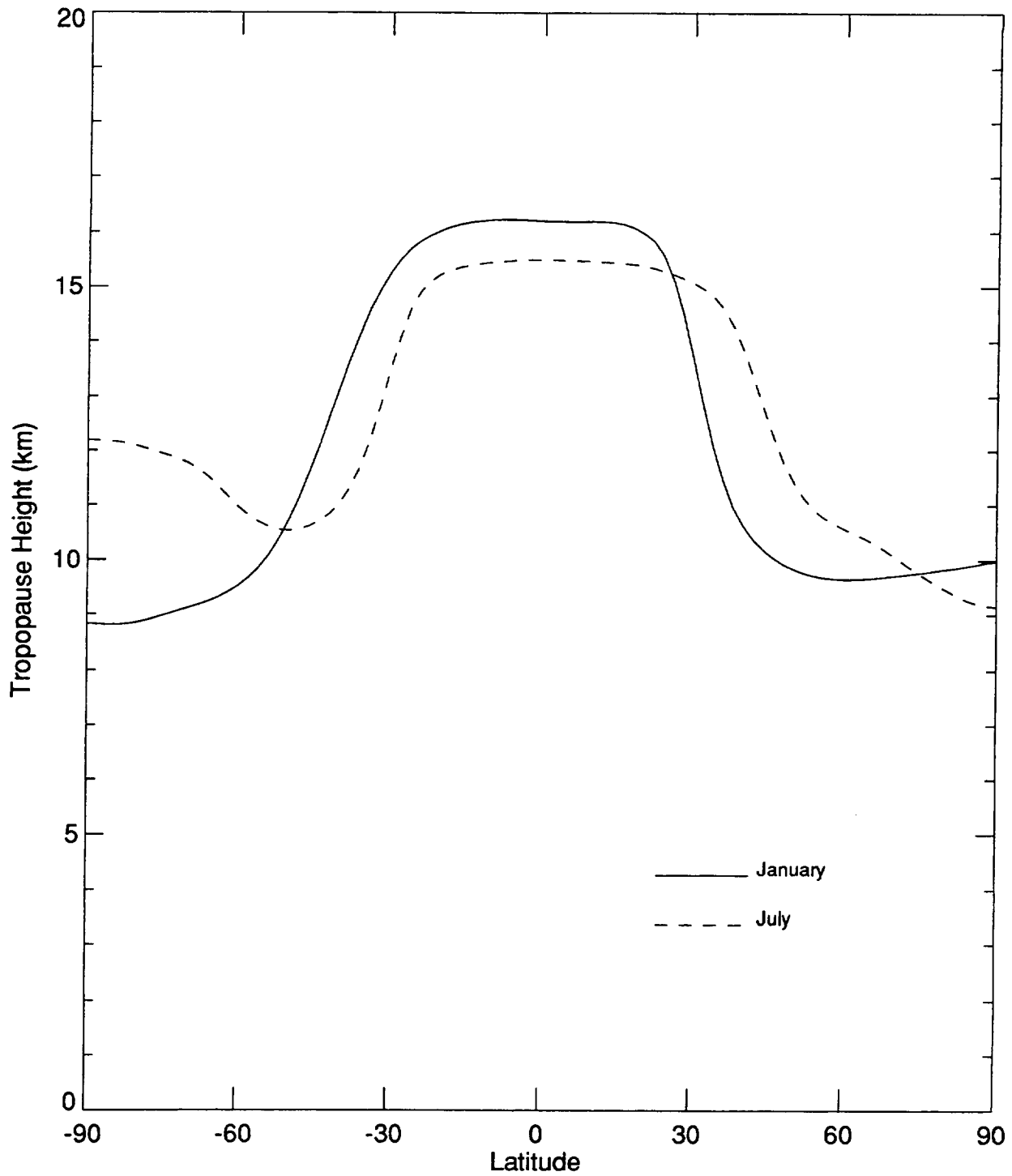


Figure 3-3. Comparison of the zonal mean tropopause heights for January (solid line) and July (dashed line) averaged over the time period of 1983 to 1993.

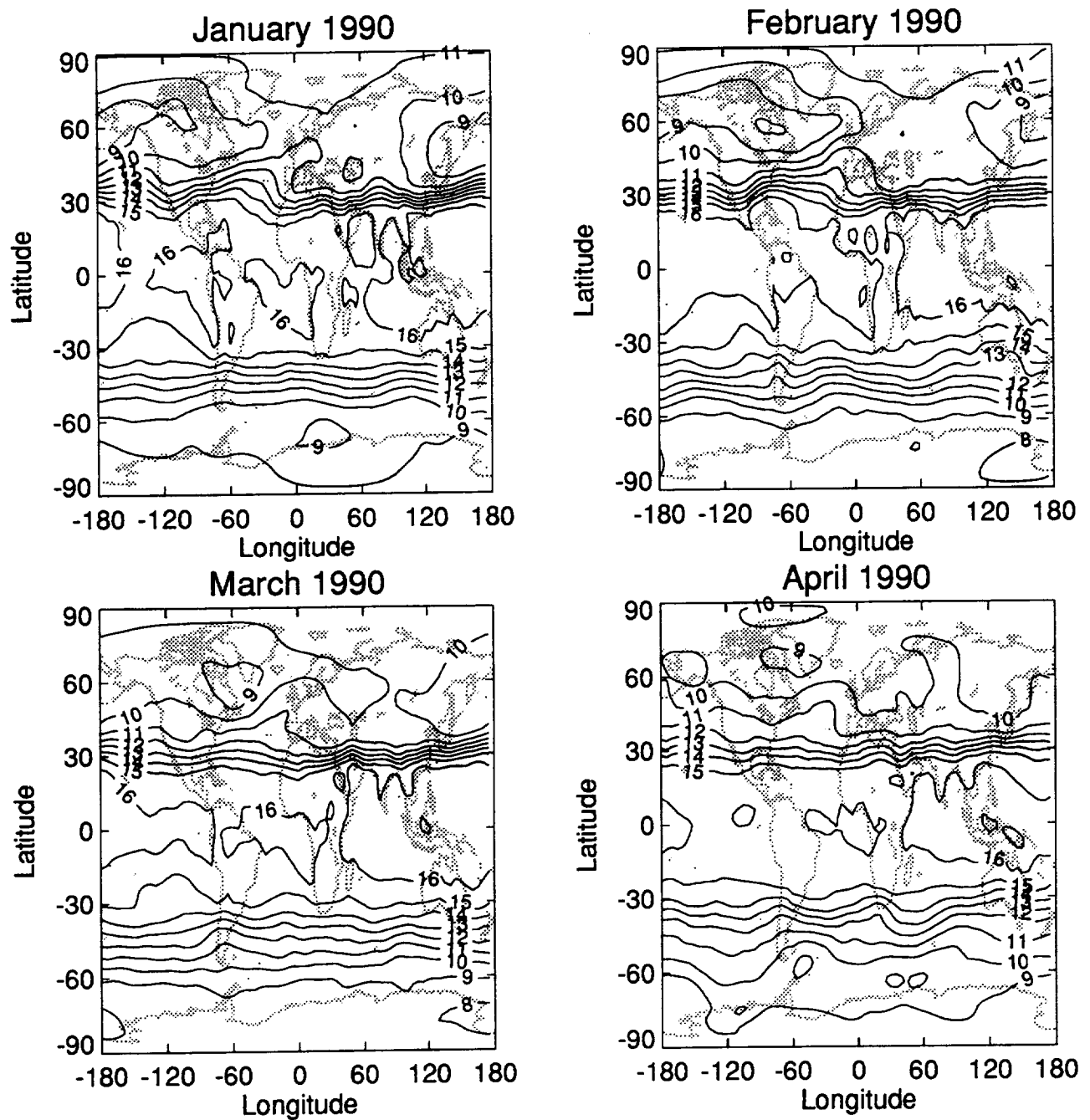


Figure 3-4. Monthly average tropopause heights in kilometers for 1990.

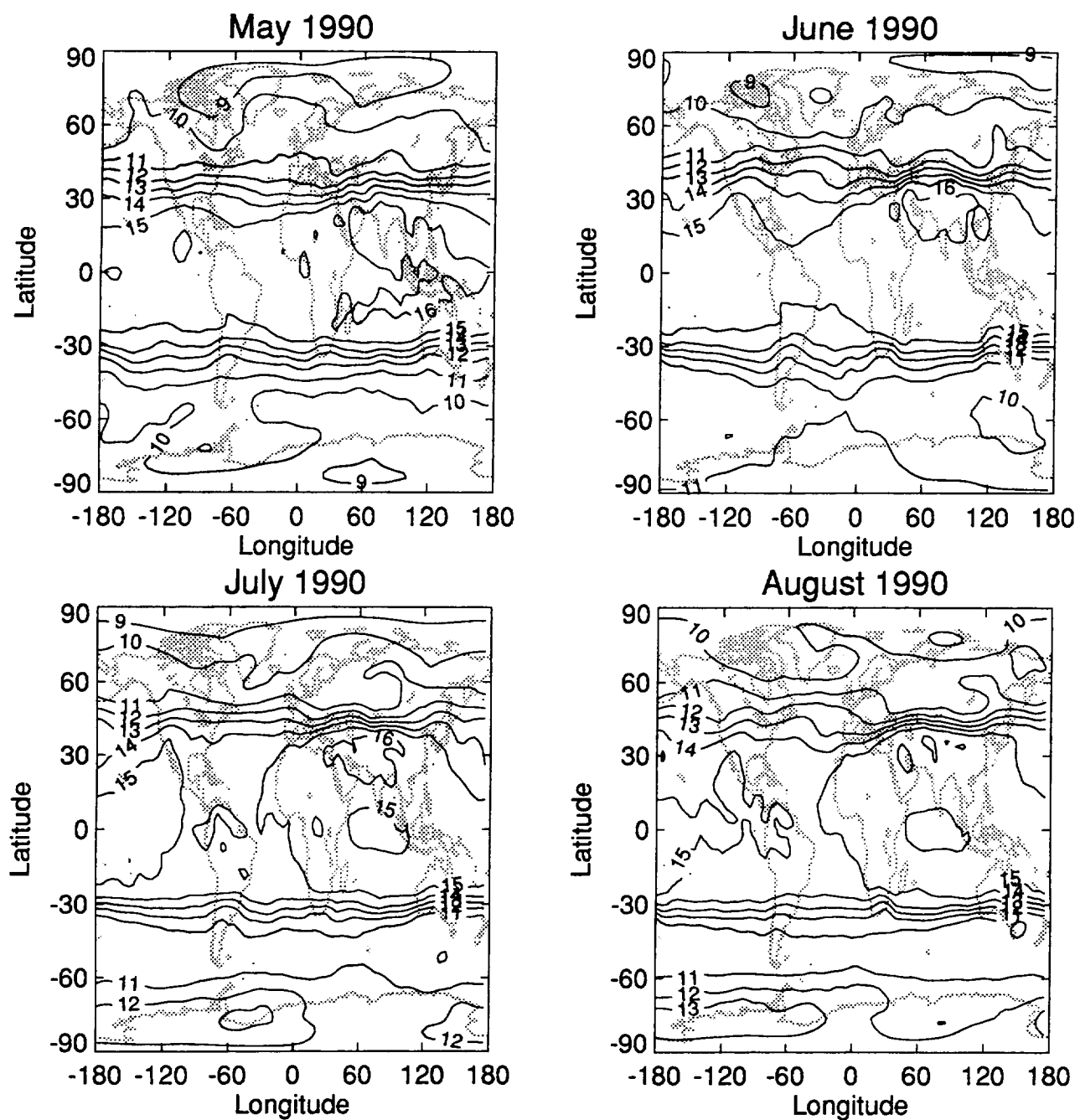


Figure 3-4 (cont). Monthly average tropopause heights in kilometers for 1990.

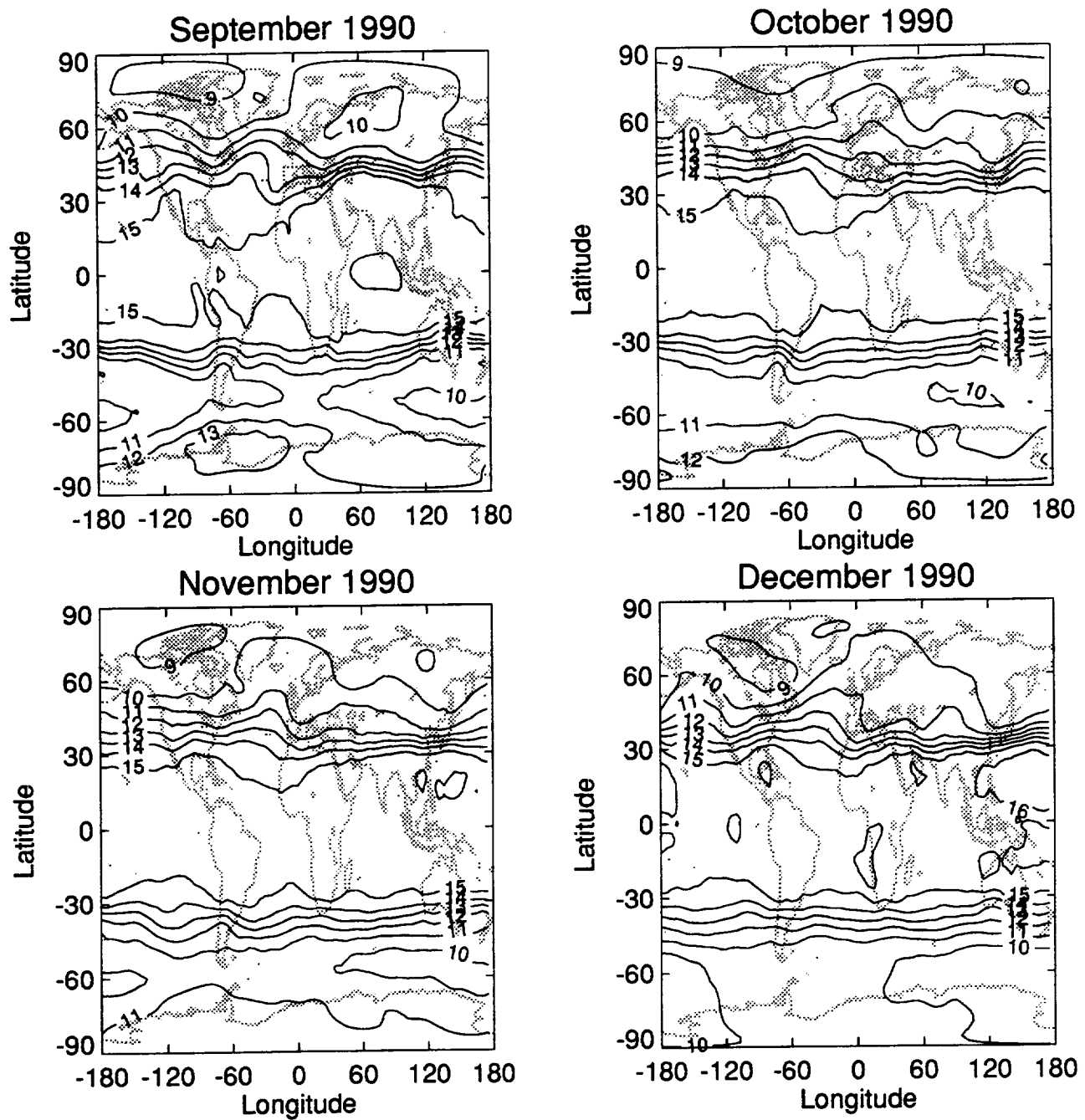


Figure 3-4 (cont). Monthly average tropopause heights in kilometers for 1990.

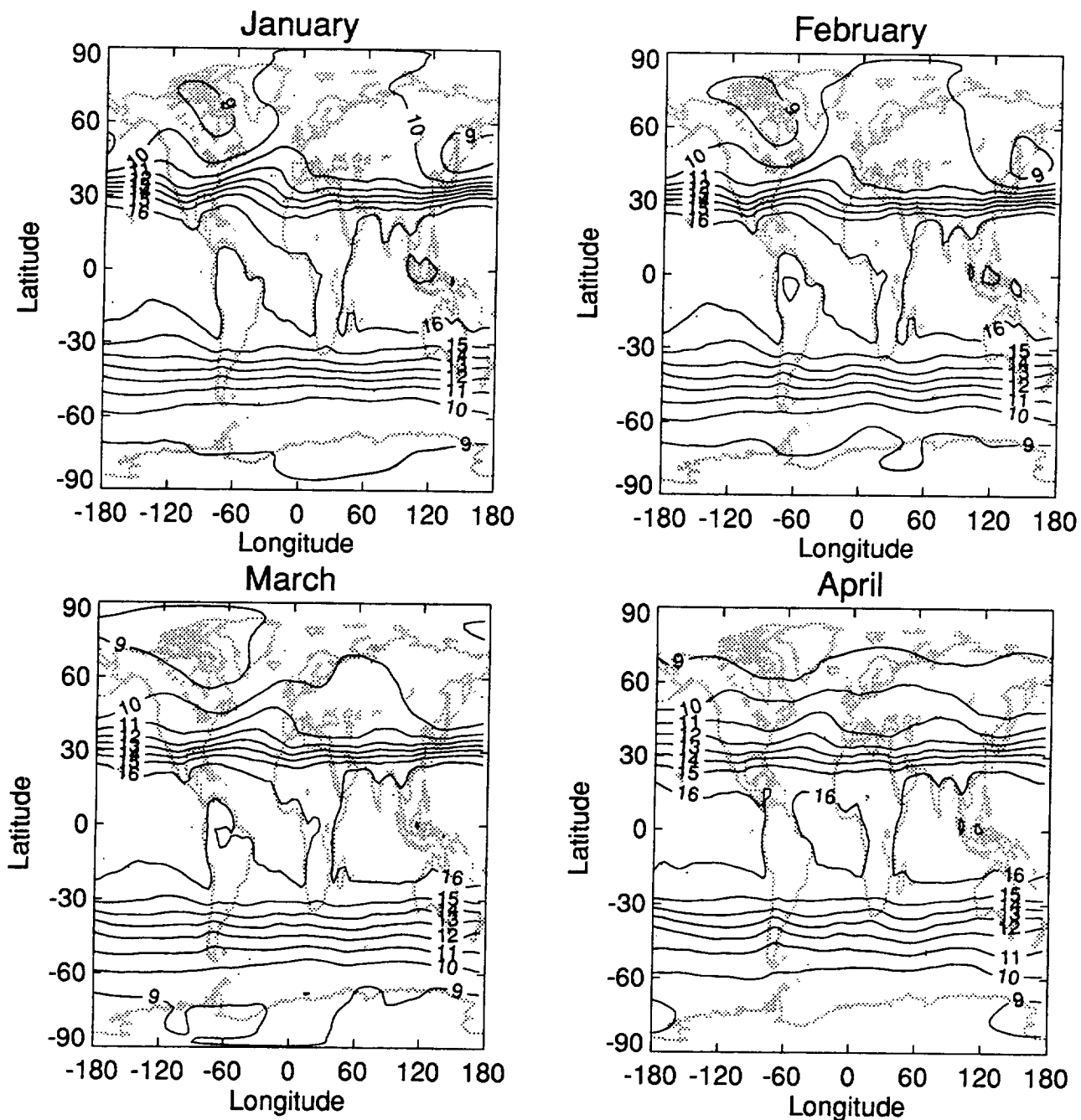


Figure 3-5. Monthly average tropopause heights in kilometers for the time period 1983-93.

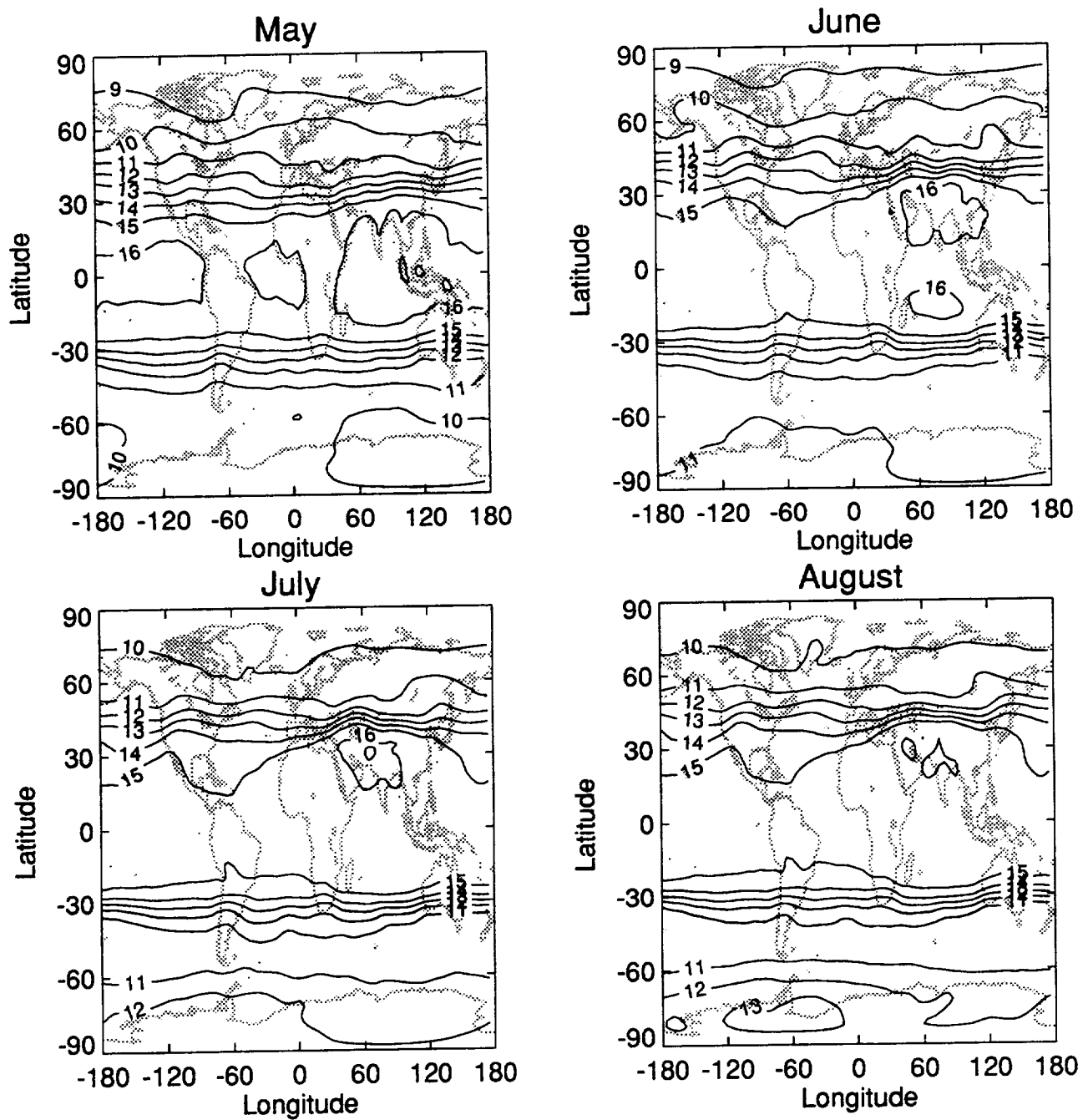


Figure 3-5 (cont). Monthly average tropopause heights in kilometers for the time period 1983-93.

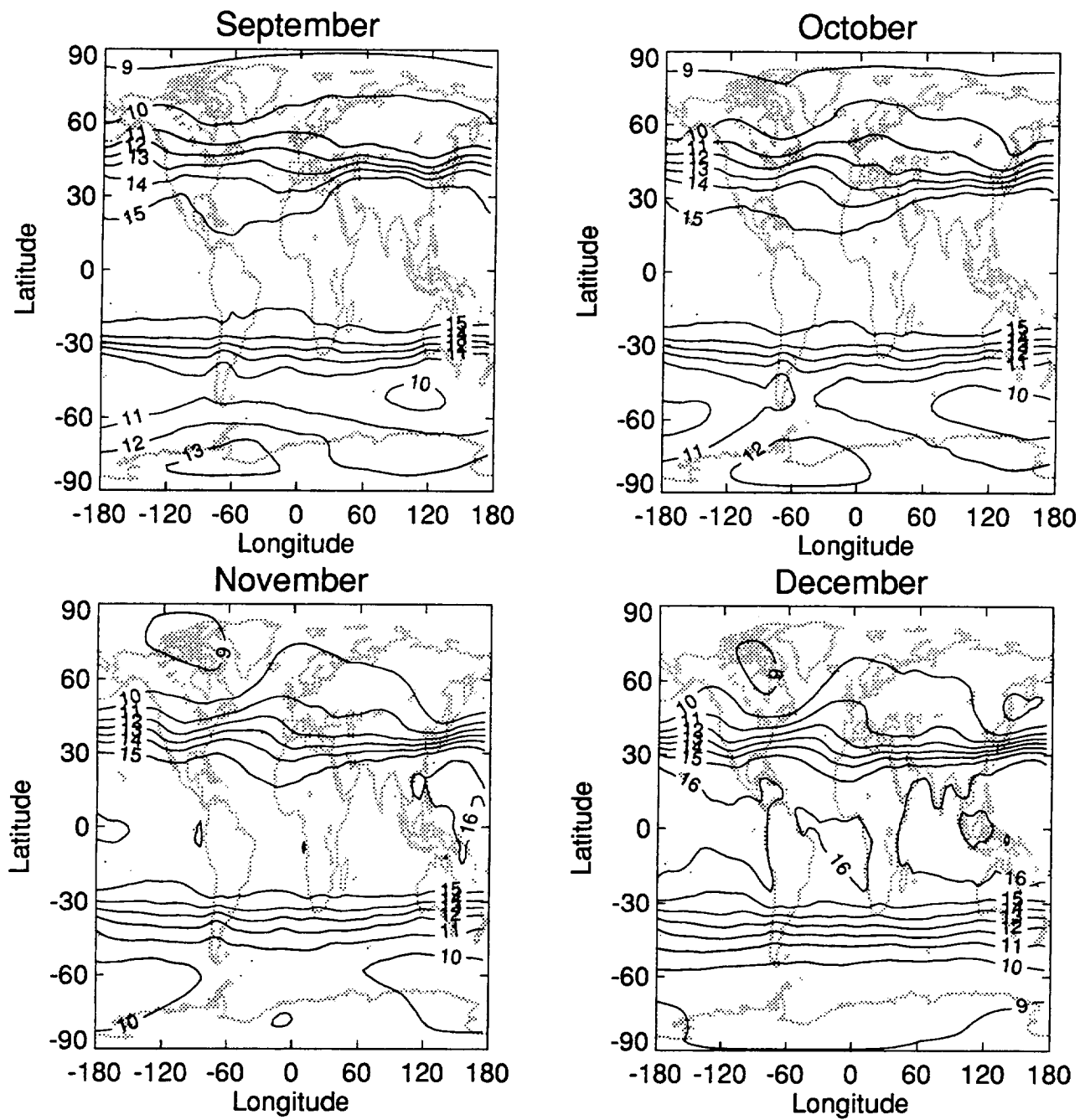


Figure 3-5 (cont.). Monthly average tropopause heights in kilometers for the time period 1983-93.

3.2 Analysis of Emissions above the Tropopause

The subsonic aircraft emission inventories have been previously reported using May 1990 as representative of the annual average. These inventories consist of scheduled air traffic (jet airliners, cargo jets, and turboprops), charter, military, and non-scheduled flights in the former Soviet Union and China. [Wuebbles, et. al., 1993; Baughcum, et. al., 1994; Landau, et. al., 1994]

The geographical distribution of the subsonic emissions is illustrated in Figure 3-6. Air traffic occurs over much of the Northern Hemisphere with cruise altitudes in the 9-13 kilometer altitude. These cruise altitudes are near the tropopause.

To analyze the aircraft emissions in the stratosphere, the 1° latitude \times 1° longitude \times 1 kilometer altitude aircraft emission inventories were interpolated onto the 2° latitude \times 5° longitude NMC grid. The emission inventories are reported on an altitude grid corresponding to the US Standard Atmosphere geopotential altitudes. Each day of tropopause height data was read (in units of mb) and converted to geopotential altitudes using US Standard Atmosphere altitude profiles. Since flight altitudes are pressure-based coordinates, this conversion is only necessary for interpolations near the tropopause. Then, for each latitude \times longitude grid point, the altitude bin containing the tropopause was identified. The emissions (fuel burned, NOx, CO, and HC [hydrocarbons]) in the stratosphere were then calculated by summing emissions at altitudes above the tropopause height, linearly interpolating within the altitude bin containing the tropopause.

Since subsonic aircraft frequently fly at altitudes close to the tropopause, studies were also conducted to evaluate the amount emissions occurring within a specified delta of the tropopause height. This allows one to evaluate how the result might change with alterations of the aircraft cruise altitudes or conversely how sensitive the result is to the exact location of the tropopause.

Figure 3-7 shows the fraction of aircraft emissions (fuel burned, NOx, CO, and hydrocarbons) injected into the stratosphere, using the meteorology of 1990 and the aircraft emission inventory for scheduled air traffic. As the figure shows, there is a strong seasonal variation with the minimum in the summer and the maximum in the winter. The annual average fraction of emissions above the tropopause is shown in the upper right corner of Figure 3-7. Approximately 16-17% of the fuel burned and NOx are calculated to be above the tropopause, with 8% of the hydrocarbons and 10% of the carbon monoxide in the stratosphere. The smaller fraction for CO and hydrocarbons arises because a larger fraction of these emissions occur at lower altitudes (e.g., 62-68% of the CO and hydrocarbon emissions from commercial aircraft are calculated to be below 9 km altitude).

The global fuel use calculated for scheduled air traffic was 9.3×10^{10} kg/year. Emissions of water vapor and sulfur compounds to the stratosphere

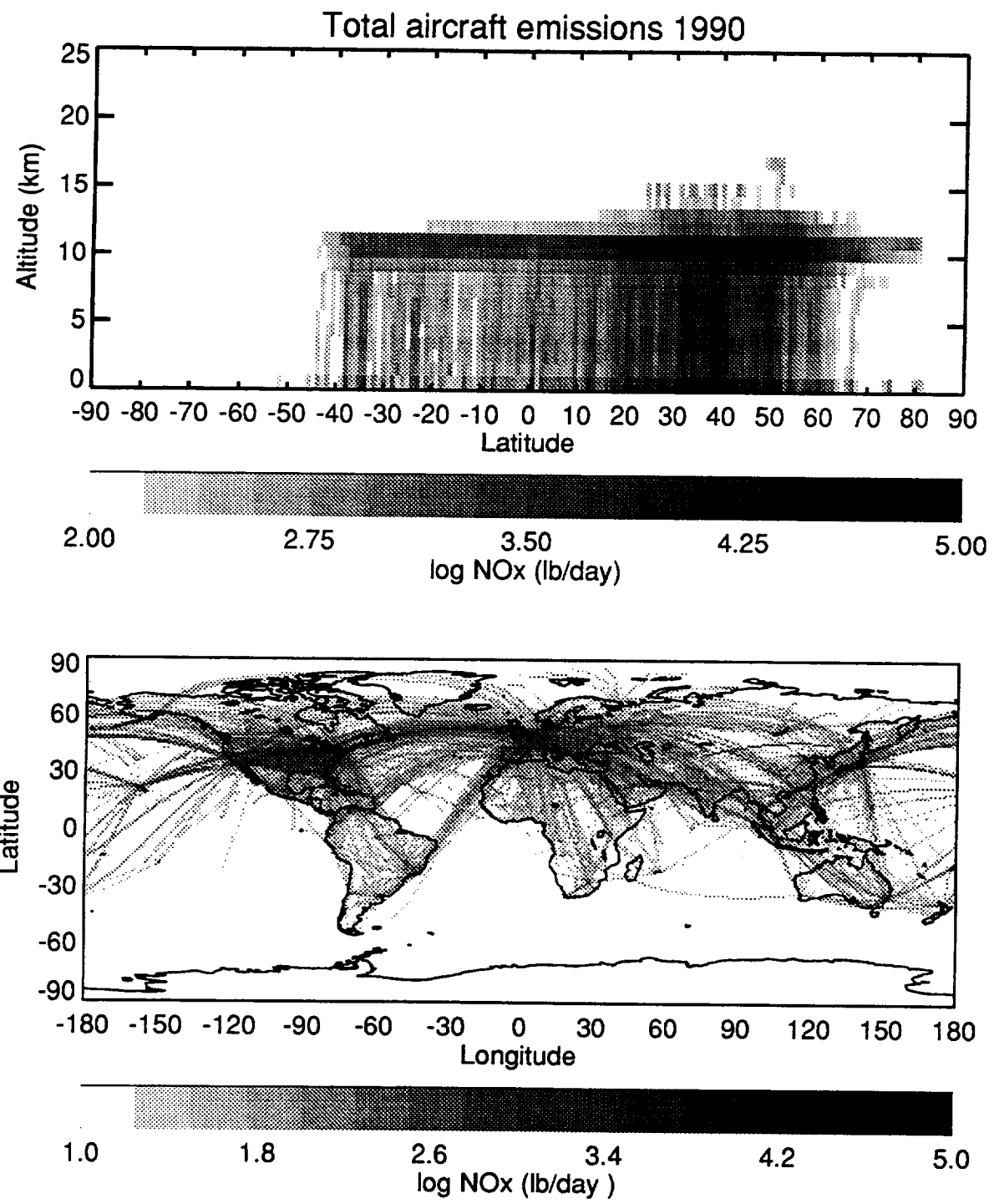


Figure 3-6. NO_x emissions for all 1990 aircraft traffic as a function of altitude and latitude (summed over longitude) (top panel) and as a function of latitude and longitude (summed over altitude) (bottom panel)

Emissions Deposited in Stratosphere
1990 Scheduled Air Traffic; 1990 Meteorology

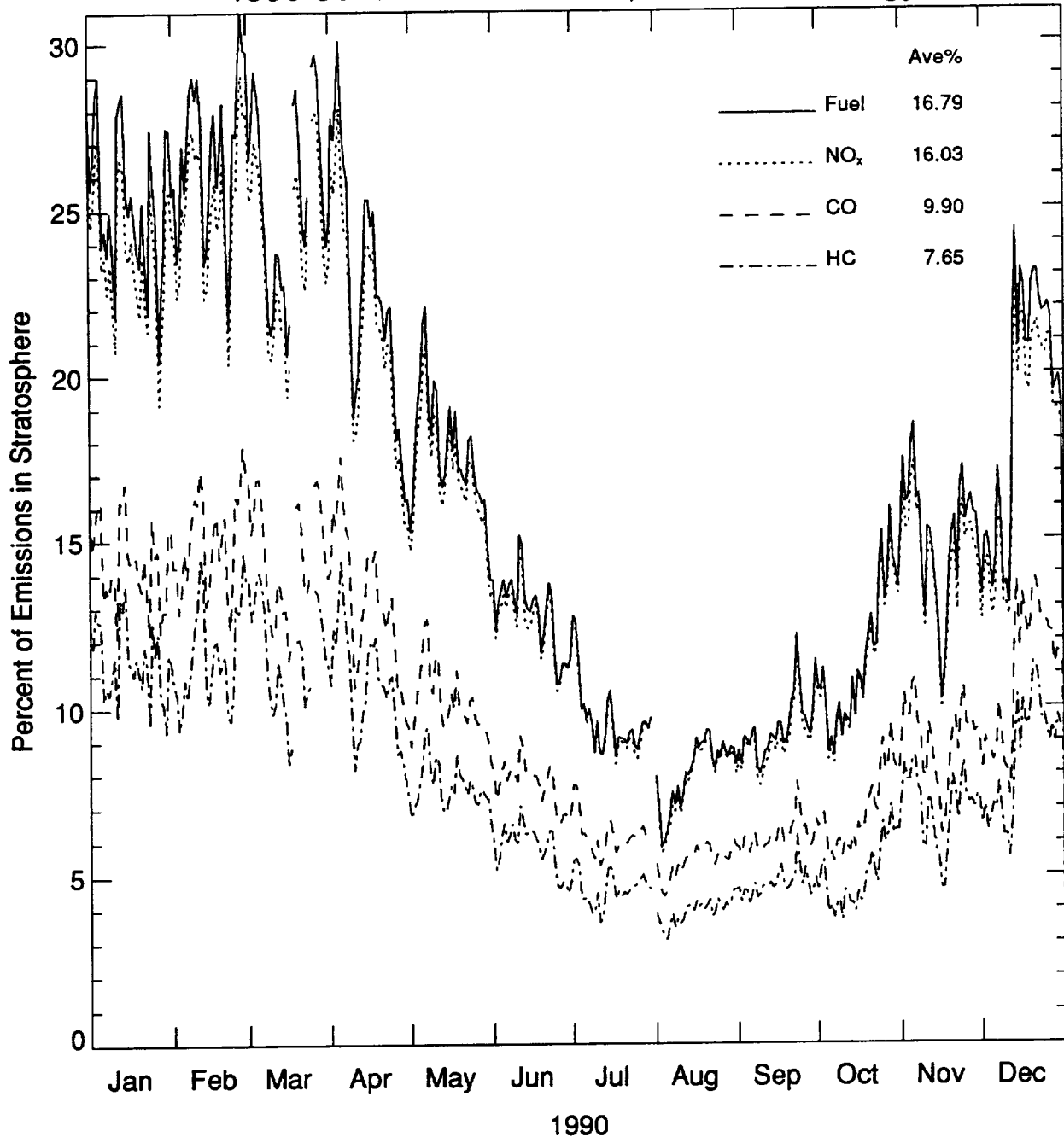


Figure 3-7. Fraction of emissions (fuel burned, NO_x, CO, and hydrocarbons) deposited in the stratosphere globally from scheduled air traffic in 1990, based on air traffic data for May 1990. This analysis used the daily tropopause heights for 1990.

can be calculated using a water emission index of 1237 g/kg fuel burned and a sulfur emission index of 0.8 g (as SO₂)/kg fuel burned.

For the analyses presented here, we examine the sensitivity using an "annual average" emission inventory represented by May 1990. Recent studies have shown that the emissions vary significantly with season as well [Baughcum, et. al, 1996]. The amplitude of the seasonal modulation varies for different geographical regions but peaks in the summer and has a minimum in the winter. More realistic calculations are in progress but are beyond the scope of this report.

To evaluate the sensitivity to the meteorology of one year versus another, Figures 3-8 and 3-9 show the same analysis using the meteorology of 1989 and 1991, respectively. Although there are large day-to-day variations, the annual average (shown in the upper right corner of the figures) is very close to that obtained using the 1990 NMC data.

Figure 3-10 shows a similar analysis, using the total 1990 emission inventory and the meteorology of 1990. The fraction emitted into the stratosphere (see the upper right corner of Figure 3-10) is quite similar to the results for the scheduled aircraft for the fuel burned and NOx but the fraction of CO and hydrocarbon (HC) emissions are much higher. The calculated hydrocarbon and carbon monoxide emission indices used for military aircraft at cruise altitudes were much higher than for commercial aircraft [see Landau, et. al., 1994 for a description of the military scenarios]. Analysis of the component (scheduled, charter, military, and former Soviet Union) emission inventories indicates that the military contribution (relative to the total) for CO and hydrocarbon emissions at cruise altitudes is greater than for fuel burned and NOx. The total global fuel use calculated for 1990 in the aircraft emission inventories was 1.34×10^{11} kg/year [Wuebbles, et. al., 1993].

A larger fraction of the emissions will be in the stratosphere for some geographical regions. This is illustrated in Figure 3-11 where the results are shown for flights occurring in the North Atlantic. In that case, the fractions of fuel burned, NOx, carbon monoxide and hydrocarbons (shown in the lower left corner of Figure 3-11) are all very similar since aircraft are flying at cruise with no takeoffs or landings. Approximately 65% of the emissions are calculated to be in the stratosphere, with large day-to-day variability. By comparison, an earlier study by Hoinka and co-workers (1993) concluded that 44% of the NOx emissions in the North Atlantic were in the stratosphere. Whether the difference in the results between the two studies is due to the flight altitudes that they assumed or in the source of their tropopause data is not clear. The Hoinka study used a dynamical definition of the tropopause, rather than the thermal definition.

At cruise altitudes, commercial aircraft are flying in the vicinity of the tropopause. Thus, we might expect that the results will be sensitive to our calculated flight altitudes or to our definitions of the tropopause.

To test the sensitivity of the results to flight altitudes, the emissions occurring within a specified displacement were calculated. These results are shown in Figure 3-12 with the annual averages shown in the upper right corner of Figure 3-12. The delta Z considers a displacement of the tropopause height by that amount. For example, a delta Z of -1 km is equivalent to moving the tropopause height down by 1 km or the flight altitudes up by 1 km.

If the aircraft emissions were 1 kilometer higher, the fraction of fuel burn above the tropopause would increase from 17% to 25%. If they were 1 km lower, the fraction would decrease from 17% to 9%. Sixteen percent of the global fuel burn occurs within +/- 1 kilometers of the tropopause; 29% occurs within +/- 2 kilometers of the tropopause. From this, we conclude that the calculated amount of emissions in the stratosphere will be sensitive to our assumptions about the flight altitudes of individual aircraft and to our definition of the tropopause.

As expected, a similar calculation using the emission inventory for a fleet of 500 Mach 2.4 HSCTs [Baughcum and Henderson, 1995], indicates that most of the fuel use occurs above the tropopause. (see Figure 3-13). Since the HSCT is projected to cruise supersonically at 18-21 km altitudes, well above the tropopause, it is no surprise that relatively little seasonal variation is observed in the result shown in Figure 3-13.

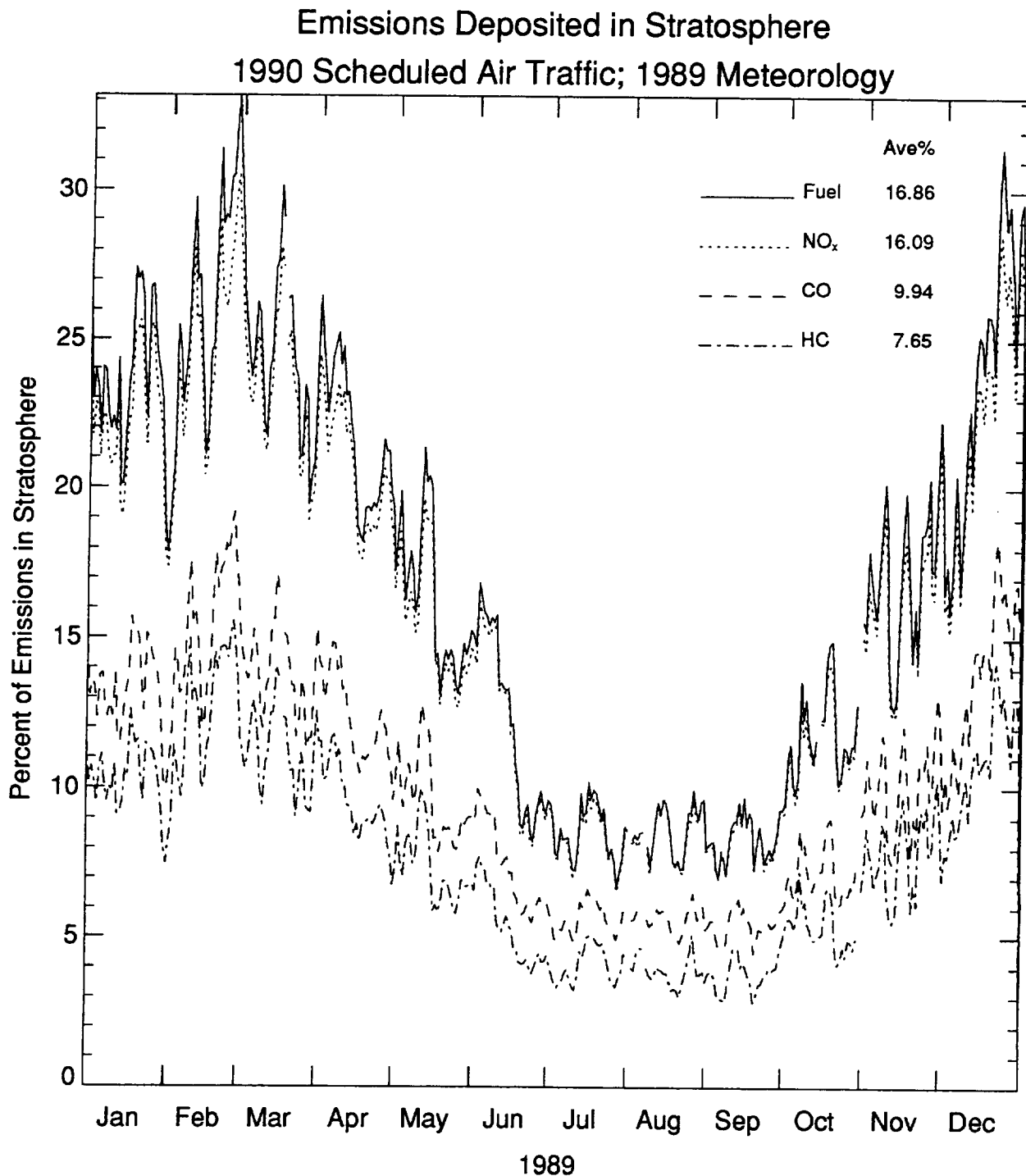


Figure 3-8. Fraction of emissions (fuel burned, NO_x, CO, and hydrocarbons) deposited in the stratosphere globally from scheduled air traffic in 1990, based on air traffic data for May 1990. This analysis used the daily tropopause heights for 1989.

Emissions Deposited in Stratosphere
1990 Scheduled Air Traffic; 1991 Meteorology

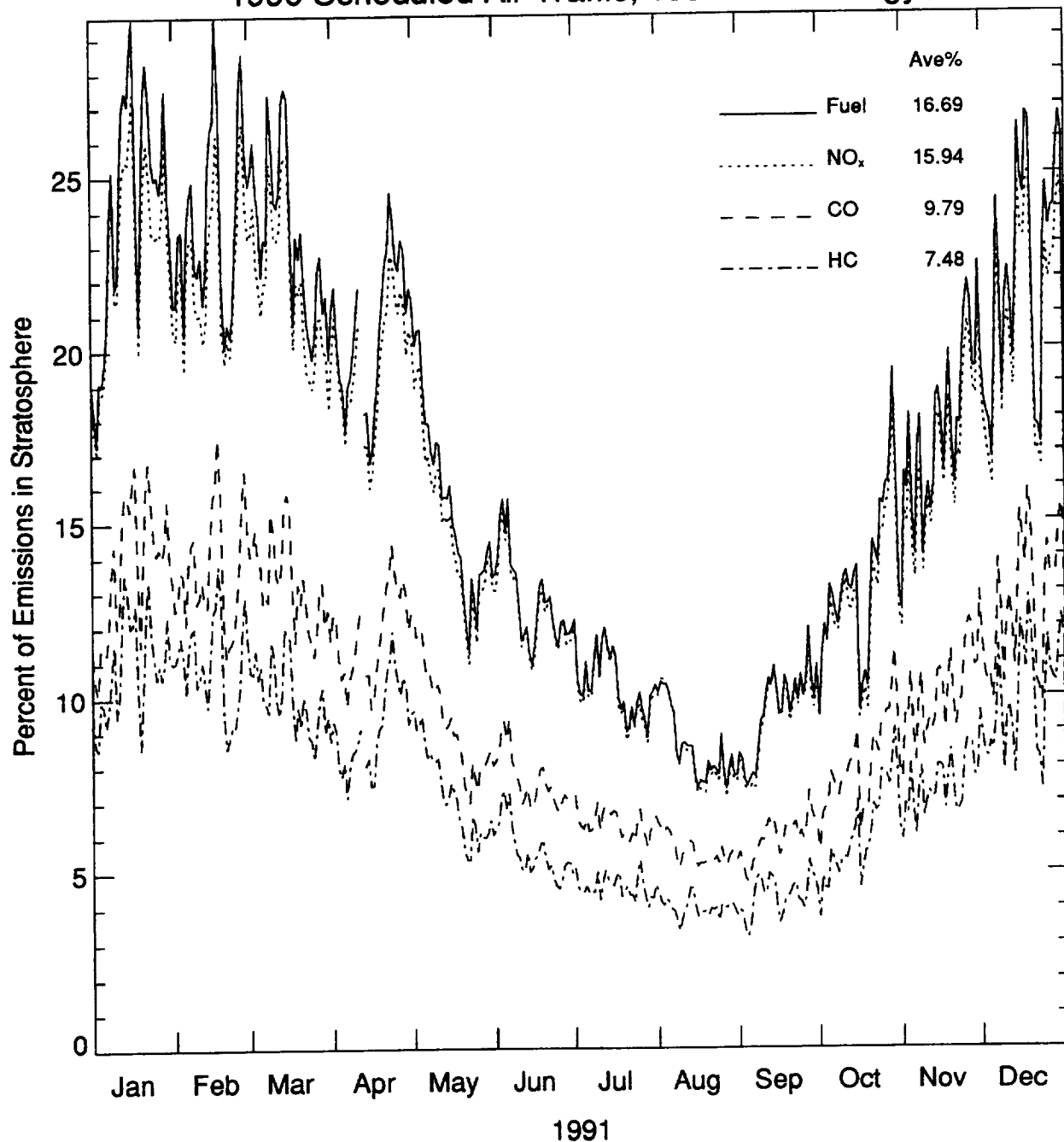


Figure 3-9. Fraction of emissions (fuel burned, NO_x, CO, and hydrocarbons) deposited in the stratosphere globally from scheduled air traffic in 1990, based on air traffic data for May 1990. This analysis used the daily tropopause heights for 1991.

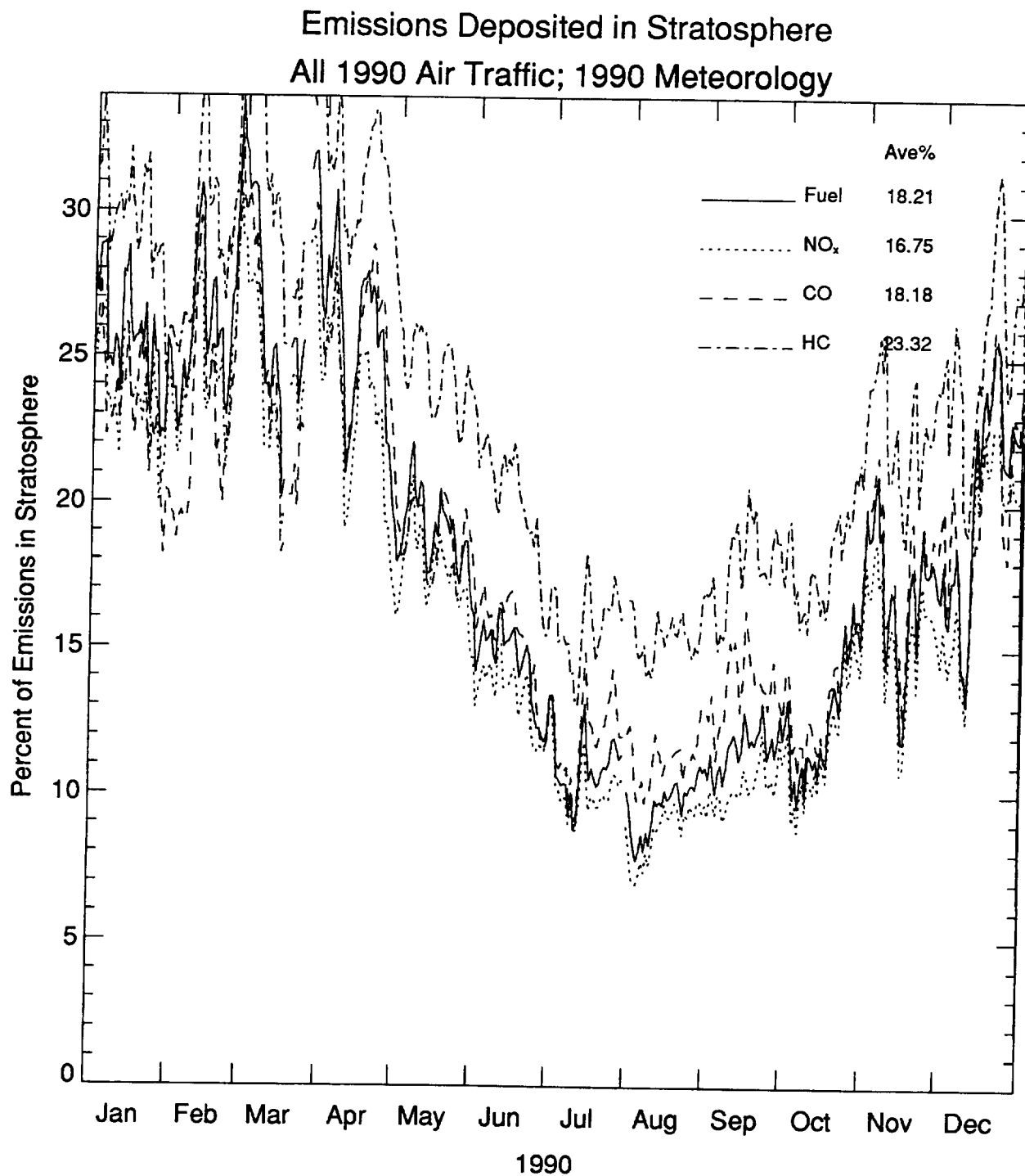


Figure 3-10. Fraction of emissions (fuel burned, NO_x, CO, and hydrocarbons) deposited in the stratosphere globally from all air traffic in 1990, based on air traffic data for May 1990. This analysis used the daily tropopause heights for 1990.

Emissions Deposited in Stratosphere
1990 Scheduled Air Traffic in North Atlantic; 1990 Meteorology

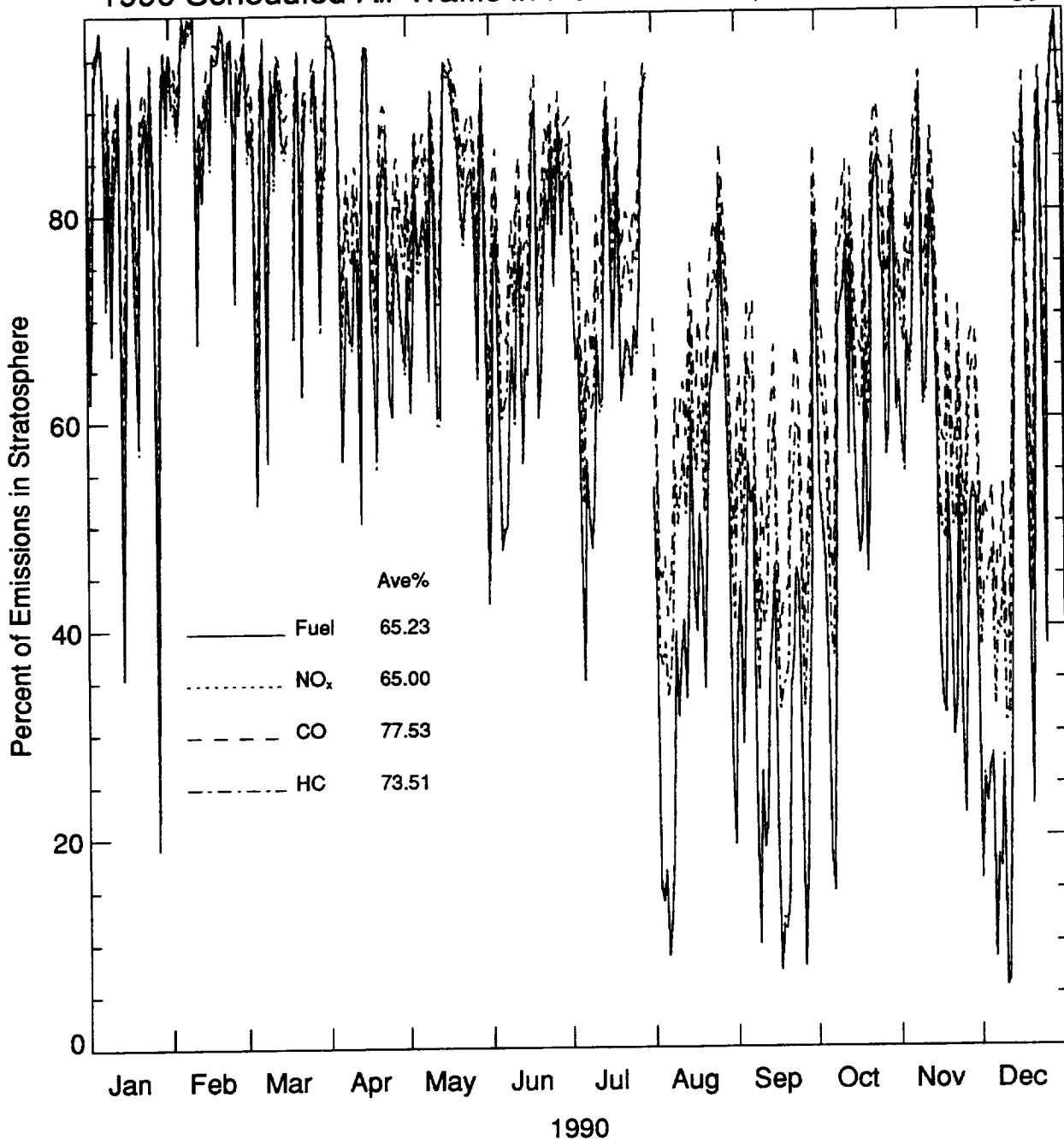


Figure 3-11. Fraction of emissions (fuel burned, NO_x, CO, and hydrocarbons) deposited in the stratosphere in the North Atlantic from scheduled air traffic in 1990, based on air traffic data for May 1990. This analysis used the daily tropopause heights for 1990.

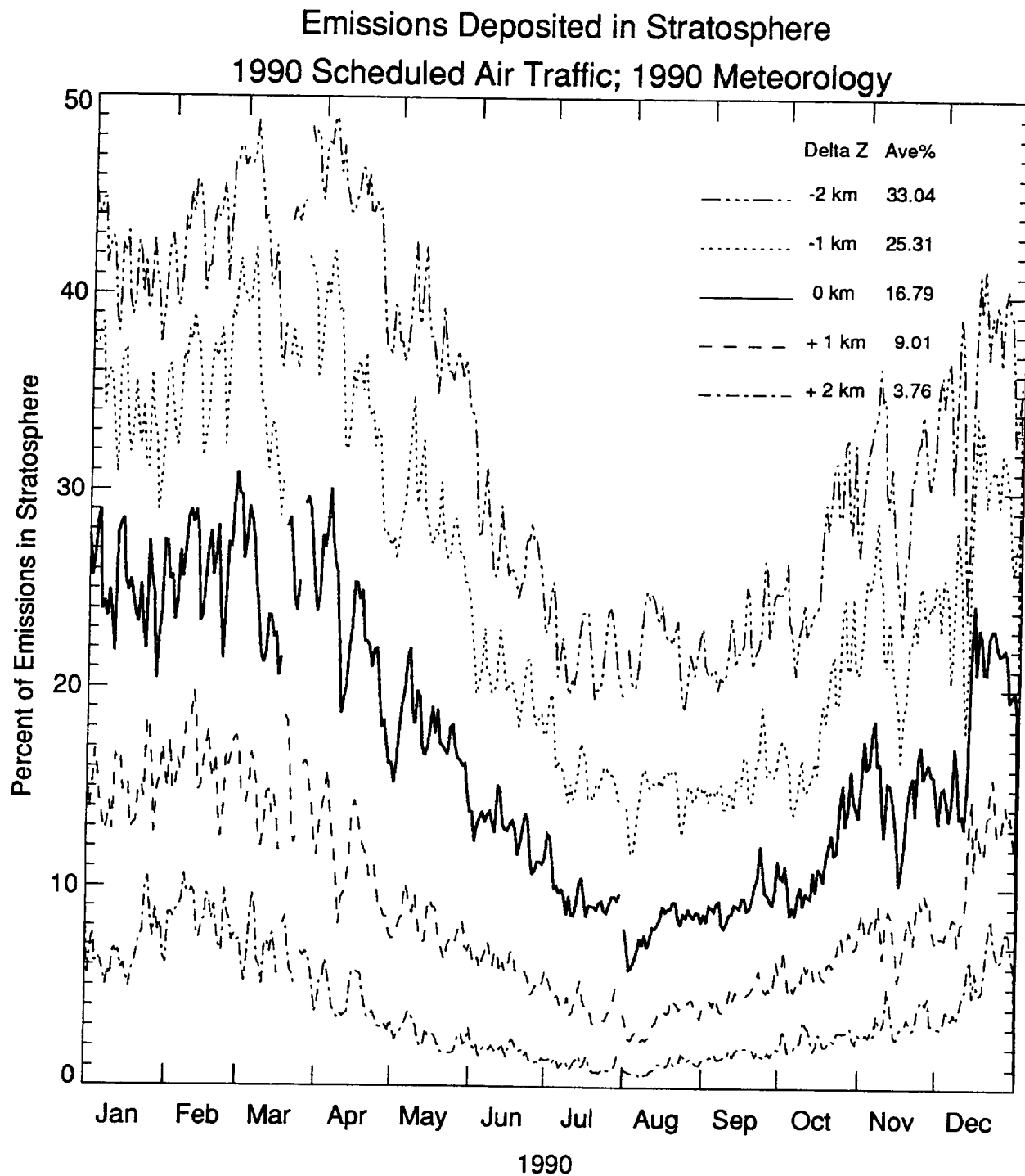


Figure 3-12. Sensitivity of amount of fuel use in the stratosphere globally to the aircraft flight altitudes for scheduled air traffic in 1990 using May 1990 as representative.

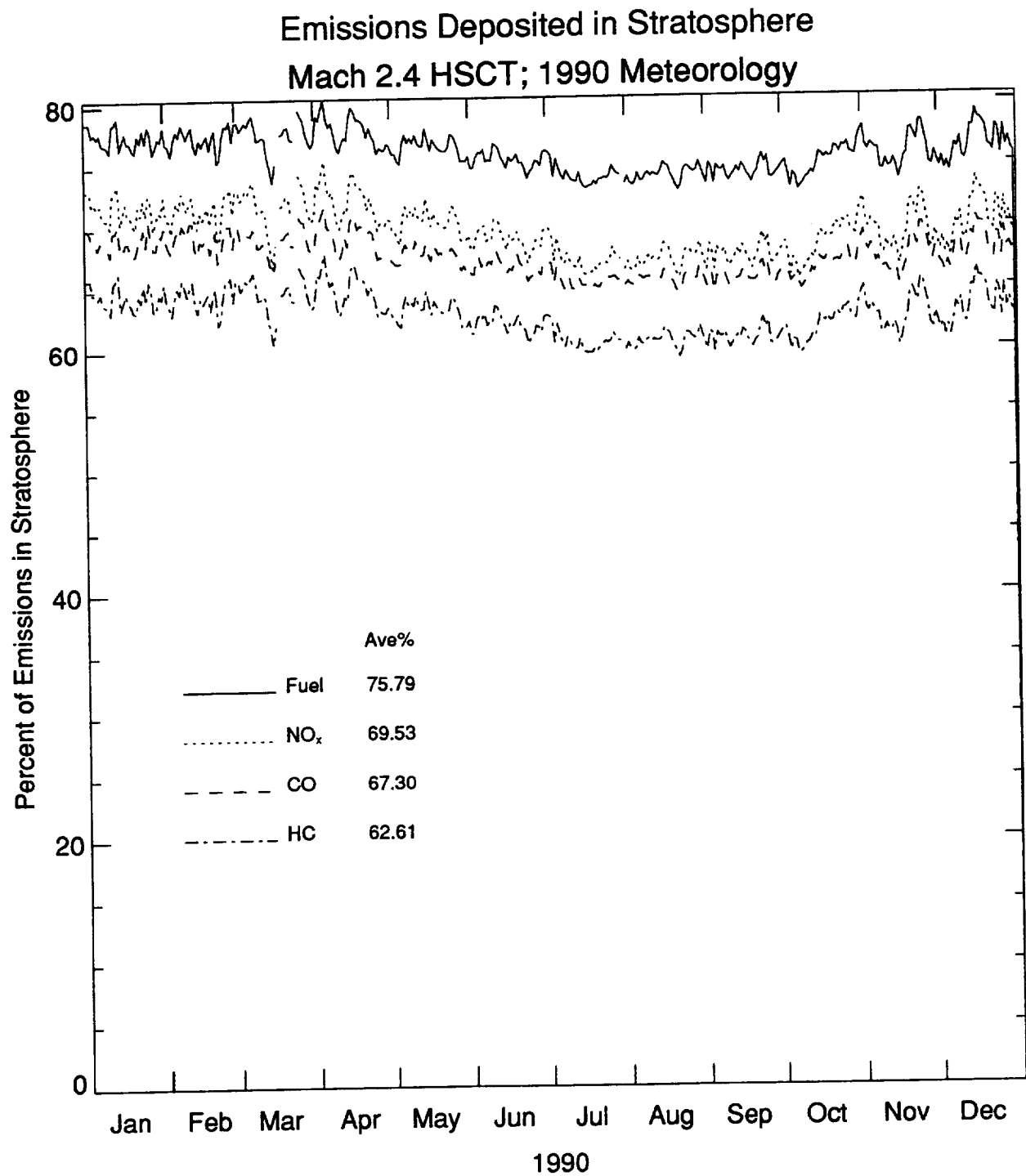


Figure 3-13. Fraction of emissions (fuel burned, NO_x, CO, and hydrocarbons) deposited in the stratosphere globally from a fleet of 500 Mach 2.4 HSCTs. This analysis used the daily tropopause heights for 1990.

3.3 Conclusions

This preliminary analysis based on one month of aircraft emissions data shows that approximately 17% of the global fuel burned by the subsonic fleet may occur in the stratosphere. This would correspond to about 2.0×10^{10} kg/year of water emissions and 2.5×10^8 kg/year of NOx into the lower stratosphere due to aircraft. Approximately 16% of the fuel burned occurs within 1 kilometer of the tropopause and 29% occurs within 2 kilometers of the tropopause. The results for NOx emissions are similar. This indicates that the amount of emissions calculated to occur in the lower stratosphere will be sensitive to both the definition (dynamical versus static) of the tropopause and the assumed flight altitudes of the aircraft.

A larger fraction of the emissions will be in the stratosphere for some geographical regions. The tropopause height varies with geographical location, being highest in the tropics. In some regions (e.g., the North Atlantic or North Pacific), aircraft are primarily at cruise altitudes and thus a larger fraction of their emissions will be above the tropopause than for regions which include landing/takeoff operations.

Emissions from air traffic are highest in the summer and lowest in the winter. The tropopause is highest in the summer and lowest in the winter. Since both air traffic and tropopause heights are seasonally dependent, a more detailed analysis is required to provide a reliable answer to the question of how much water vapor and NOx is emitted to the stratosphere from the subsonic fleet. Such an analysis is now been conducted using the tropopause height data described here and monthly aircraft emission inventories that have recently been developed [Baughcum, et. al., 1996a]. The results of that study will be reported in the future.

4. References

- Albritton, D. L., W. H. Brune, A. R. Douglass, F. L. Dryer, M. K. W. Ko, C. E. Kolb, R. C. Miake-Lye, M. J. Prather, A. R. Ravishankara, R. B. Rood, R. S. Stolarski, R. T. Watson, and D. J. Wuebbles, *The Atmospheric Effects of Stratospheric Aircraft: Interim Assessment Report of the NASA High-Speed Research Program*, NASA Reference Publication 1333, 1993.
- Baughcum, S. L., S. C. Henderson, P. S. Hertel, D. R. Maggiora, and C. A. Oncina, *Stratospheric Emissions Effects Database Development*, NASA CR-4592, 1994.
- Baughcum, S. L., and S. C. Henderson, *Aircraft Emission Inventories Projected in Year 2015 for a High Speed Civil Transport (HSCT) Universal Airline Network*, NASA CR-4659, 1995.
- Baughcum, S. L., T. G. Tritz, S. C. Henderson, and D. C. Pickett, *Scheduled Civil Aircraft Emission Inventories for 1992: Database Development and Analysis*, NASA CR-4700, 1996.
- Baughcum, S. L., S. C. Henderson, and T. G. Tritz, *Scheduled Civil Aircraft Emission Inventories for 1976 and 1984: Database Development and Analysis*, NASA CR-4722, 1996.
- Cressman, G. P., "An Operational Objective Analysis System", *Monthly Weather Review*, **87**, pp. 367-374 (1959).
- Finger, F. G., H. M. Woolf, and C. E. Anderson, "A Method for Objective Analysis of Stratospheric Constant- Pressure Charts, *Monthly Weather Review*, **93**, pp. 619-638 (1965).
- Gelman, M., et. al., "Detection of Long-Term Trends in Global Stratospheric Temperature from NMC Analyses Derived from NOAA Satellite Data," *Adv. Space Res.* **6**, pp. 17-25, 1986.
- Hoinka, K. P., M. E. Reinhardt, and W. Metz, "North Atlantic Air Traffic within the Lower Stratosphere: Cruising Times and Corresponding Emissions", *J. Geophys. Res.*, **98**, pp. 23,113-23,131 (1993).
- Kawa, S. R., D. W. Fahey, L. C. Anderson, M. Loewenstein, and K. R. Chan, "Measurements of Total Reactive Nitrogen during the Airborne Arctic Stratospheric Expedition", *Geophys. Res. Lett.*, **17**, pp. 485-488 (1990).
- Kelly, K. K., A. F. Tuck, L. E. Heidt, M. Loewenstein, J. R. Podolske, S. E. Strahan, and J. F. Vedder, "A Comparison of ER-2 Measurements of Stratospheric Water Vapor Between the 1987 Antarctic and 1989 Arctic Airborne Missions," *Geophys. Res. Lett.*, **17**, pp. 465-468 (1990).

Landau, Z. H., M. Metwally, R. Van Alstyne, and C. A. Ward, "Jet Aircraft Engine Exhaust Emissions Database Development -- Year 1990 and 2015 Scenarios," NASA CR-4613, 1994.

Metwally, M., *Jet Aircraft Engine Emissions Database Development--1992 Military, Charter, and Nonscheduled Traffic*, NASA CR-4684, 1995.

Nagatani, R. M., et. al., "An Eight Year Climatology of Meteorological and SBUV Ozone Data, NOAA Tech. Report, NWS 40, pp. 1-125, 1988.

Nagatani, R. M., A. J. Miller, M. E. Gelman, and P. A. Newman, "A Comparison of Arctic Lower Stratospheric Winter Temperatures for 1988-89 with Temperatures since 1964", *Geophys. Res. Lett.* **17**, 333-336, 1990.

Nash, E. R., P. A. Newman, J. E. Rosenfield, and M. R. Schoeberl, "An Objective Determination of the Polar Vortex using Ertel's Potential Vorticity", *J. Geophys. Res.*, in press, 1996.

Newman, P. A., D. J. Lamich, M. Gelman, M. R. Schoeberl, W. Baker and A. J. Krueger, *Meteorological Atlas of the Southern Hemisphere Lower Stratosphere for August and September 1987*, NASA Technical Memorandum 4049, pp. 1-131, 1988.

Newman, P. A., L. R. Lait, M. R. Schoeberl, R. M. Nagatani, and A. J. Krueger, *Meteorological Atlas of the Northern Hemisphere Lower Stratosphere for January and February 1989 During the Airborne Arctic Stratospheric Expedition*, NASA Technical Memorandum 4145, pp. 1-185, 1989.

Newman, P. A. L. R. Lait, M. R. Schoeberl, and R. M. Nagatani, "Stratospheric Temperatures during the 88-89 Northern Hemisphere Winter, *Geophys. Res. Lett.* **17**, 329-332, 1990.

Newman, P. A., L. Lait, M. Schoeberl, E. Nash, K. Kelly, D. W. Fahey, R. Nagatani, D. Toohey, J. Anderson, and L. Avallone, AASE II Stratospheric Meteorological Conditions, *Science*, **261**, 1143-1145, 1993.

Peter, Th., C. Bruhl, and P. J. Crutzen, "Increase in the PSC-Formation Probability Caused by High-Flying Aircraft," *Geophys. Res. Lett.* **18**, 1465-1468, 1991.

Randel, W. J., "Global Atmospheric Circulation Statistics, 1000-1 mb", NCAR technical note, NCAR/TN-295+STR, pp. 1-245, 1987.

Schoeberl, M. R. and D. L. Hartmann, "The Dynamics of the Stratospheric Polar Vortex and its Relation to Springtime Ozone Depletions", *Science*, **251**, pp. 46-52 ,1991.

Schoeberl, M. R. , L. R. Lait, P. A. Newman, and J. E. Rosenfield, "The Structure of the Polar Vortex," *J. Geophys. Res.* **97**, pp. 7859-7882, 1992.

Stolarski, R. S., and H. L. Wesoky (eds.), *The Atmospheric Effects of Stratospheric Aircraft: A Third Program Report*, NASA Reference Publication 1313, 1993.

Stolarski, R. S., S. L. Baughcum, W. H. Brune, A. R. Douglass, D. W. Fahey, R. R. Friedl, S. C. Liu, R. A. Plumb, L. R. Poole, H. L. Wesoky, and D. R. Worsnop, *1995 Scientific Assessment of the Atmospheric Effects of Stratospheric Aircraft*, NASA Reference Publication 1381, 1995.

Trenberth, K., and J. Olsen, "Evaluation of NMC Global Analyses: 1979-87, NCAR/TN-299+STR, pp. 1-82, 1988.

WMO, *Scientific Assessment of Ozone Depletion: 1994*, WMO Report 37, 1995.

Wu, M., et. al., "Global Atmospheric Circulation Statistics - Four Year Averages," NASA Technical Memorandum 100690, pp. 1-70, 1987.

Wuebbles, D. J., D. Maiden, R. K. Seals, Jr., S. L. Baughcum, M. Metwally, and A. Mortlock, "Emissions Scenarios Development: Report of the Emissions Scenarios Committee," in *The Atmospheric Effects of Stratospheric Aircraft: A Third Program Report*, R. S. Stolarski and H. L. Wesoky, eds., NASA Reference Publication 1313, 1993.

Yanai, M., "An Experimental Objective Analysis in the Tropics," Technical Paper No. 62, Department of Atmospheric Science, Colorado State University, pp. 1-21, 1964.

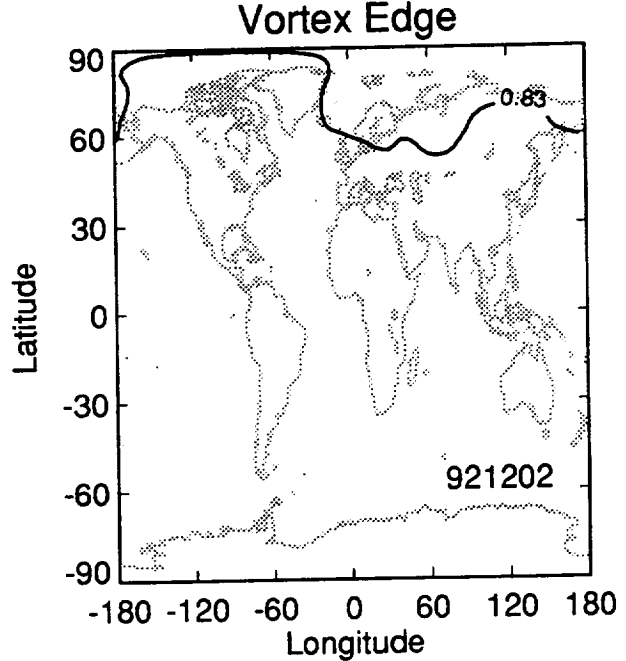
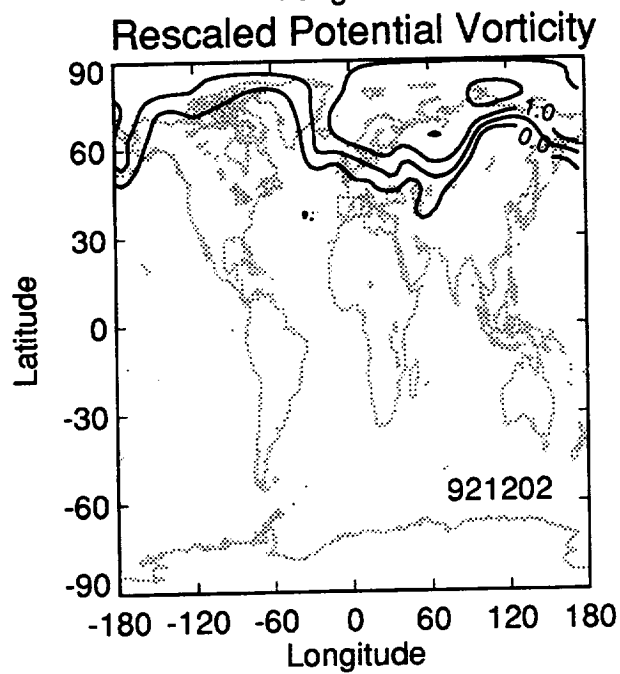
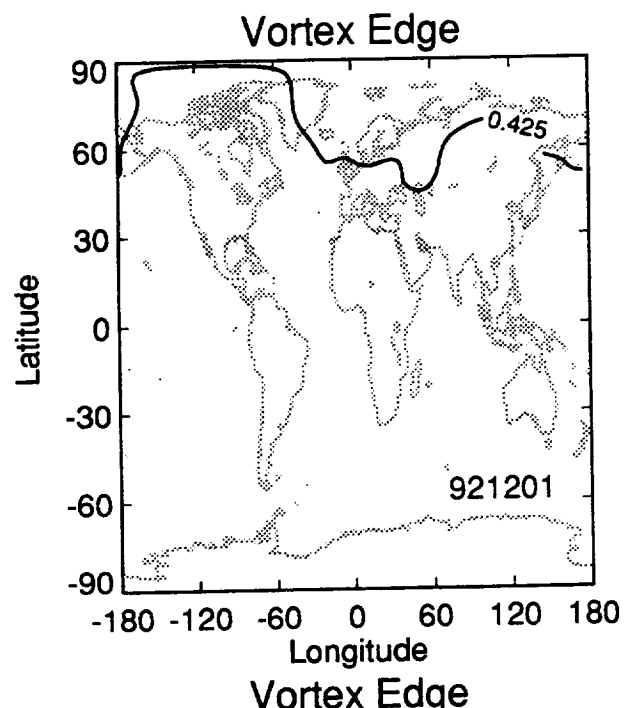
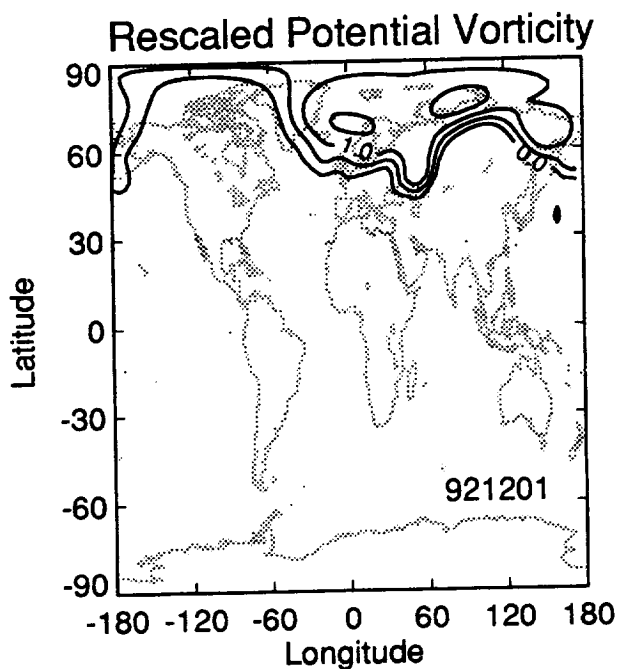
Appendix A. Arctic Polar Vortex, Winter of 1992-93

In this appendix, plots of the polar vortex location are shown for each day for which data were available for the winter of 1992-93. These plots show the results for a typical winter, according to Dr. Paul Newman at NASA Goddard Space Flight Center.

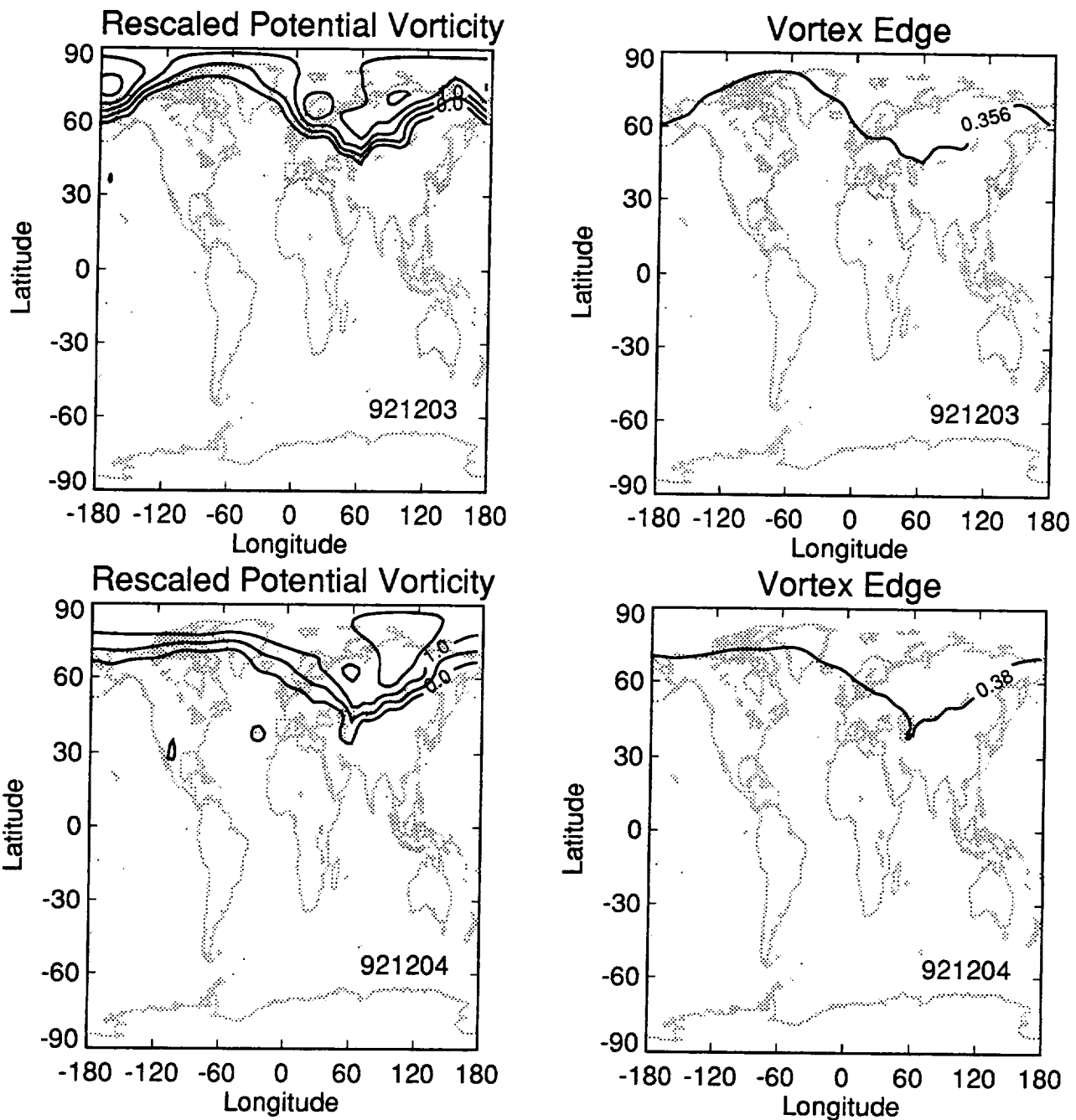
For each day, two contour plots are shown as a function of latitude and longitude. Longitudes are referenced to Greenwich as zero longitude, with positive values east of Greenwich. The plots on the left show the rescaled potential vorticity as discussed in Section 2. Only positive values are plotted; and the zero contour line corresponds to the liberal definition of the vortex as discussed in Section 2. The plots on the right of each page are the vortex edge as calculated using the method of Nash, et. al. (1996).

Each plot is labeled with the date used in the analysis. The date is given as a two digit representation of the year, month, and day (YYMMDD). For example, 921201 is December 1, 1992.

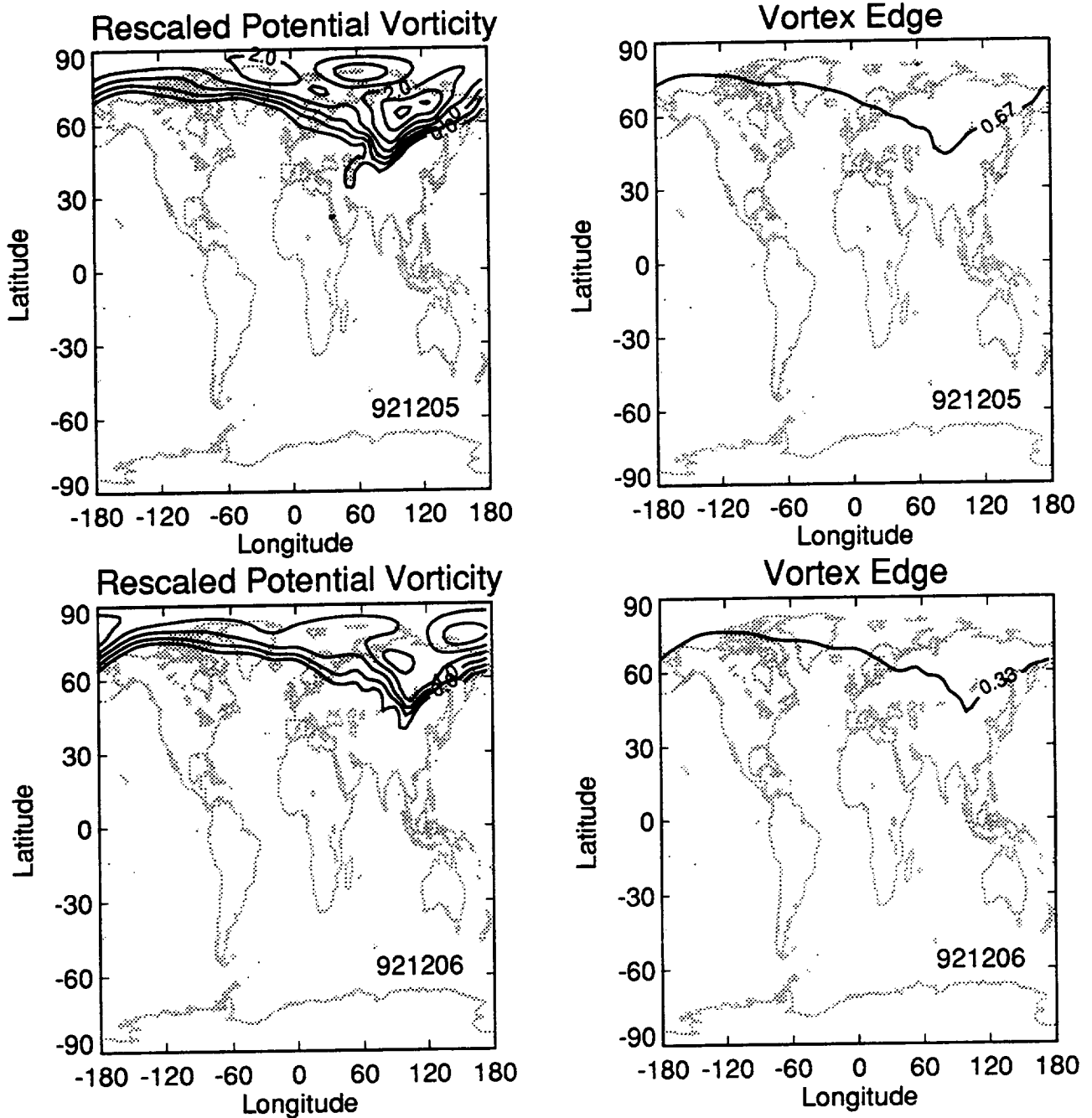
Each page shows the rescaled potential vorticity data for two days. The available data for the winter of 1992-3 begins on December 1, 1992 and extends through February 28, 1993. Some days are missing because data files from NASA Goddard were not available for those days.



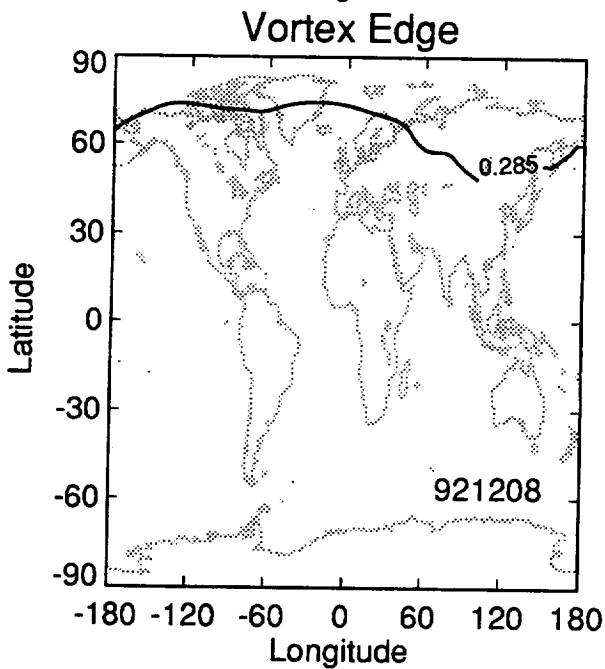
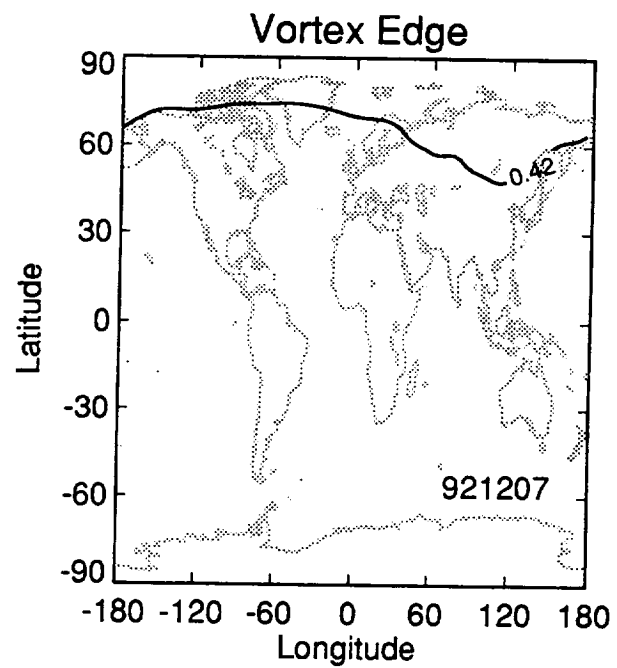
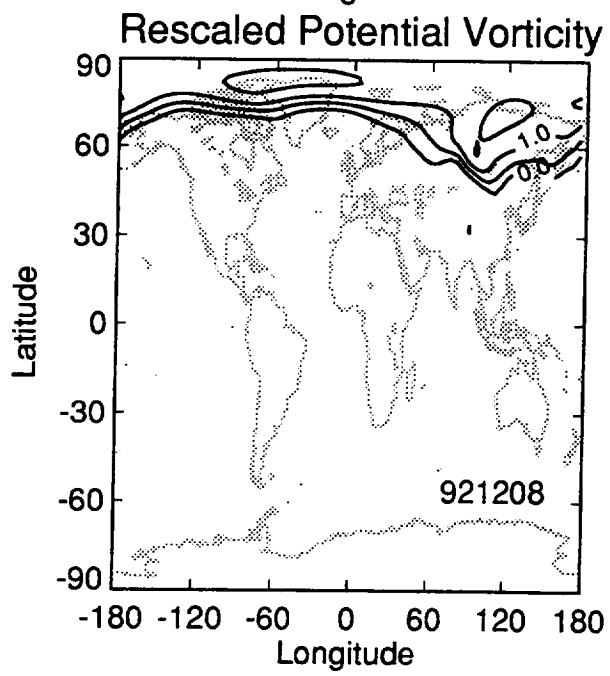
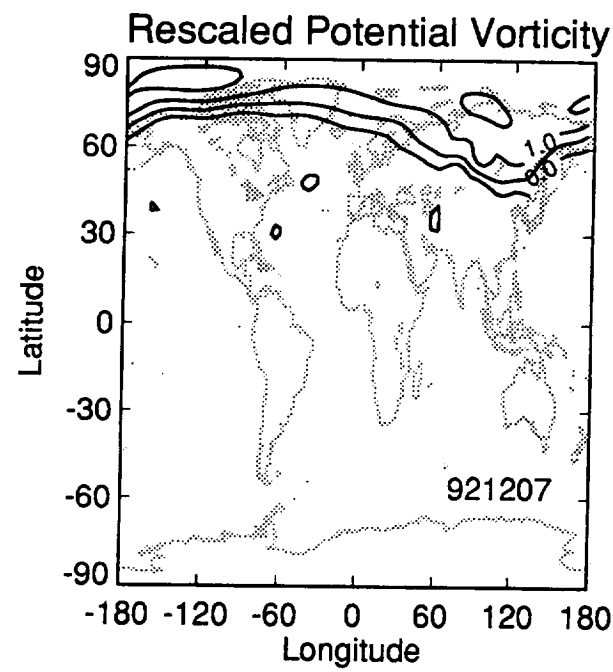
Appendix A. Plots of rescaled potential vorticity and the vortex edge for each day of available data for the winter of 1992-93. Dates are labeled as YYMMDD (year, month, day).



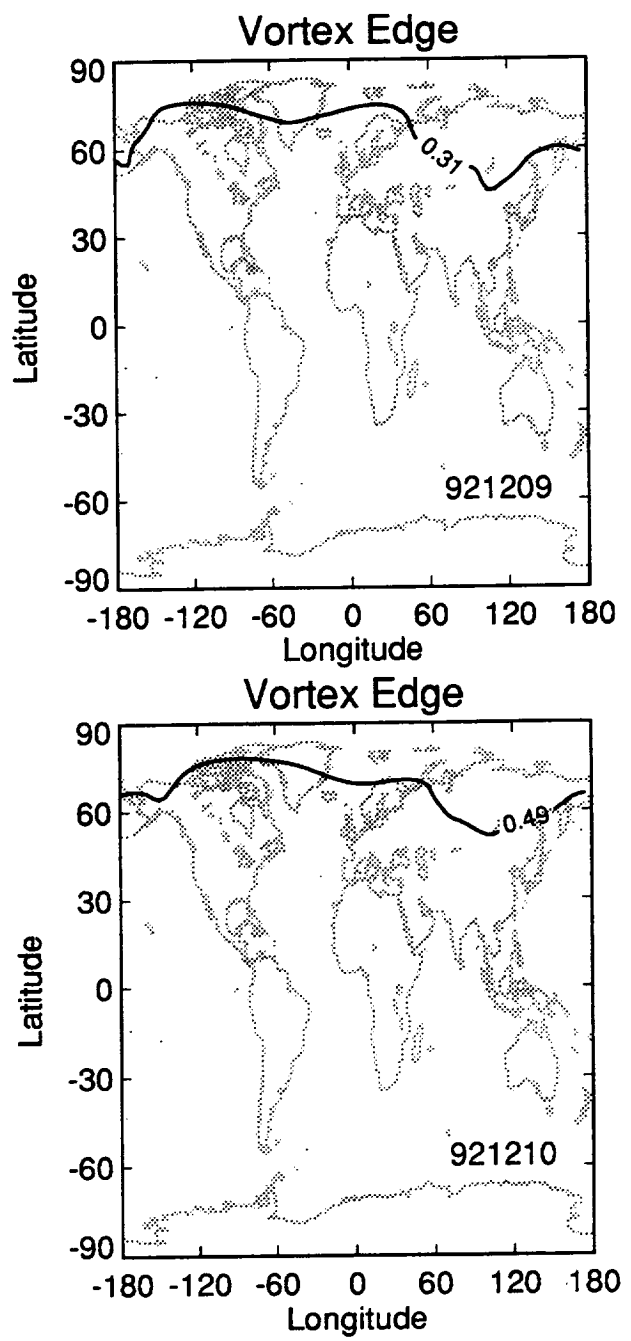
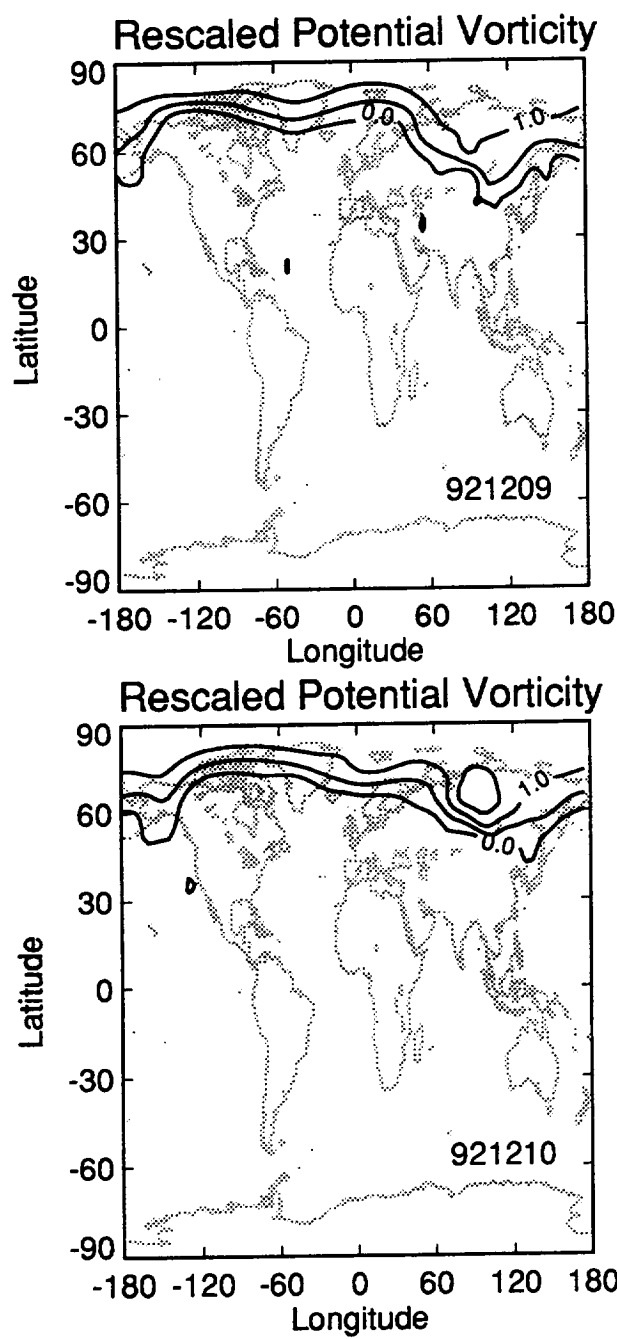
Appendix A. Plots of rescaled potential vorticity and the vortex edge for each day of available data for the winter of 1992-93. Dates are labeled as YYMMDD (year, month, day).



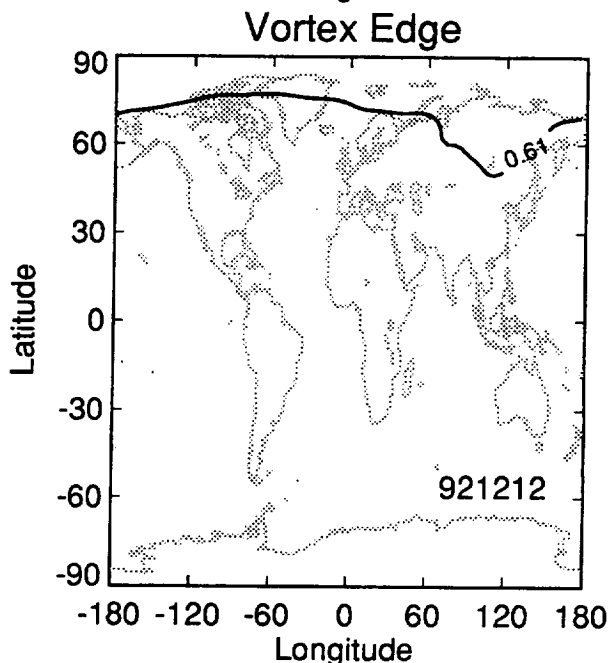
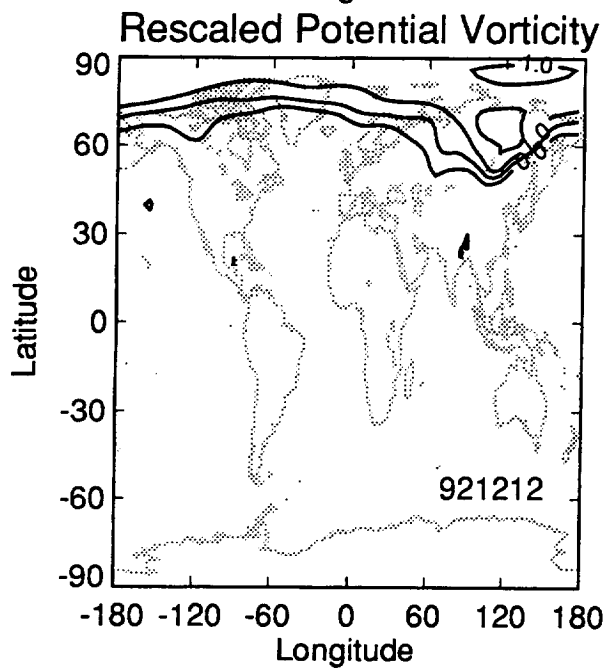
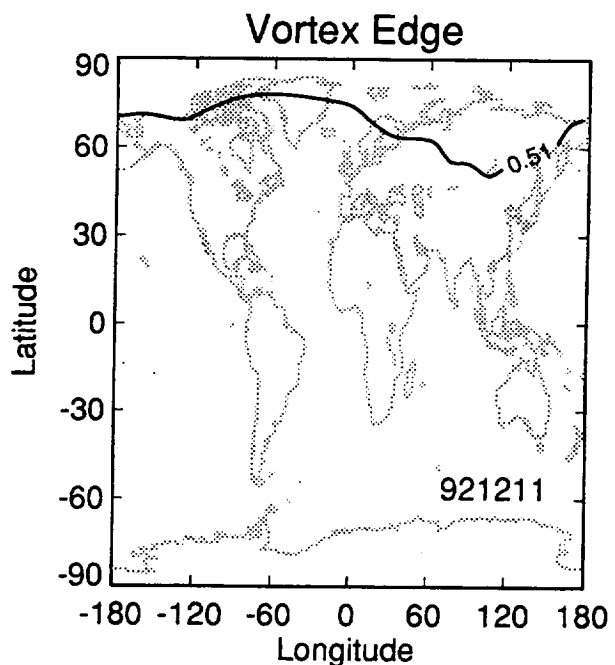
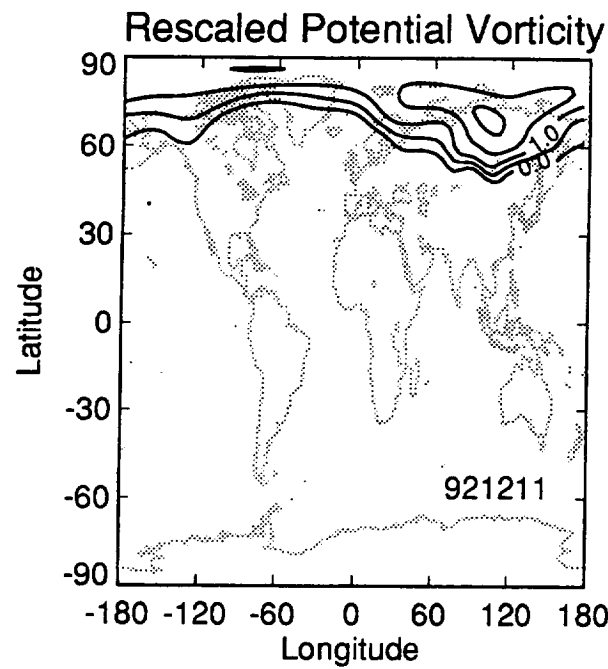
Appendix A. Plots of rescaled potential vorticity and the vortex edge for each day of available data for the winter of 1992-93. Dates are labeled as YYMMDD (year, month, day).



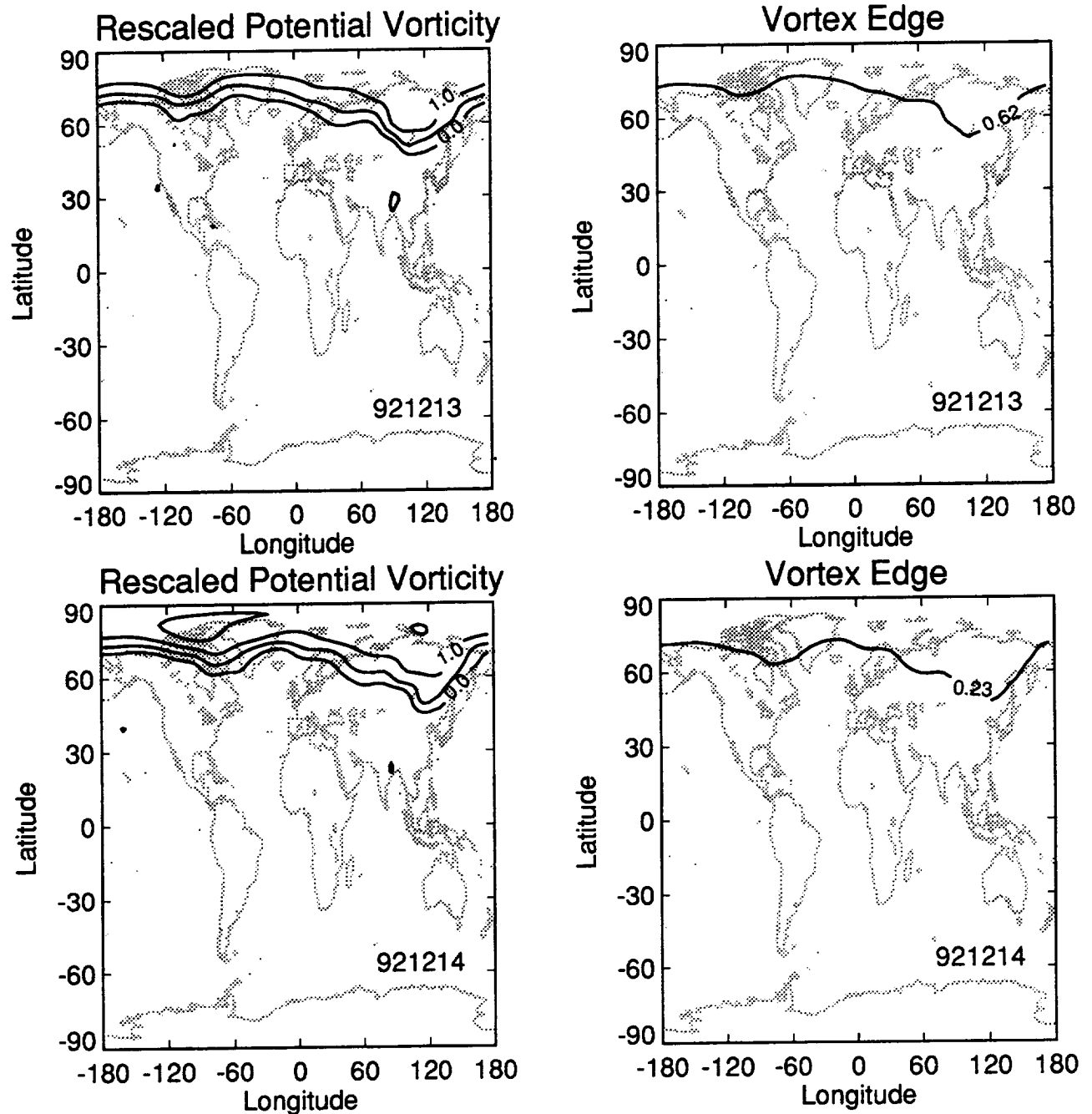
Appendix A. Plots of rescaled potential vorticity and the vortex edge for each day of available data for the winter of 1992-93. Dates are labeled as YYMMDD (year, month, day).



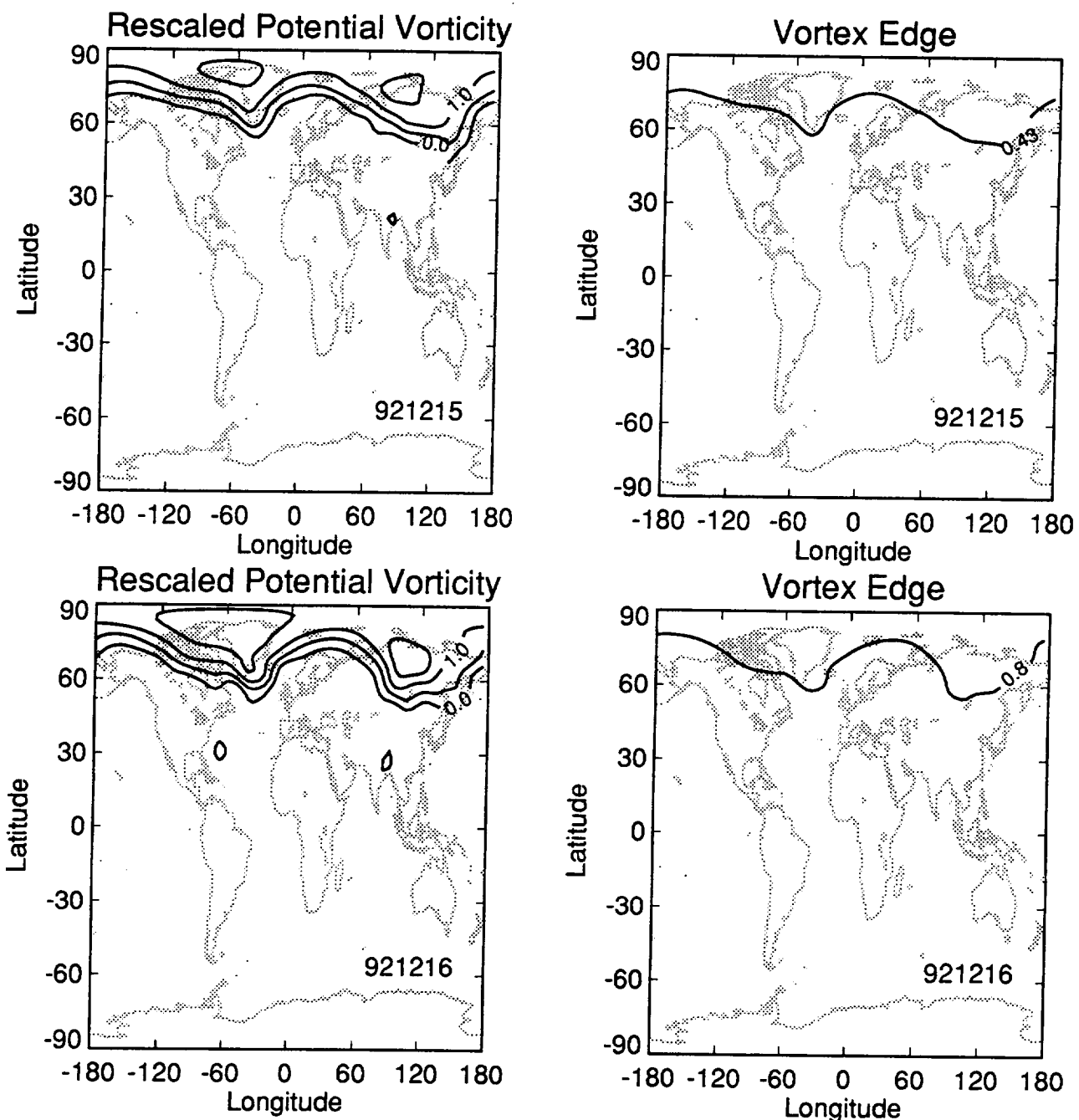
Appendix A. Plots of rescaled potential vorticity and the vortex edge for each day of available data for the winter of 1992-93. Dates are labeled as YYMMDD (year, month, day).



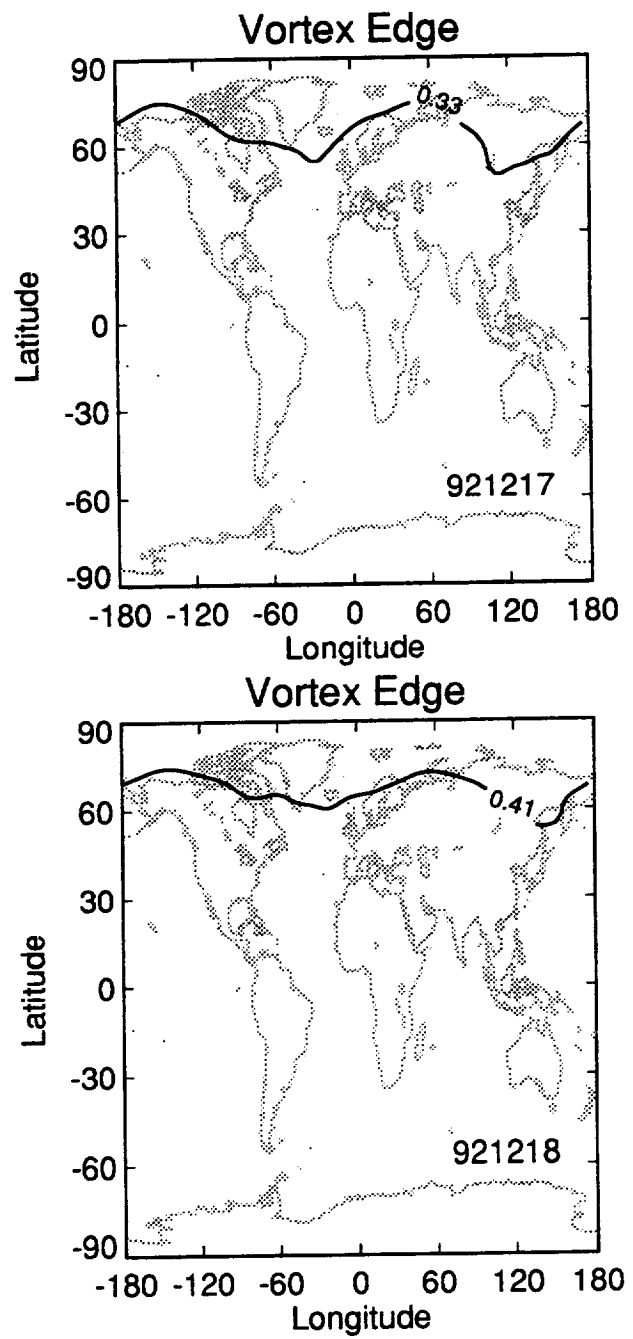
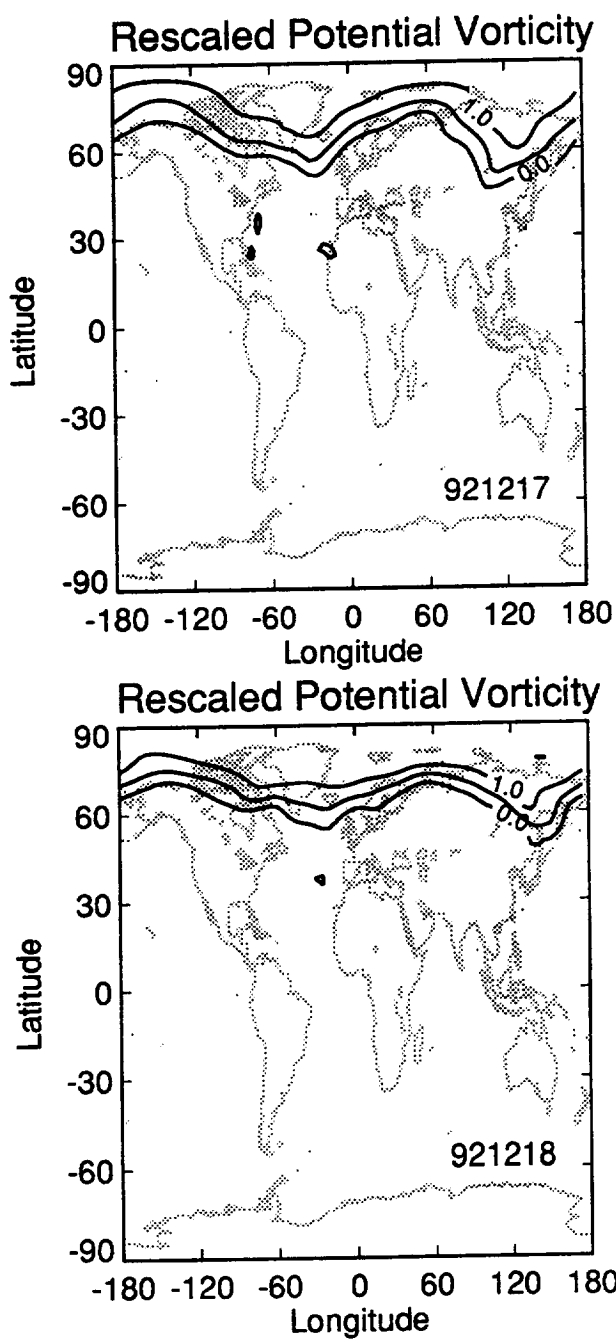
Appendix A. Plots of rescaled potential vorticity and the vortex edge for each day of available data for the winter of 1992-93. Dates are labeled as YYMMDD (year, month, day).



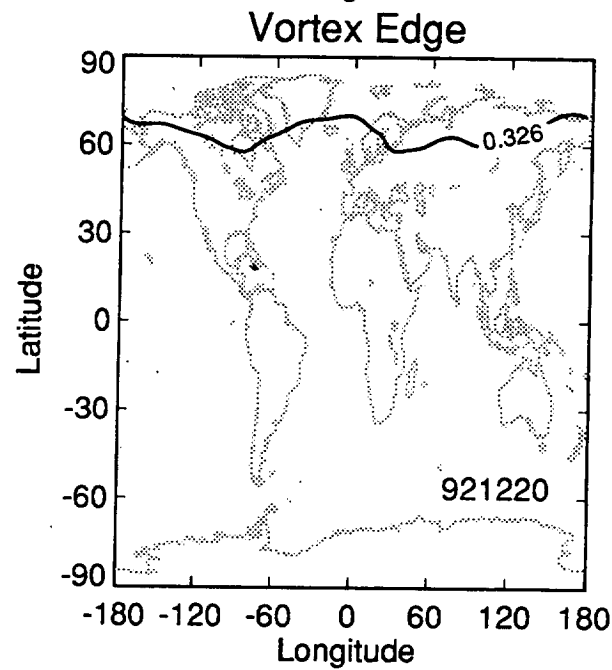
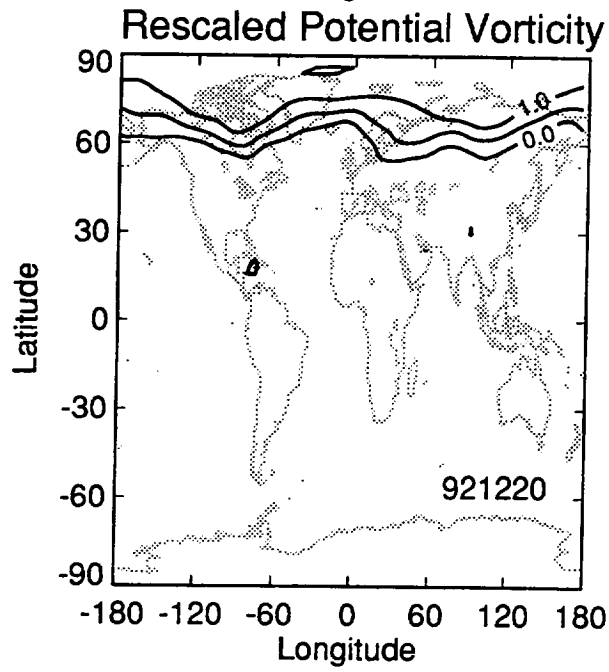
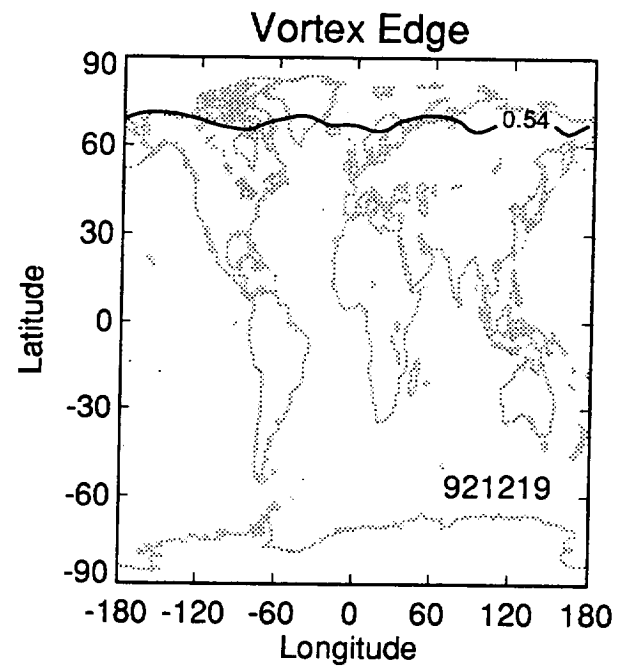
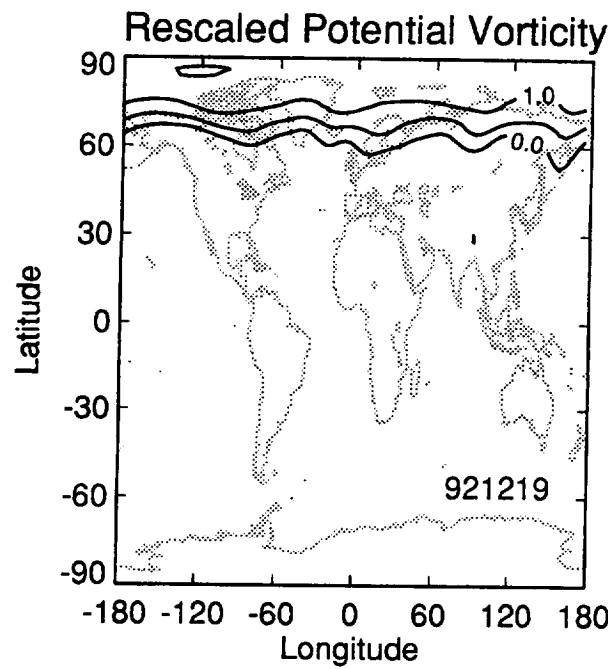
Appendix A. Plots of rescaled potential vorticity and the vortex edge for each day of available data for the winter of 1992-93. Dates are labeled as YYMMDD (year, month, day).



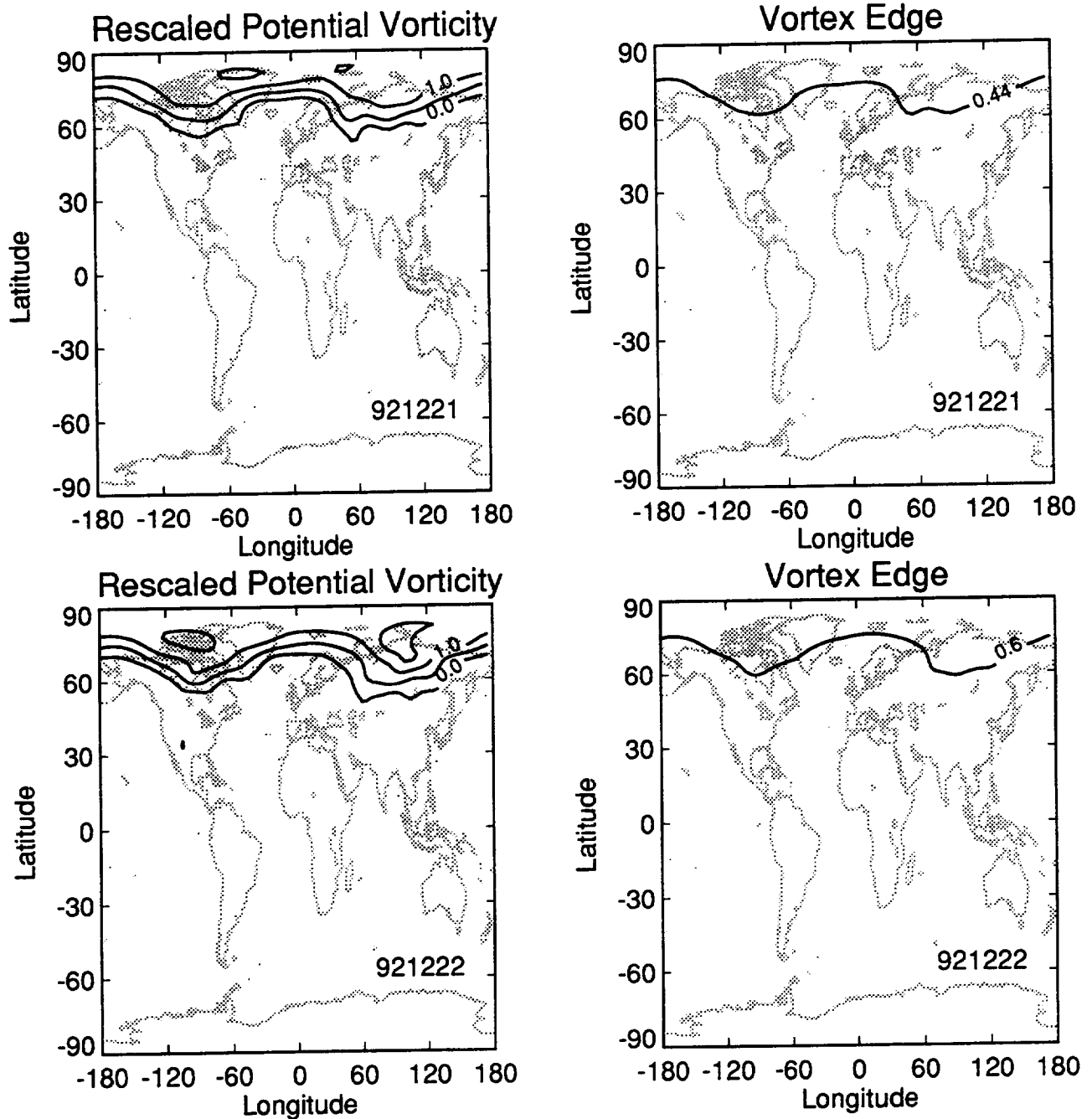
Appendix A. Plots of rescaled potential vorticity and the vortex edge for each day of available data for the winter of 1992-93. Dates are labeled as YYMMDD (year, month, day).



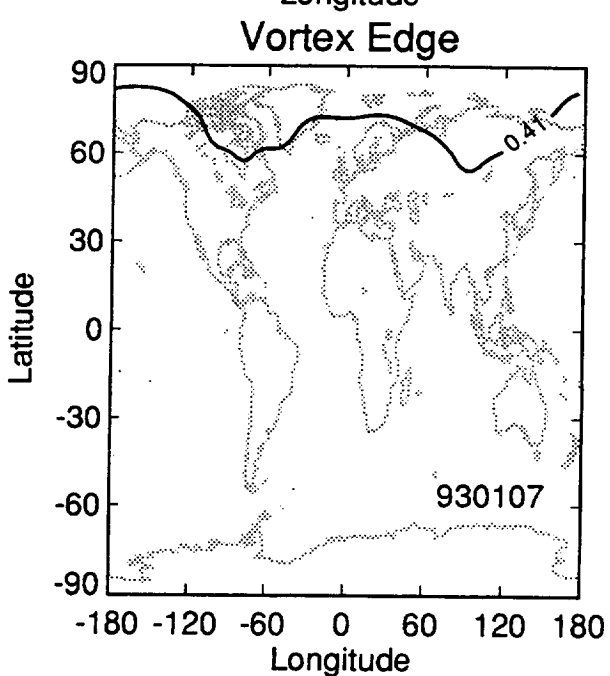
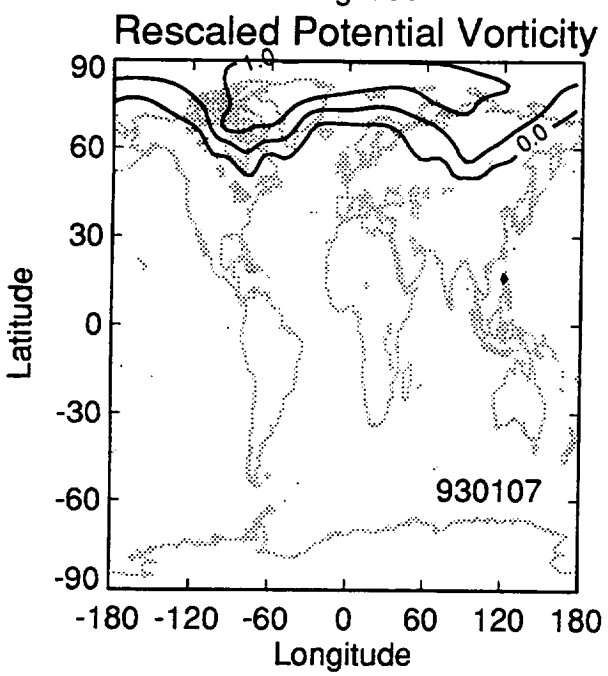
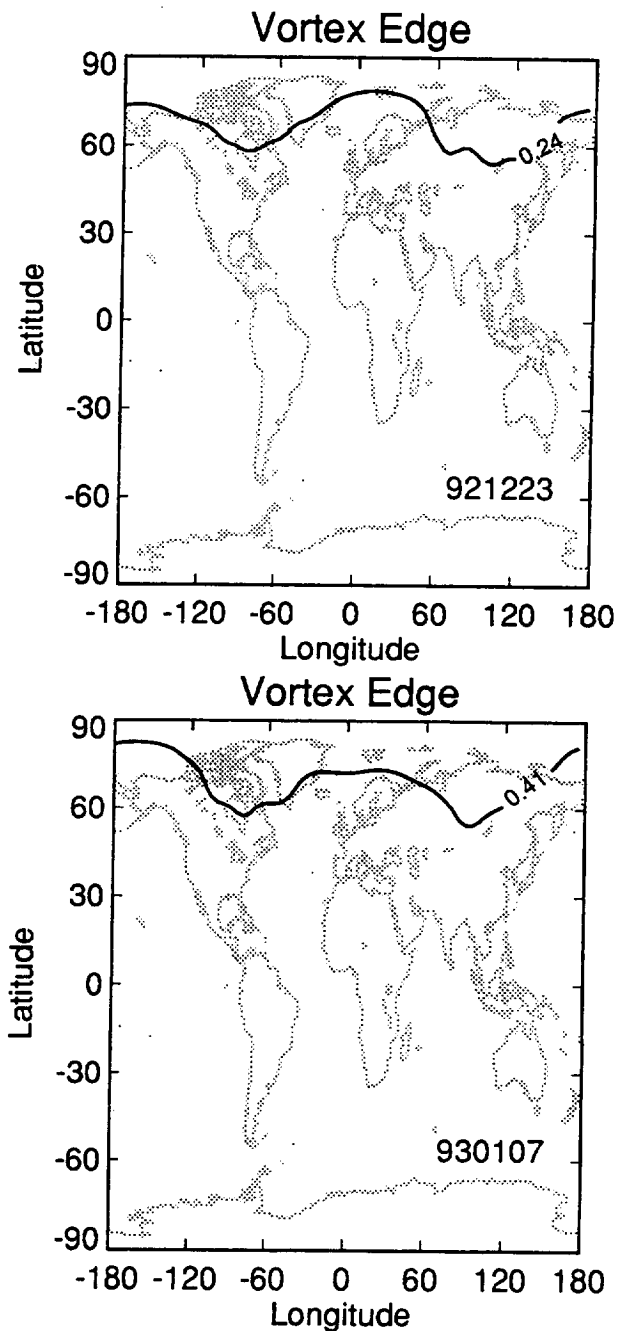
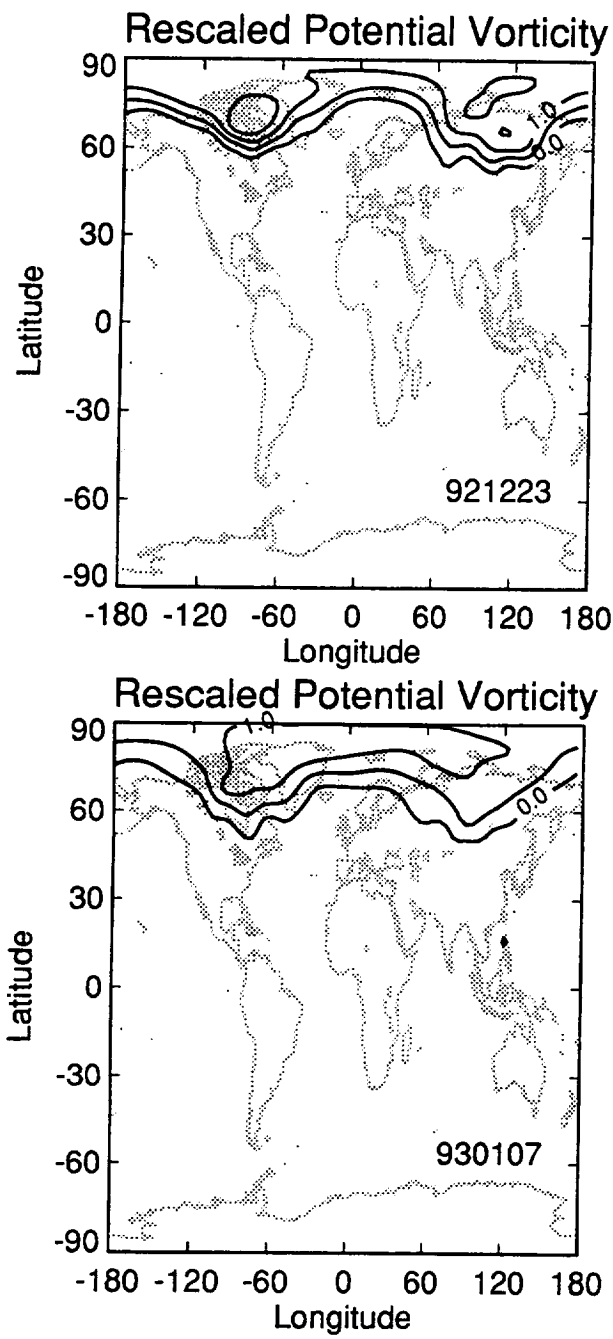
Appendix A. Plots of rescaled potential vorticity and the vortex edge for each day of available data for the winter of 1992-93. Dates are labeled as YYMMDD (year, month, day).



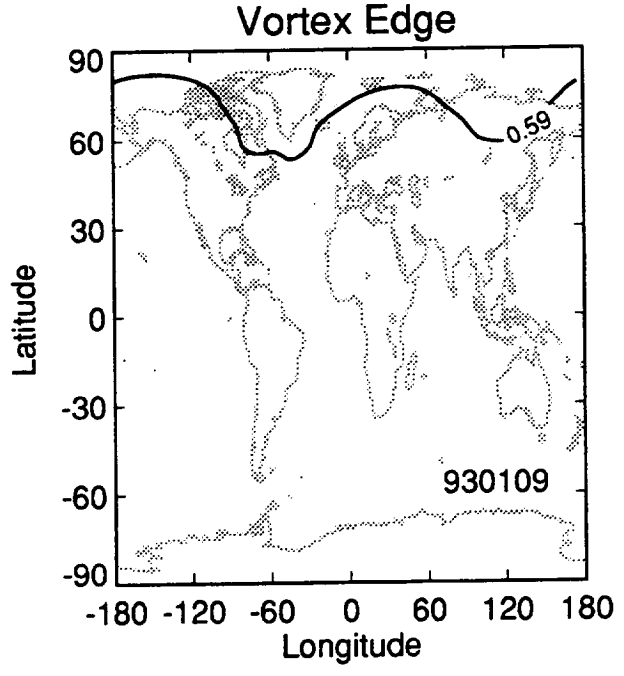
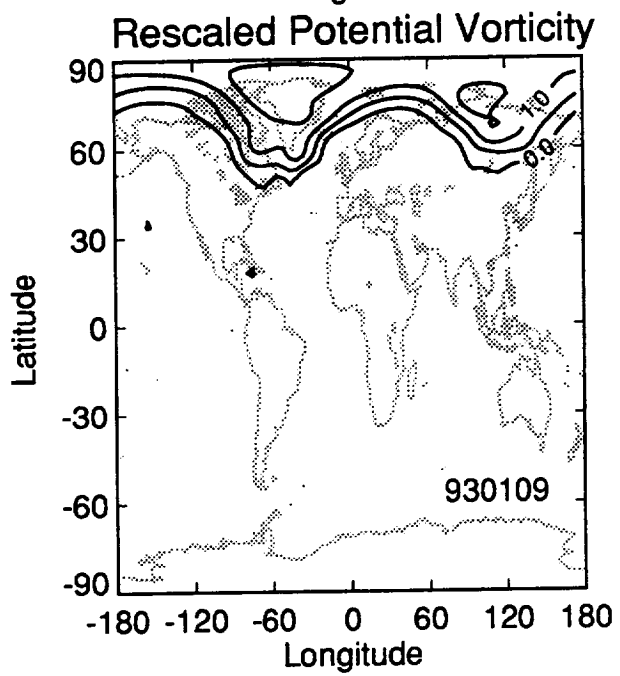
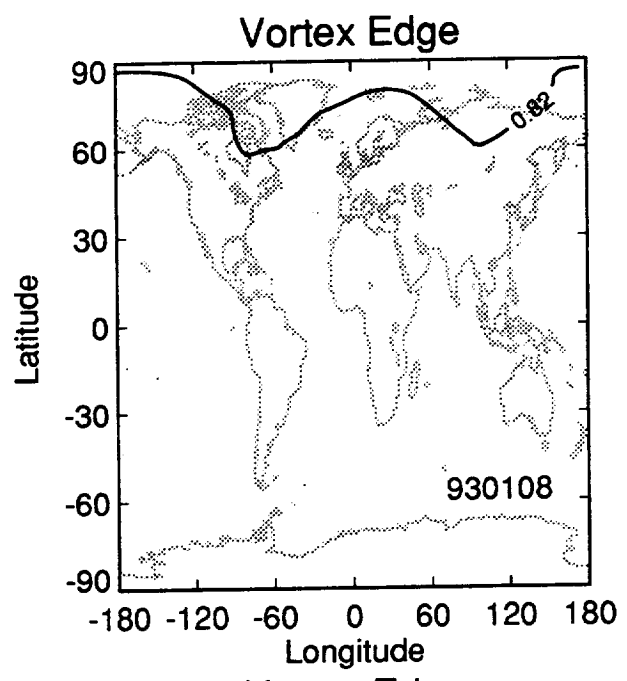
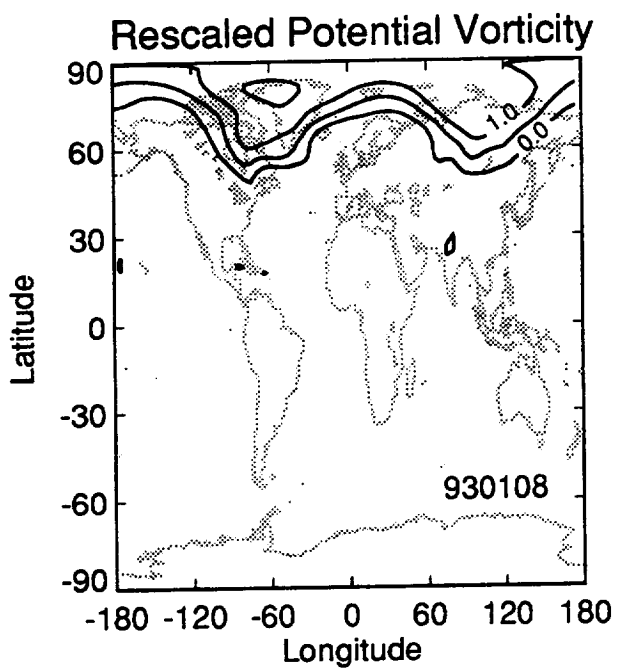
Appendix A. Plots of rescaled potential vorticity and the vortex edge for each day of available data for the winter of 1992-93. Dates are labeled as YYMMDD (year, month, day).



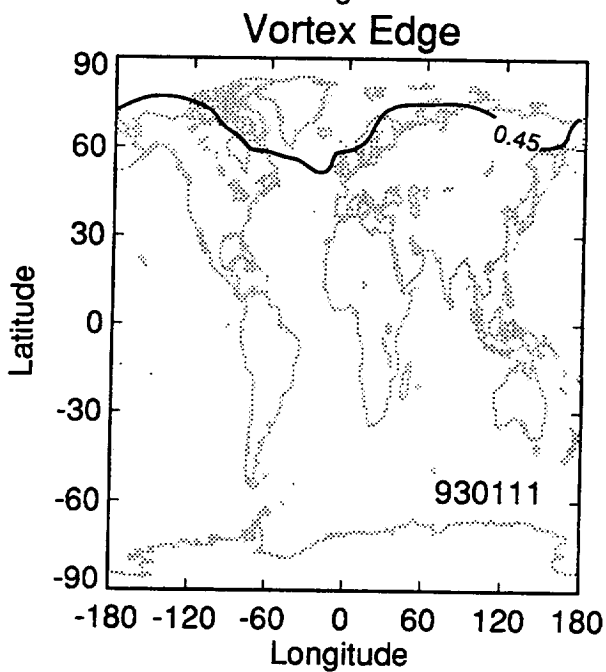
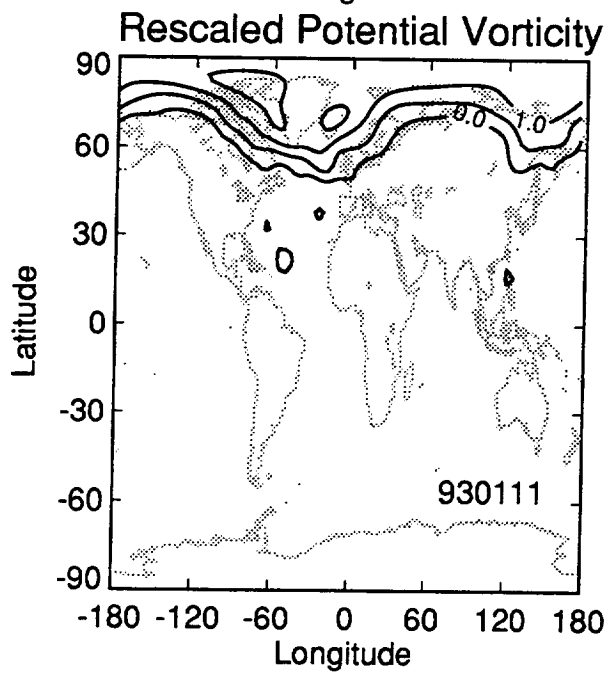
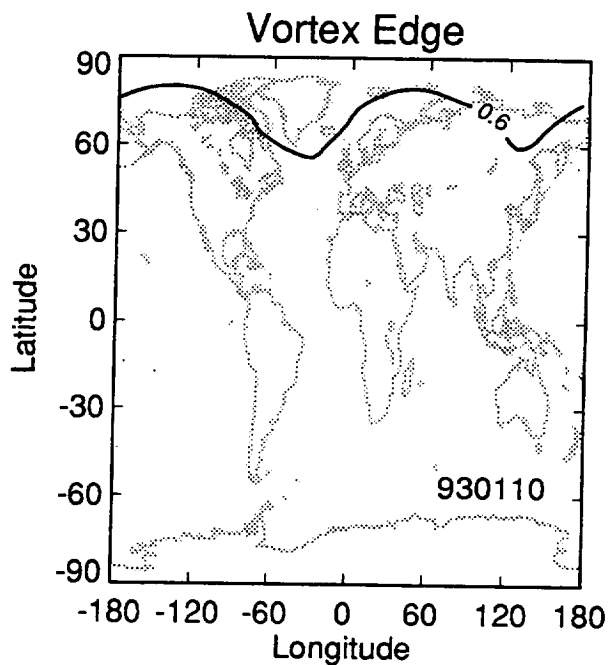
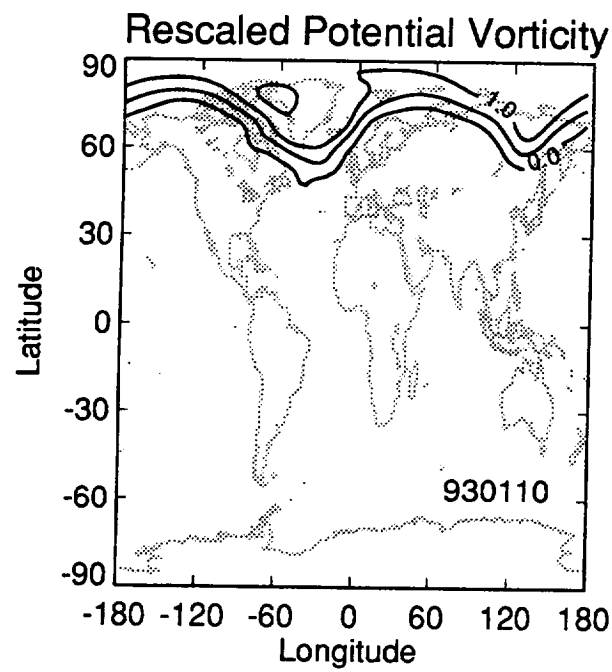
Appendix A. Plots of rescaled potential vorticity and the vortex edge for each day of available data for the winter of 1992-93. Dates are labeled as YYMMDD (year, month, day).



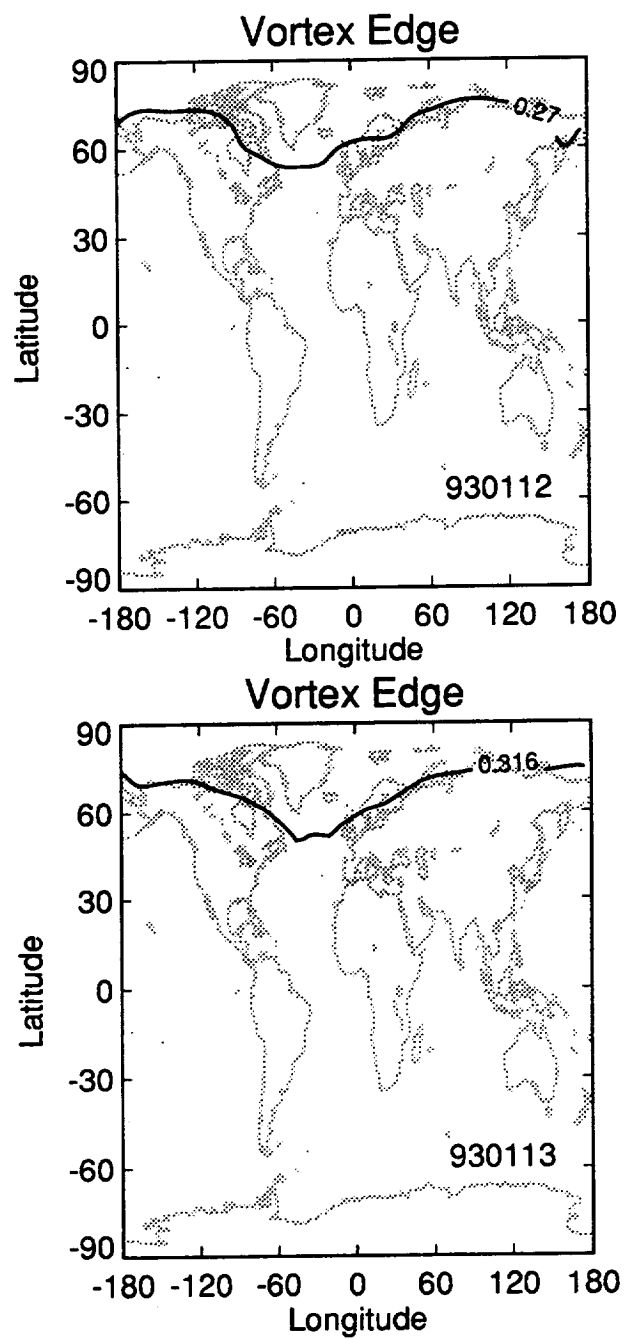
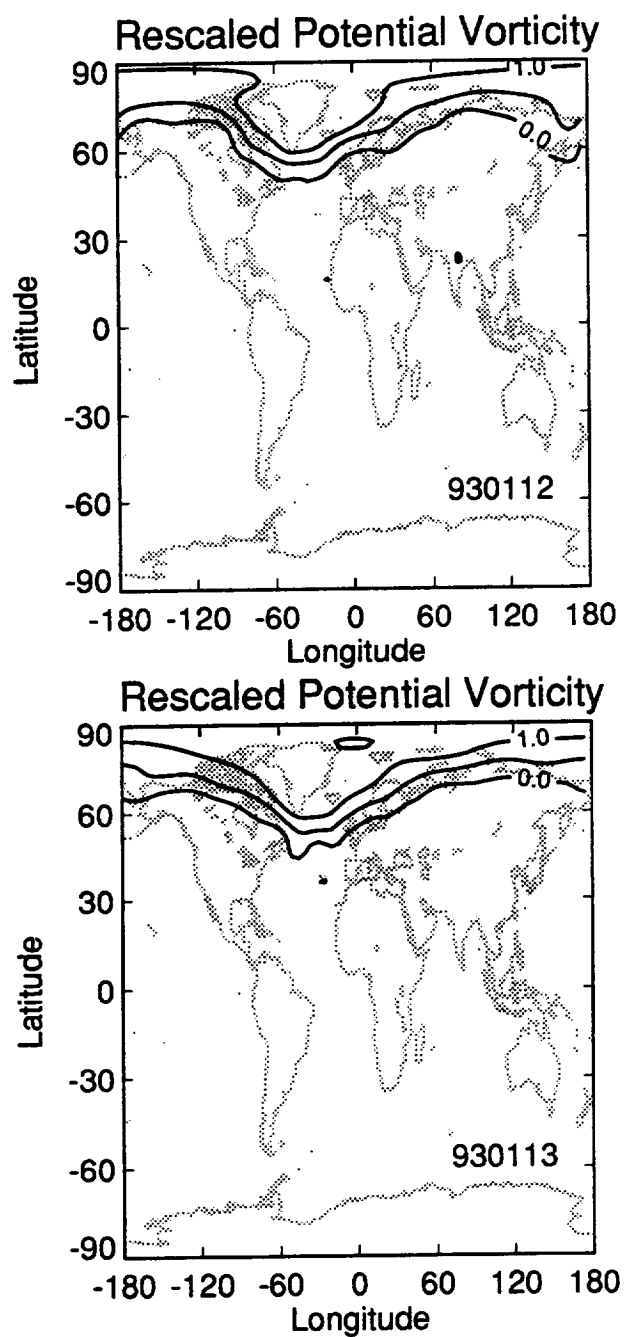
Appendix A. Plots of rescaled potential vorticity and the vortex edge for each day of available data for the winter of 1992-93. Dates are labeled as YYMMDD (year, month, day).



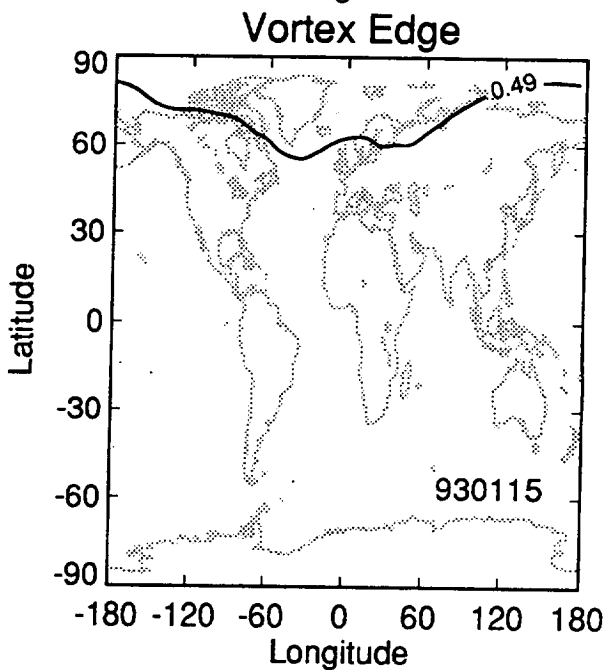
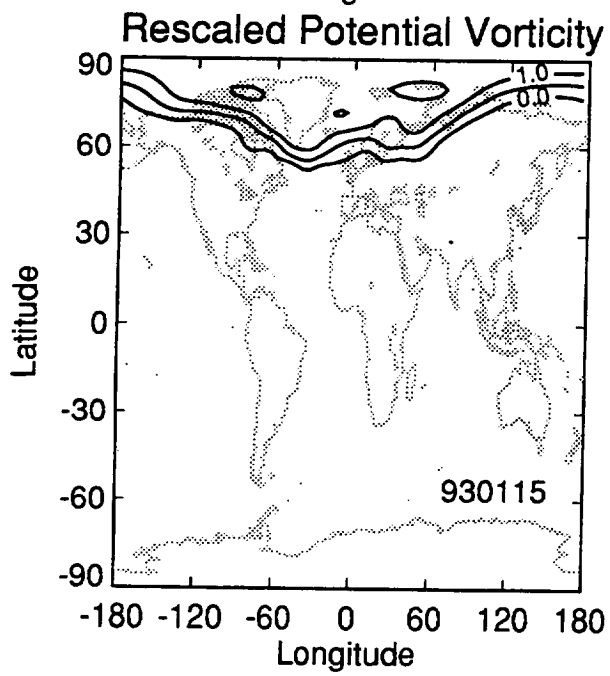
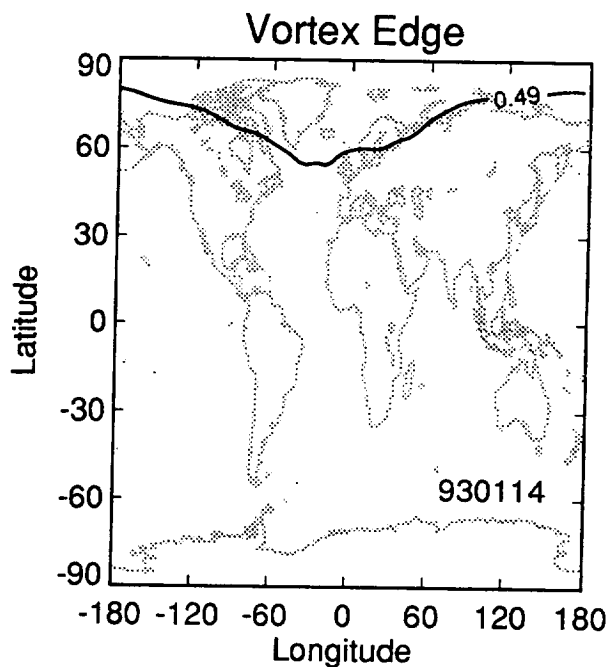
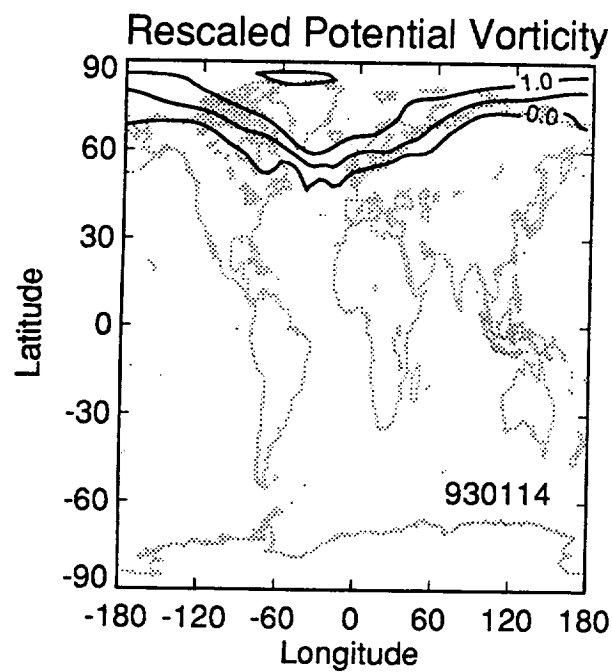
Appendix A. Plots of rescaled potential vorticity and the vortex edge for each day of available data for the winter of 1992-93. Dates are labeled as YYMMDD (year, month, day).



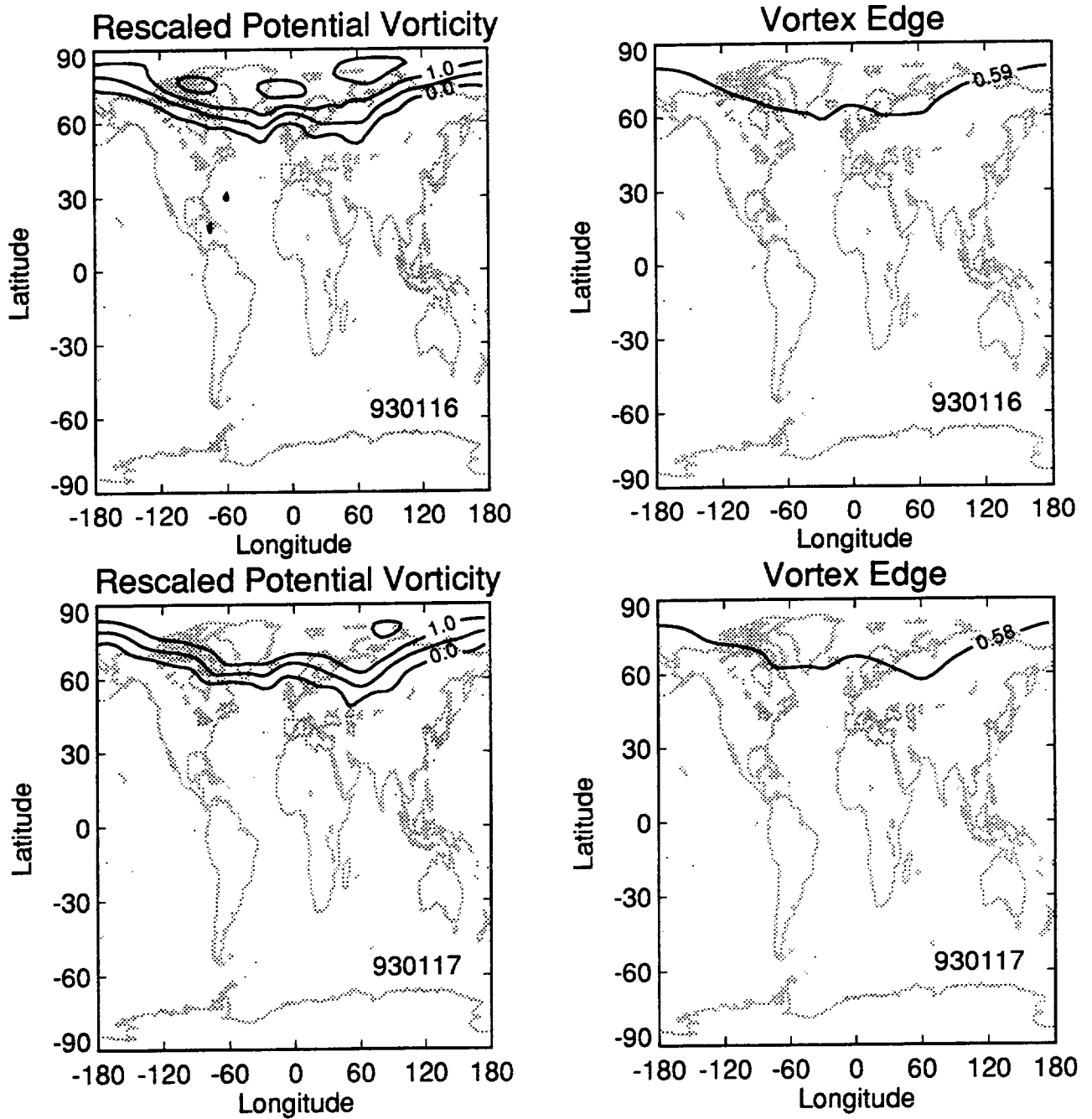
Appendix A. Plots of rescaled potential vorticity and the vortex edge for each day of available data for the winter of 1992-93. Dates are labeled as YYMMDD (year, month, day).



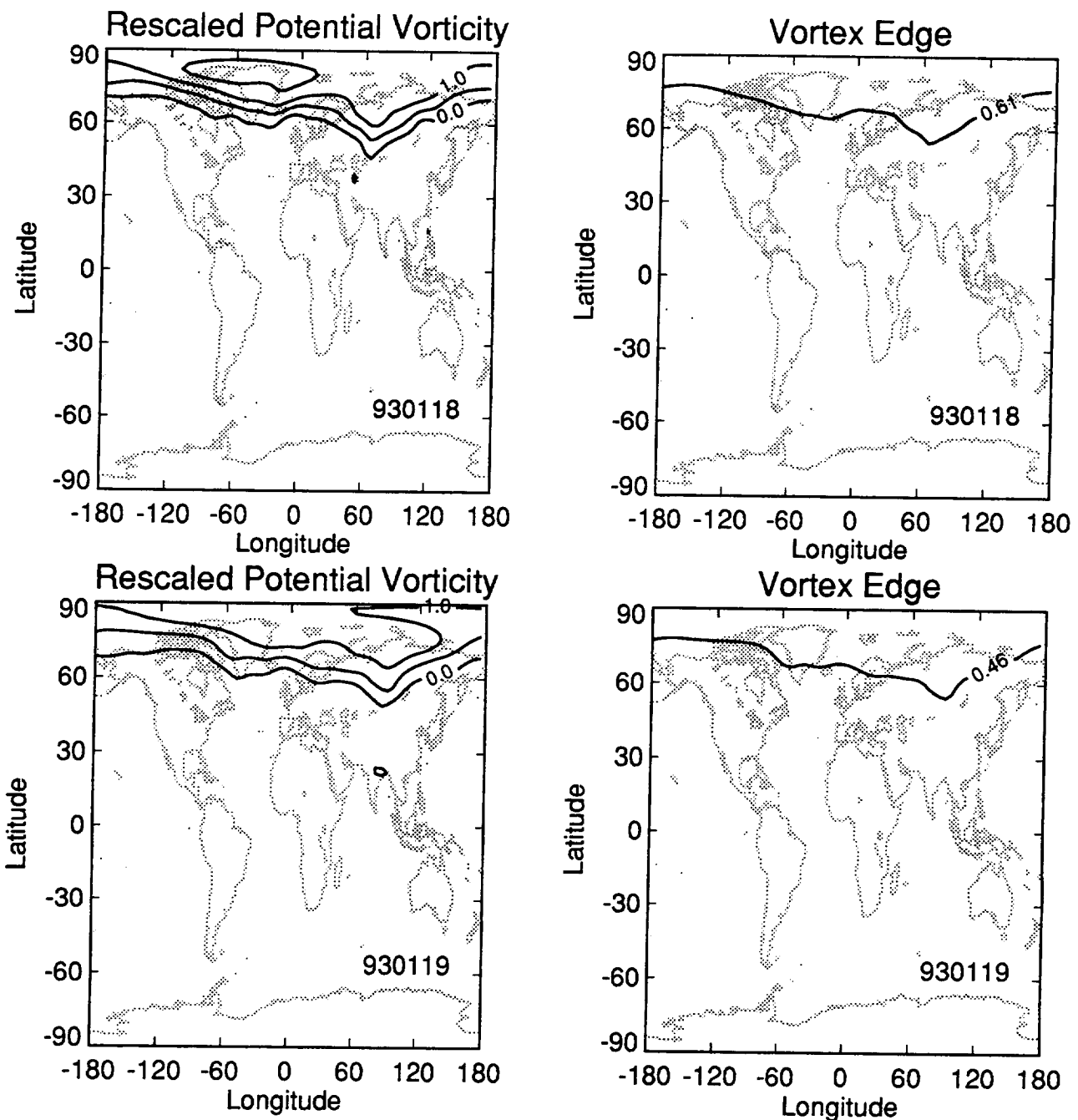
Appendix A. Plots of rescaled potential vorticity and the vortex edge for each day of available data for the winter of 1992-93. Dates are labeled as YYMMDD (year, month, day).



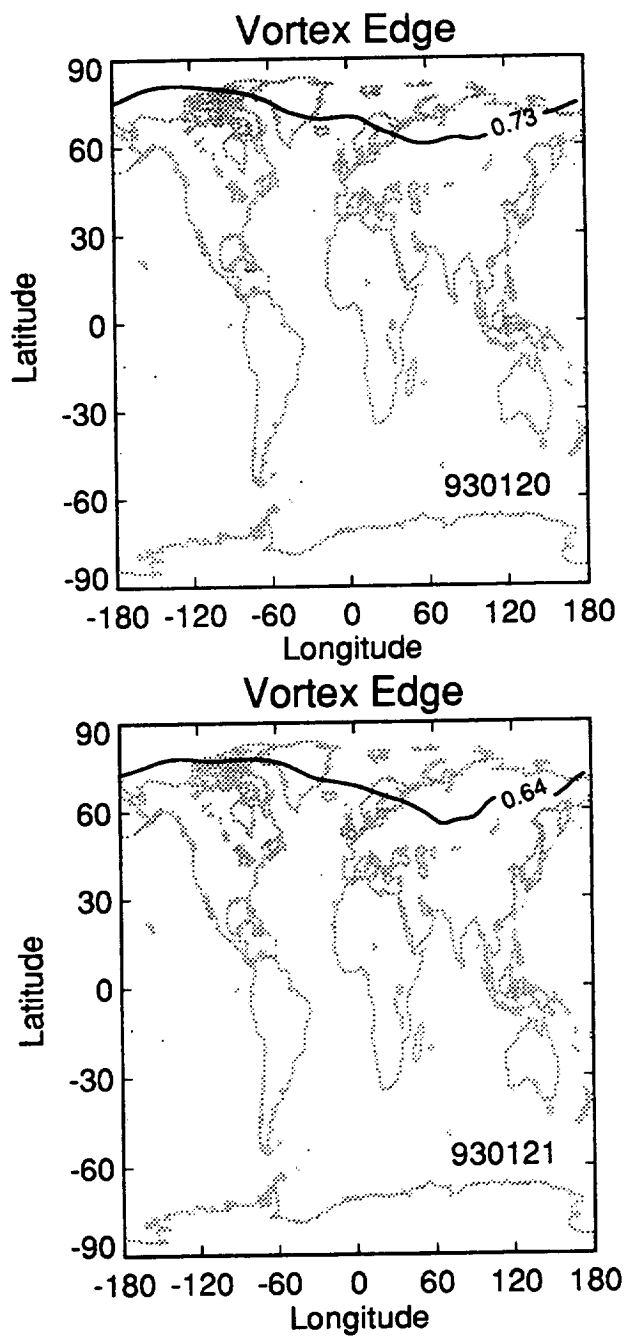
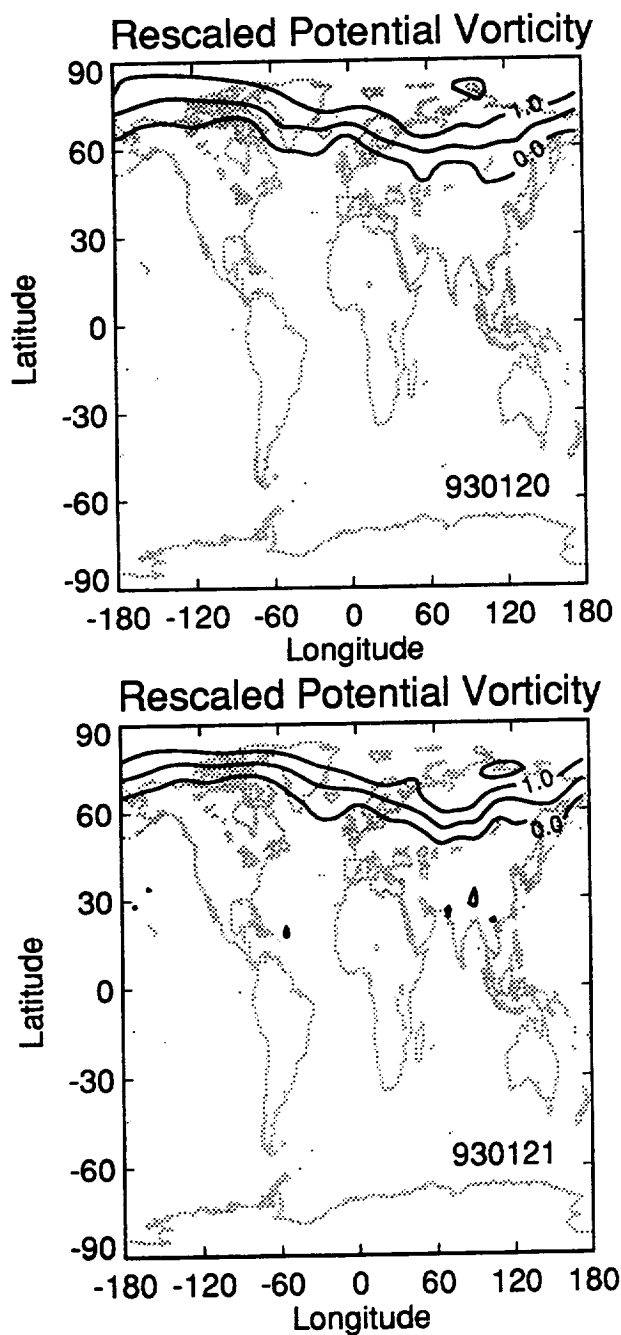
Appendix A. Plots of rescaled potential vorticity and the vortex edge for each day of available data for the winter of 1992-93. Dates are labeled as YYMMDD (year, month, day).



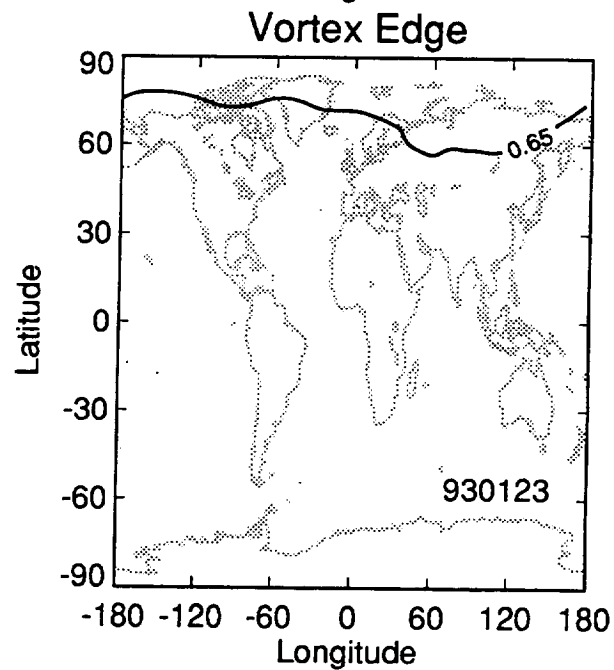
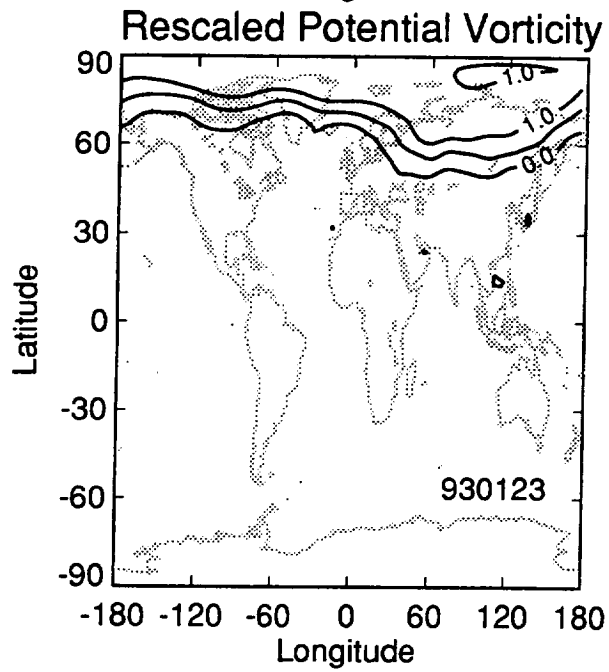
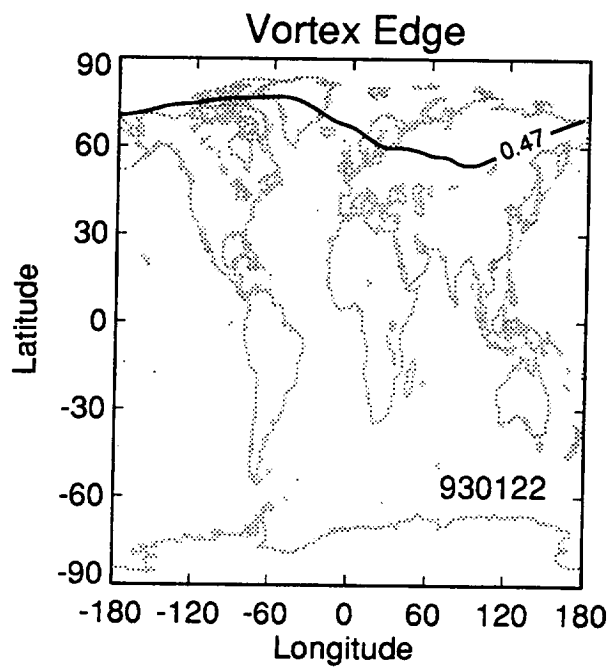
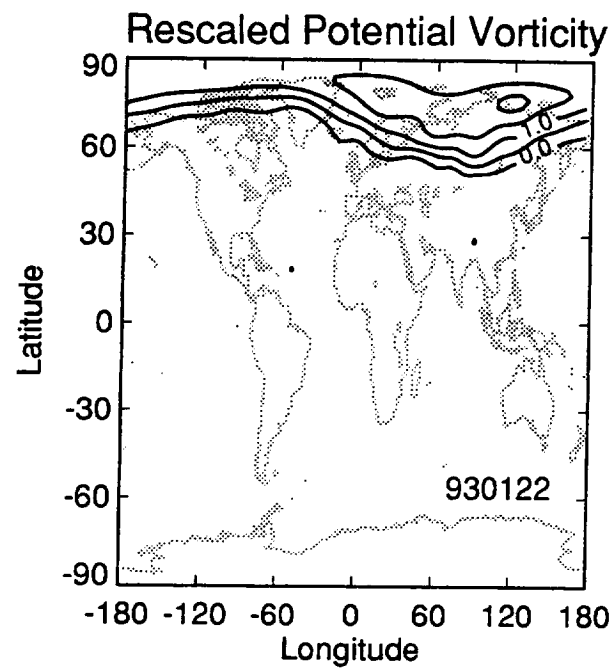
Appendix A. Plots of rescaled potential vorticity and the vortex edge for each day of available data for the winter of 1992-93. Dates are labeled as YYMMDD (year, month, day).



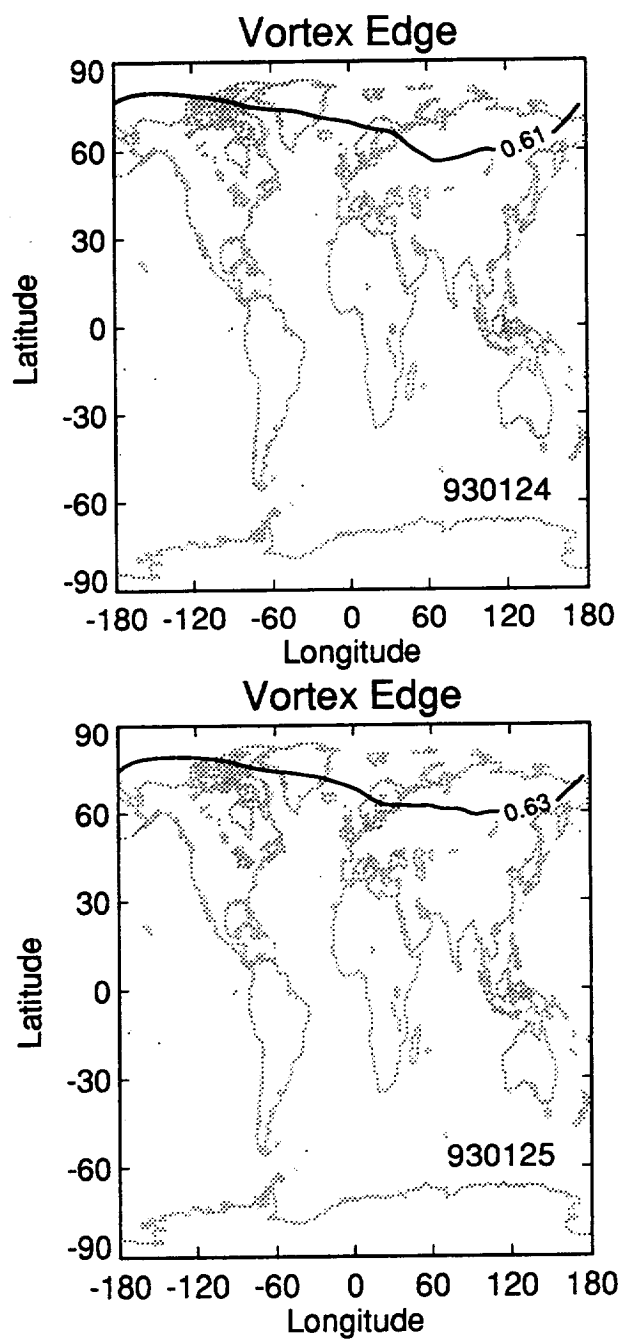
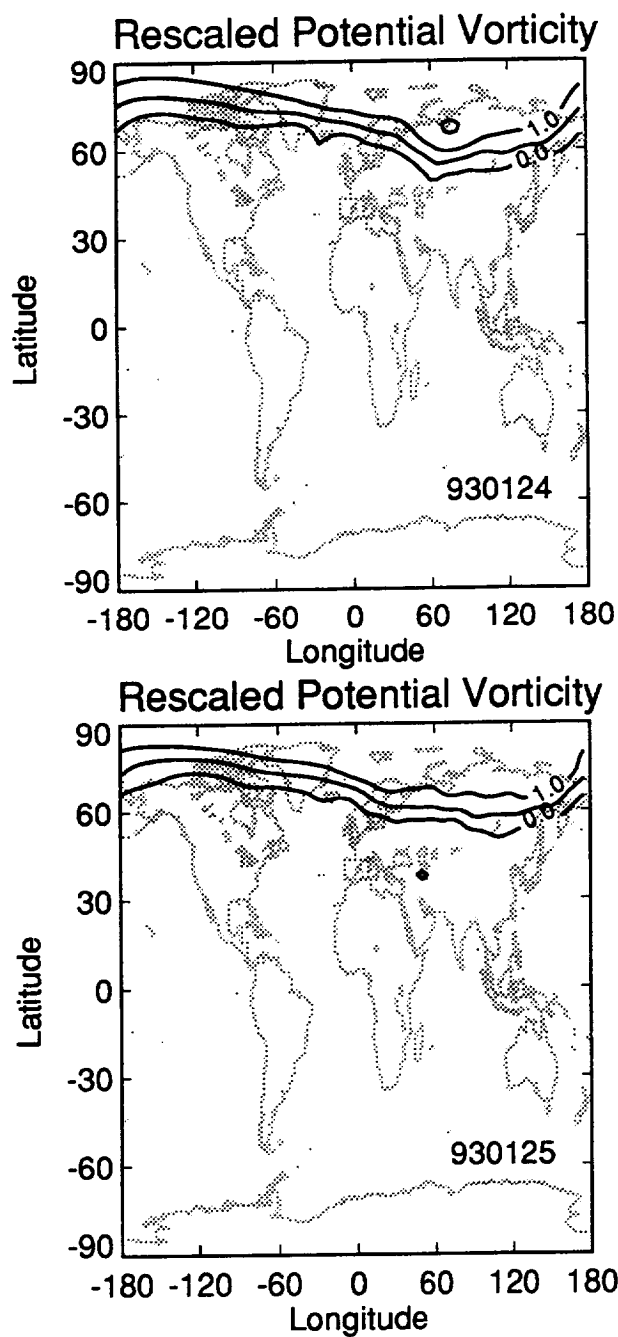
Appendix A. Plots of rescaled potential vorticity and the vortex edge for each day of available data for the winter of 1992-93. Dates are labeled as YYMMDD (year, month, day).



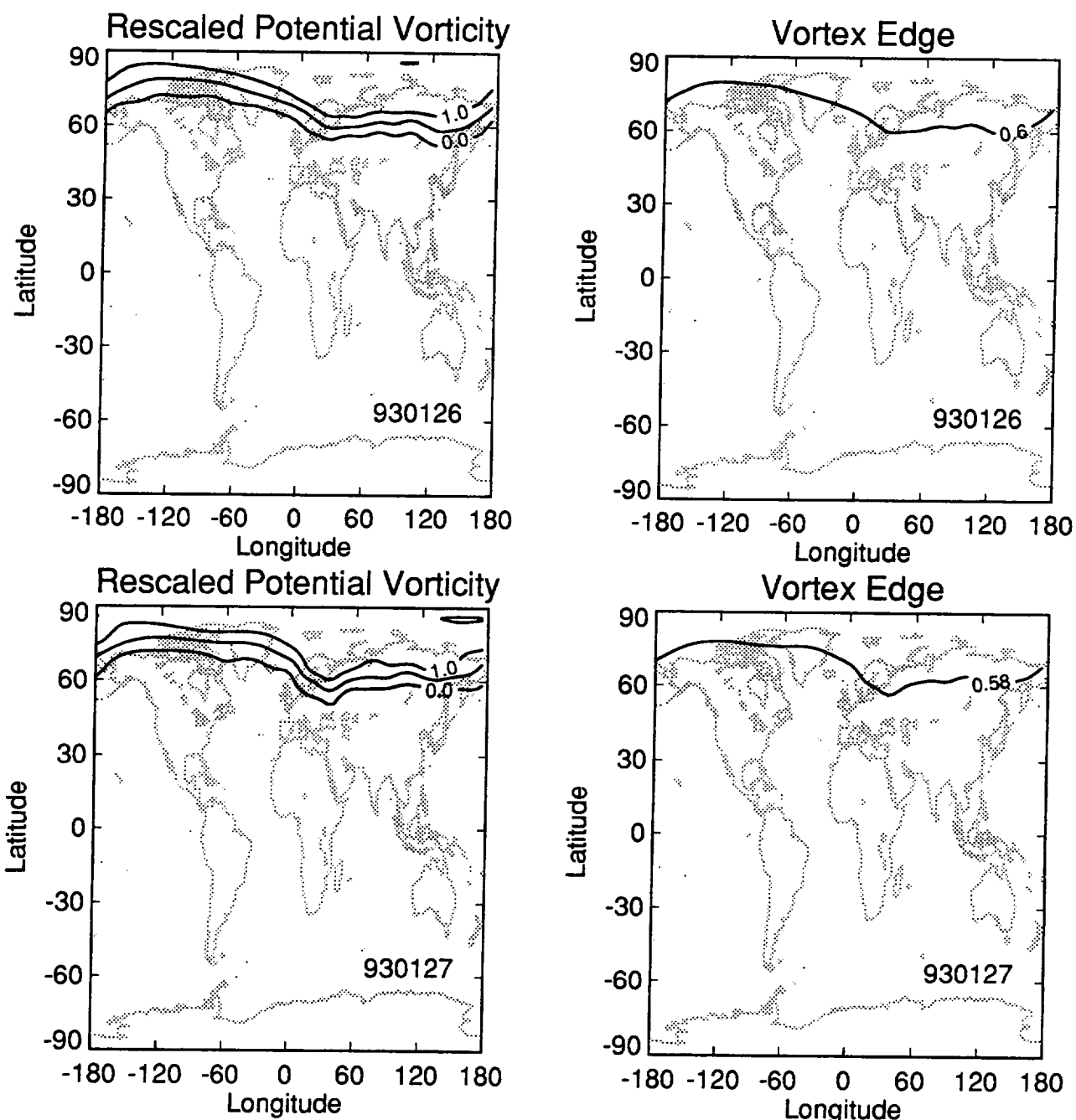
Appendix A. Plots of rescaled potential vorticity and the vortex edge for each day of available data for the winter of 1992-93. Dates are labeled as YYMMDD (year, month, day).



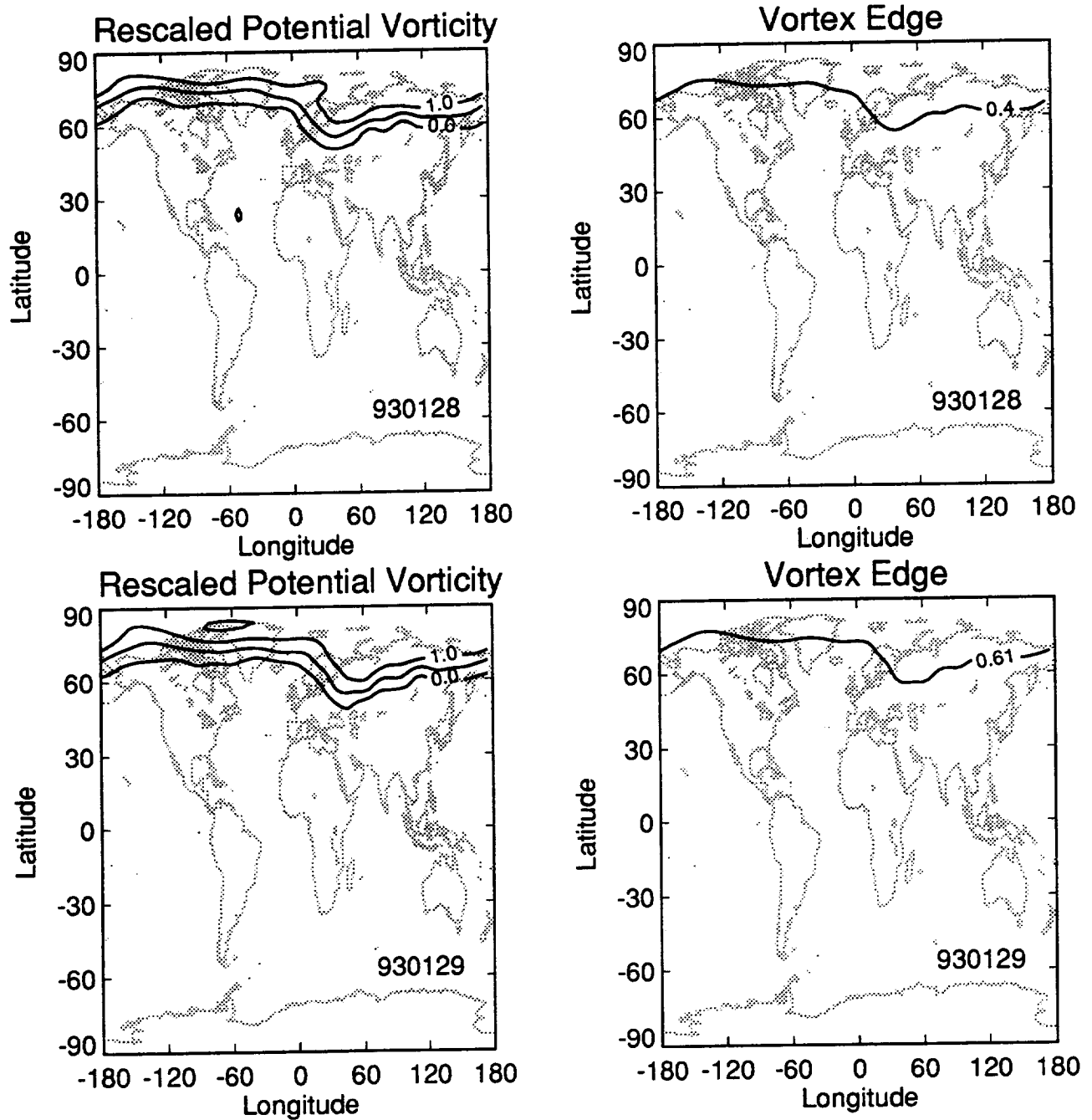
Appendix A. Plots of rescaled potential vorticity and the vortex edge for each day of available data for the winter of 1992-93. Dates are labeled as YYMMDD (year, month, day).



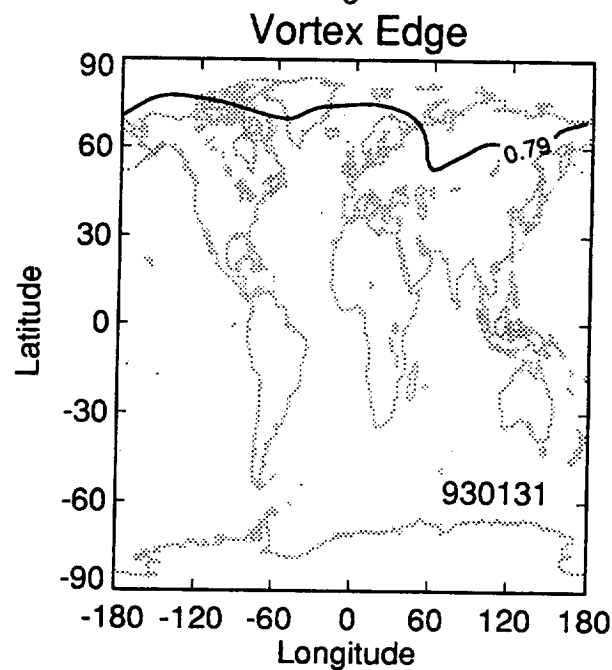
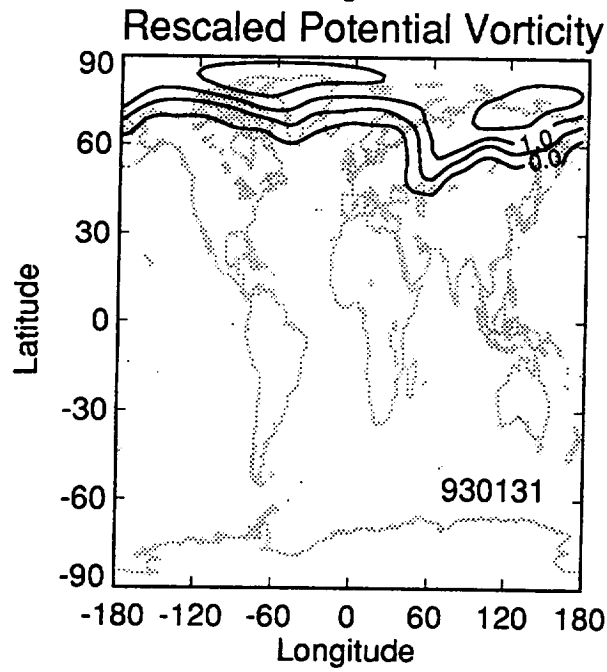
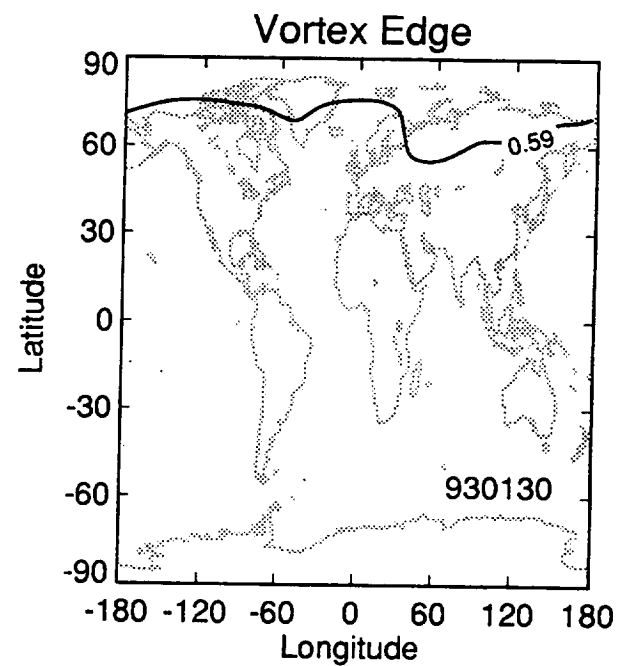
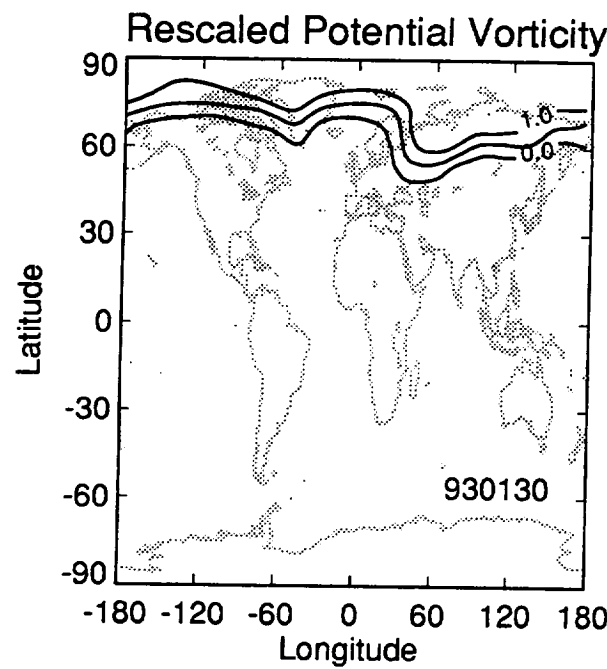
Appendix A. Plots of rescaled potential vorticity and the vortex edge for each day of available data for the winter of 1992-93. Dates are labeled as YYMMDD (year, month, day).



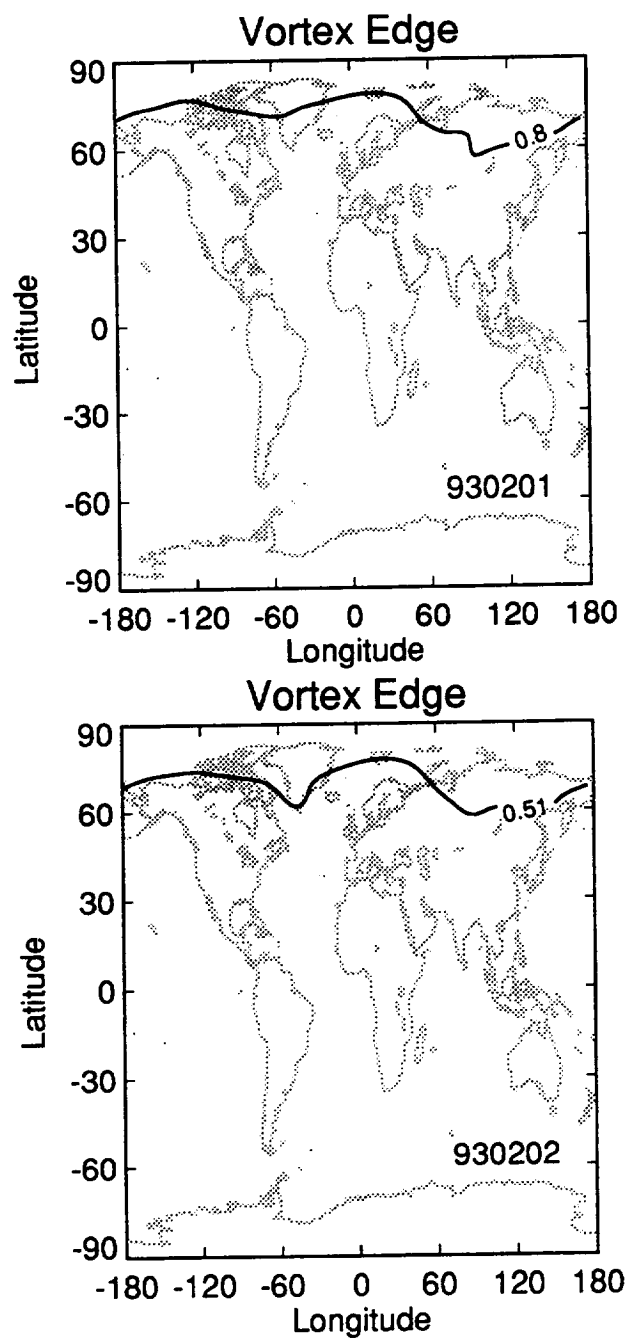
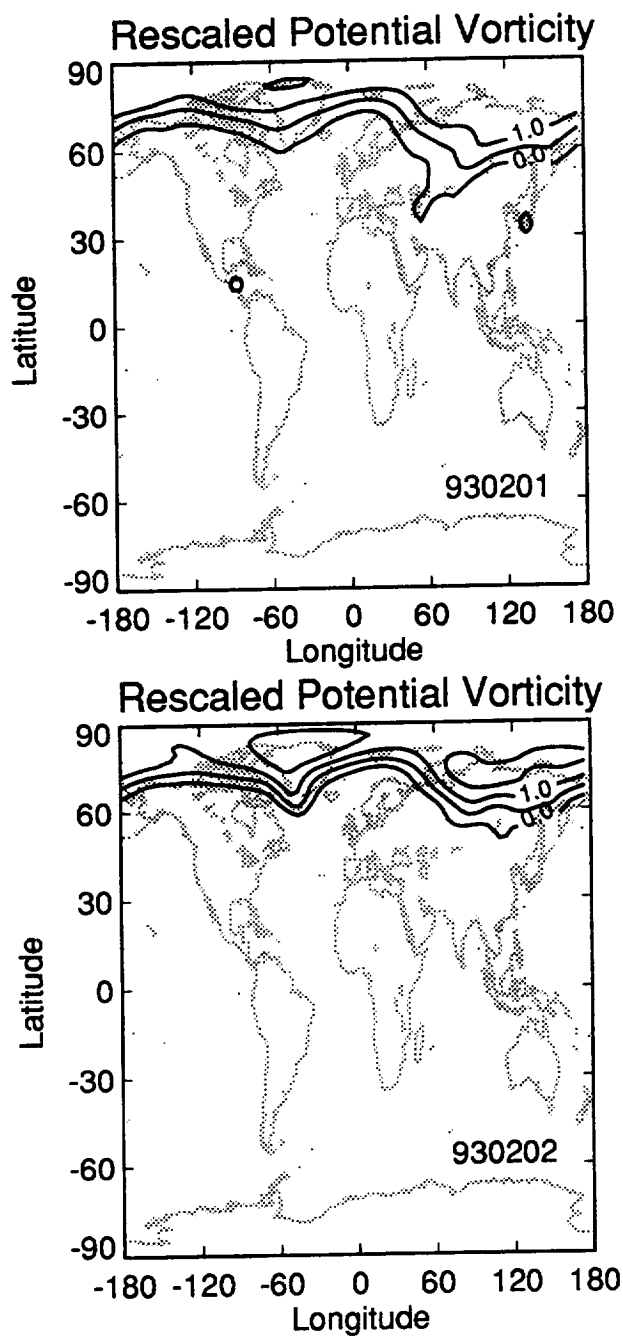
Appendix A. Plots of rescaled potential vorticity and the vortex edge for each day of available data for the winter of 1992-93. Dates are labeled as YYMMDD (year, month, day).



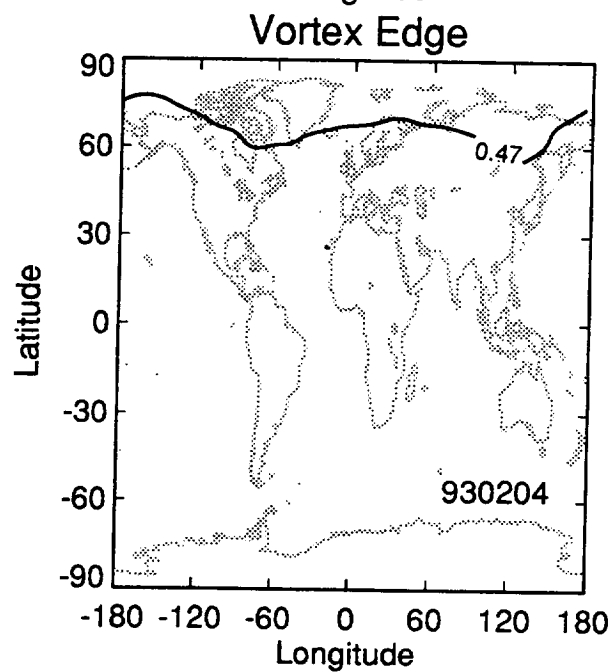
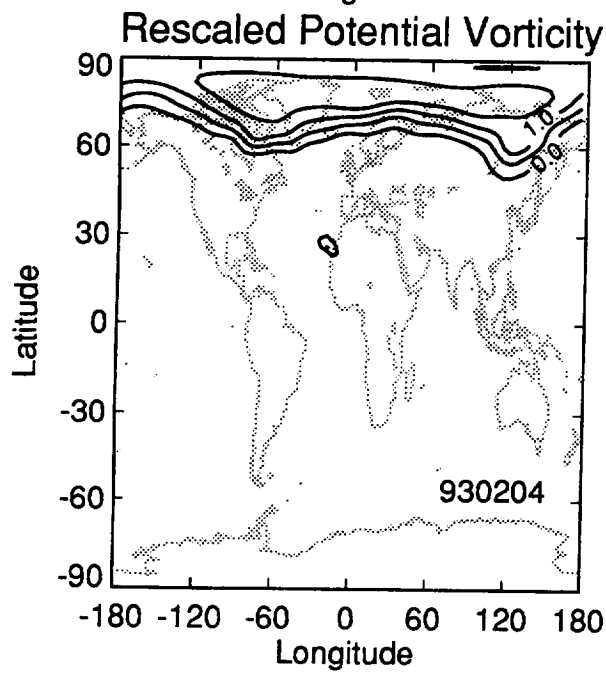
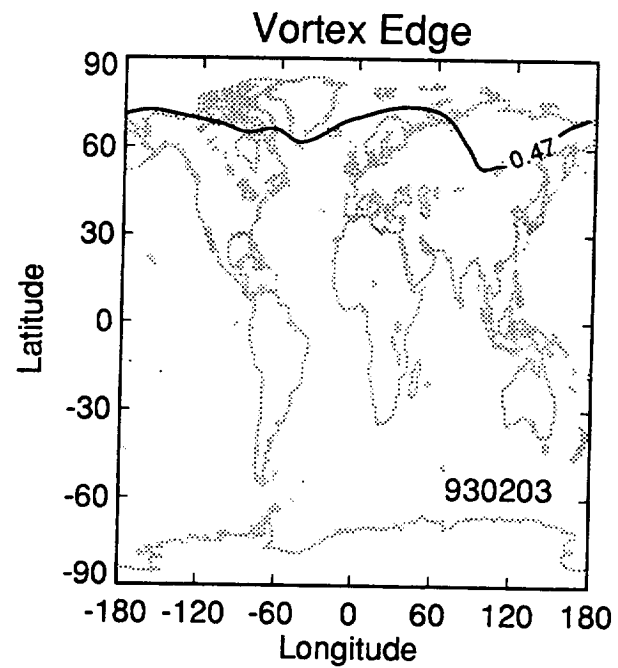
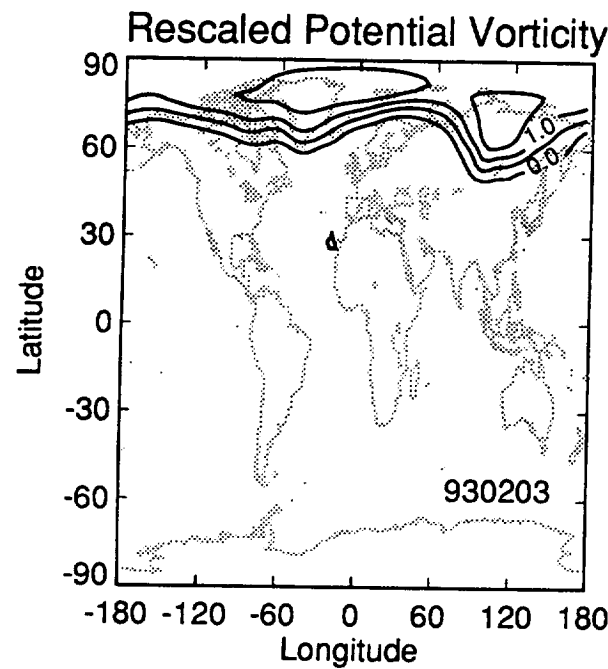
Appendix A. Plots of rescaled potential vorticity and the vortex edge for each day of available data for the winter of 1992-93. Dates are labeled as YYMMDD (year, month, day).



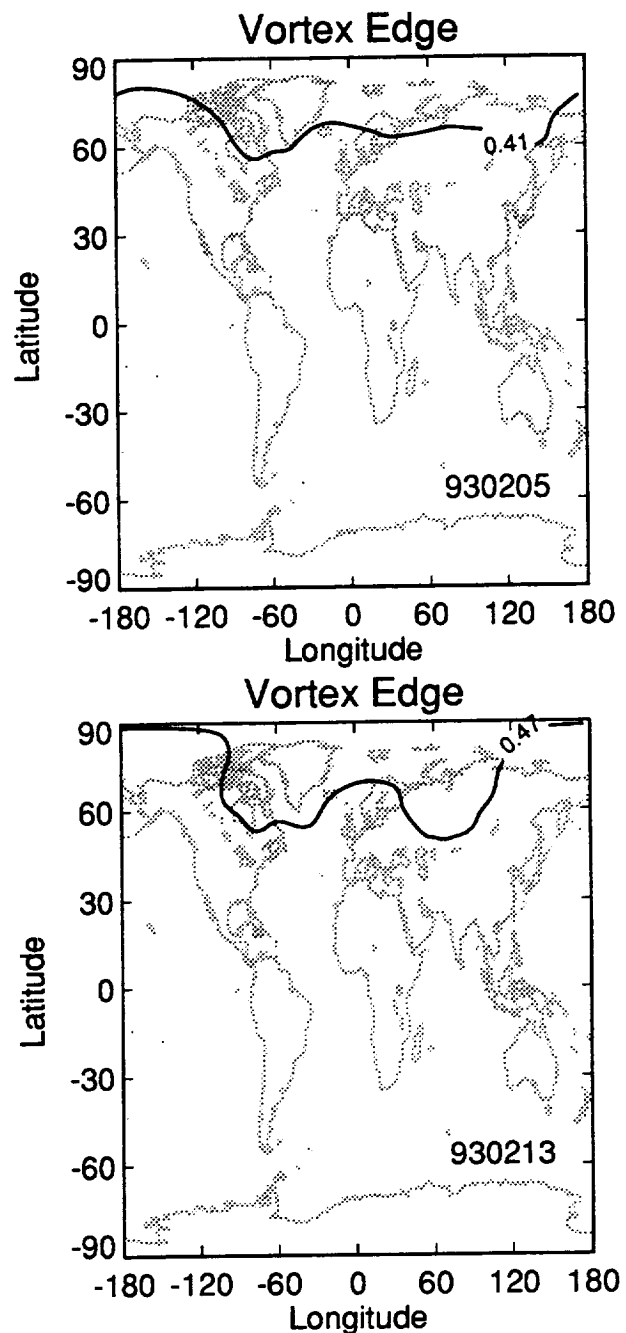
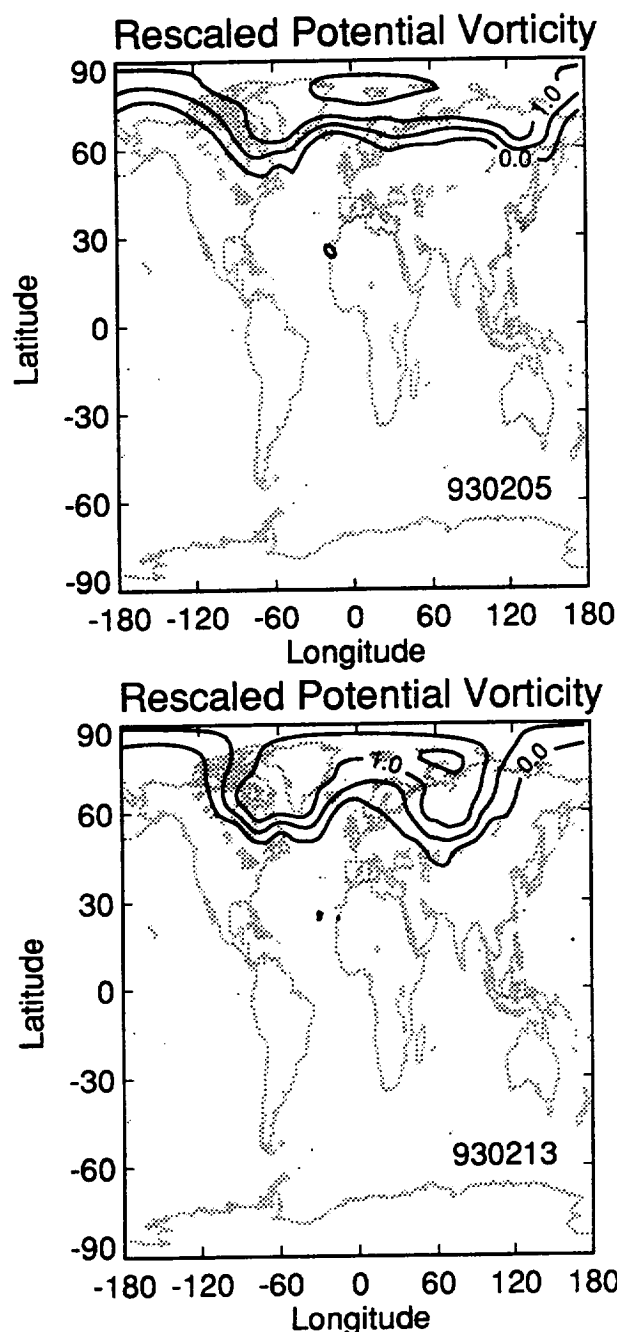
Appendix A. Plots of rescaled potential vorticity and the vortex edge for each day of available data for the winter of 1992-93. Dates are labeled as YYMMDD (year, month, day).



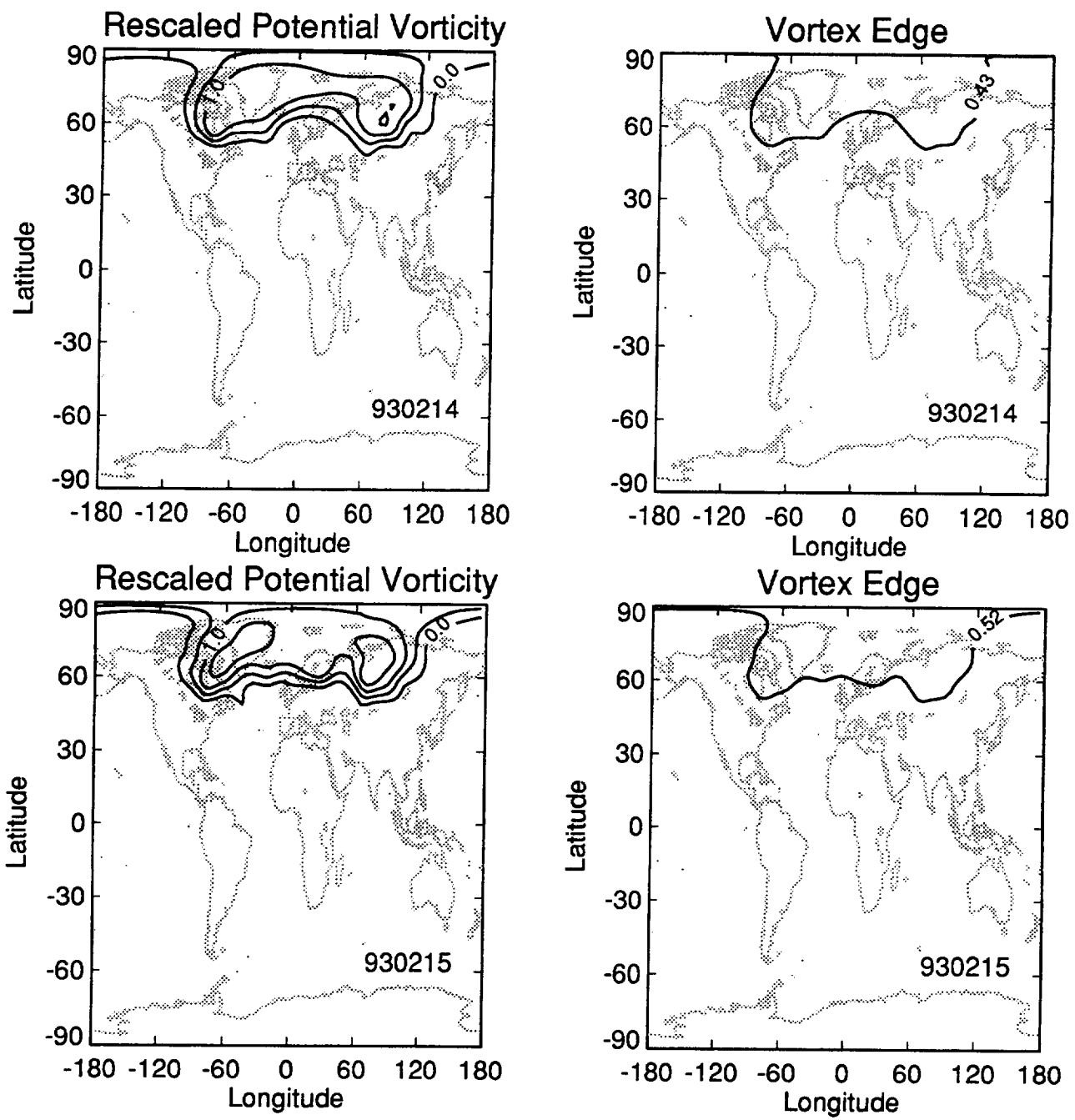
Appendix A. Plots of rescaled potential vorticity and the vortex edge for each day of available data for the winter of 1992-93. Dates are labeled as YYMMDD (year, month, day).



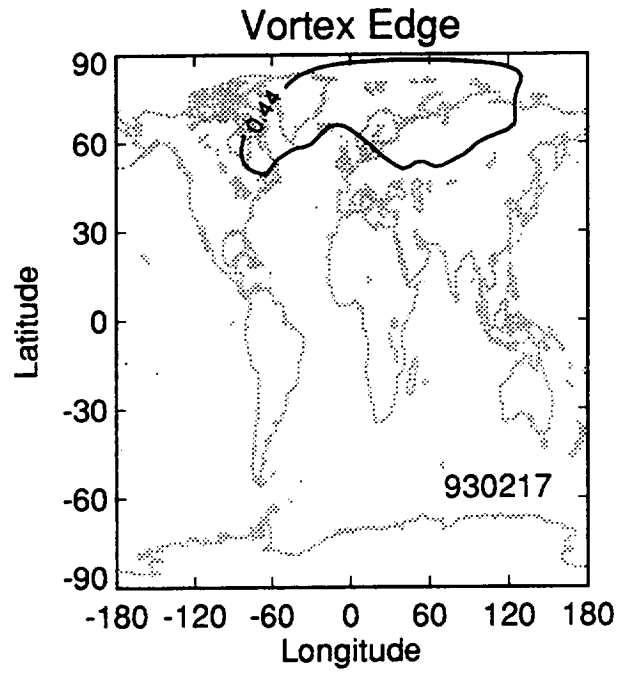
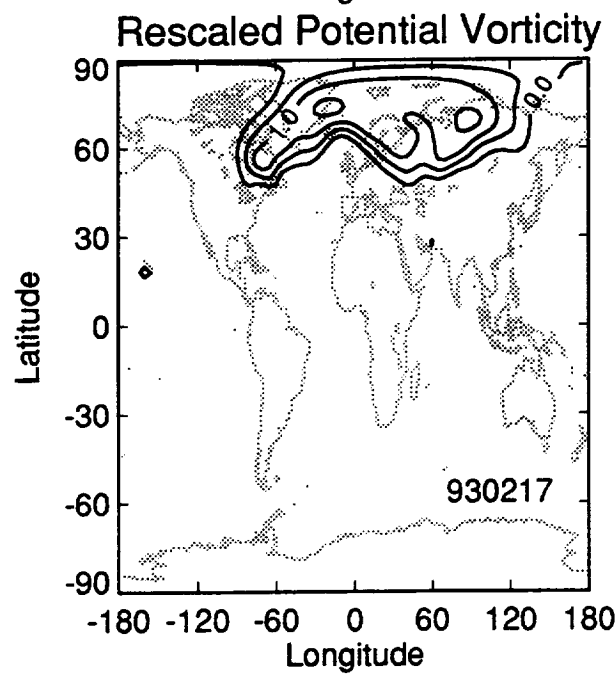
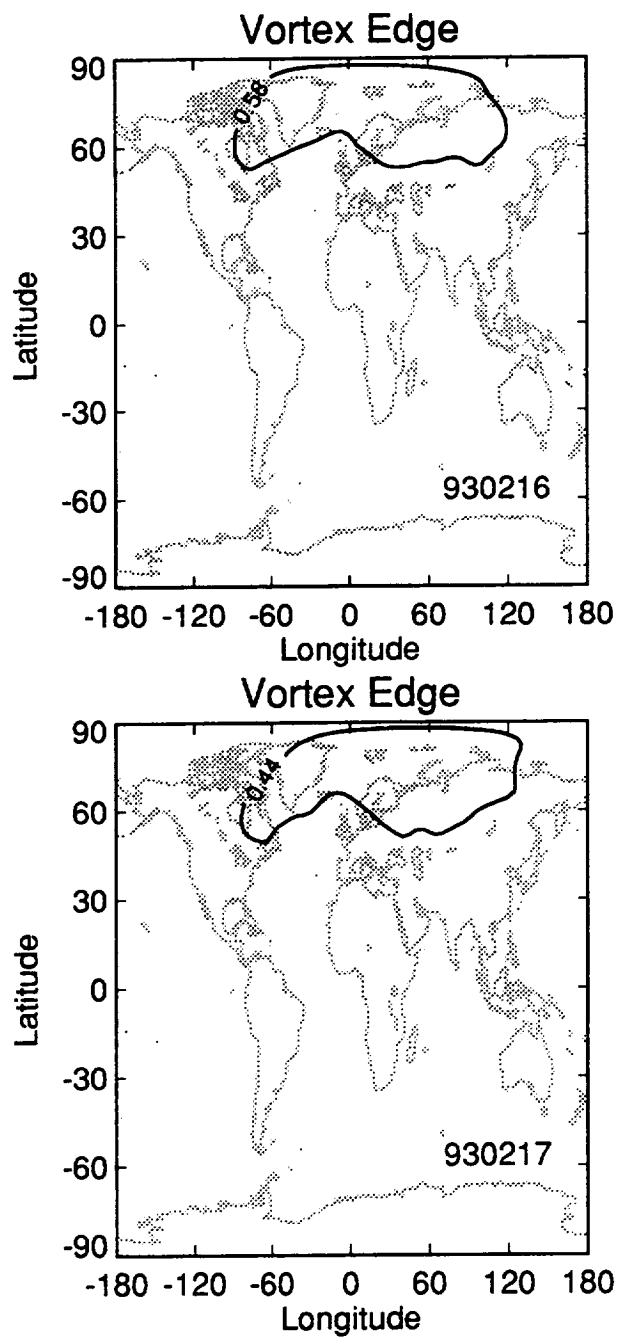
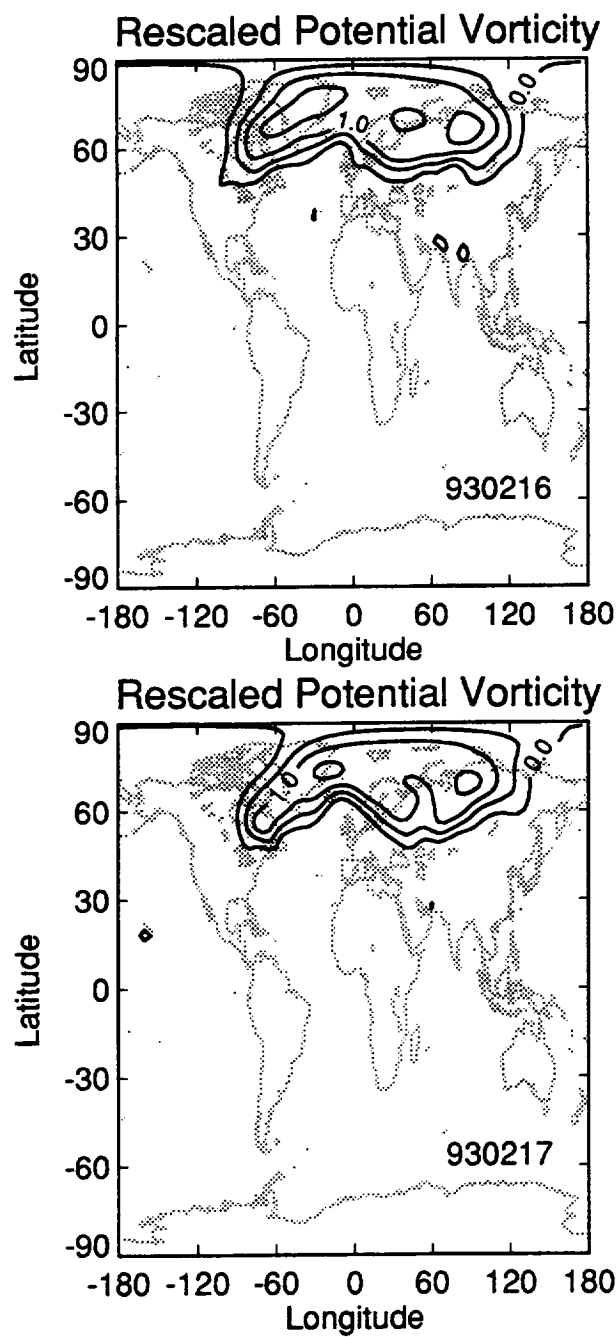
Appendix A. Plots of rescaled potential vorticity and the vortex edge for each day of available data for the winter of 1992-93. Dates are labeled as YYMMDD (year, month, day).



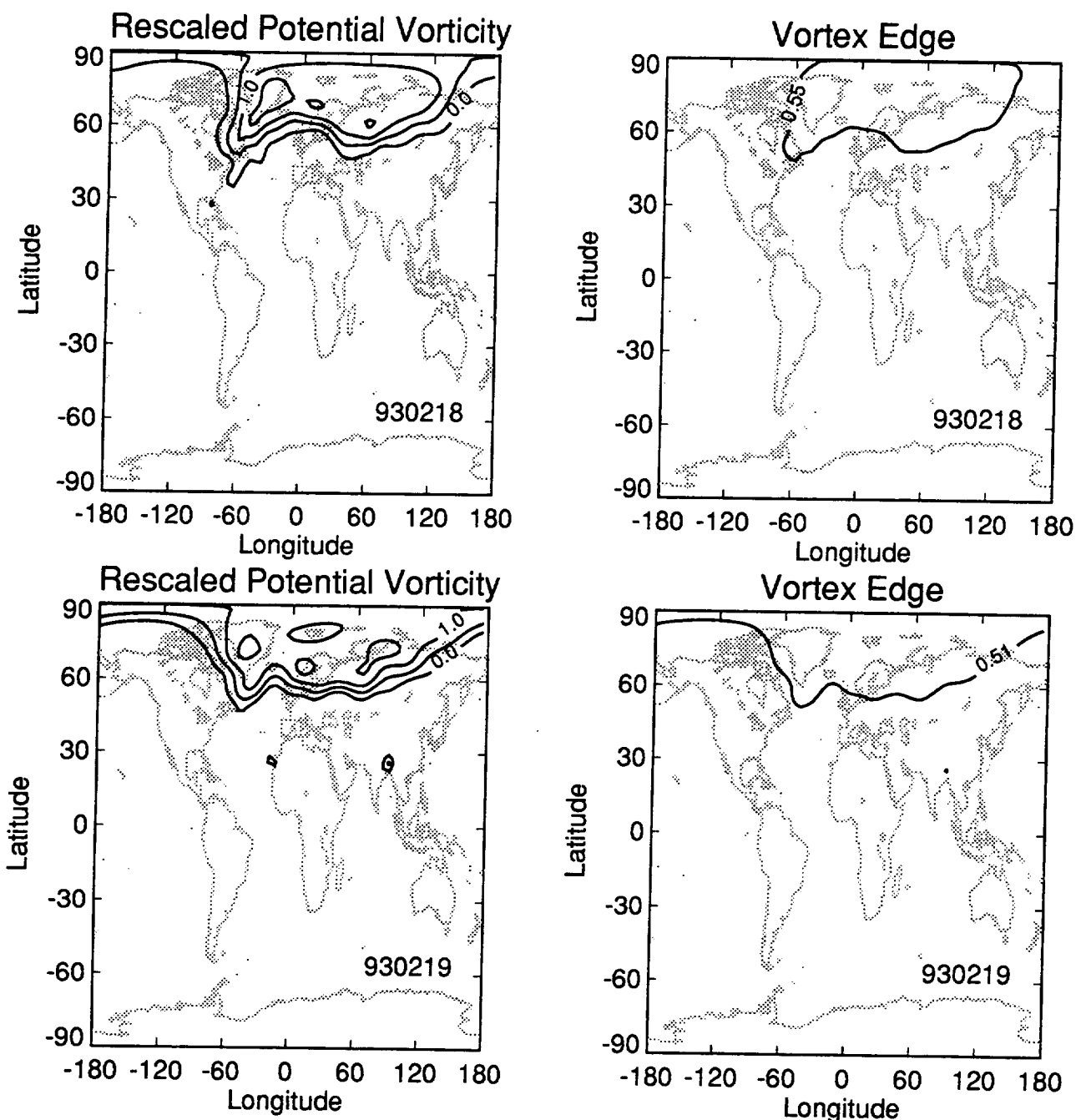
Appendix A. Plots of rescaled potential vorticity and the vortex edge for each day of available data for the winter of 1992-93. Dates are labeled as YYMMDD (year, month, day).



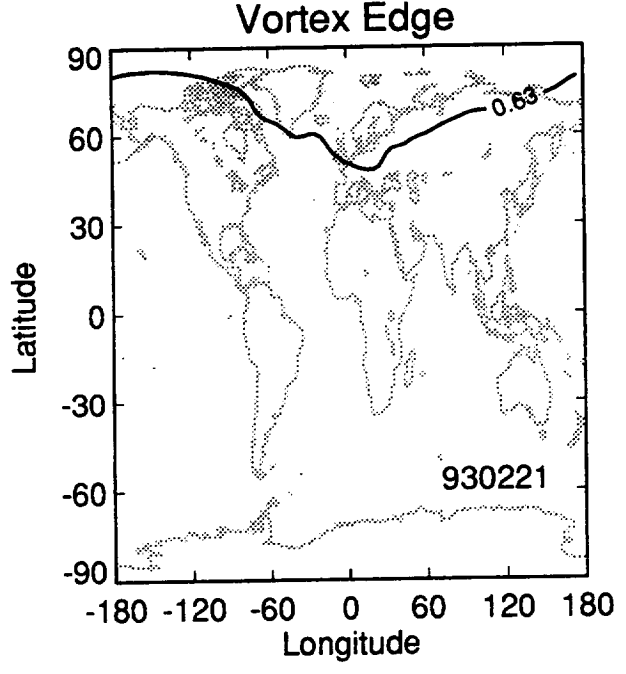
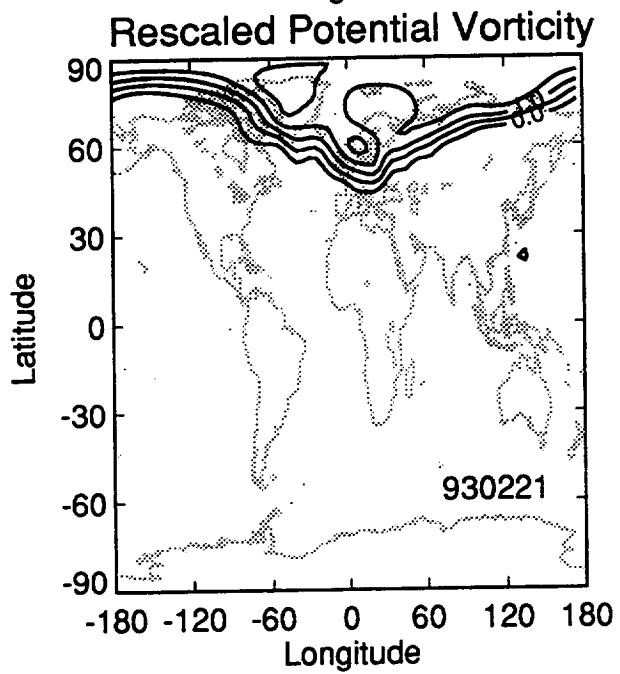
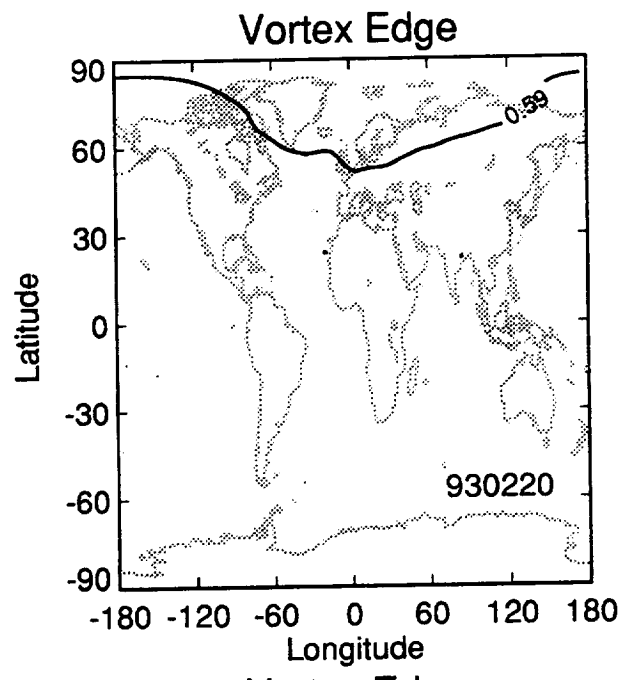
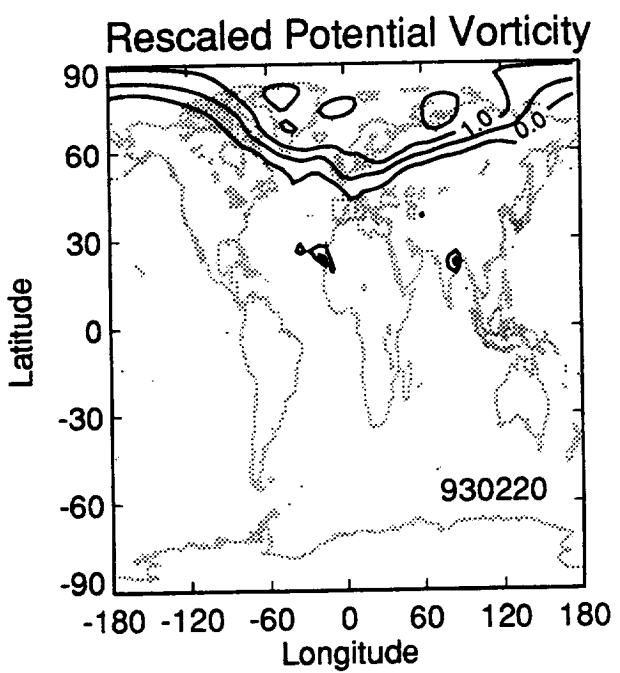
Appendix A. Plots of rescaled potential vorticity and the vortex edge for each day of available data for the winter of 1992-93. Dates are labeled as YYMMDD (year, month, day).



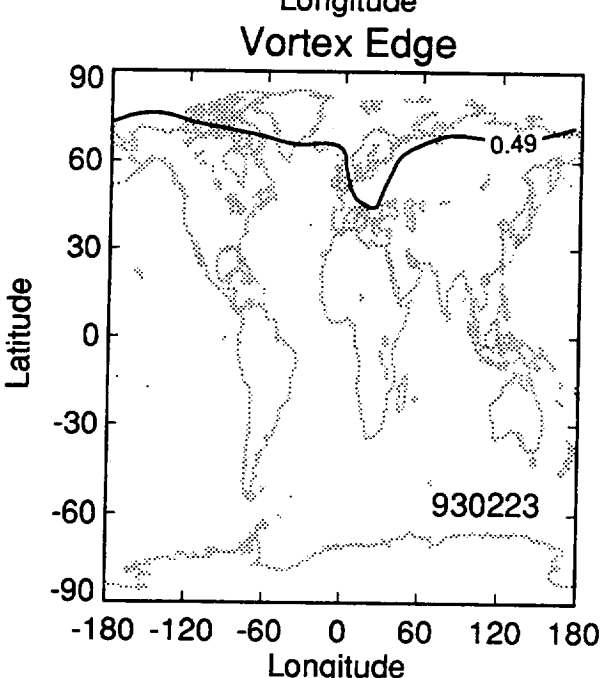
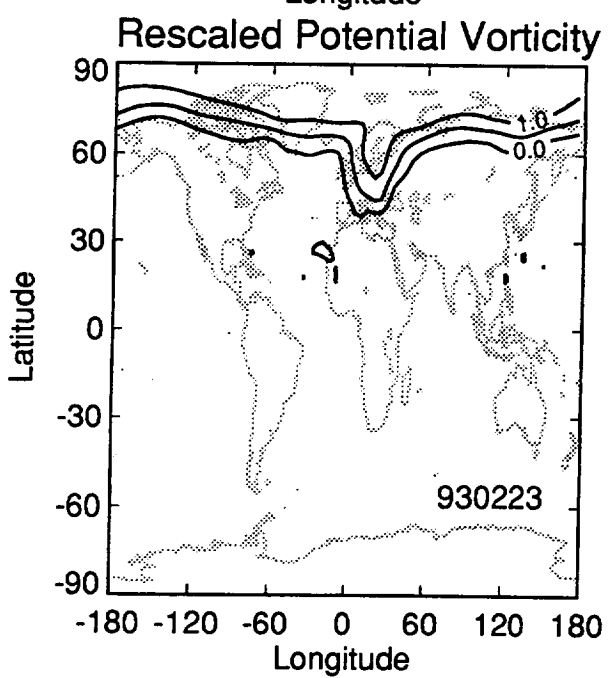
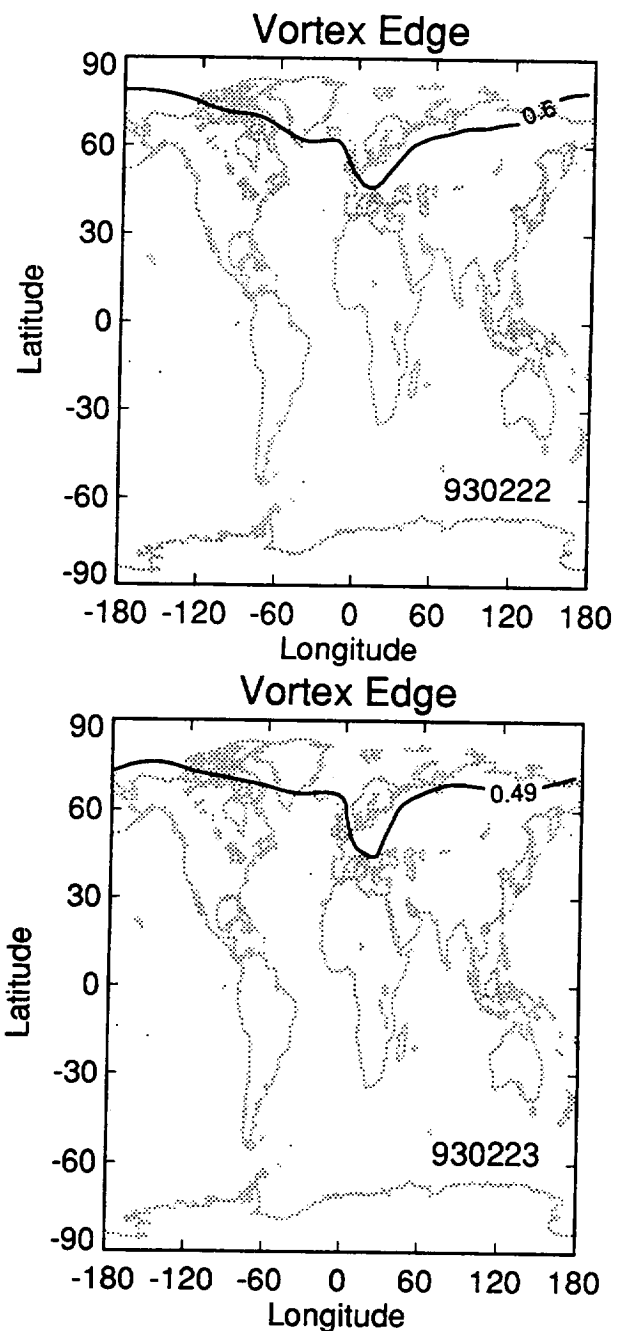
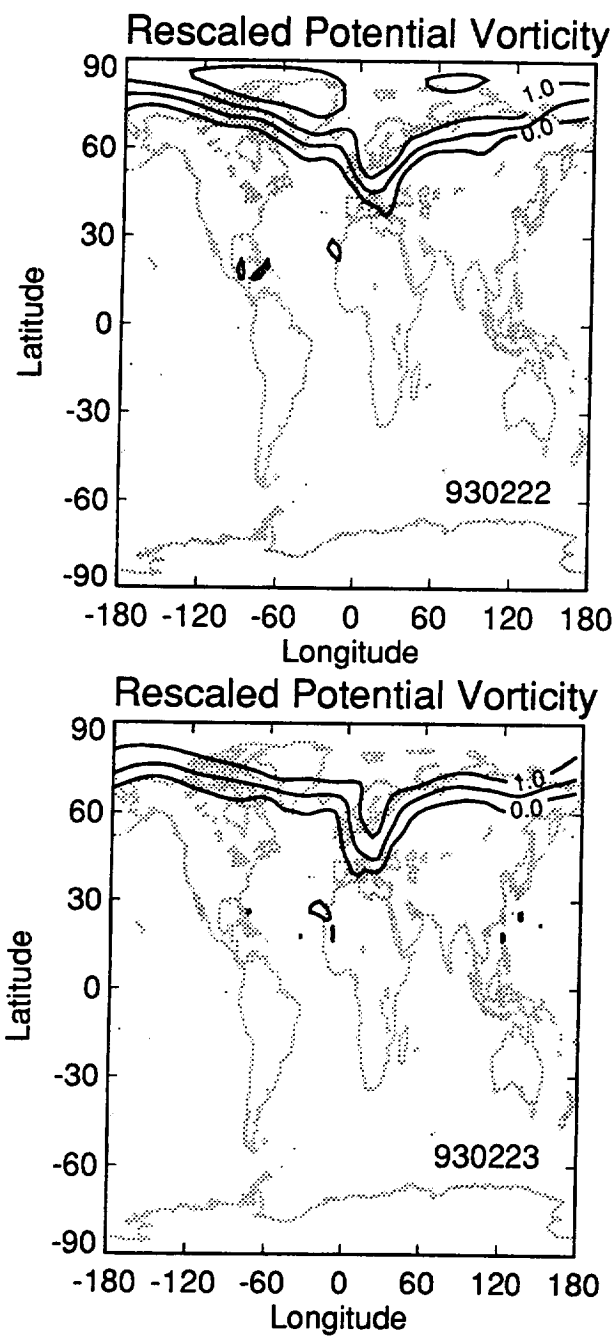
Appendix A. Plots of rescaled potential vorticity and the vortex edge for each day of available data for the winter of 1992-93. Dates are labeled as YYMMDD (year, month, day).



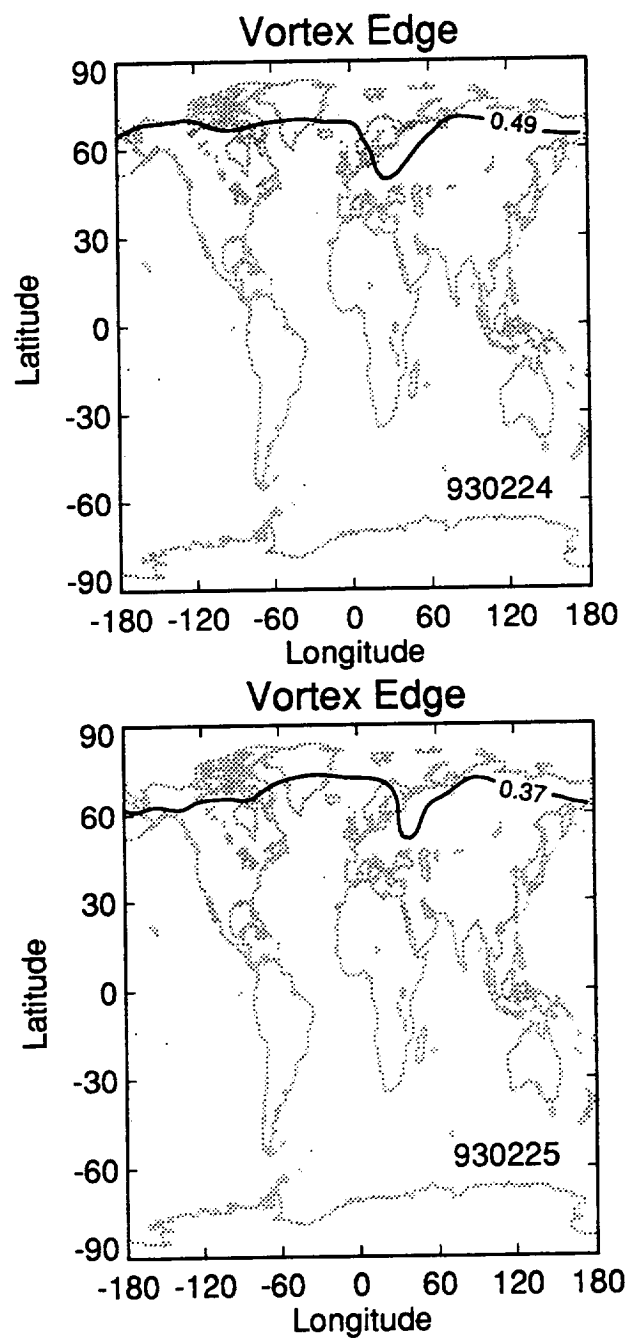
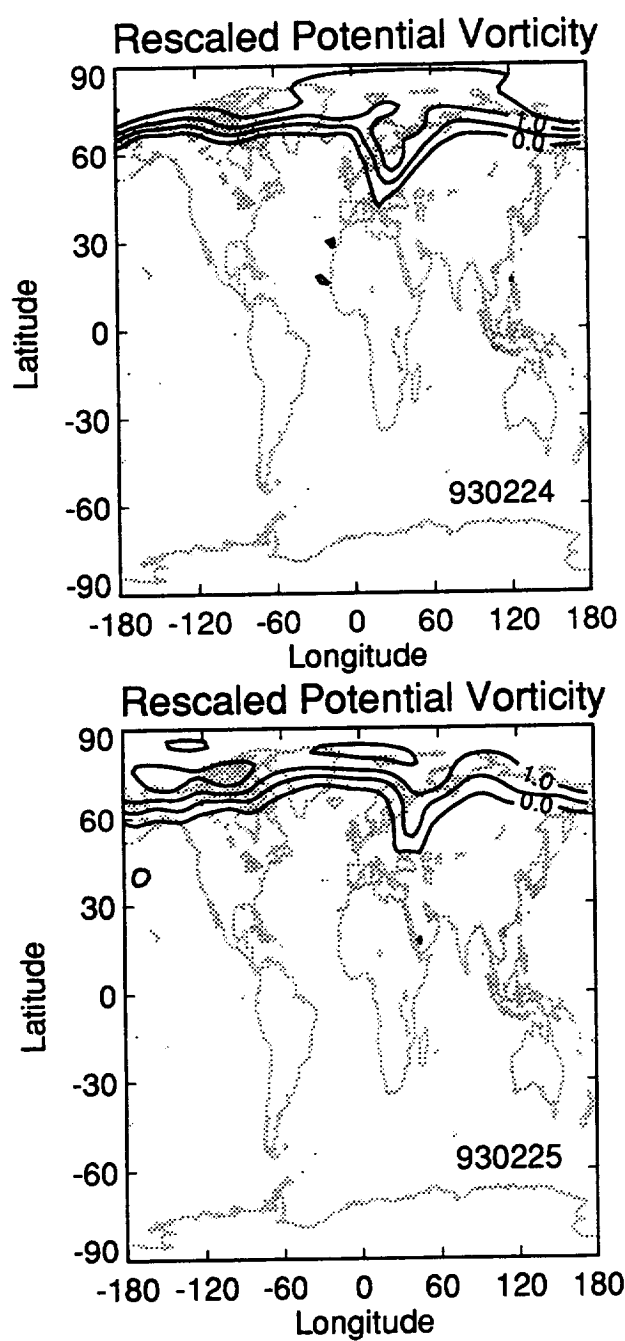
Appendix A. Plots of rescaled potential vorticity and the vortex edge for each day of available data for the winter of 1992-93. Dates are labeled as YYMMDD (year, month, day).



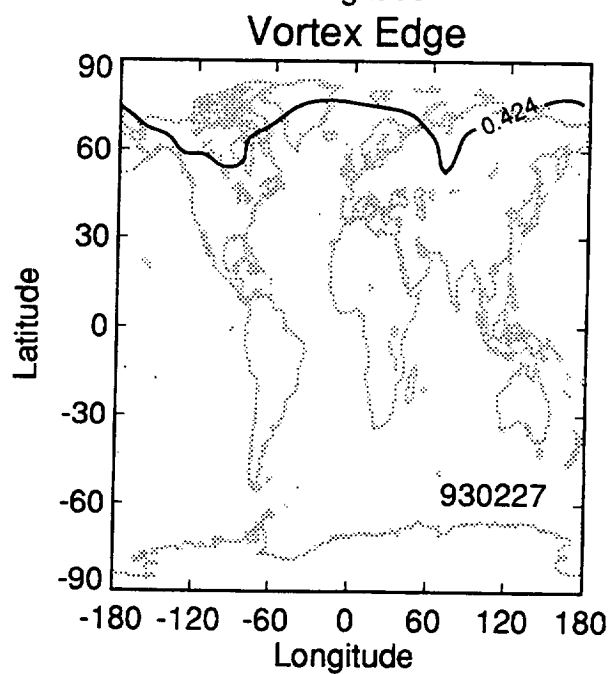
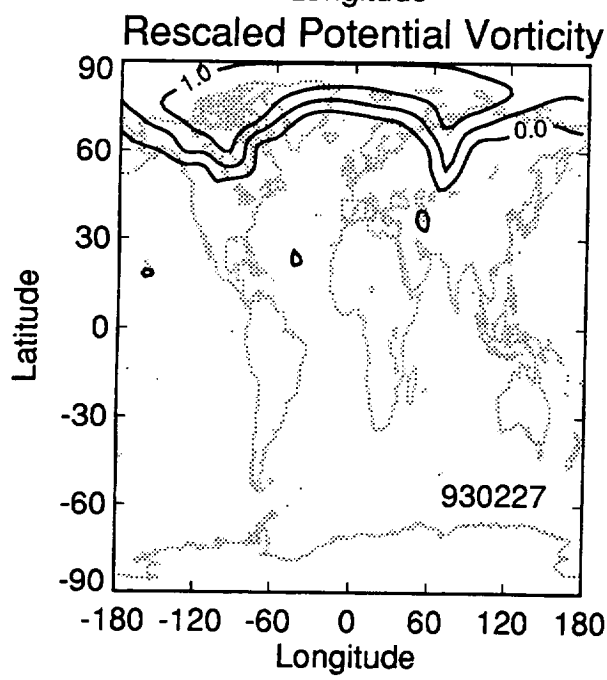
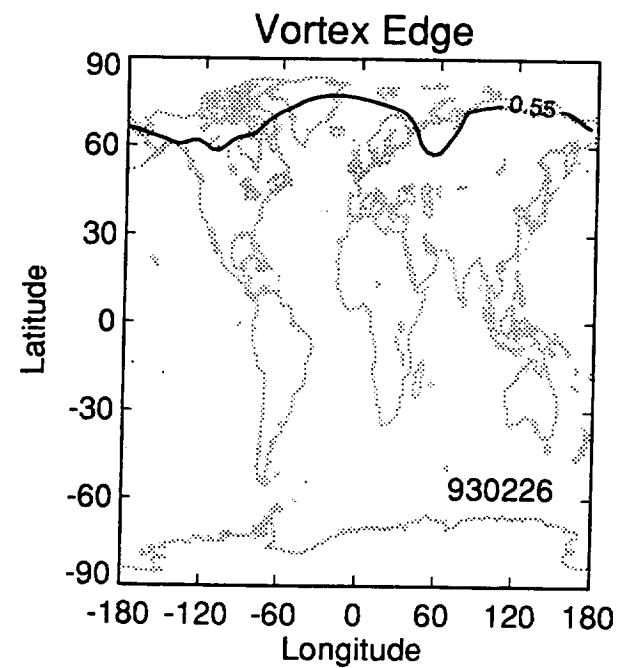
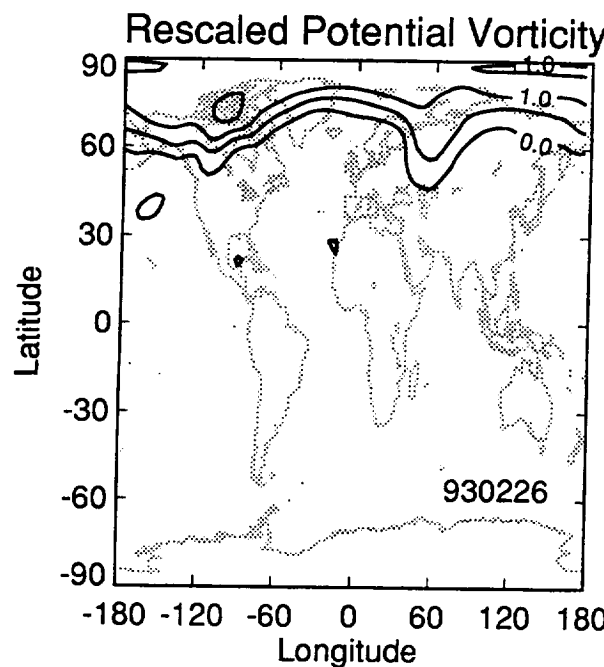
Appendix A. Plots of rescaled potential vorticity and the vortex edge for each day of available data for the winter of 1992-93. Dates are labeled as YYMMDD (year, month, day).



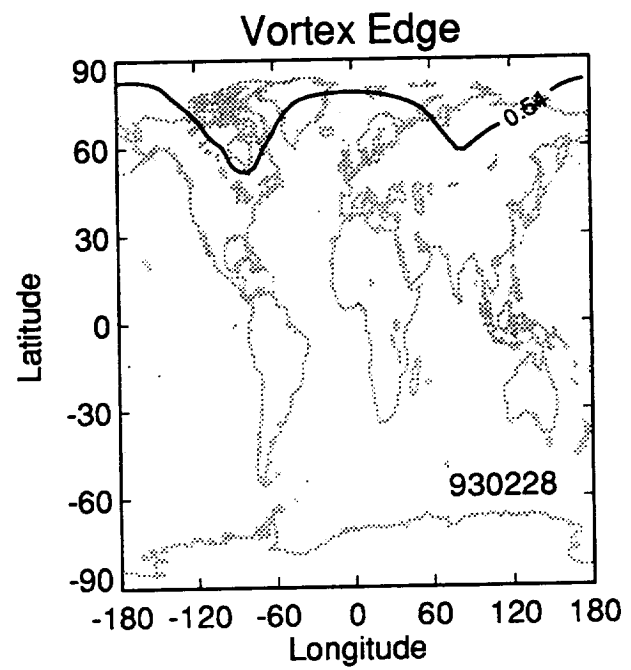
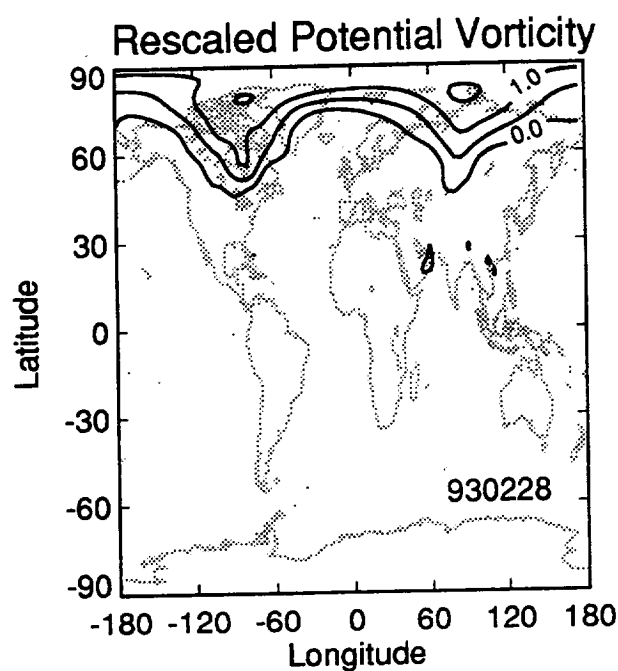
Appendix A. Plots of rescaled potential vorticity and the vortex edge for each day of available data for the winter of 1992-93. Dates are labeled as YYMMDD (year, month, day).



Appendix A. Plots of rescaled potential vorticity and the vortex edge for each day of available data for the winter of 1992-93. Dates are labeled as YYMMDD (year, month, day).



Appendix A. Plots of rescaled potential vorticity and the vortex edge for each day of available data for the winter of 1992-93. Dates are labeled as YYMMDD (year, month, day).



Appendix A. Plots of rescaled potential vorticity and the vortex edge for each day of available data for the winter of 1992-93. Dates are labeled as YYMMDD (year, month, day).

Appendix B. Plots of Emissions within the Polar Vortex for 1978-94

In this appendix, plots of the amount of emissions deposited within the Arctic polar vortex as a function of each day of the winters from 1978 to 1994 are plotted. For these calculations the emission inventory for a fleet of 500 Mach 2.4 HSCTs flying on the universal airline network [Baughcum and Henderson, 1995] were used.

For each winter studied, the fuel burned per day within the vortex was calculated using both the liberal and conservative analyses, as described in Section 2. Plots are provided for each. The top panel of each plot shows the daily fuel burned within the polar vortex as a function of day relative to January 1 of that winter. The bottom panel shows the fraction of global fuel burned above 17 kilometers altitude which was deposited directly within the vortex.

On all plots, the dark solid line corresponds to the average value for that winter. The dashed lines in the plots corresponds to the average plus one standard deviation.

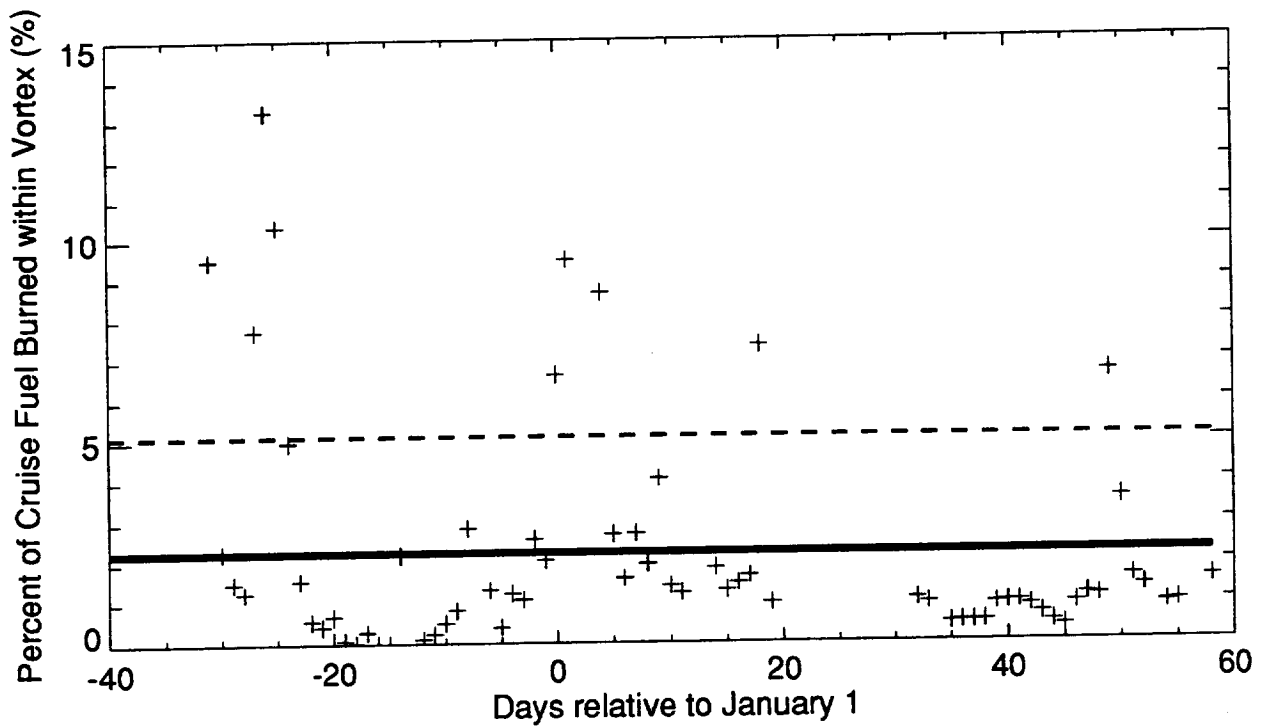
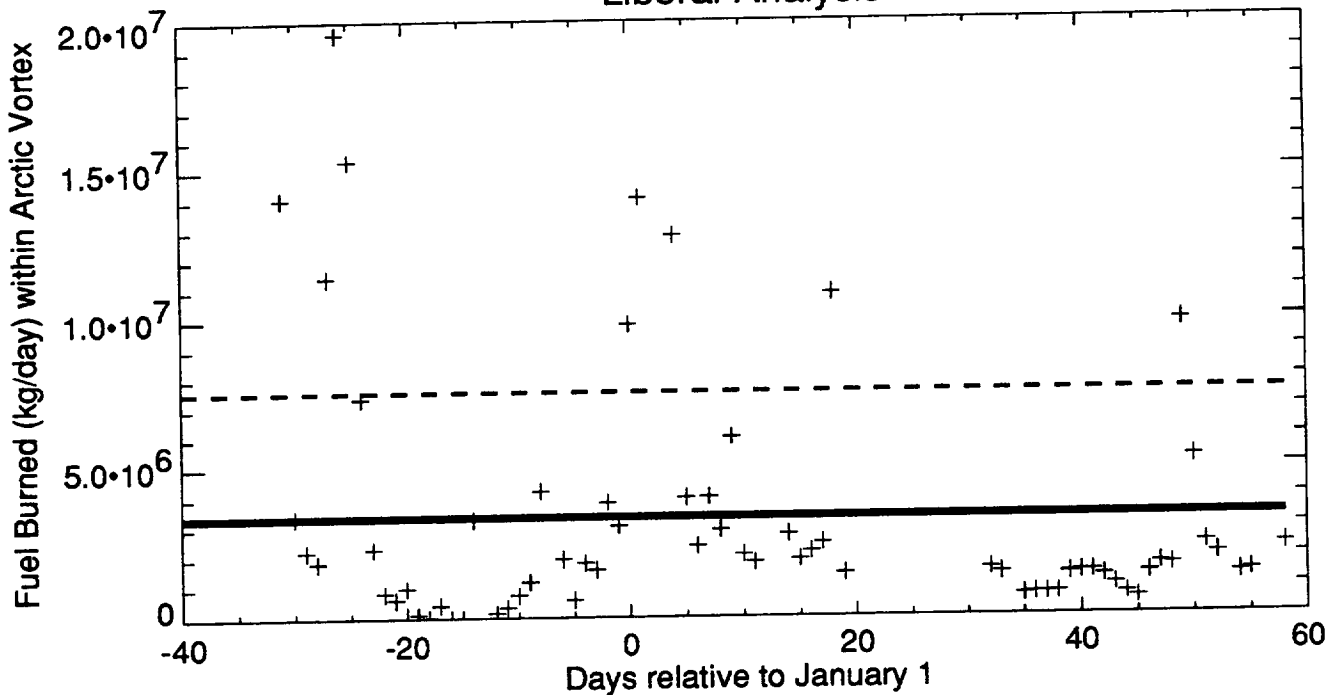
As the plots show, approximately 1-3% of the cruise fuel burn occurs within the vortex on most days. But for every winter, episodes occur in which the polar vortex extends into the North Atlantic. For those days a much larger fraction of the emissions would occur within the vortex.

The plots are only shown for fuel burned. Since flights within the vortex would only occur during stratospheric cruise, the other emissions (NOx, H₂O, CO, and hydrocarbons) can be calculated from the fuel burned using the emission indices corresponding to stratospheric cruise conditions. These are summarized in Table B-1.

Table B-1. Recommended emission indices in units of grams of emission/kilogram fuel burned for the year 2015.

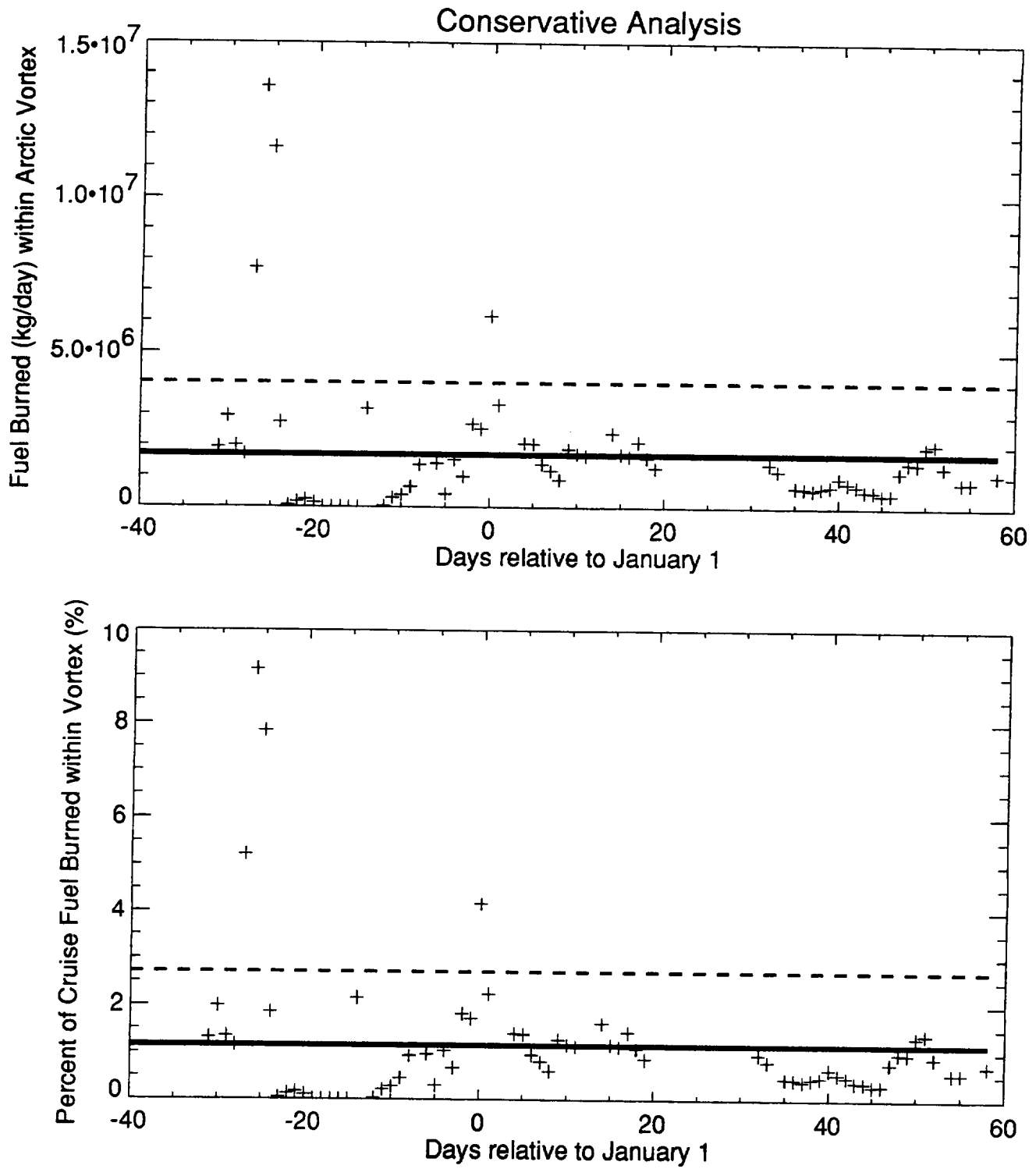
Emission	Emission Index
NOx (as NO ₂)	5.0
Carbon Monoxide (CO)	2.9
Hydrocarbons	0.3
Carbon Dioxide (CO ₂)	3155
Water (H ₂ O)	1237
Sulfur oxides (as SO ₂)	0.4

Liberal Analysis



Winter of 1978-9
 Universal Airline Network 500 Mach 2.4 HSCTs EI(NOx)=5

Solid line = Mean value
 Dashed line = Mean value + 1 standard deviation



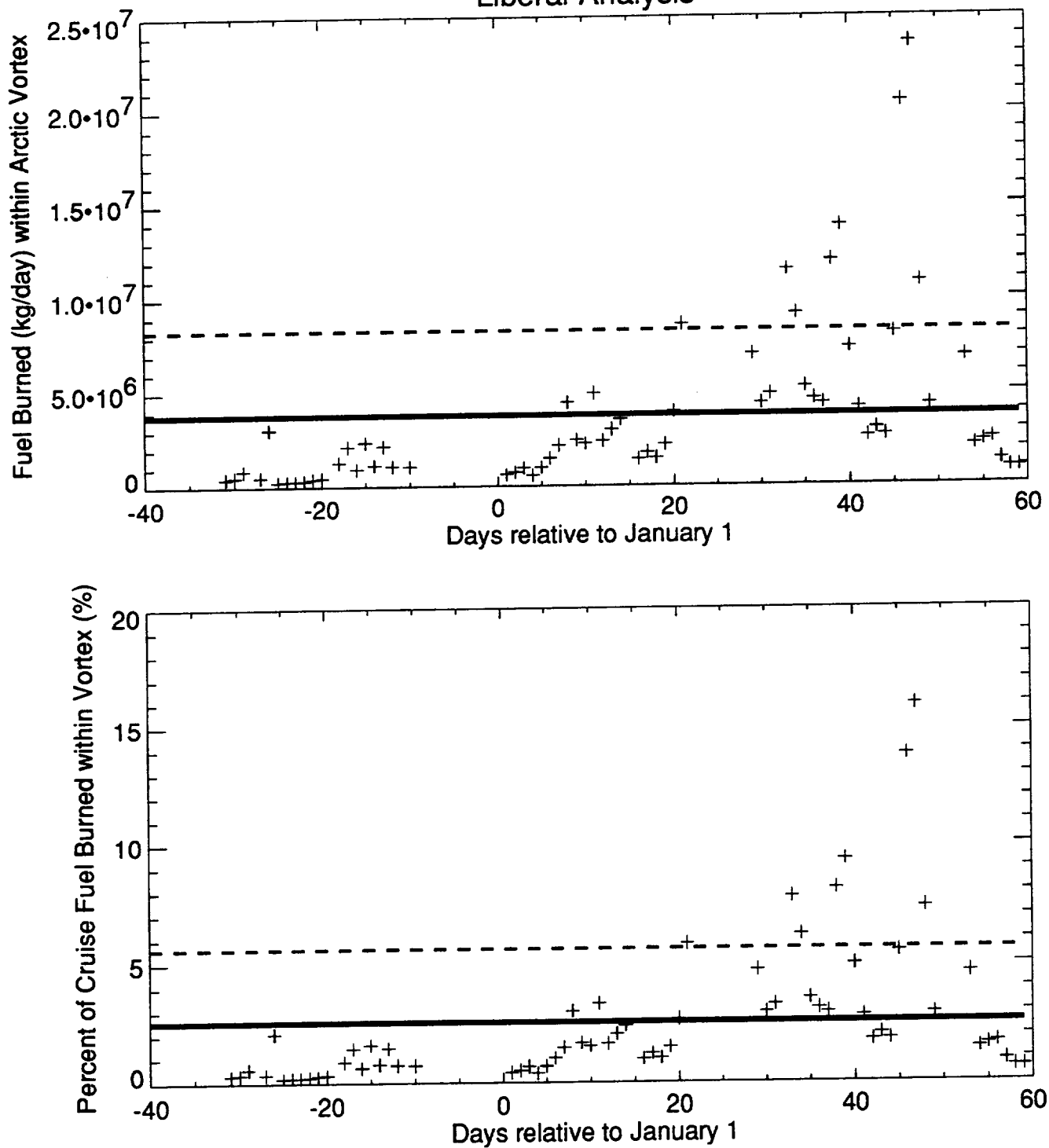
Winter of 1978-9

Universal Airline Network 500 Mach 2.4 HSCTs EI(NOx)=5

Solid line = Mean value

Dashed line = Mean value + 1 standard deviation

Liberal Analysis

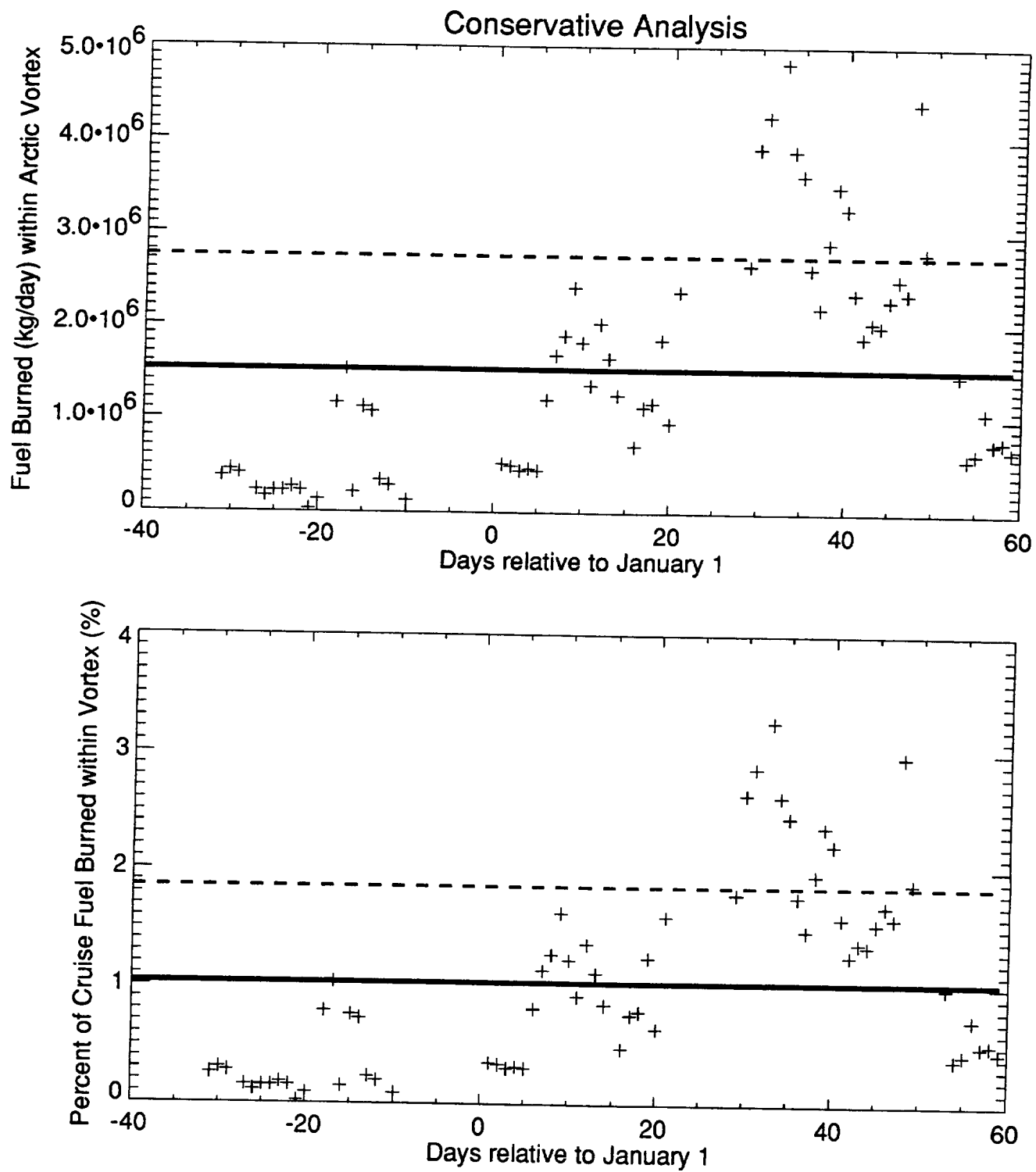


Winter of 1979-80

Universal Airline Network 500 Mach 2.4 HSCTs EI(NOx)=5

Solid line = Mean value

Dashed line = Mean value + 1 standard deviation



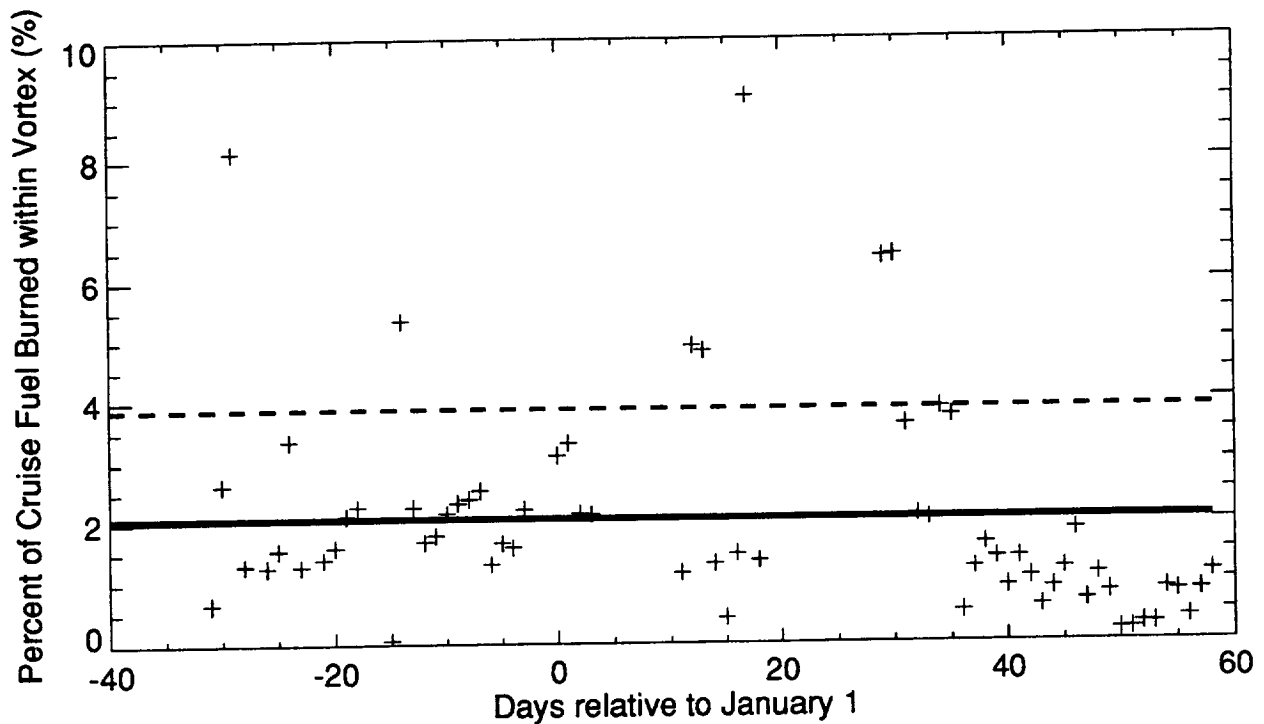
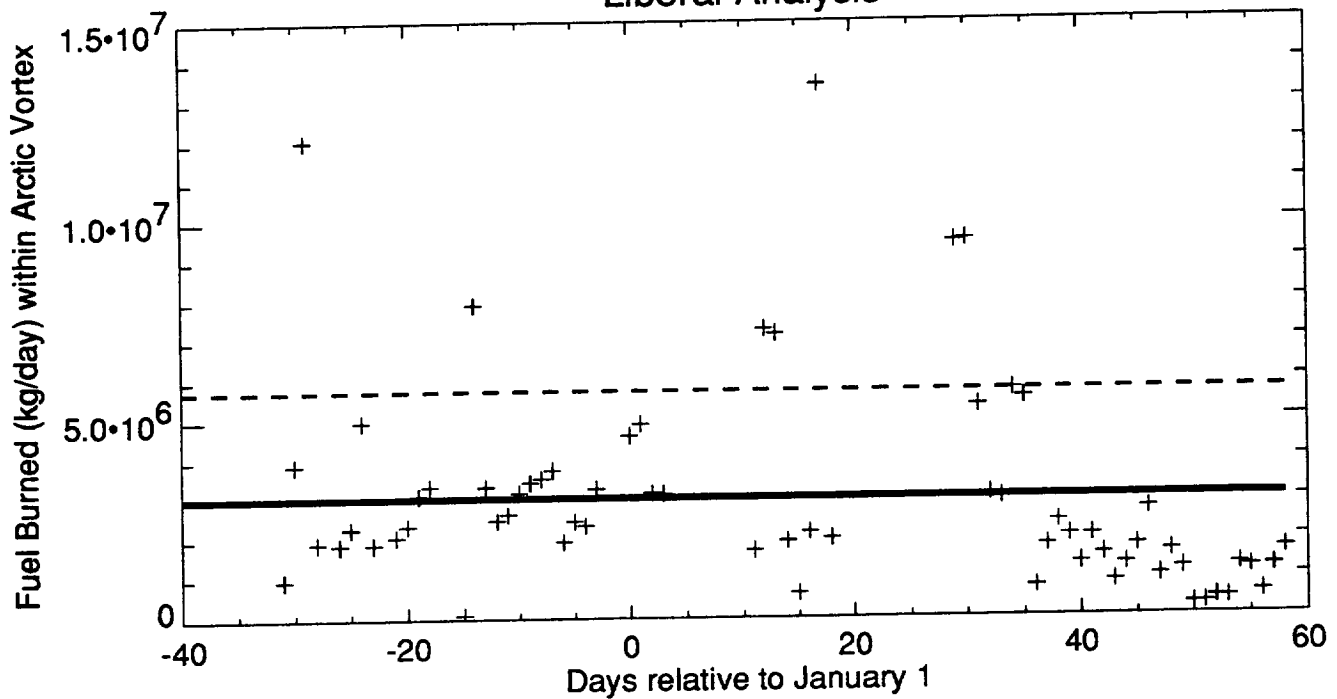
Winter of 1979-80

Universal Airline Network 500 Mach 2.4 HSCTs EI(NOx)=5

Solid line = Mean value

Dashed line = Mean value + 1 standard deviation

Liberal Analysis

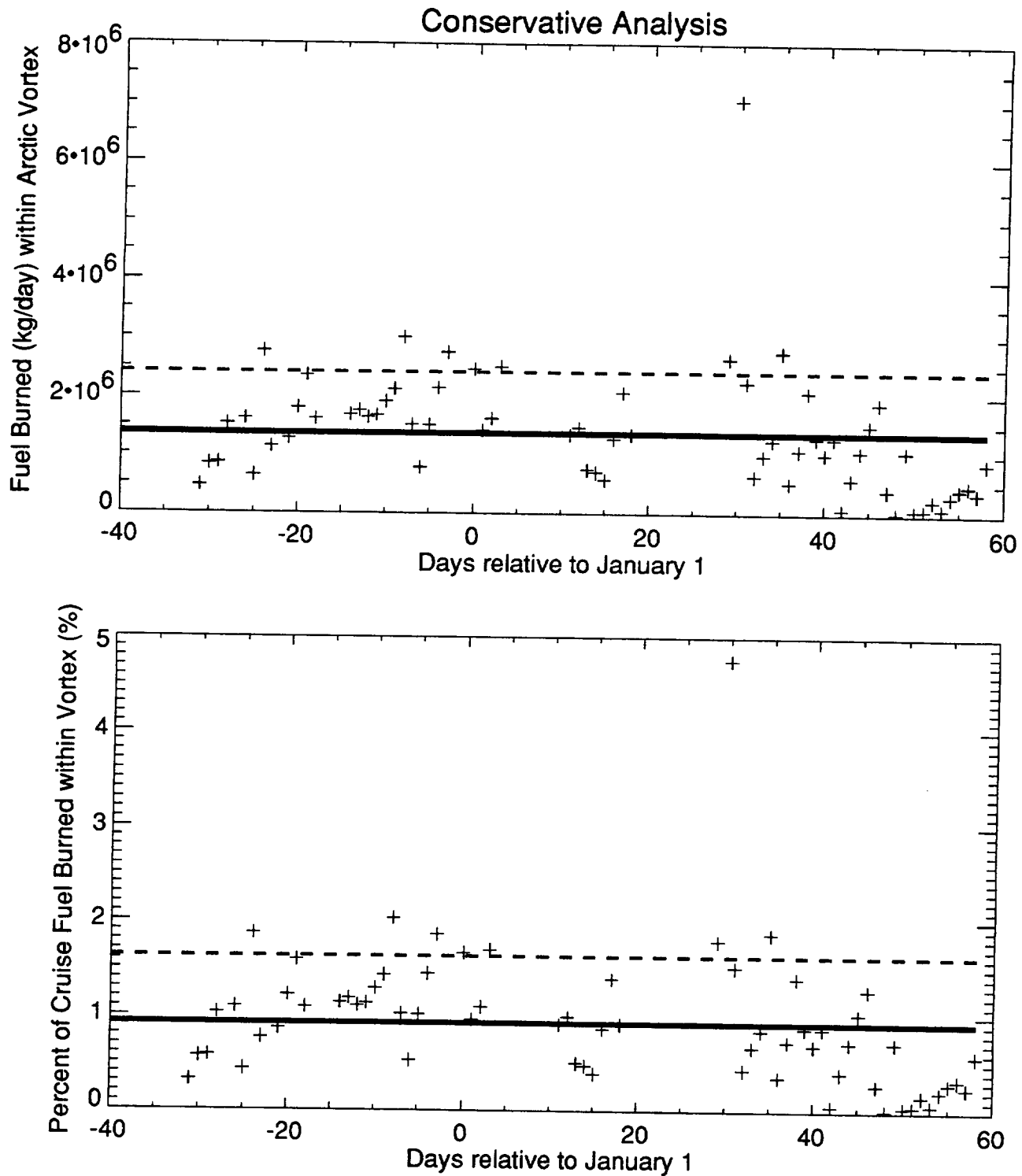


Winter of 1980-1

Universal Airline Network 500 Mach 2.4 HSCTs EI(NO_x)=5

Solid line = Mean value

Dashed line = Mean value + 1 standard deviation

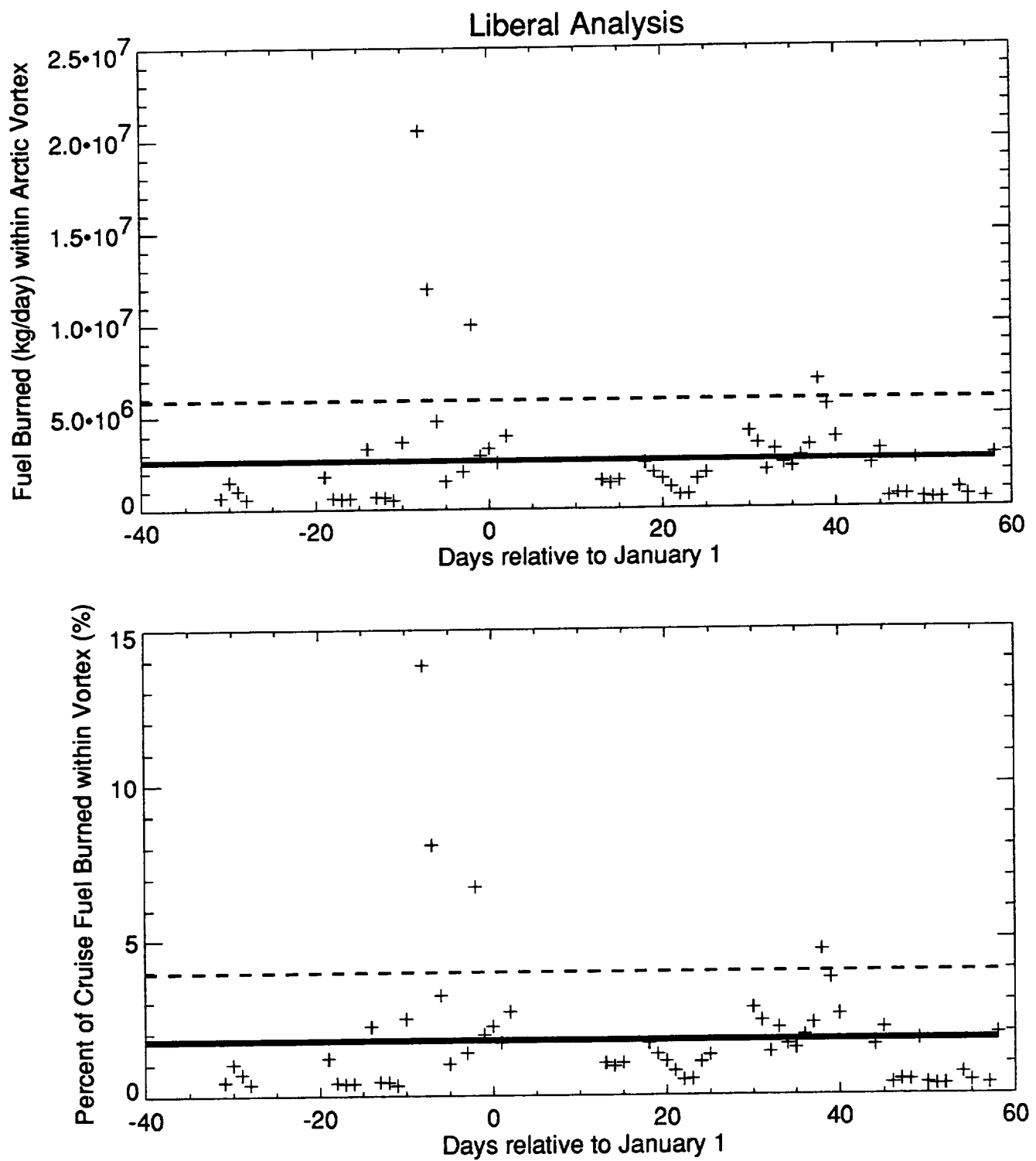


Winter of 1980-1

Universal Airline Network 500 Mach 2.4 HSCTs EI(NO_x)=5

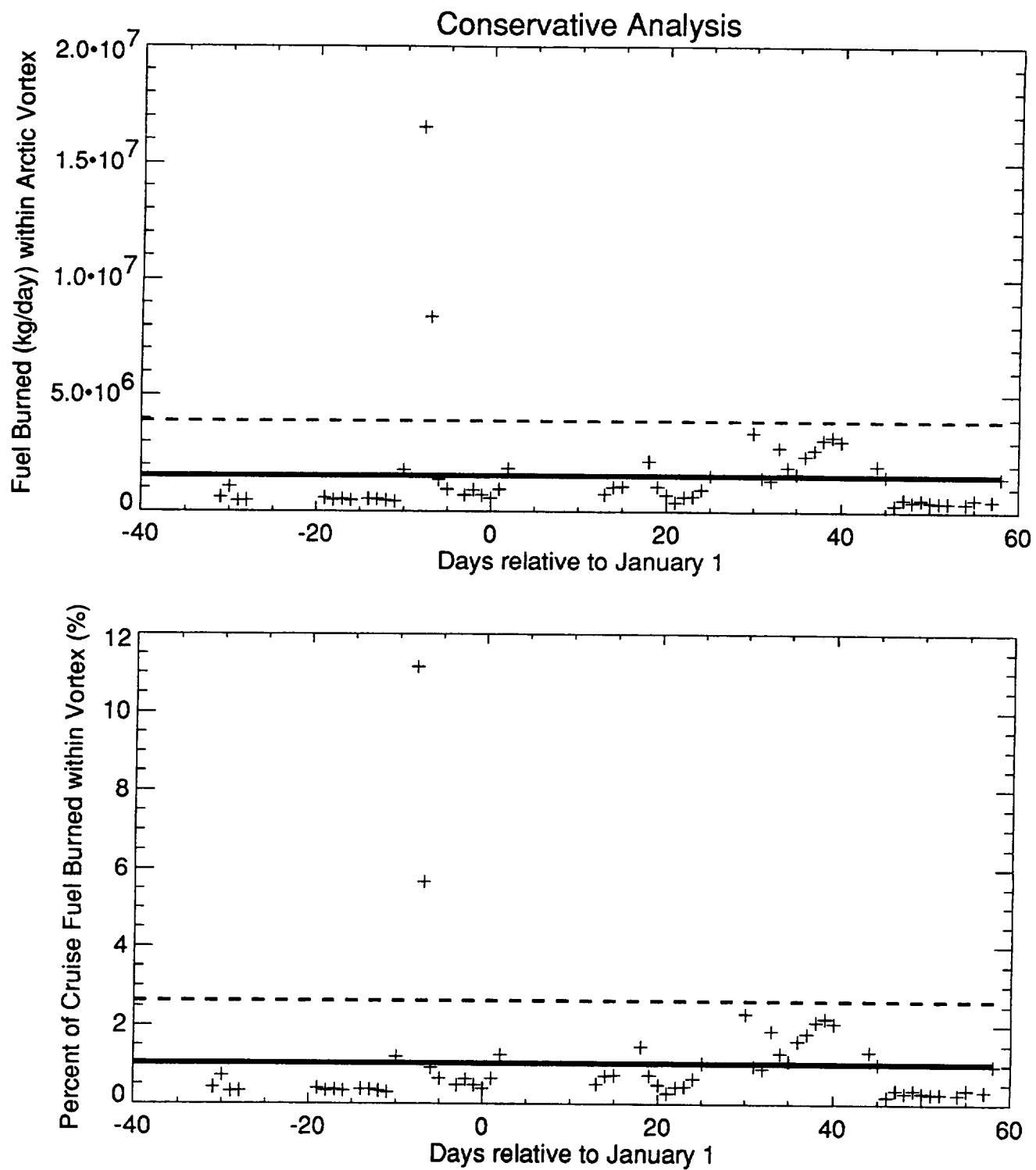
Solid line = Mean value

Dashed line = Mean value + 1 standard deviation



Winter of 1981-2
Universal Airline Network 500 Mach 2.4 HSCTs EI(NOx)=5

Solid line = Mean value
Dashed line = Mean value + 1 standard deviation

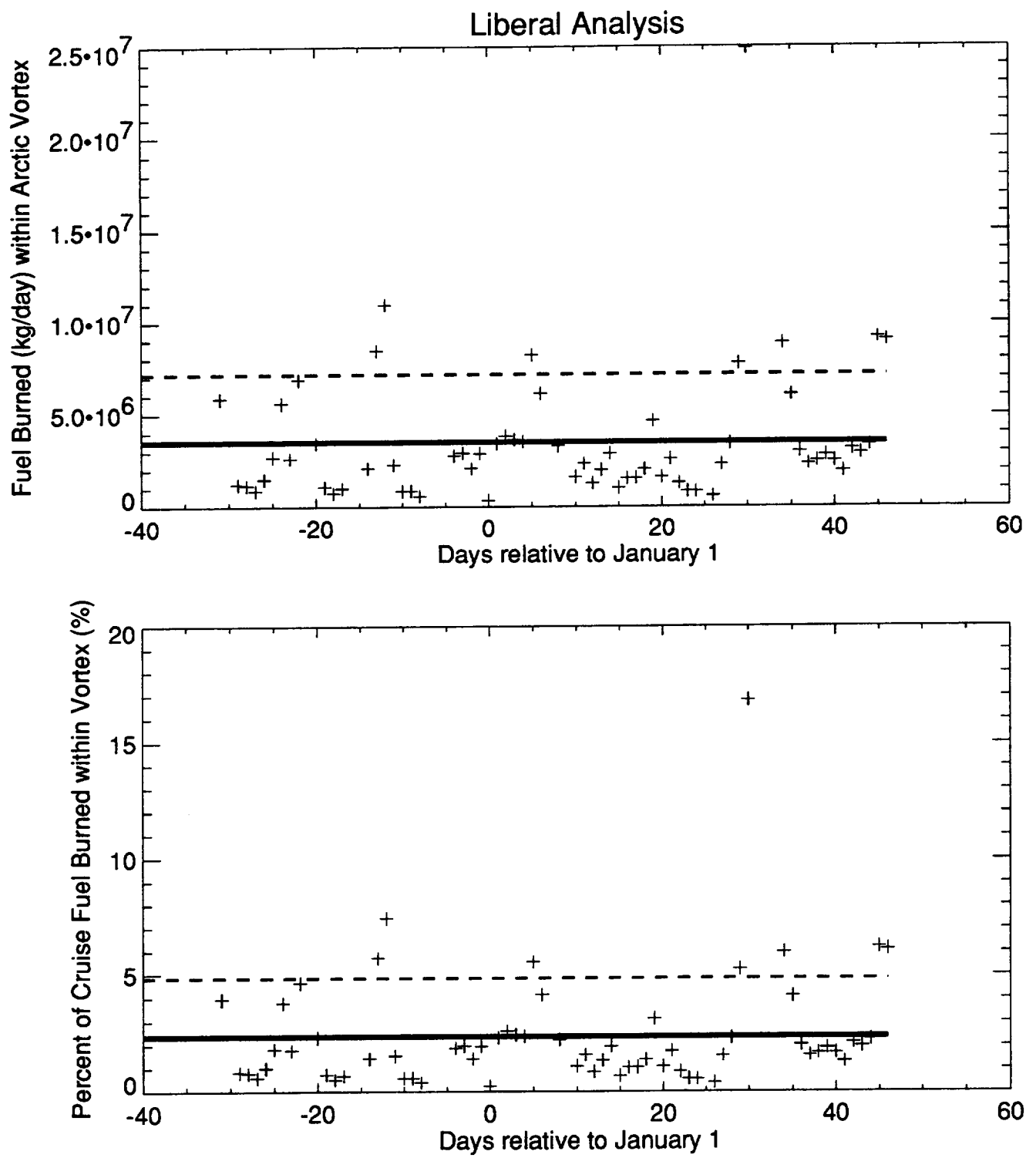


Winter of 1981-2

Universal Airline Network 500 Mach 2.4 HSCTs EI(NOx)=5

Solid line = Mean value

Dashed line = Mean value + 1 standard deviation

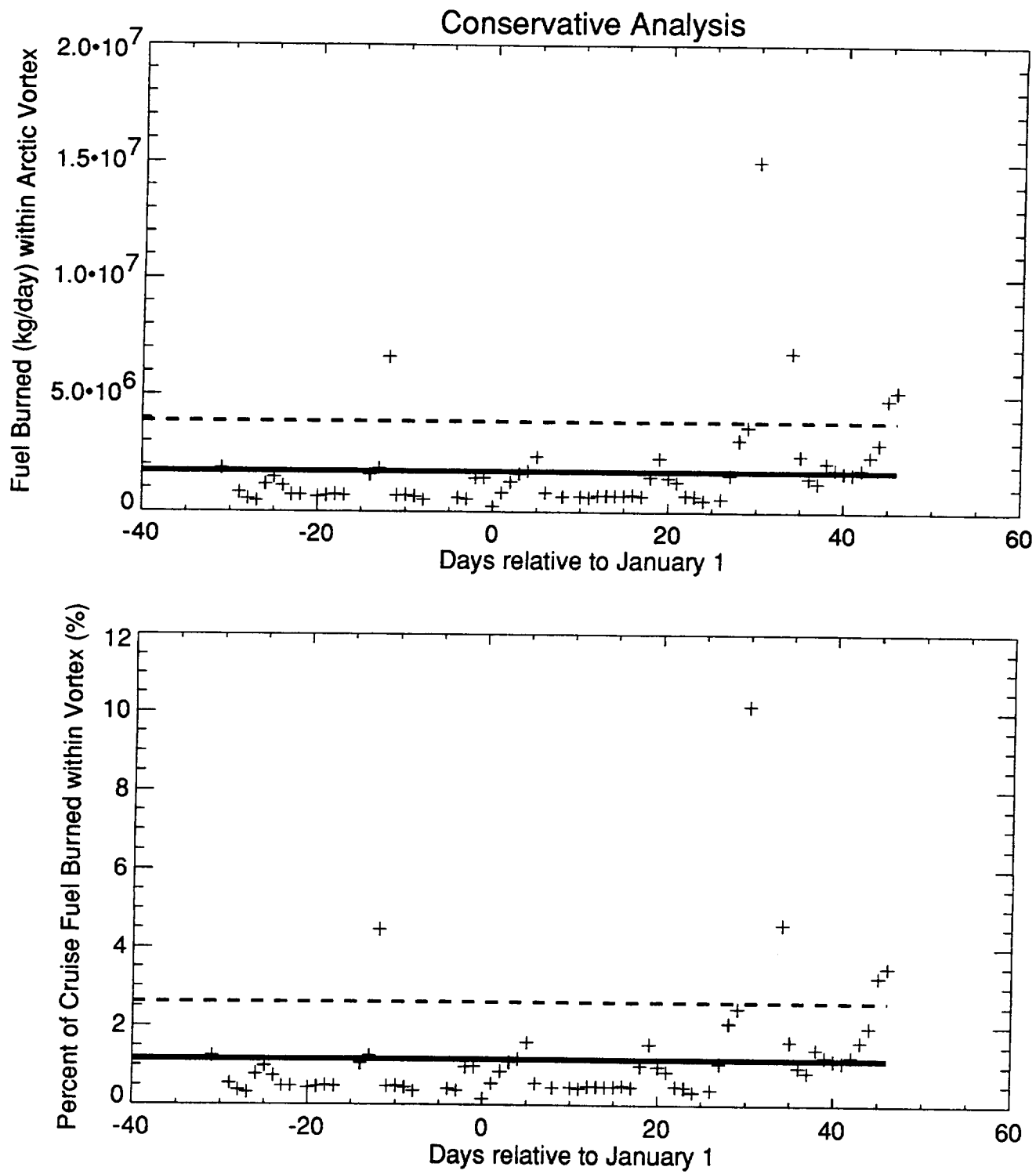


Winter of 1982-3

Universal Airline Network 500 Mach 2.4 HSCTs EI(NO_x)=5

Solid line = Mean value

Dashed line = Mean value + 1 standard deviation

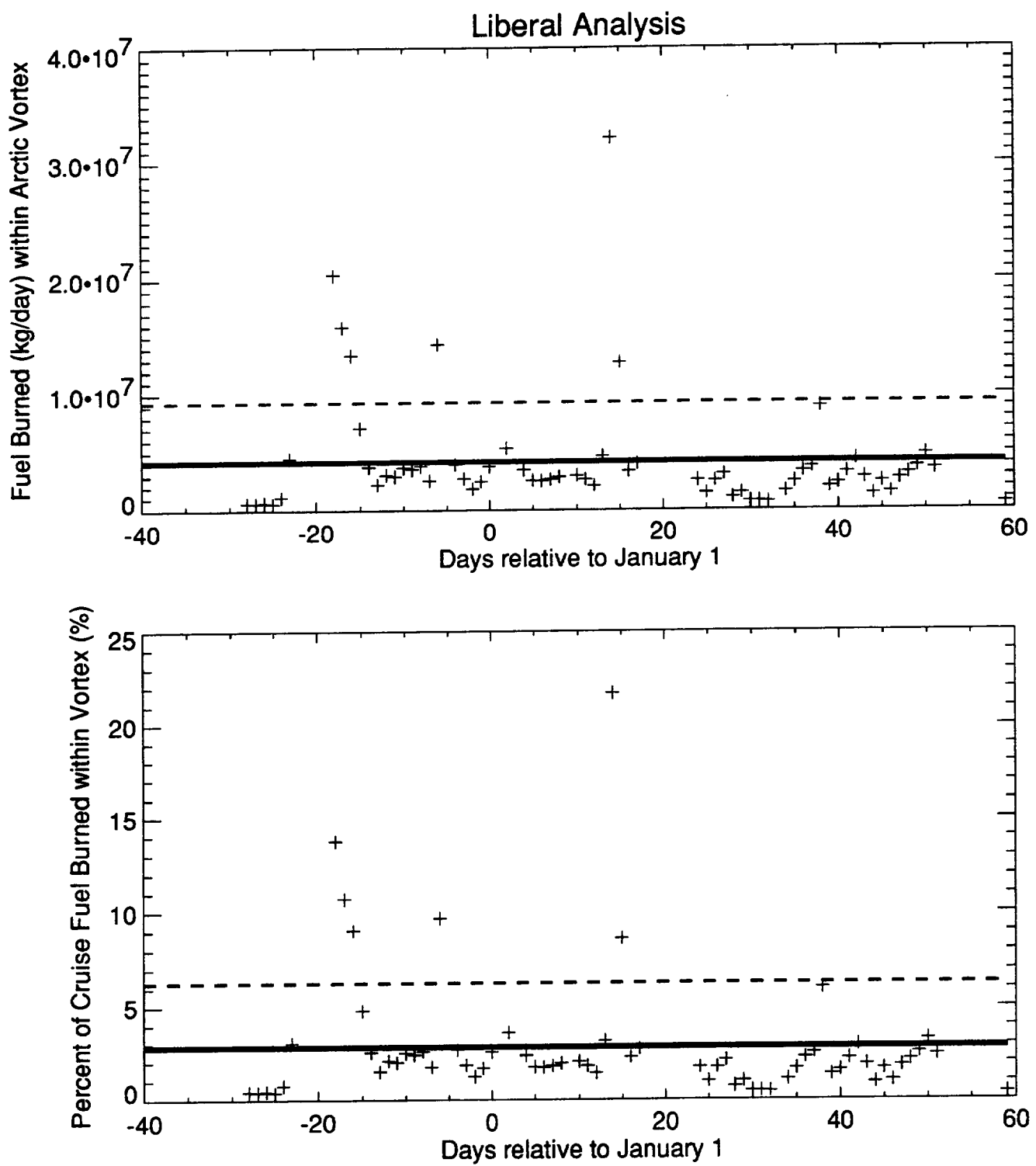


Winter of 1982-3

Universal Airline Network 500 Mach 2.4 HSCTs EI(NOx)=5

Solid line = Mean value

Dashed line = Mean value + 1 standard deviation

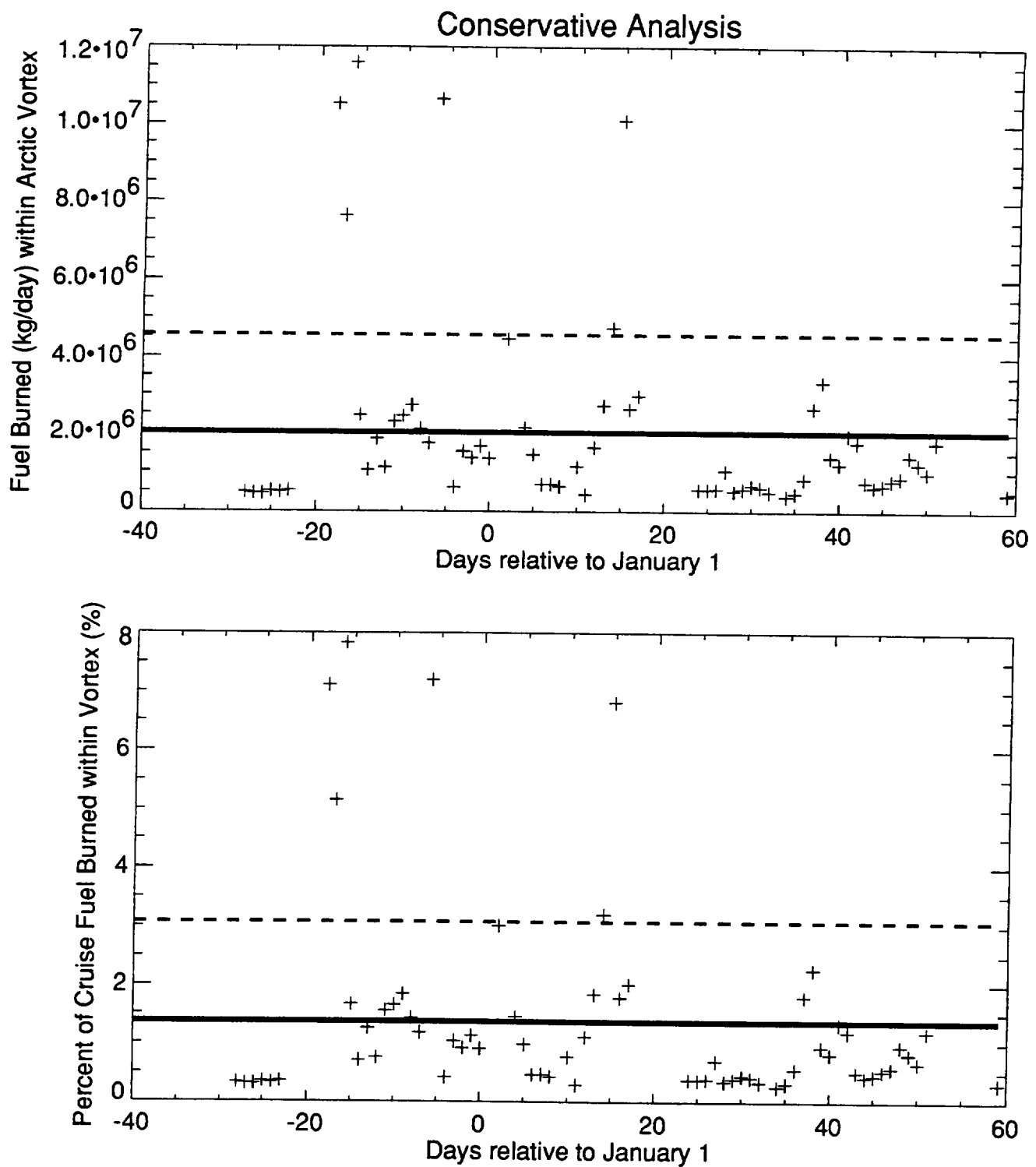


Winter of 1983-4

Universal Airline Network 500 Mach 2.4 HSCTs EI(NOx)=5

Solid line = Mean value

Dashed line = Mean value + 1 standard deviation



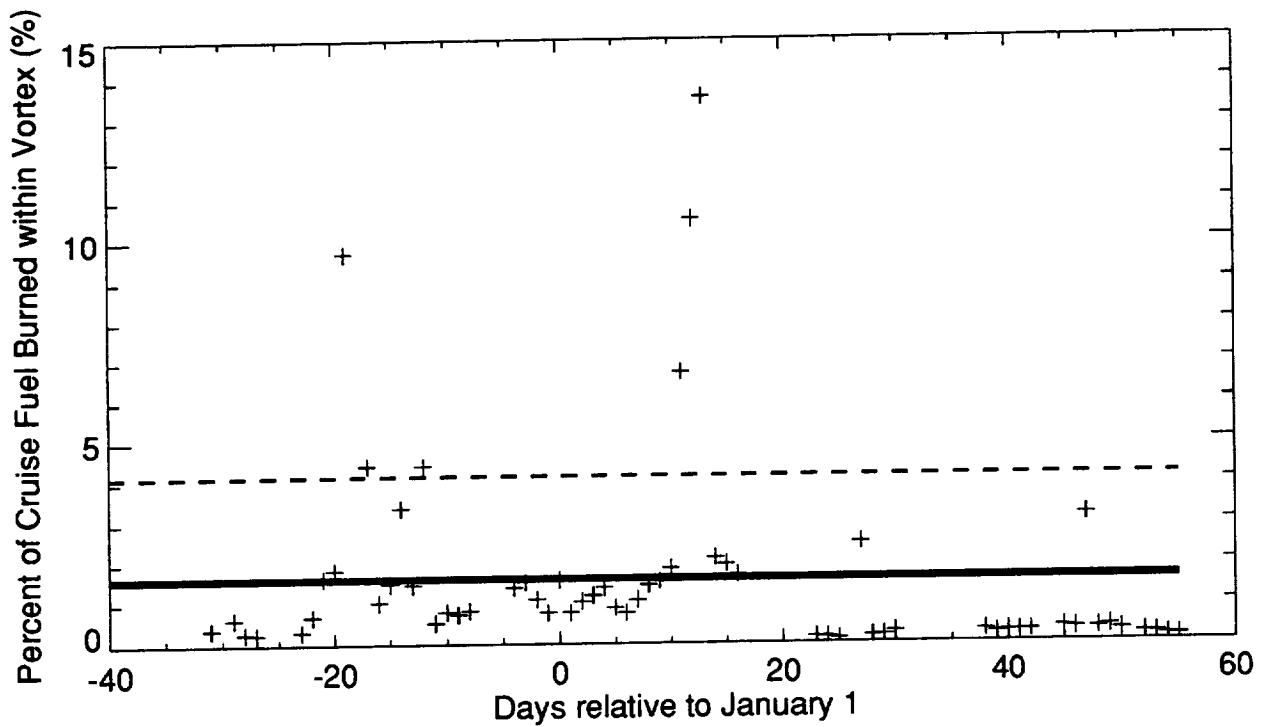
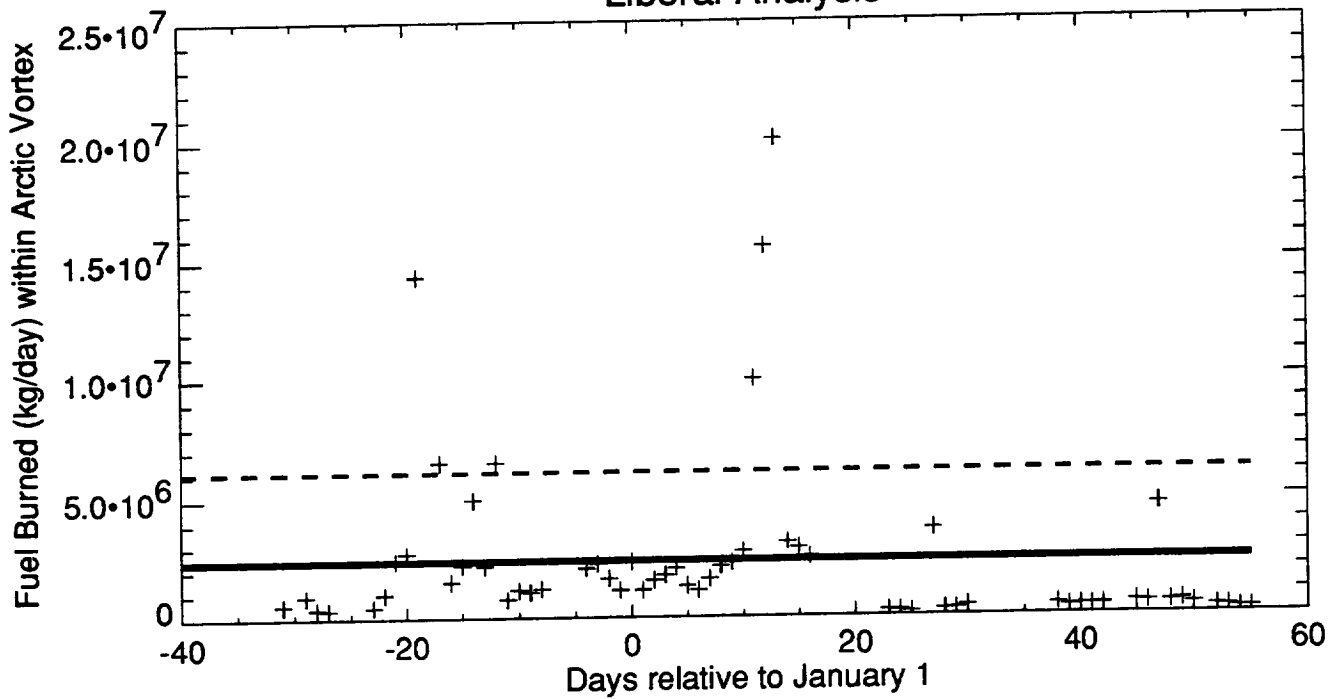
Winter of 1983-4

Universal Airline Network 500 Mach 2.4 HSCTs EI(NO_x)=5

Solid line = Mean value

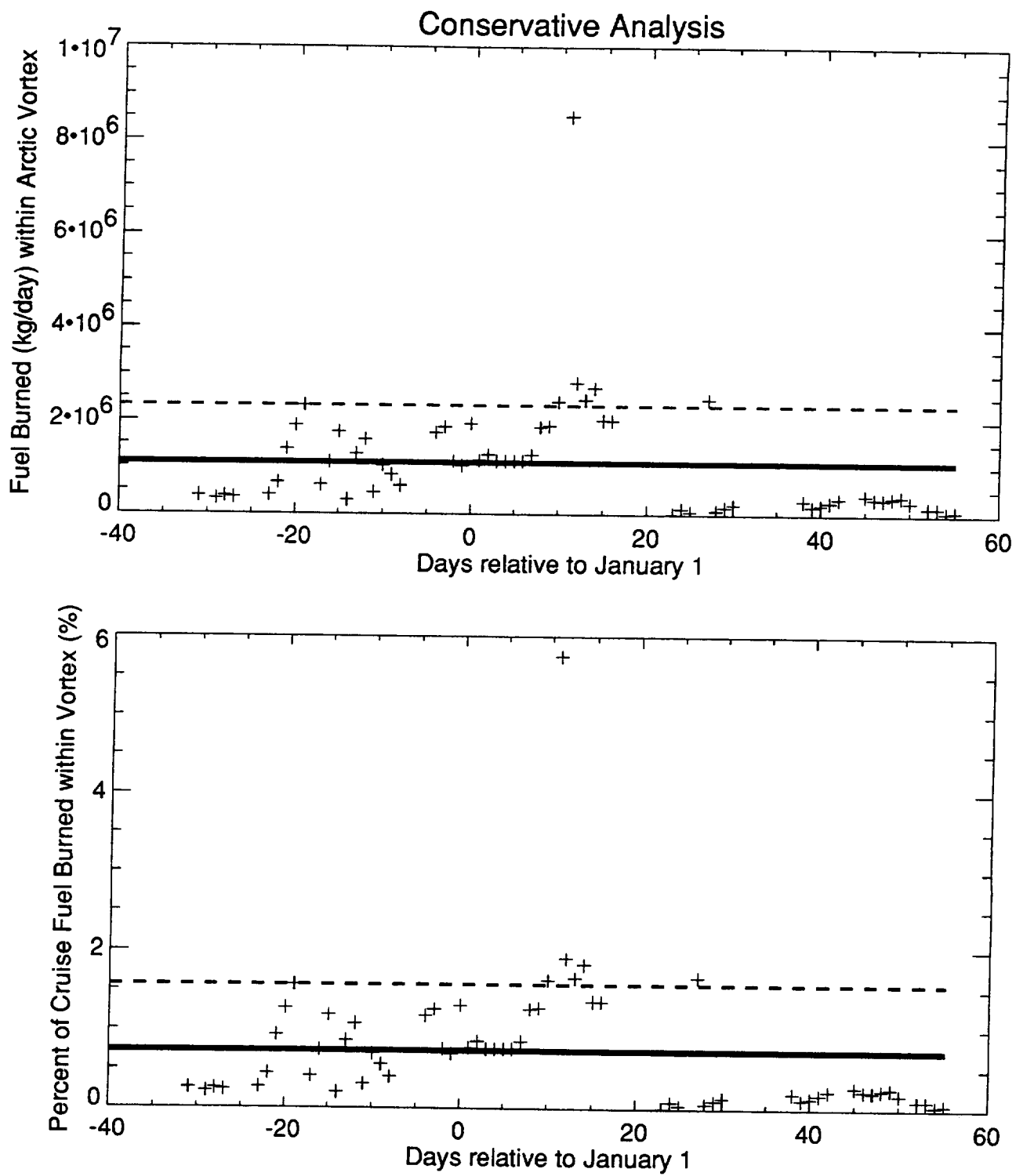
Dashed line = Mean value + 1 standard deviation

Liberal Analysis



Winter of 1984-5
 Universal Airline Network 500 Mach 2.4 HSCTs EI(NO_x)=5

Solid line = Mean value
 Dashed line = Mean value + 1 standard deviation

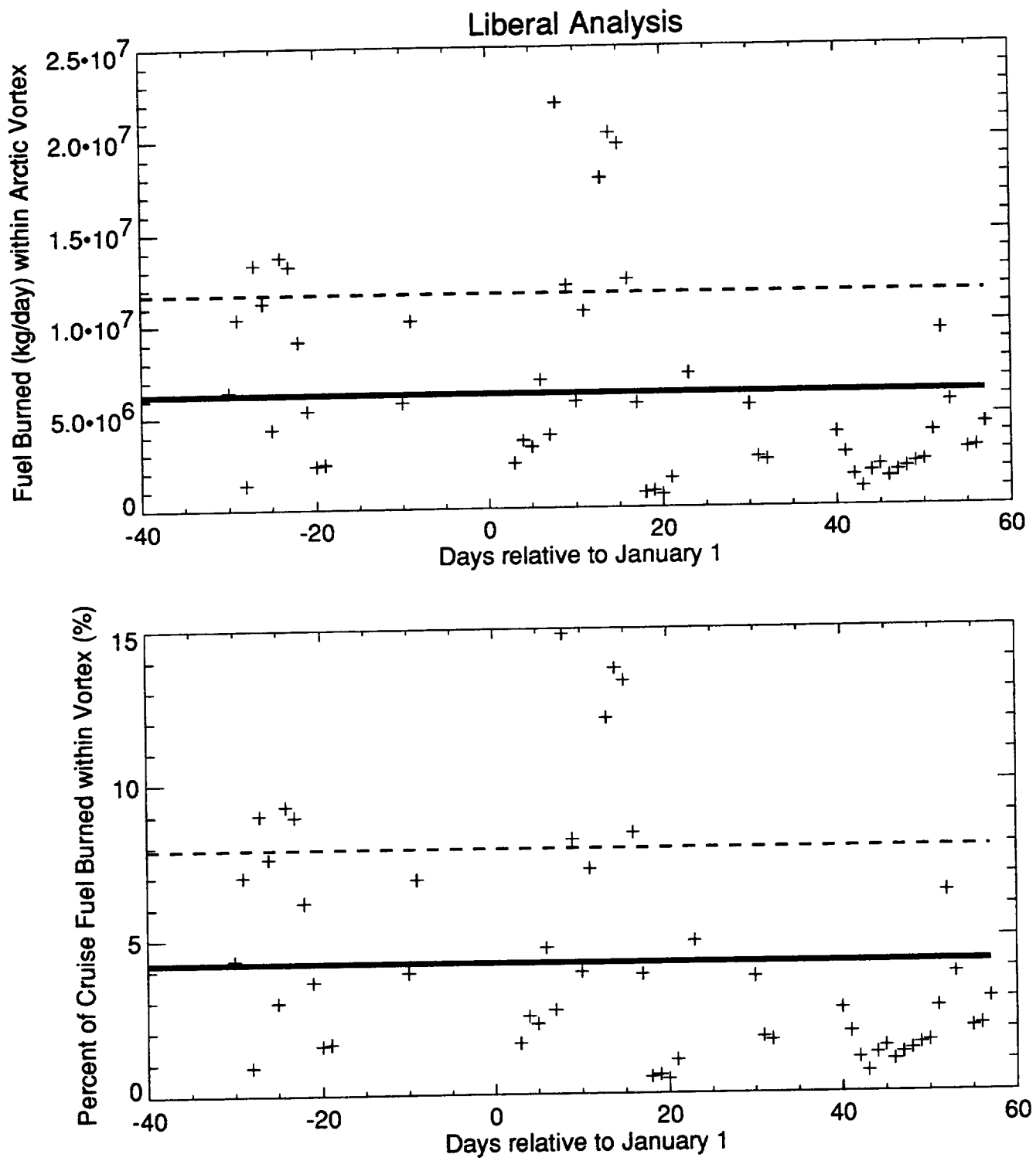


Winter of 1984-5

Universal Airline Network 500 Mach 2.4 HSCTs EI(NOx)=5

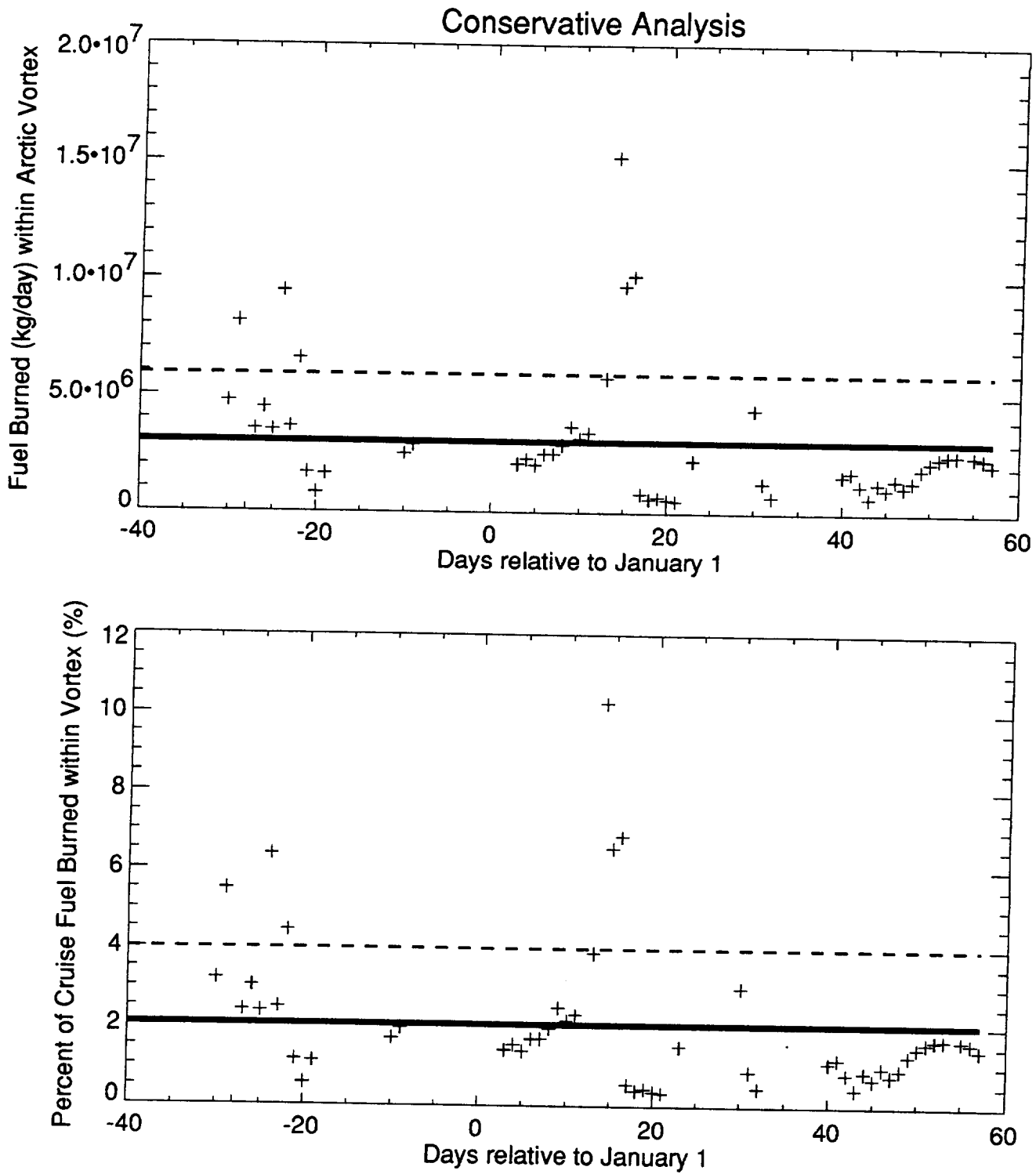
Solid line = Mean value

Dashed line = Mean value + 1 standard deviation



Winter of 1985-6
 Universal Airline Network 500 Mach 2.4 HSCTs EI(NO_x)=5

Solid line = Mean value
 Dashed line = Mean value + 1 standard deviation



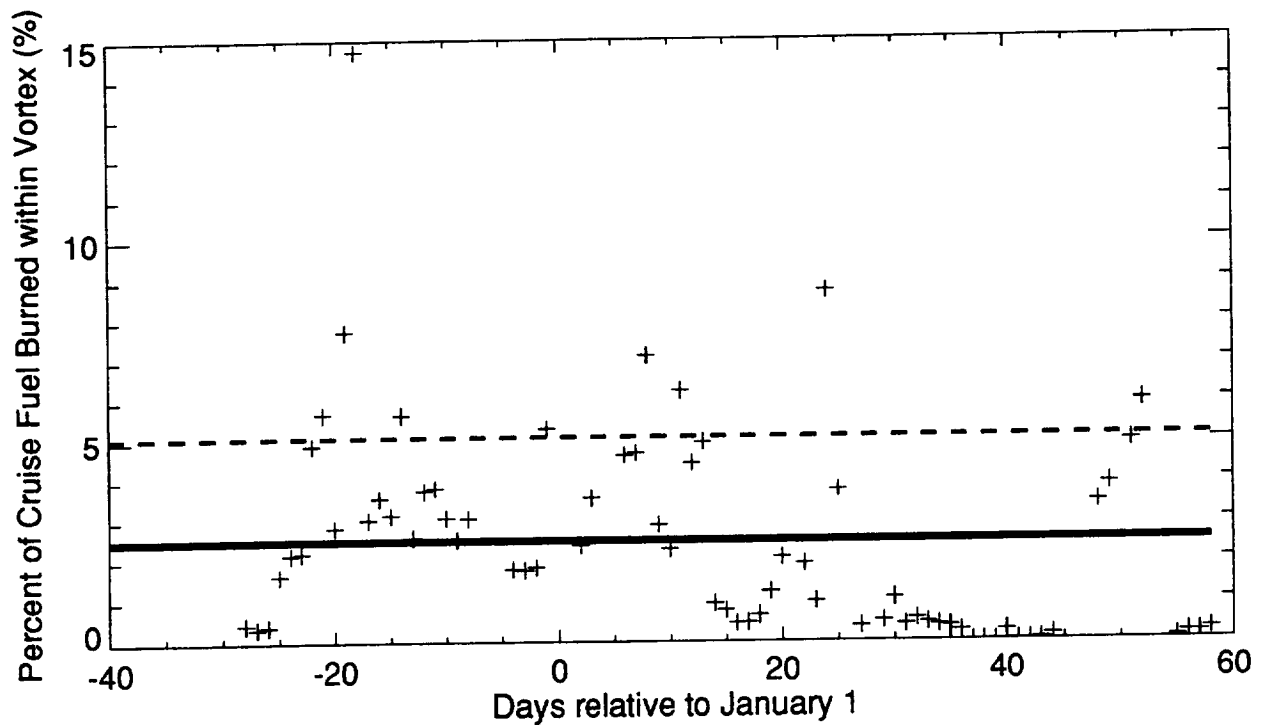
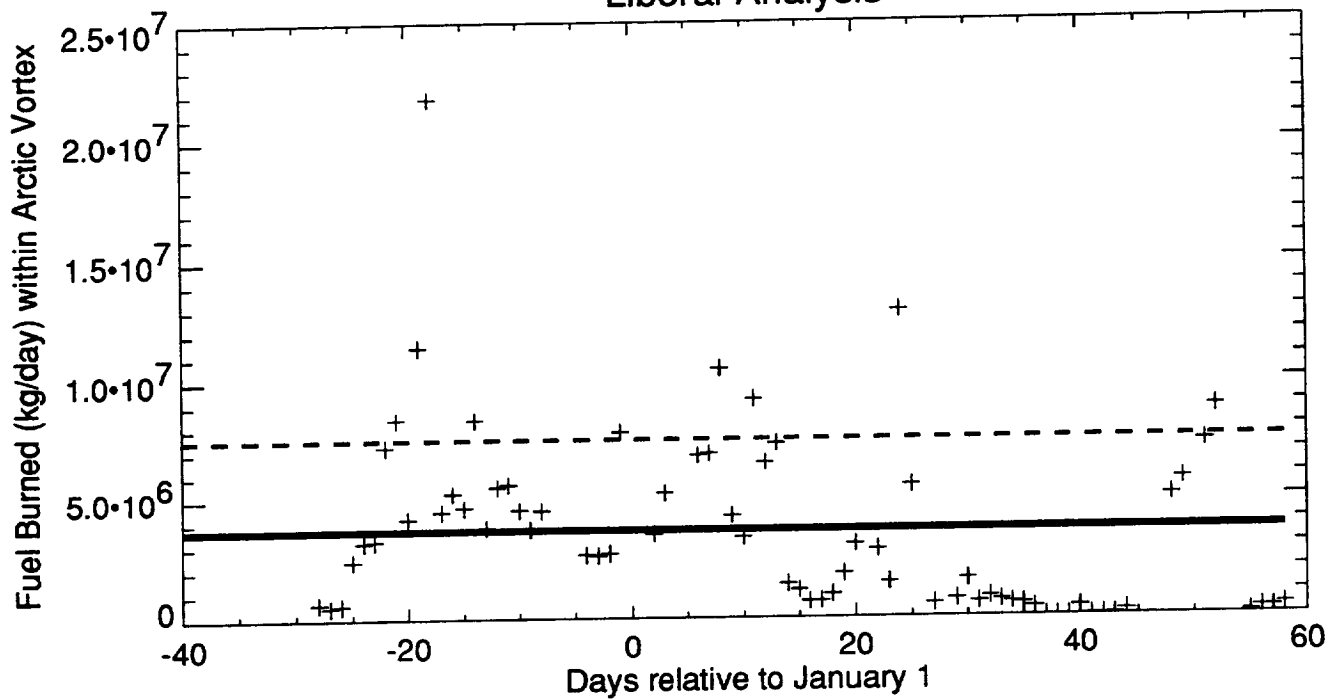
Winter of 1985-6

Universal Airline Network 500 Mach 2.4 HSCTs EI(NOx)=5

Solid line = Mean value

Dashed line = Mean value + 1 standard deviation

Liberal Analysis

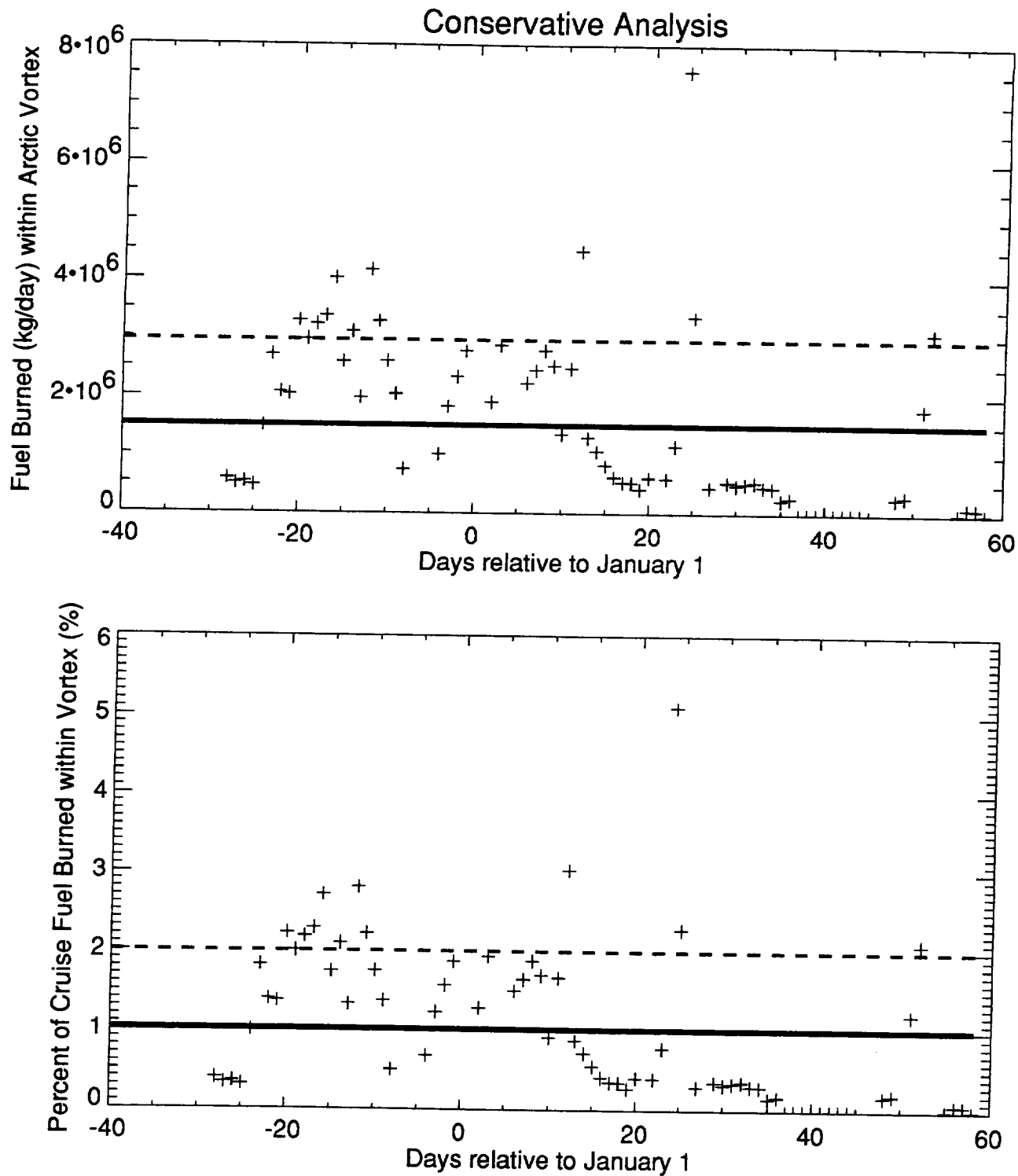


Winter of 1986-7

Universal Airline Network 500 Mach 2.4 HSCTs EI(NO_x)=5

Solid line = Mean value

Dashed line = Mean value + 1 standard deviation



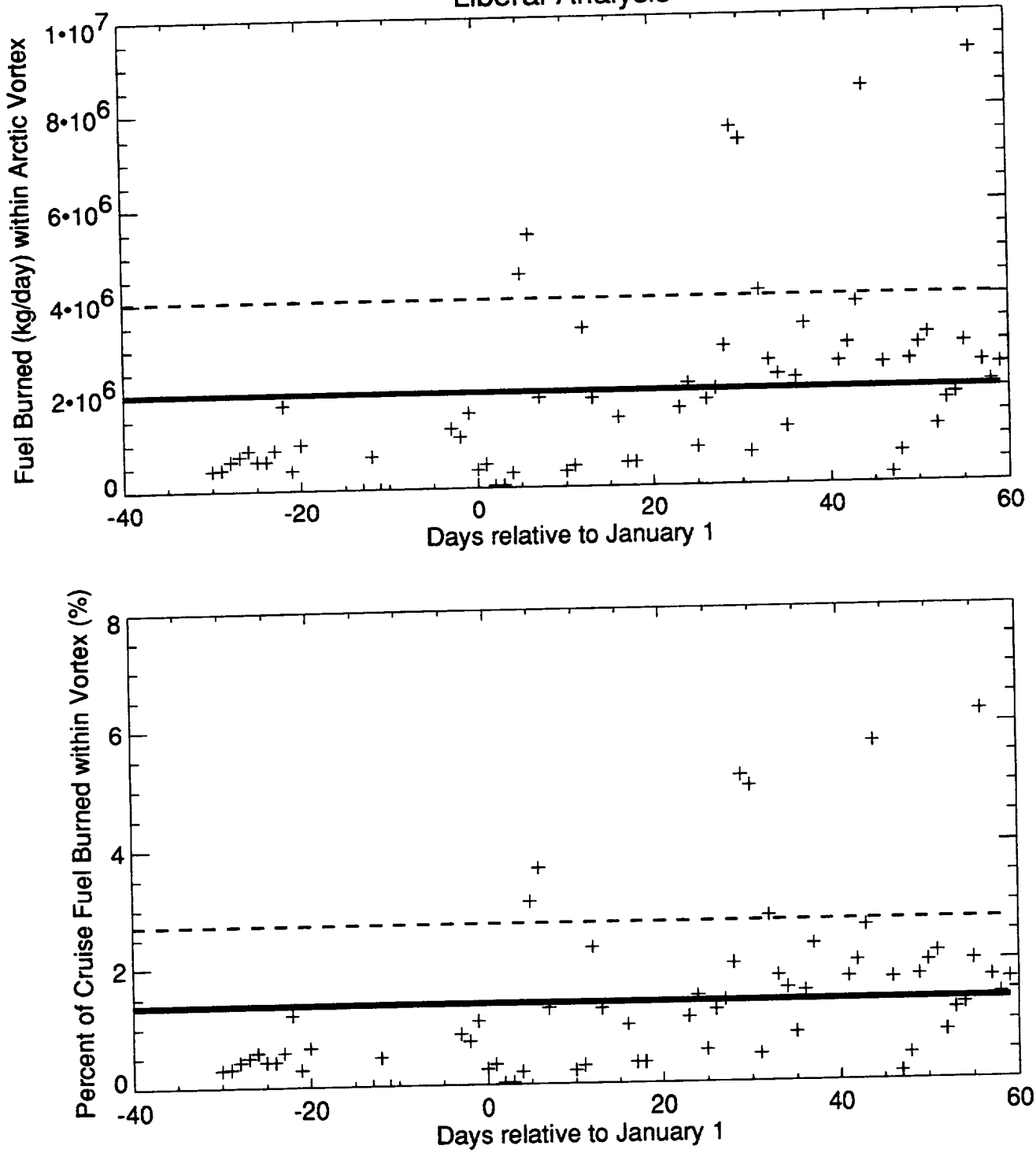
Winter of 1986-7

Universal Airline Network 500 Mach 2.4 HSCTs EI(NO_x)=5

Solid line = Mean value

Dashed line = Mean value + 1 standard deviation

Liberal Analysis

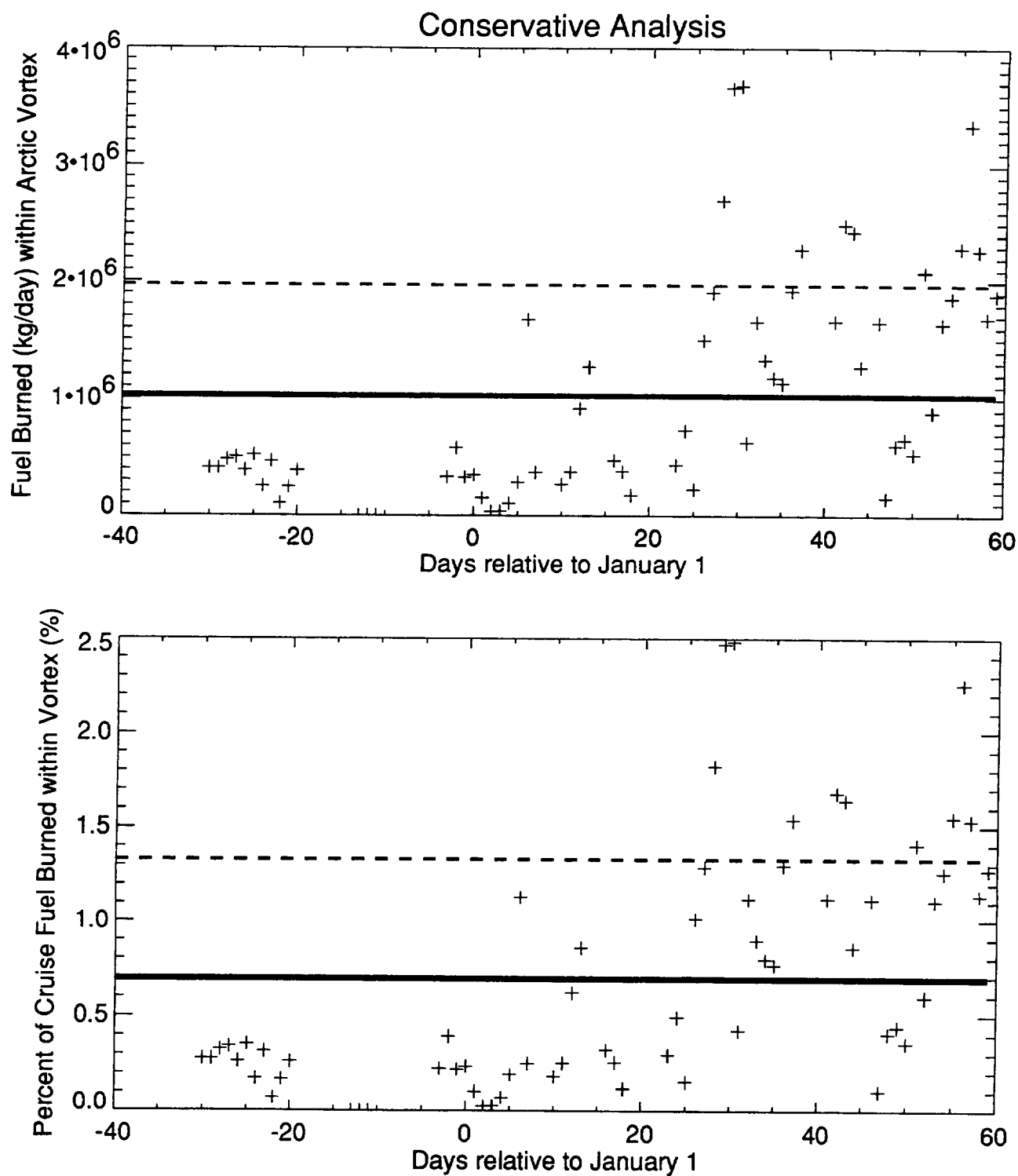


Winter of 1987-8

Universal Airline Network 500 Mach 2.4 HSCTs EI(NOx)=5

Solid line = Mean value

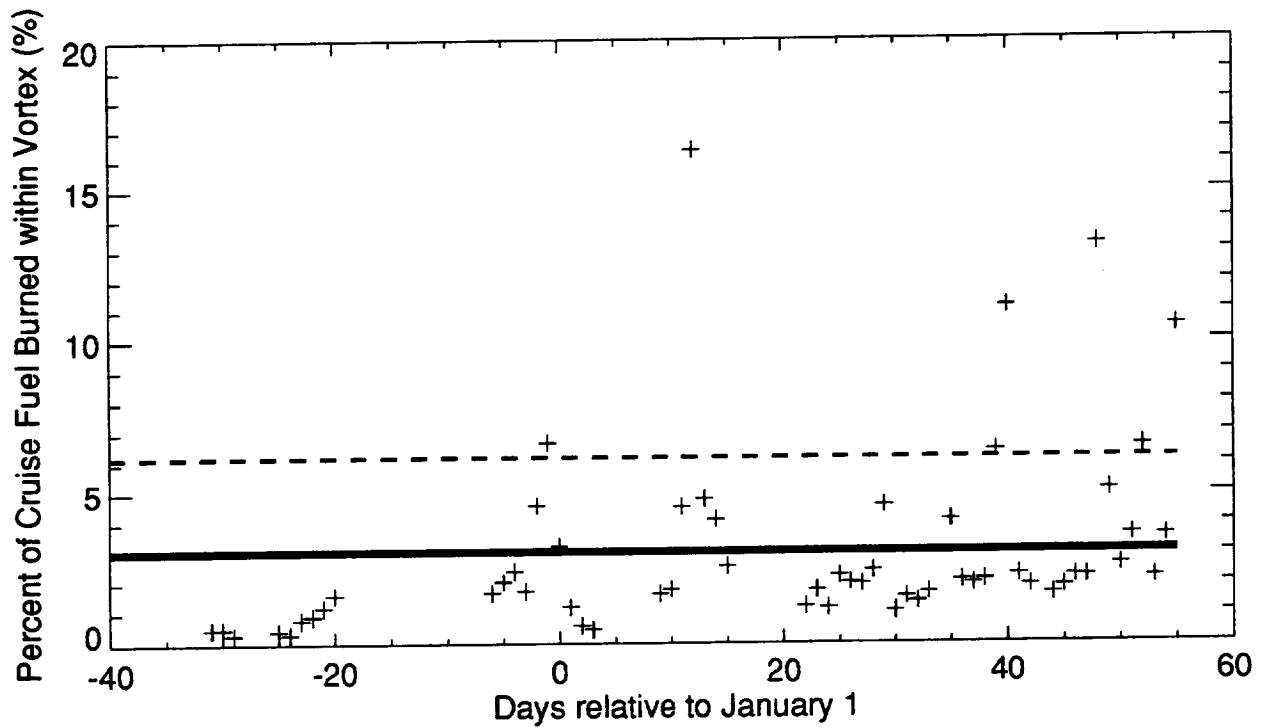
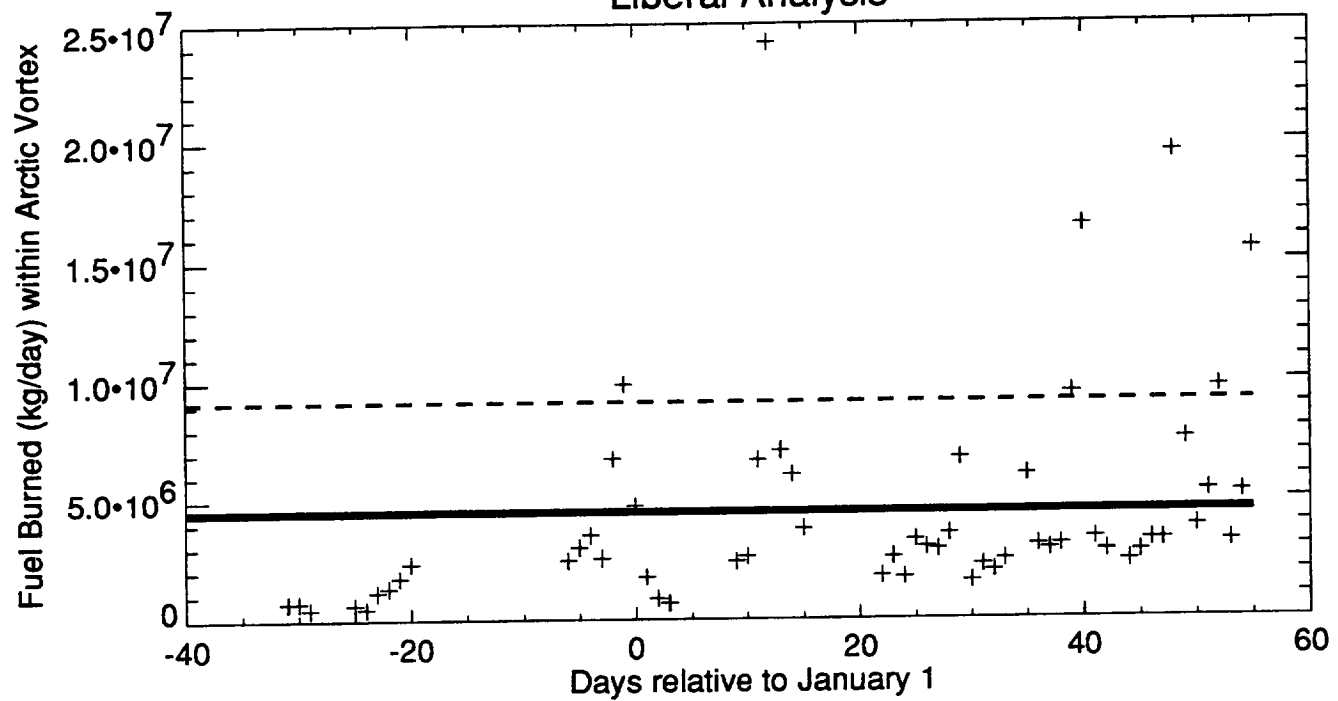
Dashed line = Mean value + 1 standard deviation



Winter of 1987-8
 Universal Airline Network 500 Mach 2.4 HSCTs EI(NO_x)=5

Solid line = Mean value
 Dashed line = Mean value + 1 standard deviation

Liberal Analysis

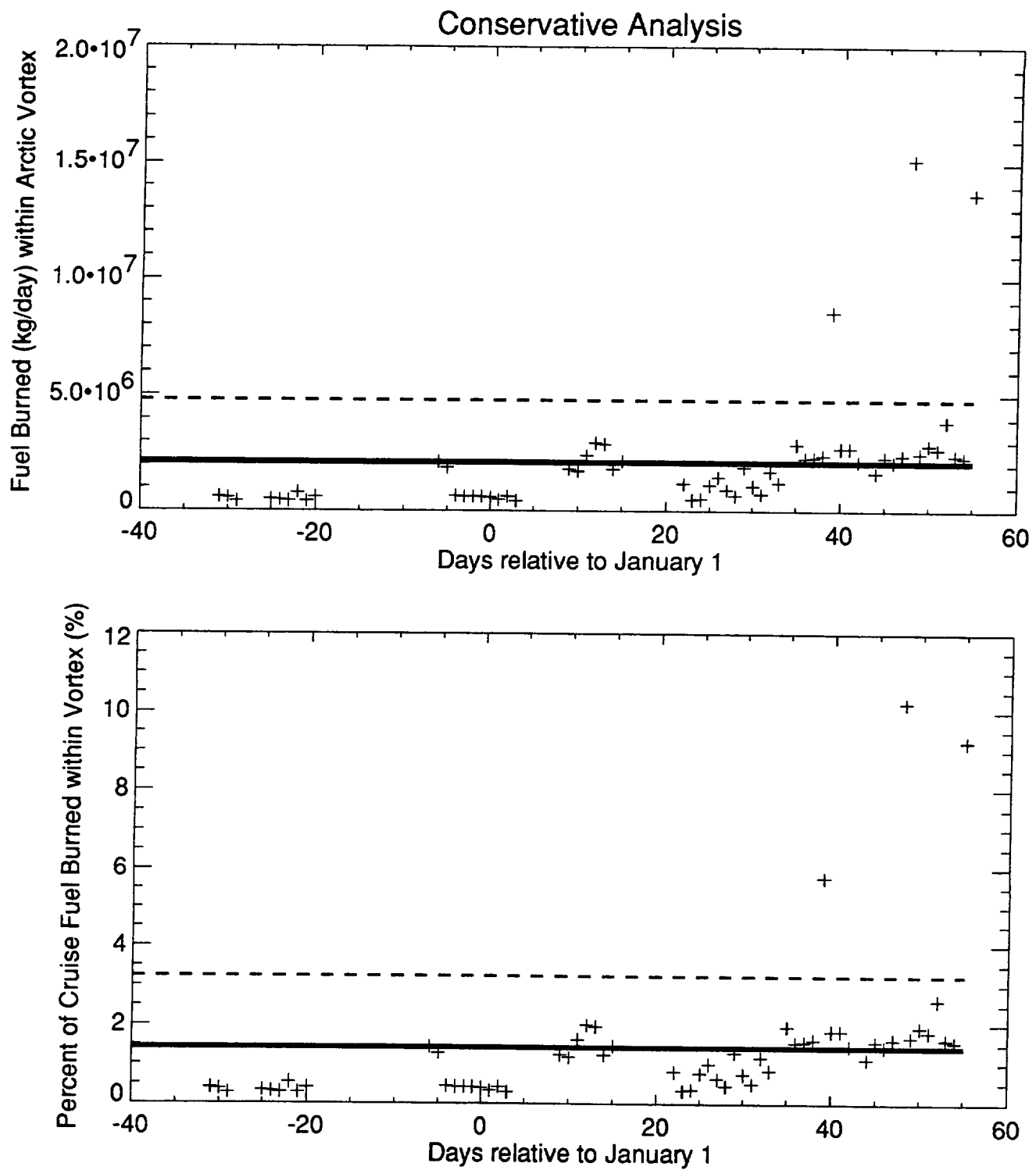


Winter of 1988-9

Universal Airline Network 500 Mach 2.4 HSCTs EI(NOx)=5

Solid line = Mean value

Dashed line = Mean value + 1 standard deviation

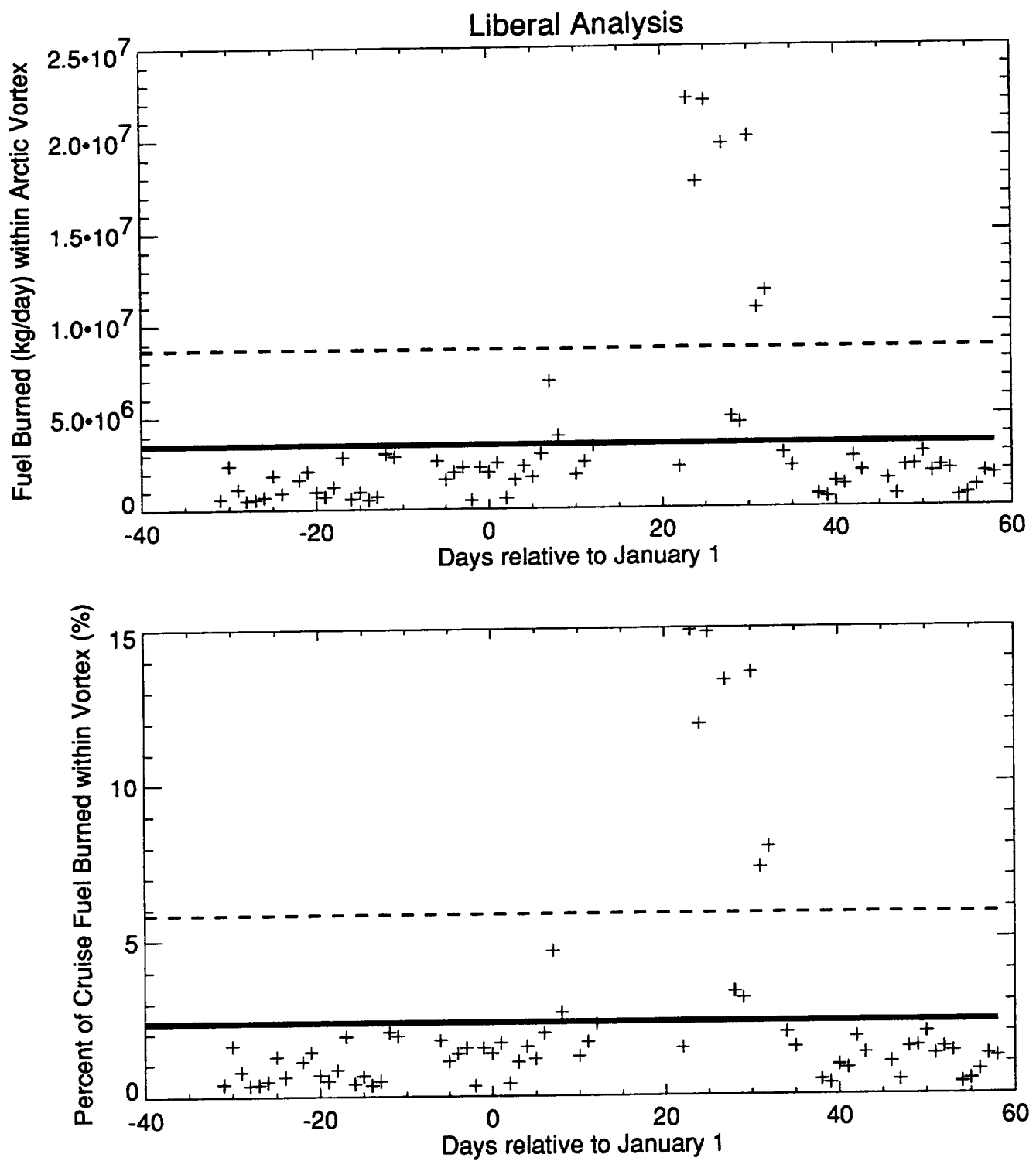


Winter of 1988-9

Universal Airline Network 500 Mach 2.4 HSCTs EI(NOx)=5

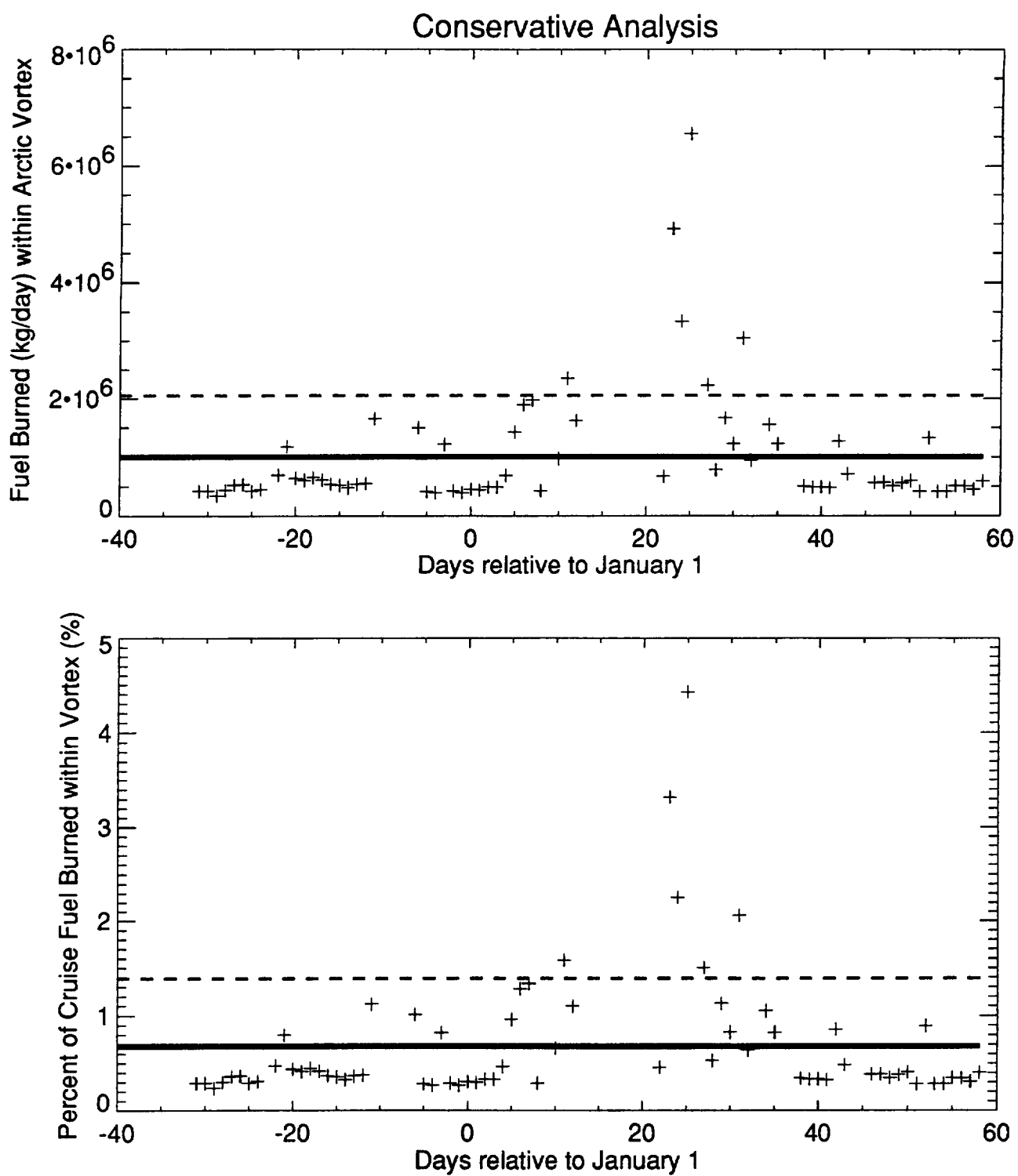
Solid line = Mean value

Dashed line = Mean value + 1 standard deviation



Winter of 1989-90
 Universal Airline Network 500 Mach 2.4 HSCTs EI(NOx)=5

Solid line = Mean value
 Dashed line = Mean value + 1 standard deviation



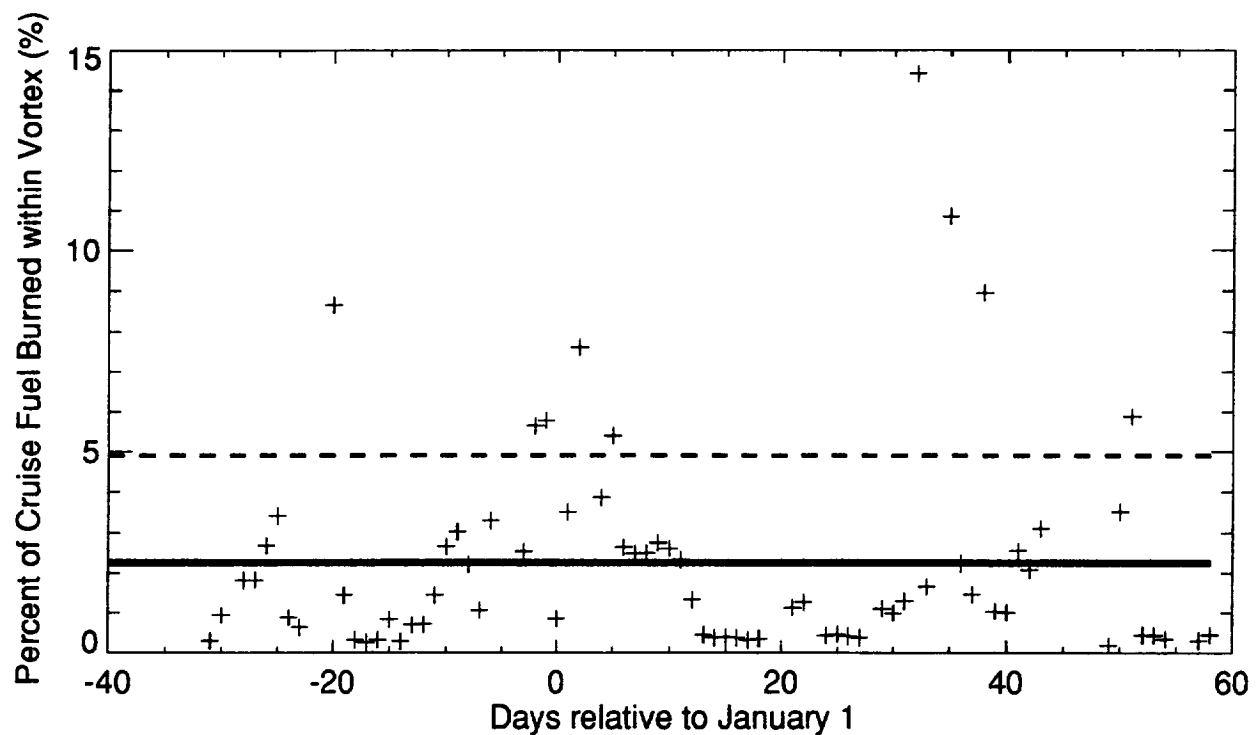
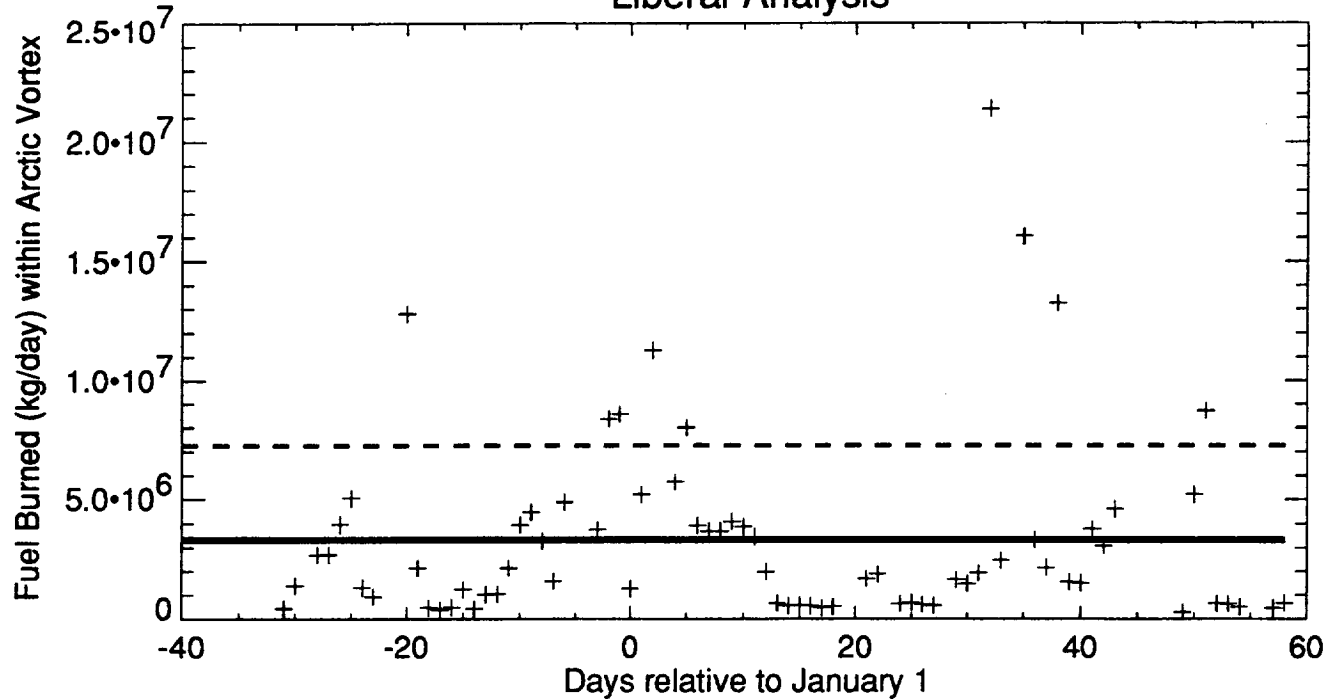
Winter of 1989-90

Universal Airline Network 500 Mach 2.4 HSCTs EI(NOx)=5

Solid line = Mean value

Dashed line = Mean value + 1 standard deviation

Liberal Analysis

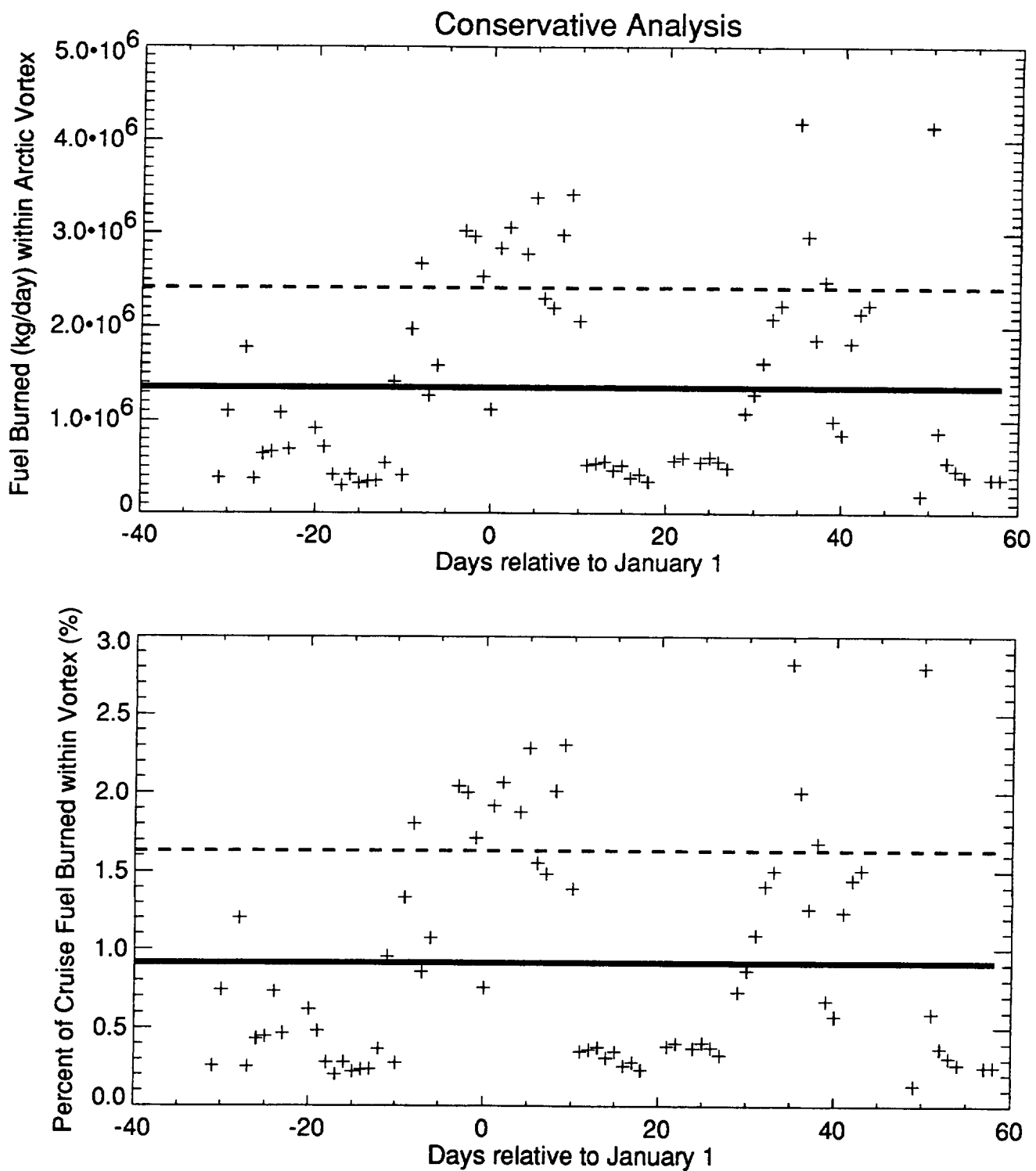


Winter of 1990-1

Universal Airline Network 500 Mach 2.4 HSCTs EI(NOx)=5

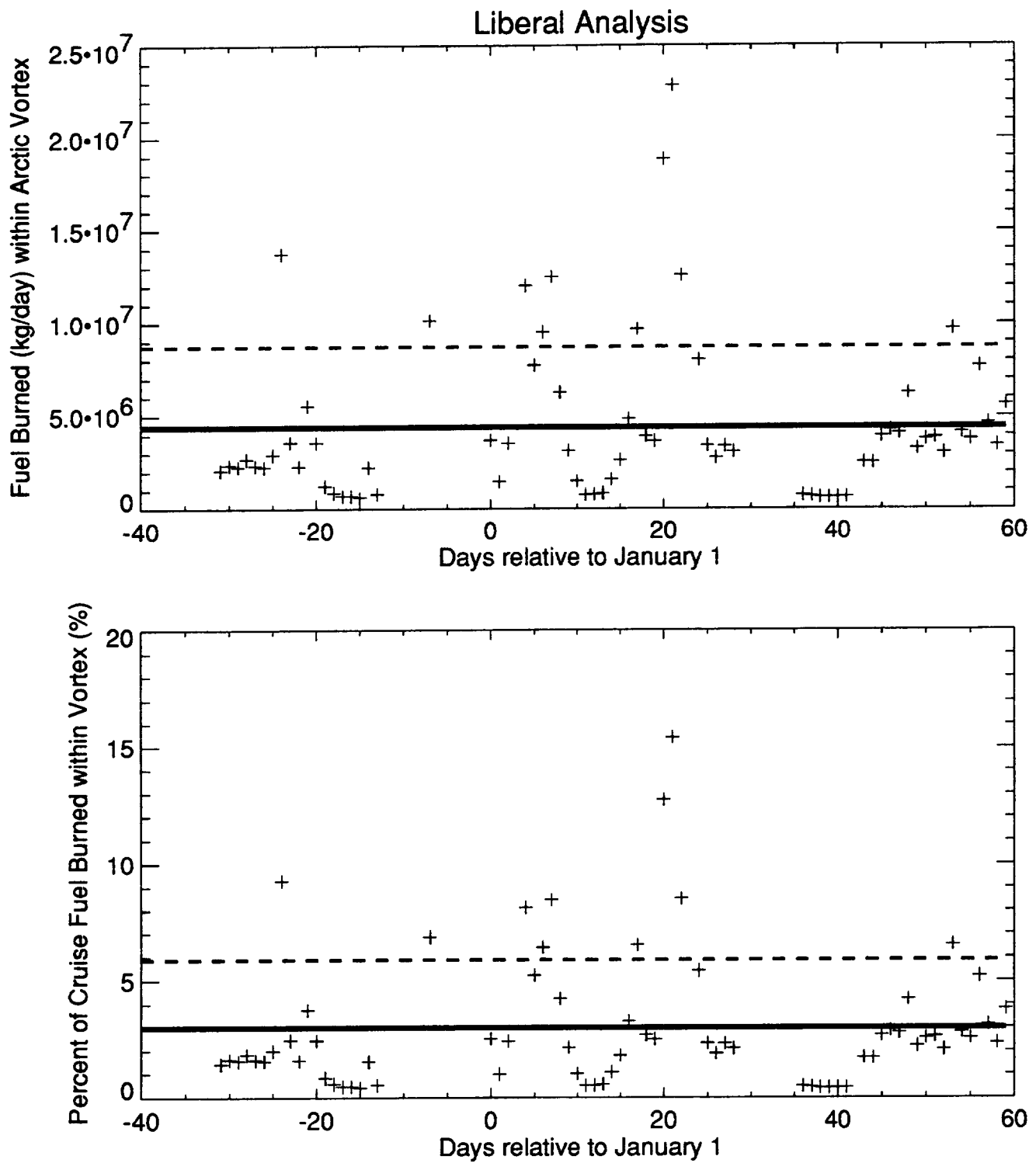
Solid line = Mean value

Dashed line = Mean value + 1 standard deviation



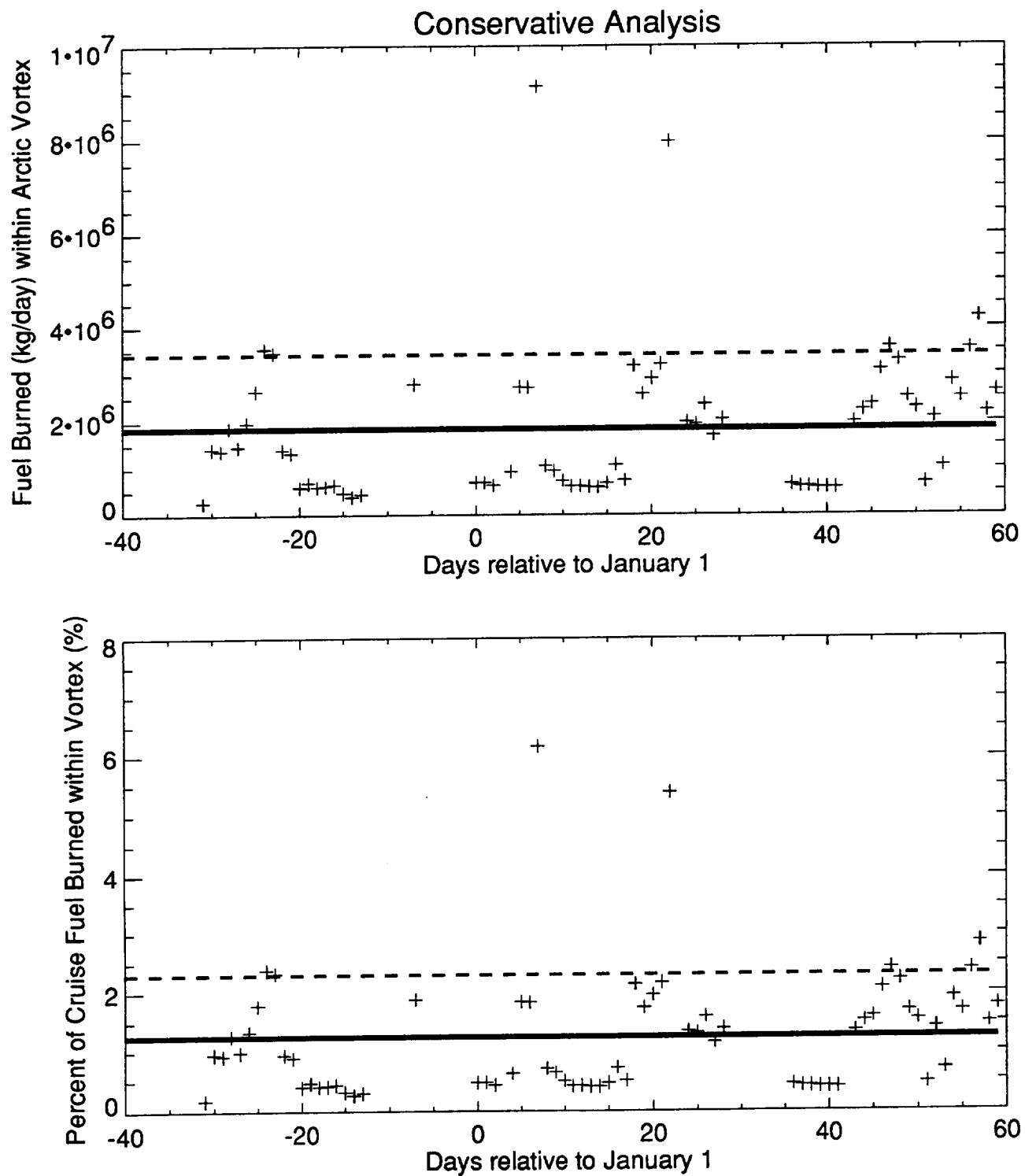
Winter of 1990-1
 Universal Airline Network 500 Mach 2.4 HSCTs EI(NO_x)=5

Solid line = Mean value
 Dashed line = Mean value + 1 standard deviation



Winter of 1991-2
 Universal Airline Network 500 Mach 2.4 HSCTs EI(NO_x)=5

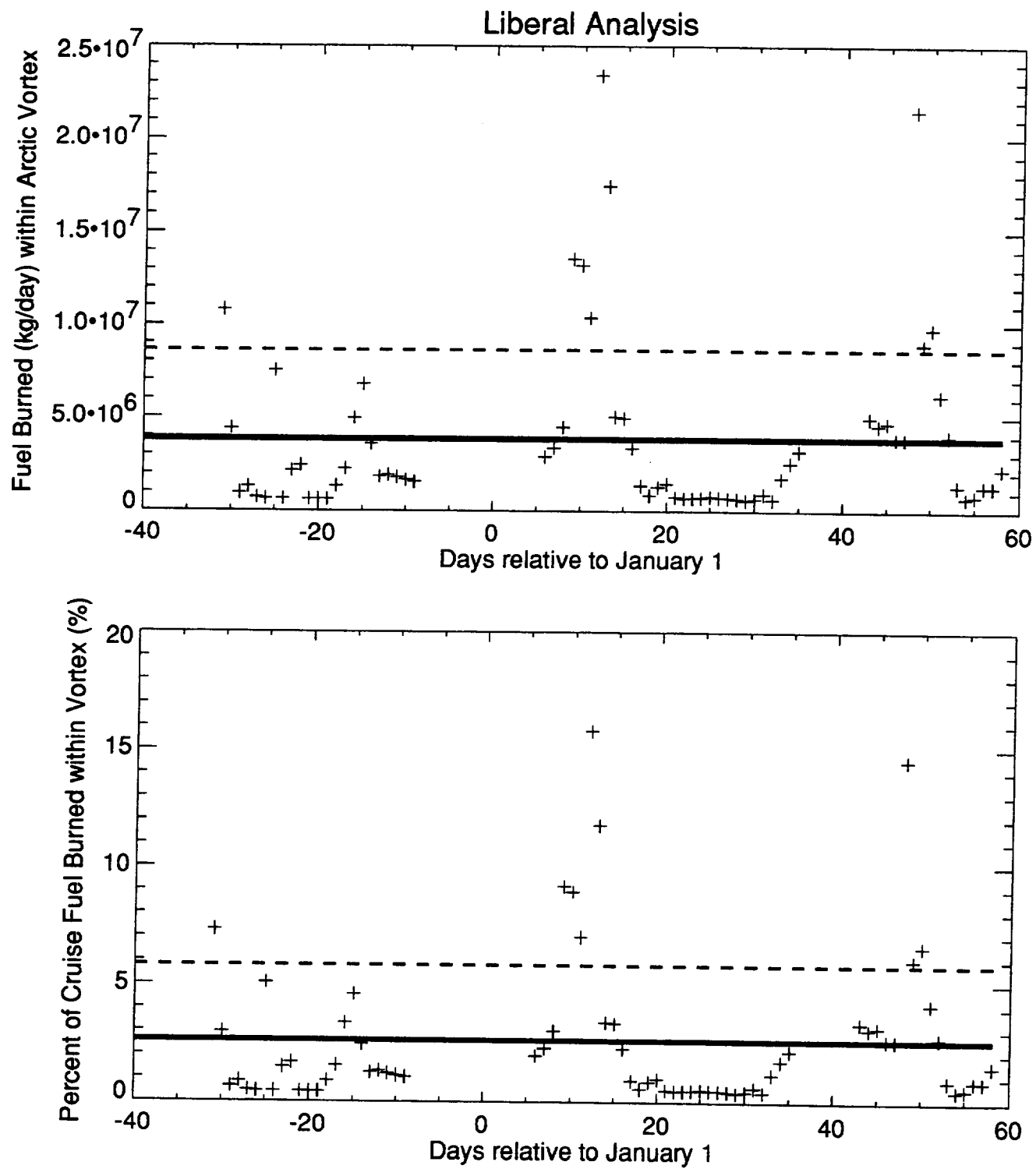
Solid line = Mean value
 Dashed line = Mean value + 1 standard deviation



Winter of 1991-2
 Universal Airline Network 500 Mach 2.4 HSCTs EI(NO_x)=5

Solid line = Mean value

Dashed line = Mean value + 1 standard deviation

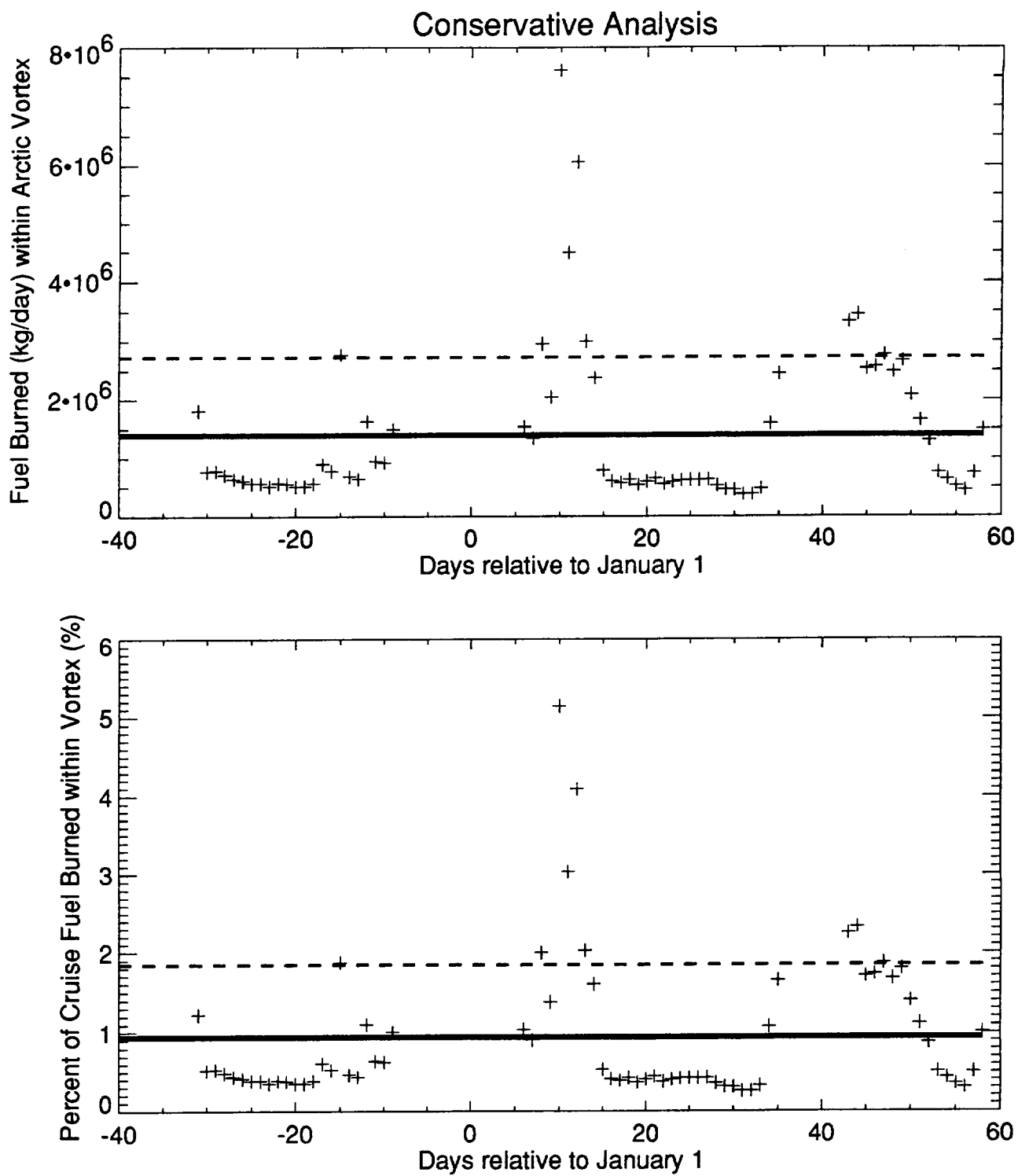


Winter of 1992-3

Universal Airline Network 500 Mach 2.4 HSCTs EI(NOx)=5

Solid line = Mean value

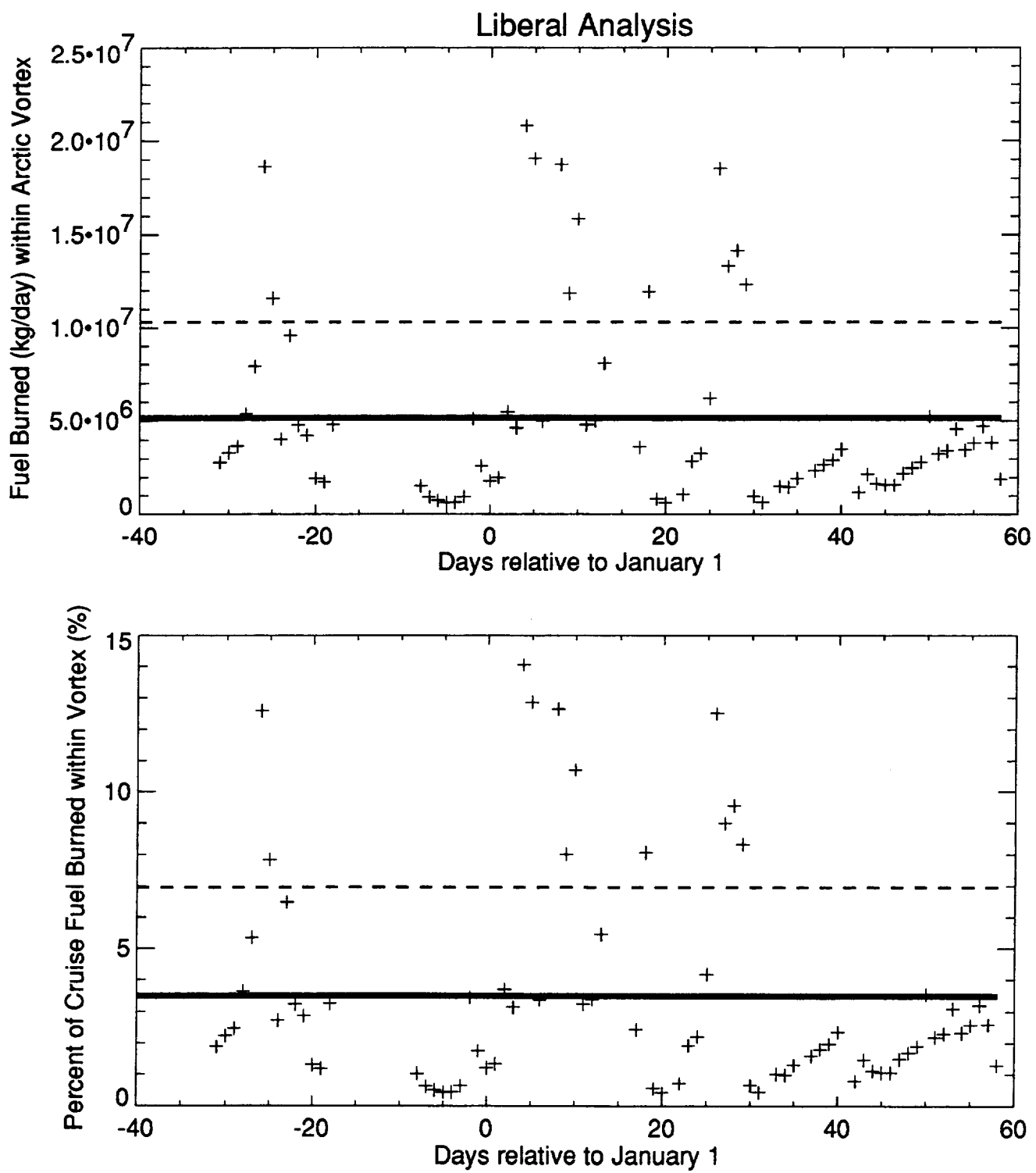
Dashed line = Mean value + 1 standard deviation



Winter of 1992-3
 Universal Airline Network 500 Mach 2.4 HSCTs EI(NOx)=5

Solid line = Mean value

Dashed line = Mean value + 1 standard deviation



Winter of 1993-4

Universal Airline Network 500 Mach 2.4 HSCTs EI(NOx)=5

Solid line = Mean value

Dashed line = Mean value + 1 standard deviation

Appendix C. Tables of Results for the Polar Vortex Calculations

1993 AESA assessment network

Winter	Conservative Analysis				Liberal Analysis			
	Mean Daily Fuel (million kg/day)	Std. Dev.	Mean Fraction	Std. Deviation	Mean Daily Fuel (million kg/day)	Std. Dev.	Mean Fraction	Std. Deviation
1978-79	2.5	2.0	1.8%	1.4%	4.1	3.5	2.9%	2.5%
1979-80	2.4	1.1	1.7%	0.8%	4.5	3.7	3.2%	2.6%
1980-81	2.2	1.3	1.6%	0.9%	3.7	2.5	2.6%	1.7%
1981-82	2.6	1.9	1.9%	1.4%	3.7	2.6	2.6%	1.8%
1982-83	2.9	1.7	2.0%	1.2%	4.5	3.0	3.2%	2.1%
1983-84	3.1	2.0	2.2%	1.4%	4.8	4.1	3.4%	2.9%
1984-85	1.4	1.2	1.0%	0.8%	2.7	3.2	1.9%	2.2%
1985-86	3.8	2.5	2.7%	1.7%	6.6	4.5	4.7%	3.2%
1986-87	2.4	1.6	1.7%	1.1%	4.5	3.7	3.2%	2.6%
1987-88	2.0	1.1	1.4%	0.8%	3.1	1.7	2.2%	1.2%
1988-89	3.2	2.1	2.2%	1.5%	5.4	3.9	3.8%	2.8%
1989-90	2.3	0.8	1.7%	0.5%	4.5	4.2	3.2%	2.9%
1990-91	2.1	0.6	1.5%	0.4%	4.1	3.3	2.9%	2.3%
1991-92	2.9	1.2	2.1%	0.8%	5.1	3.5	3.6%	2.4%
1992-93	2.6	0.9	1.8%	0.7%	4.8	3.9	3.4%	2.7%
1993-94	3.2	2.4	2.3%	1.7%	5.7	4.1	4.0%	2.9%
Average (1978-94)	2.6	1.8%			4.5		3.2%	

Appendix C. Tables of Results for the Polar Vortex Calculations

Universal HSCT network (500 HSCTs)

Winter	Conservative Analysis			Liberal Analysis				
	Mean	Std.	Daily Dev.	Mean	Std.	Daily Dev.		
	Daily Fuel (million kg/day)	(million kg/day)	Fraction	Deviation	Daily Fuel (million kg/day)	(million kg/day)	Fraction	Deviation
1978-79	1.7	2.3	1.2%	1.6%	3.4	4.2	2.3%	2.8%
1979-80	1.5	1.2	1.0%	0.8%	3.8	4.5	2.6%	3.0%
1980-81	1.4	1.1	0.9%	0.7%	3.1	2.7	2.1%	1.8%
1981-82	1.5	2.4	1.0%	1.6%	2.6	3.2	1.8%	2.2%
1982-83	1.7	2.2	1.2%	1.5%	3.5	3.7	2.4%	2.5%
1983-84	2.0	2.5	1.4%	1.7%	4.2	5.1	2.8%	3.5%
1984-85	1.1	1.3	0.7%	0.8%	2.4	3.8	1.6%	2.5%
1985-86	3.0	2.9	2.1%	1.9%	6.2	5.5	4.2%	3.7%
1986-87	1.5	1.5	1.0%	1.0%	3.7	3.9	2.5%	2.6%
1987-88	1.0	0.9	0.7%	0.6%	2.0	2.0	1.4%	1.4%
1988-89	2.1	2.7	1.4%	1.8%	4.5	4.7	3.0%	3.1%
1989-90	1.0	1.1	0.7%	0.7%	3.5	5.1	2.4%	3.5%
1990-91	1.4	1.1	0.9%	0.7%	3.3	3.9	2.3%	2.7%
1991-92	1.9	1.6	1.3%	1.1%	4.4	4.3	3.0%	2.9%
1992-93	1.4	1.3	0.9%	0.9%	3.8	4.8	2.6%	3.2%
1993-94	2.4	3.0	1.6%	2.0%	5.2	5.2	3.5%	3.5%
Average (1978-94)	1.7		1.1%		3.7		2.5%	

Appendix C. Tables of Results for the Polar Vortex Calculations

Universal HSCT network (1000 HSCTs)

Winter	Conservative Analysis				Liberal Analysis			
	Mean Daily Fuel (million kg/day)	Std. Dev. (million kg/day)	Mean Fraction	Std. Deviation	Mean Daily Fuel (million kg/day)	Std. Dev. (million kg/day)	Mean Fraction	Std. Deviation
1978-79	4.6	4.0	1.7%	1.5%	7.7	7.1	2.9%	2.7%
1979-80	4.5	2.7	1.7%	1.0%	8.7	7.9	3.2%	3.0%
1980-81	4.1	2.5	1.5%	0.9%	7.2	5.1	2.7%	1.9%
1981-82	4.5	4.1	1.7%	1.5%	6.7	5.5	2.5%	2.1%
1982-83	5.4	3.7	2.0%	1.4%	8.7	6.1	3.3%	2.3%
1983-84	5.8	4.5	2.2%	1.7%	9.7	8.6	3.6%	3.2%
1984-85	2.8	2.3	1.0%	0.9%	5.3	6.4	2.0%	2.4%
1985-86	7.6	5.1	2.8%	1.9%	13.2	9.2	4.9%	3.4%
1986-87	4.5	3.1	1.7%	1.2%	8.4	6.9	3.1%	2.6%
1987-88	3.4	2.2	1.3%	0.8%	5.5	3.7	2.1%	1.4%
1988-89	5.4	4.5	2.0%	1.7%	9.8	7.7	3.6%	2.9%
1989-90	3.9	2.1	1.5%	0.8%	8.4	8.8	3.1%	3.3%
1990-91	3.8	1.6	1.4%	0.6%	7.6	6.5	2.8%	2.4%
1991-92	5.4	2.6	2.0%	1.0%	10.2	7.2	3.8%	2.7%
1992-93	4.6	2.5	1.7%	0.9%	9.1	8.1	3.4%	3.0%
1993-94	6.2	5.2	2.3%	2.0%	11.2	8.8	4.2%	3.3%
Average (1978-94)	4.8	1.8%			8.6		3.2%	

REPORT DOCUMENTATION PAGE			Form Approved OMB No. 0704-0188
<p>Public reporting burden for this collection of information is estimated to average 1 hour per response, including the time for reviewing instructions, searching existing data sources, gathering and maintaining the data needed, and completing and reviewing the collection of information. Send comments regarding this burden estimate or any other aspect of this collection of information, including suggestions for reducing this burden, to Washington Headquarters Services, Directorate for Information Operations and Reports, 1215 Jefferson Davis Highway, Suite 1204, Arlington, VA 22202-4302, and to the Office of Management and Budget, Paperwork Reduction Project (0704-0188), Washington, DC 20503.</p>			
1. AGENCY USE ONLY (Leave blank)	2. REPORT DATE	3. REPORT TYPE AND DATES COVERED	
	April 1996	Contractor Report	
4. TITLE AND SUBTITLE		5. FUNDING NUMBERS	
Aircraft Emissions Deposited in the Stratosphere and within the Arctic Polar Vortex		C NAS1-19360 WU 537-09-23-02	
6. AUTHOR(S)			
Steven L. Baughcum			
7. PERFORMING ORGANIZATION NAME(S) AND ADDRESS(ES)		8. PERFORMING ORGANIZATION REPORT NUMBER	
Boeing Commercial Airplane Group P. O. Box 3707 Seattle, WA 98124-2207			
9. SPONSORING/MONITORING AGENCY NAME(S) AND ADDRESS(ES)		10. SPONSORING/MONITORING AGENCY REPORT NUMBER	
National Aeronautics and Space Administration Langley Research Center Hampton, VA 23681-0001		NASA CR-4714	
11. SUPPLEMENTARY NOTES Langley Technical Monitor: Donald L. Maiden Final Report - Task 36			
12a. DISTRIBUTION / AVAILABILITY STATEMENT		12b. DISTRIBUTION CODE	
Unclassified - Unlimited Subject Category 45			
13. ABSTRACT (Maximum 200 words)			
<p>This report describes an analysis of the quantity of emissions (water vapor, NOx) projected to be deposited directly within the Arctic polar vortex by projected fleets of Mach 2.4 high speed civil transports (HSCTs). It also evaluates the amount of emissions from subsonic aircraft which are emitted into the lower stratosphere using aircraft emission inventories developed earlier for May 1990 as representative of the annual average.</p>			
14. SUBJECT TERMS			15. NUMBER OF PAGES
aircraft emissions, ozone impact, emissions inventory, atmospheric impact			131
16. PRICE CODE			A07
17. SECURITY CLASSIFICATION OF REPORT	18. SECURITY CLASSIFICATION OF THIS PAGE	19. SECURITY CLASSIFICATION OF ABSTRACT	20. LIMITATION OF ABSTRACT
Unclassified	Unclassified	Unclassified	



